7 Clouds and Aerosols

Coordinating Lead Authors:
Olivier Boucher (France), David Randall (USA)

Lead Authors:
Paulo Artaxo (Brazil), Christopher Bretherton (USA), Graham Feingold (USA), Piers Forster (UK), Veli-Matti Kerminen (Finland), Yutaka Kondo (Japan), Hong Liao (China), Ulrike Lohmann (Switzerland), Philip Rasch (USA), S.K. Satheesh (India), Steven Sherwood (Australia), Bjorn Stevens (Germany), Xiao-Ye Zhang (China)

Contributing Authors:
Govindasamy Bala (India), Nicolas Bellouin (UK), Angela Benedetti (UK), Sandrine Bony (France), Ken Caldeira (USA), Anthony Del Genio (USA), Maria Cristina Facchini (Italy), Mark Flanner (USA), Steven Ghan (USA), Claire Granier (France), Corinna Hoose (Germany), Andy Jones (UK), Makoto Koike (Japan), Ben Kravitz (USA), Benjamin Laken (Spain), Matthew Lebsock (USA), Natalie Mahowald (USA), Gunnar Myhre (Norway), Colin O'Dowd (Ireland), Alan Robock (USA), Bjørn Samset (Norway), Hauke Schmidt (Germany), Michael Schulz (Norway), Graeme Stephens (USA), Philip Stier (UK), Trude Storelvmo (USA), Dave Winker (USA), Matthew Wyant (USA)

Review Editors:
Sandro Fuzzi (Italy), Joyce Penner (USA), Venkatachalam Ramaswamy (USA), Claudia Stubenrauch (France)

This chapter should be cited as:
Boucher, O., D. Randall, P. Artaxo, C. Bretherton, G. Feingold, P. Forster, V.-M. Kerminen, Y. Kondo, H. Liao, U. Lohmann, P. Rasch, S.K. Satheesh, S. Sherwood, B. Stevens and X.Y. Zhang, 2013: Clouds and Aerosols. In: *Climate Change 2013: The Physical Science Basis. Contribution of Working Group I to the Fifth Assessment Report of the Intergovernmental Panel on Climate Change* [Stocker, T.F., D. Qin, G.-K. Plattner, M. Tignor, S.K. Allen, J. Boschung, A. Nauels, Y. Xia, V. Bex and P.M. Midgley (eds.)]. Cambridge University Press, Cambridge, United Kingdom and New York, NY, USA.

Table of Contents

Executive Summary

Clouds and aerosols continue to contribute the largest uncertainty to estimates and interpretations of the Earth's changing energy budget. This chapter focuses on process understanding and considers observations, theory and models to assess how clouds and aerosols contribute and respond to climate change. The following conclusions are drawn.

Progress in Understanding

Many of the cloudiness and humidity changes simulated by climate models in warmer climates are now understood as responses to large-scale circulation changes that do not appear to depend strongly on sub-grid scale model processes, increasing confidence in these changes. For example, multiple lines of evidence now indicate positive feedback contributions from circulation-driven changes in both the height of high clouds and the latitudinal distribution of clouds (*medium to high confidence*[1]). However, some aspects of the overall cloud response vary substantially among models, and these appear to depend strongly on sub-grid scale processes in which there is less confidence. {7.2.4, 7.2.5, 7.2.6, Figure 7.11}

Climate-relevant aerosol processes are better understood, and climate-relevant aerosol properties better observed, than at the time of AR4. However, the representation of relevant processes varies greatly in global aerosol and climate models and it remains unclear what level of sophistication is required to model their effect on climate. Globally, between 20 and 40% of aerosol optical depth (*medium confidence*) and between one quarter and two thirds of cloud condensation nucleus concentrations (*low confidence*) are of anthropogenic origin. {7.3, Figures 7.12 to 7.15}

Cosmic rays enhance new particle formation in the free troposphere, but the effect on the concentration of cloud condensation nuclei is too weak to have any detectable climatic influence during a solar cycle or over the last century (*medium evidence, high agreement*). No robust association between changes in cosmic rays and cloudiness has been identified. In the event that such an association existed, a mechanism other than cosmic ray-induced nucleation of new aerosol particles would be needed to explain it. {7.4.6}

Recent research has clarified the importance of distinguishing forcing (instantaneous change in the radiative budget) and rapid adjustments (which modify the radiative budget indirectly through fast atmospheric and surface changes) from feedbacks (which operate through changes in climate variables that are mediated by a change in surface temperature). Furthermore, one can distinguish between the traditional concept of radiative forcing (RF) and the relatively new concept of effective radiative forcing (ERF) that also includes rapid adjustments. For aerosols one can further distinguish forcing processes arising from aerosol–radiation interactions (ari) and aerosol–cloud interactions (aci). {7.1, Figures 7.1 to 7.3}

The quantification of cloud and convective effects in models, and of aerosol–cloud interactions, continues to be a challenge. Climate models are incorporating more of the relevant processes than at the time of AR4, but confidence in the representation of these processes remains weak. Cloud and aerosol properties vary at scales significantly smaller than those resolved in climate models, and cloud-scale processes respond to aerosol in nuanced ways at these scales. Until sub-grid scale parameterizations of clouds and aerosol–cloud interactions are able to address these issues, model estimates of aerosol–cloud interactions and their radiative effects will carry large uncertainties. Satellite-based estimates of aerosol–cloud interactions remain sensitive to the treatment of meteorological influences on clouds and assumptions on what constitutes pre-industrial conditions. {7.3, 7.4, 7.5.3, 7.5.4, 7.6.4, Figures 7.8, 7.12, 7.16}

Precipitation and evaporation are expected to increase on average in a warmer climate, but also undergo global and regional adjustments to carbon dioxide (CO_2) and other forcings that differ from their warming responses. Moreover, there is *high confidence* that, as climate warms, extreme precipitation rates on for example, daily time scales will increase faster than the time average. Changes in average precipitation must remain consistent with changes in the net rate of cooling of the troposphere, which is affected by its temperature but also by greenhouse gases (GHGs) and aerosols. Consequently, while the increase in global mean precipitation would be 1.5 to 3.5% $°C^{-1}$ due to surface temperature change alone, warming caused by CO_2 or absorbing aerosols results in a smaller sensitivity, even more so if it is partially offset by albedo increases. The complexity of land surface and atmospheric processes limits confidence in regional projections of precipitation change, especially over land, although there is a component of a 'wet-get-wetter' and 'dry-get-drier' response over oceans at the large scale. Changes in local extremes on daily and sub-daily time scales are strongly influenced by lower-tropospheric water vapour concentrations, and on average will increase by roughly 5 to 10% per degree Celsius of warming (*medium confidence*). Aerosol–cloud interactions can influence the character of individual storms, but evidence for a systematic aerosol effect on storm or precipitation intensity is more limited and ambiguous. {7.2.4, 7.4, 7.6, Figures 7.20, 7.21}

[1] In this Report, the following summary terms are used to describe the available evidence: limited, medium, or robust; and for the degree of agreement: low, medium, or high. A level of confidence is expressed using five qualifiers: very low, low, medium, high, and very high, and typeset in italics, e.g., *medium confidence*. For a given evidence and agreement statement, different confidence levels can be assigned, but increasing levels of evidence and degrees of agreement are correlated with increasing confidence (see Section 1.4 and Box TS.1 for more details).

Water Vapour, Cloud and Aerosol Feedbacks

The net feedback from water vapour and lapse rate changes combined, as traditionally defined, is *extremely likely*[2] positive (amplifying global climate changes). The sign of the net radiative feedback due to all cloud types is less certain but *likely* positive. Uncertainty in the sign and magnitude of the cloud feedback is due primarily to continuing uncertainty in the impact of warming on low clouds. We estimate the water vapour plus lapse rate feedback[3] to be +1.1 (+0.9 to +1.3) W m^{-2} $°C^{-1}$ and the cloud feedback from all cloud types to be +0.6 (–0.2 to +2.0) W m^{-2} $°C^{-1}$. These ranges are broader than those of climate models to account for additional uncertainty associated with processes that may not have been accounted for in those models. The mean values and ranges in climate models are essentially unchanged since AR4, but are now supported by stronger indirect observational evidence and better process understanding, especially for water vapour. Low clouds contribute positive feedback in most models, but that behaviour is not well understood, nor effectively constrained by observations, so we are not confident that it is realistic. {7.2.4, 7.2.5, 7.2.6, Figures 7.9 to 7.11}.

Aerosol–climate feedbacks occur mainly through changes in the source strength of natural aerosols or changes in the sink efficiency of natural and anthropogenic aerosols; a limited number of modelling studies have bracketed the feedback parameter within ±0.2 W m^{-2} $°C^{-1}$ with *low confidence*. There is *medium confidence* for a weak dimethylsulphide–cloud condensation nuclei–cloud albedo feedback due to a weak sensitivity of cloud condensation nuclei population to changes in dimethylsulphide emissions. {7.3.5}

Quantification of climate forcings[4] due to aerosols and clouds

The ERF due to aerosol–radiation interactions that takes rapid adjustments into account (ERFari) is assessed to be –0.45 (–0.95 to +0.05) W m^{-2}. The RF from absorbing aerosol on snow and ice is assessed separately to be +0.04 (+0.02 to +0.09) W m^{-2}. Prior to adjustments taking place, the RF due to aerosol–radiation interactions (RFari) is assessed to be –0.35 (–0.85 to +0.15) W m^{-2}. The assessment for RFari is less negative than reported in AR4 because of a re-evaluation of aerosol absorption. The uncertainty estimate is wider but more robust, based on multiple lines of evidence from models, remotely sensed data, and ground-based measurements. Fossil fuel and biofuel emissions[4] contribute to RFari via sulphate aerosol: –0.4 (–0.6 to –0.2) W m^{-2}, black carbon (BC) aerosol: +0.4 (+0.05 to +0.8) W m^{-2}, and primary and secondary organic aerosol: –0.12 (–0.4 to +0.1) W m^{-2}. Additional RFari contributions occur via biomass burning emissions[5]: +0.0 (–0.2 to +0.2) W m^{-2}, nitrate aerosol: –0.11 (–0.3 to –0.03) W m^{-2}, and mineral dust: –0.1 (–0.3 to +0.1) W m^{-2} although the latter may not be entirely of anthropogenic origin. While there is robust evidence for the existence of rapid adjustment of clouds in response to aerosol absorption, these effects are multiple and not well represented in climate models, leading to large uncertainty. Unlike in the last IPCC assessment, the RF from BC on snow and ice includes the effects on sea ice, accounts for more physical processes and incorporates evidence from both models and observations. This RF has a 2 to 4 times larger global mean surface temperature change per unit forcing than a change in CO_2. {7.3.4, 7.5.2, Figures 7.17, 7.18}

The total ERF due to aerosols (ERFari+aci, excluding the effect of absorbing aerosol on snow and ice) is assessed to be –0.9 (–1.9 to –0.1) W m^{-2} with *medium confidence*. The ERFari+aci estimate includes rapid adjustments, such as changes to the cloud lifetime and aerosol microphysical effects on mixed-phase, ice and convective clouds. This range was obtained from expert judgement guided by climate models that include aerosol effects on mixed-phase and convective clouds in addition to liquid clouds, satellite studies and models that allow cloud-scale responses. This forcing can be much larger regionally but the global mean value is consistent with several new lines of evidence suggesting less negative estimates for the ERF due to aerosol–cloud interactions than in AR4. {7.4, 7.5.3, 7.5.4, Figure 7.19}

Persistent contrails from aviation contribute a RF of +0.01 (+0.005 to +0.03) W m^{-2} for year 2011, and the combined contrail and contrail-cirrus ERF from aviation is assessed to be +0.05 (+0.02 to +0.15) W m^{-2}. This forcing can be much larger regionally but there is now *medium confidence* that it does not produce observable regional effects on either the mean or diurnal range of surface temperature. {7.2.7}

Geoengineering Using Solar Radiation Management Methods

Theory, model studies and observations suggest that some Solar Radiation Management (SRM) methods, if practicable, could substantially offset a global temperature rise and partially offset some other impacts of global warming, but the compensation for the climate change caused by GHGs would be imprecise (*high confidence*). SRM methods are unimplemented and untested. Research on SRM is in its infancy, though it leverages understanding of how the climate responds to forcing more generally. The efficacy of a number of SRM strategies was assessed, and there is *medium confidence* that stratospheric aerosol SRM is scalable to counter the RF from increasing GHGs at least up to approximately 4 W m^{-2}; however,

---

[2] In this Report, the following terms have been used to indicate the assessed likelihood of an outcome or a result: Virtually certain 99–100% probability, Very likely 90–100%, Likely 66–100%, About as likely as not 33–66%, Unlikely 0–33%, Very unlikely 0–10%, Exceptionally unlikely 0–1%. Additional terms (Extremely likely: 95–100%, More likely than not >50–100%, and Extremely unlikely 0–5%) may also be used when appropriate. Assessed likelihood is typeset in italics, e.g., *very likely* (see Section 1.4 and Box TS.1 for more details).

[3] This and all subsequent ranges given with this format are 90% uncertainty ranges unless otherwise specified.

[4] All climate forcings (RFs and ERFs) are anthropogenic and relate to the period 1750–2010 unless otherwise specified.

[5] This species breakdown is less certain than the total RFari and does not sum to the total exactly.

the required injection rate of aerosol precursors remains very uncertain. There is no consensus on whether a similarly large RF could be achieved from cloud brightening SRM owing to uncertainties in understanding and representation of aerosol–cloud interactions. It does not appear that land albedo change SRM can produce a large RF. Limited literature on other SRM methods precludes their assessment. Models consistently suggest that SRM would generally reduce climate differences compared to a world with elevated GHG concentrations and no SRM; however, there would also be residual regional differences in climate (e.g., temperature and rainfall) when compared to a climate without elevated GHGs. {7.4.3, 7.7}

Numerous side effects, risks and shortcomings from SRM have been identified. Several lines of evidence indicate that SRM would produce a small but significant decrease in global precipitation (with larger differences on regional scales) if the global surface temperature were maintained. A number of side effects have been identified. One that is relatively well characterized is the likelihood of modest polar stratospheric ozone depletion associated with stratospheric aerosol SRM. There could also be other as yet unanticipated consequences. As long as GHG concentrations continued to increase, the SRM would require commensurate increase, exacerbating side effects. In addition, scaling SRM to substantial levels would carry the risk that if the SRM were terminated for any reason, there is *high confidence* that surface temperatures would increase rapidly (within a decade or two) to values consistent with the GHG forcing, which would stress systems sensitive to the rate of climate change. Finally, SRM would not compensate for ocean acidification from increasing CO_2. {7.6.3, 7.7, Figures 7.22 to 7.24}

7.1 Introduction

7.1.1 Clouds and Aerosols in the Atmosphere

The atmosphere is composed mostly of gases, but also contains liquid and solid matter in the form of particles. It is usual to distinguish these particles according to their size, chemical composition, water content and fall velocity into atmospheric aerosol particles, cloud particles and falling hydrometeors. Despite their small mass or volume fraction, particles in the atmosphere strongly influence the transfer of radiant energy and the spatial distribution of latent heating through the atmosphere, thereby influencing the weather and climate.

Cloud formation usually takes place in rising air, which expands and cools, thus permitting the activation of aerosol particles into cloud droplets and ice crystals in supersaturated air. Cloud particles are generally larger than aerosol particles and composed mostly of liquid water or ice. The evolution of a cloud is governed by the balance between a number of dynamical, radiative and microphysical processes. Cloud particles of sufficient size become falling hydrometeors, which are categorized as drizzle drops, raindrops, snow crystals, graupel and hailstones. Precipitation is an important and complex climate variable that is influenced by the distribution of moisture and cloudiness, and to a lesser extent by the concentrations and properties of aerosol particles.

Aerosol particles interact with solar radiation through absorption and scattering and, to a lesser extent with terrestrial radiation through absorption, scattering and emission. Aerosols[6] can serve as cloud condensation nuclei (CCN) and ice nuclei (IN) upon which cloud droplets and ice crystals form. They also play a wider role in atmospheric chemistry and biogeochemical cycles in the Earth system, for instance, by carrying nutrients to ocean ecosystems. They can be of natural or anthropogenic origin.

Cloud and aerosol amounts[7] and properties are extremely variable in space and time. The short lifetime of cloud particles in subsaturated air creates relatively sharp cloud edges and fine-scale variations in cloud properties, which is less typical of aerosol layers. While the distinction between aerosols and clouds is generally appropriate and useful, it is not always unambiguous, which can cause interpretational difficulties (e.g., Charlson et al., 2007; Koren et al., 2007).

7.1.2 Rationale for Assessing Clouds, Aerosols and Their Interactions

The representation of cloud processes in climate models has been recognized for decades as a dominant source of uncertainty in our understanding of changes in the climate system (e.g., Arakawa, 1975, 2004; Charney et al., 1979; Cess et al., 1989; Randall et al., 2003; Bony et al., 2006), but has never been systematically assessed by the IPCC before. Clouds respond to climate forcing mechanisms in multiple ways, and inter-model differences in cloud feedbacks constitute by far the primary source of spread of both equilibrium and transient climate responses simulated by climate models (Dufresne and Bony, 2008) despite the fact that most models agree that the feedback is positive (Randall et al., 2007; Section 7.2). Thus confidence in climate projections requires a thorough assessment of how cloud processes have been accounted for.

Aerosols of anthropogenic origin are responsible for a radiative forcing (RF) of climate change through their interaction with radiation, and also as a result of their interaction with clouds. Quantification of this forcing is fraught with uncertainties (Haywood and Boucher, 2000; Lohmann and Feichter, 2005) and aerosols dominate the uncertainty in the total anthropogenic RF (Forster et al., 2007; Haywood and Schulz, 2007; Chapter 8). Furthermore, our inability to better quantify non-greenhouse gas RFs, and primarily those that result from aerosol–cloud interactions, underlie difficulties in constraining climate sensitivity from observations even if we had a perfect knowledge of the temperature record (Andreae et al., 2005). Thus a complete understanding of past and future climate change requires a thorough assessment of aerosol–cloud–radiation interactions.

7.1.3 Forcing, Rapid Adjustments and Feedbacks

Figure 7.1 illustrates key aspects of how clouds and aerosols contribute to climate change, and provides an overview of important terminological distinctions. *Forcings* associated with agents such as greenhouse gases (GHGs) and aerosols act on global mean surface temperature through the global radiative (energy) budget. *Rapid adjustments* (sometimes called rapid responses) arise when forcing agents, by altering flows of energy internal to the system, affect cloud cover or other components of the climate system and thereby alter the global budget indirectly. Because these adjustments do not operate through changes in the global mean surface temperature (ΔT), which are slowed by the massive heat capacity of the oceans, they are generally rapid and most are thought to occur within a few weeks. *Feedbacks* are associated with changes in climate variables that are mediated by a change in global mean surface temperature; they contribute to amplify or damp global temperature changes via their impact on the radiative budget.

In this report, following an emerging consensus in the literature, the traditional concept of radiative forcing (RF, defined as the instantaneous radiative forcing with stratospheric adjustment only) is de-emphasized in favour of an absolute measure of the radiative effects of all responses triggered by the forcing agent that are independent of surface temperature change (see also Section 8.1). This new measure of the forcing includes rapid adjustments and the net forcing with these adjustments included is termed the *effective radiative forcing* (ERF). The climate sensitivity to ERF will differ somewhat from traditional equilibrium climate sensitivity, as the latter include adjustment effects. As shown in Figure 7.1, adjustments can occur through geographic temperature variations, lapse rate changes, cloud changes

[6] For convenience the term 'aerosol', which includes both the particles and the suspending gas, is often used in its plural form to mean 'aerosol particles' both in this chapter and the rest of this Report.

[7] In this chapter, we use 'cloud amount' as an inexact term to refer to the quantity of clouds, both in the horizontal and vertical directions. The term 'cloud cover' is used in its usual sense and refers to the horizontal cloud cover.

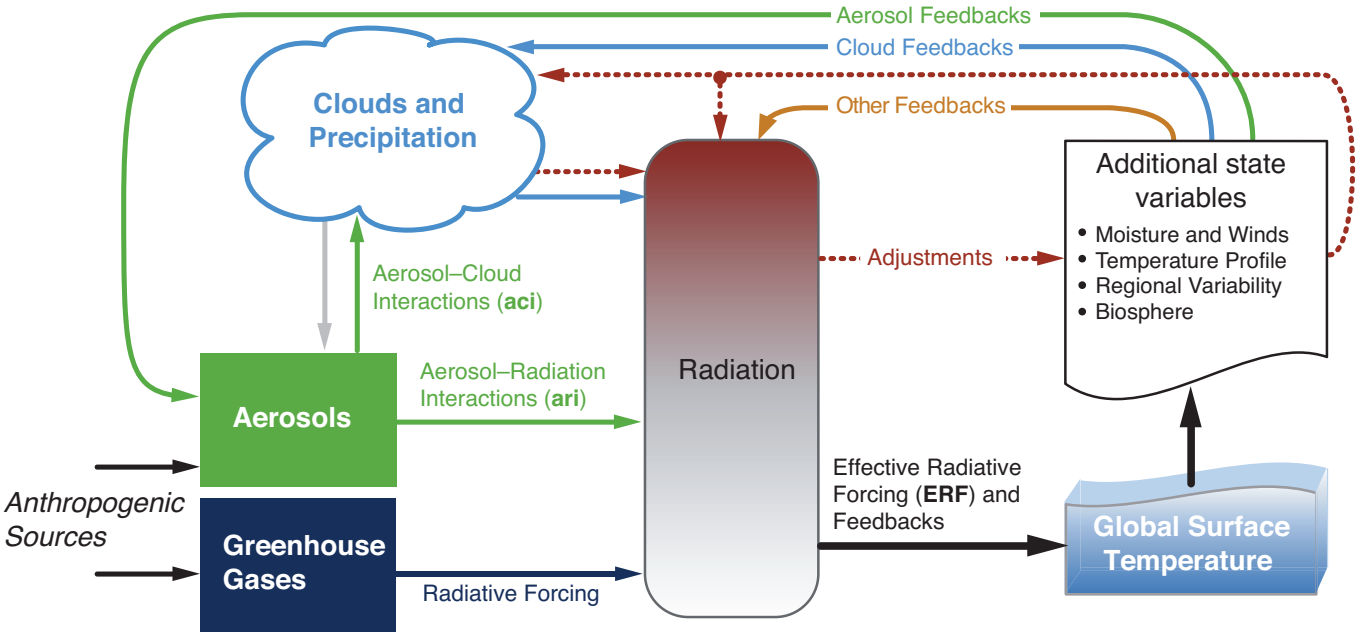

Figure 7.1 | Overview of forcing and feedback pathways involving greenhouse gases, aerosols and clouds. Forcing agents are in the green and dark blue boxes, with forcing mechanisms indicated by the straight green and dark blue arrows. The forcing is modified by rapid adjustments whose pathways are independent of changes in the globally averaged surface temperature and are denoted by brown dashed arrows. Feedback loops, which are ultimately rooted in changes ensuing from changes in the surface temperature, are represented by curving arrows (blue denotes cloud feedbacks; green denotes aerosol feedbacks; and orange denotes other feedback loops such as those involving the lapse rate, water vapour and surface albedo). The final temperature response depends on the effective radiative forcing (ERF) that is felt by the system, that is, after accounting for rapid adjustments, and the feedbacks.

and vegetation effects. Measures of ERF and rapid adjustments have existed in the literature for more than a decade, with a number of different terminologies and calculation methods adopted. These were principally aimed to help quantify the effects of aerosols on clouds (Rotstayn and Penner, 2001; Lohmann et al., 2010) and understand different forcing agent responses (Hansen et al., 2005), but it is now realized that there are rapid adjustments in response to the CO_2 forcing itself (Section 7.2.5.6).

In principle rapid adjustments are independent of ΔT, while feedbacks operate purely through ΔT. Thus, within this framework adjustments are not another type of 'feedback' but rather a non-feedback phenomenon, required in the analysis by the fact that a single scalar ΔT cannot fully characterize the system. This framework brings most efficacies close to unity although they are not necessarily exactly 1 (Hansen et al., 2005; Bond et al., 2013). There is also no clean separation in time scale between rapid adjustments and warming. Although the former occur mostly within a few days of applying a forcing (Dong et al., 2009), some adjustments such as those that occur within the stratosphere and snowpack can take several months or longer. Meanwhile the land surface warms quickly so that a small part of ΔT occurs within days to weeks of an applied forcing. This makes the two phenomena difficult to isolate in model runs. Other drawbacks are that adjustments are difficult to observe, and typically more model-dependent than RF. However, recent work is beginning to meet the challenges of quantifying the adjustments, and has noted advantages of the new framework (e.g., Vial et al., 2013; Zelinka et al., 2013).

There is no perfect method to determine ERF. Two common methods are to regress the net energy imbalance onto ΔT in a transient

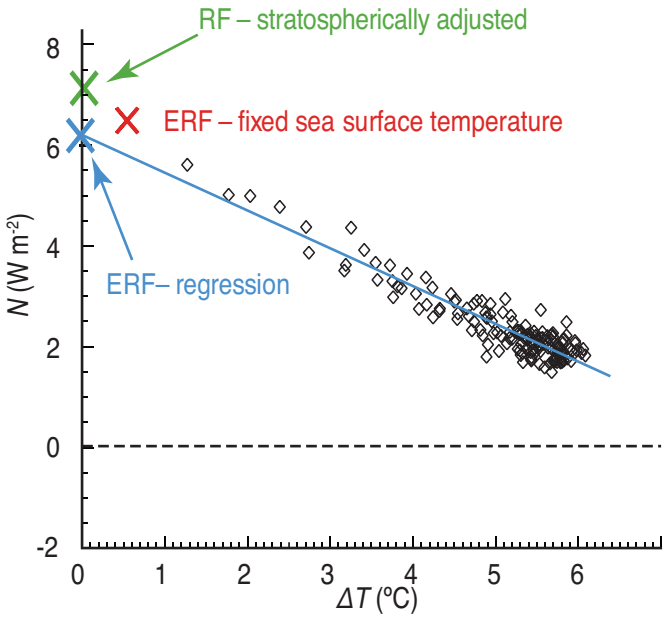

Figure 7.2 | Radiative forcing (RF) and effective radiative forcing (ERF) estimates derived by two methods, for the example of 4 × CO_2 experiments in one climate model. N is the net energy imbalance at the top of the atmosphere and ΔT the global mean surface temperature change. The fixed sea surface temperature ERF estimate is from an atmosphere–land model averaged over 30 years. The regression estimate is from 150 years of a coupled model simulation after an instantaneous quadrupling of CO_2, with the N from individual years in this regression shown as black diamonds. The stratospherically adjusted RF is the tropopause energy imbalance from otherwise identical radiation calculations at 1 × and 4 × CO_2 concentrations. (Figure follows Andrews et al., 2012.) See also Figure 8.1.

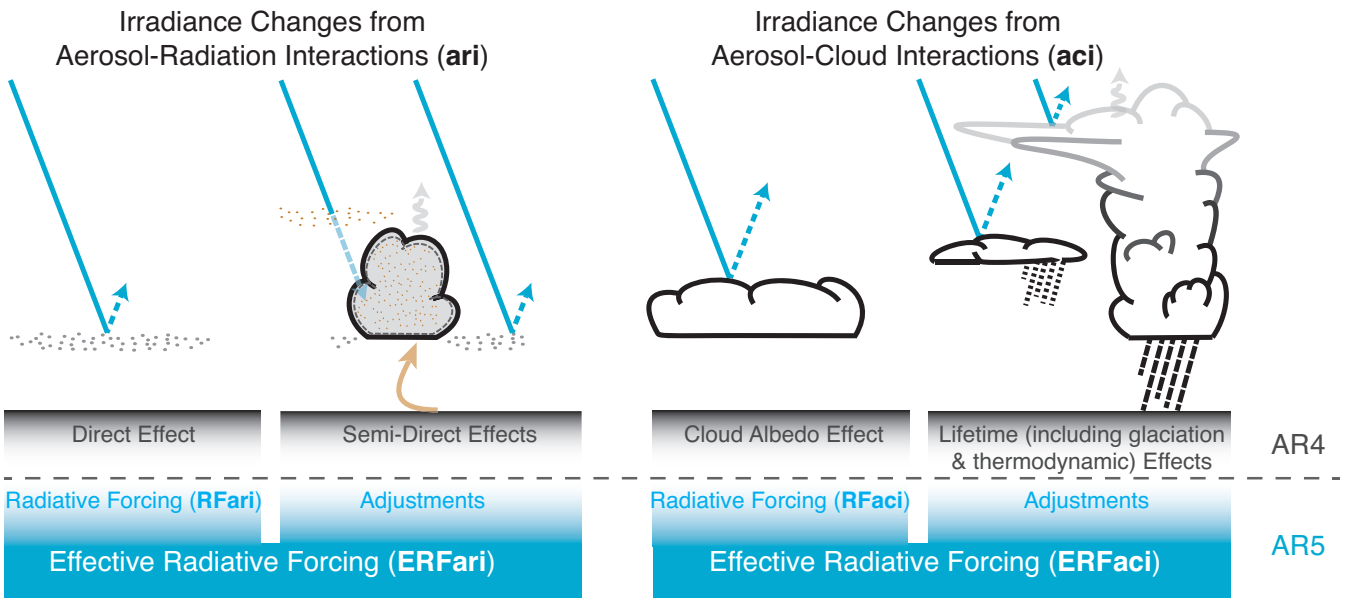

Figure 7.3 | Schematic of the new terminology used in this Assessment Report (AR5) for aerosol–radiation and aerosol–cloud interactions and how they relate to the terminology used in AR4. The blue arrows depict solar radiation, the grey arrows terrestrial radiation and the brown arrow symbolizes the importance of couplings between the surface and the cloud layer for rapid adjustments. See text for further details.

warming simulation (Gregory et al., 2004; Figure 7.2), or to simulate the climate response with sea surface temperatures (SSTs) held fixed (Hansen et al., 2005). The former can be complicated by natural variability or time-varying feedbacks, while the non-zero ΔT from land warming complicates the latter. Both methods are used in this chapter.

Figure 7.3 links the former terminology of aerosol direct, semi-direct and indirect effects with the new terminology used in this chapter and in Chapter 8. The RF from aerosol–radiation interactions (abbreviated RFari) encompasses radiative effects from anthropogenic aerosols before any adjustment takes place and corresponds to what is usually referred to as the aerosol direct effect. Rapid adjustments induced by aerosol radiative effects on the surface energy budget, the atmospheric profile and cloudiness contribute to the ERF from aerosol–radiation interactions (abbreviated ERFari). They include what has earlier been referred to as the semi-direct effect. The RF from aerosol–cloud interactions (abbreviated RFaci) refers to the instantaneous effect on cloud albedo due to changing concentrations of cloud condensation and ice nuclei, also known as the Twomey effect. All subsequent changes to the cloud lifetime and thermodynamics are rapid adjustments, which contribute to the ERF from aerosol–cloud interactions (abbreviated ERFaci). RFaci is a theoretical construct that is not easy to separate from other aerosol–cloud interactions and is therefore not quantified in this chapter.

7.1.4 Chapter Roadmap

For the first time in the IPCC WGI assessment reports, clouds and aerosols are discussed together in a single chapter. Doing so allows us to assess, and place in context, recent developments in a large and growing area of climate change research. In addition to assessing cloud feedbacks and aerosol forcings, which were covered in previous assessment reports in a less unified manner, it becomes possible to assess understanding of the multiple interactions among aerosols, clouds and precipitation and their relevance for climate and climate change. This chapter assesses the climatic roles and feedbacks of water vapour, lapse rate and clouds (Section 7.2), discusses aerosol–radiation (Section 7.3) and aerosol–cloud (Section 7.4) interactions and quantifies the resulting aerosol RF on climate (Section 7.5). It also introduces the physical basis for the precipitation responses to aerosols and climate changes (Section 7.6) noted later in the Report, and assesses geoengineering methods based on solar radiation management (Section 7.7).

7.2 Clouds

This section summarizes our understanding of clouds in the current climate from observations and process models; advances in the representation of cloud processes in climate models since AR4; assessment of cloud, water vapour and lapse rate feedbacks and adjustments; and the RF due to clouds induced by moisture released by two anthropogenic processes (air traffic and irrigation). Aerosol–cloud interactions are assessed in Section 7.4. The fidelity of climate model simulations of clouds in the current climate is assessed in Chapter 9.

7.2.1 Clouds in the Present-Day Climate System

7.2.1.1 Cloud Formation, Cloud Types and Cloud Climatology

To form a cloud, air must cool or moisten until it is sufficiently supersaturated to activate some of the available condensation or freezing nuclei. Clouds may be composed of liquid water (possibly supercooled), ice or both (mixed phase). The nucleated cloud particles are initially very small, but grow by vapour deposition. Other microphysical mechanisms dependent on the cloud phase (e.g., droplet collision and coalescence for liquid clouds, riming and Wegener–Bergeron–Findeisen processes for mixed-phase clouds and crystal aggregation in ice clouds)

can produce a broader spectrum of particle sizes and types; turbulent mixing produces further variations in cloud properties on scales from kilometres to less than a centimetre (Davis et al., 1999; Bodenschatz et al., 2010). If and when some of the droplets or ice particles become large enough, these will fall out of the cloud as precipitation.

Atmospheric flows often organize convection and associated clouds into coherent systems having scales from tens to thousands of kilometres, such as cyclones or frontal systems. These represent a significant modelling and theoretical challenge, as they are usually too large to represent within the limited domains of cloud-resolving models (Section 7.2.2.1), but are also not well resolved nor parameterized by most climate models; this gap, however, is beginning to close (Section 7.2.2.2). Finally, clouds and cloud systems are organized by larger-scale circulations into different regimes such as deep convection near the equator, subtropical marine stratocumulus, or mid-latitude storm tracks guided by the tropospheric westerly jets. Figure 7.4 shows a selection of widely occurring cloud regimes schematically and as they might appear in a typical geostationary satellite image.

New satellite sensors and new analysis of previous data sets have given us a clearer picture of the Earth's clouds since AR4. A notable example is the launch in 2006 of two coordinated, active sensors, the Cloud Profiling Radar (CPR) on the CloudSat satellite (Stephens et al., 2002) and the Cloud–Aerosol Lidar with Orthogonal Polarization (CALIOP) on board the Cloud–Aerosol Lidar and Infrared Pathfinder Satellite Observations (CALIPSO) satellite (Winker et al., 2009). These sensors have significantly improved our ability to quantify vertical profiles of cloud occurrence and water content (see Figures 7.5 and 7.6), and complement the detection capabilities of passive multispectral sensors (e.g., Stubenrauch et al., 2010; Chan and Comiso, 2011). Satellite cloud-observing capacities are reviewed by Stubenrauch et al. (2013).

Clouds cover roughly two thirds of the globe (Figure 7.5a, c), with a more precise value depending on both the optical depth threshold used to define cloud and the spatial scale of measurement (Wielicki and Parker, 1992; Stubenrauch et al., 2013). The mid-latitude oceanic storm tracks and tropical precipitation belts are particularly cloudy, while continental desert regions and the central subtropical oceans are relatively cloud-free. Clouds are composed of liquid at temperatures above 0°C, ice below about –38°C (e.g., Koop et al., 2000), and either or both phases at intermediate temperatures (Figure 7.5b). Throughout most of the troposphere, temperatures at any given altitude are usually warmer in the tropics, but clouds also extend higher there such that ice

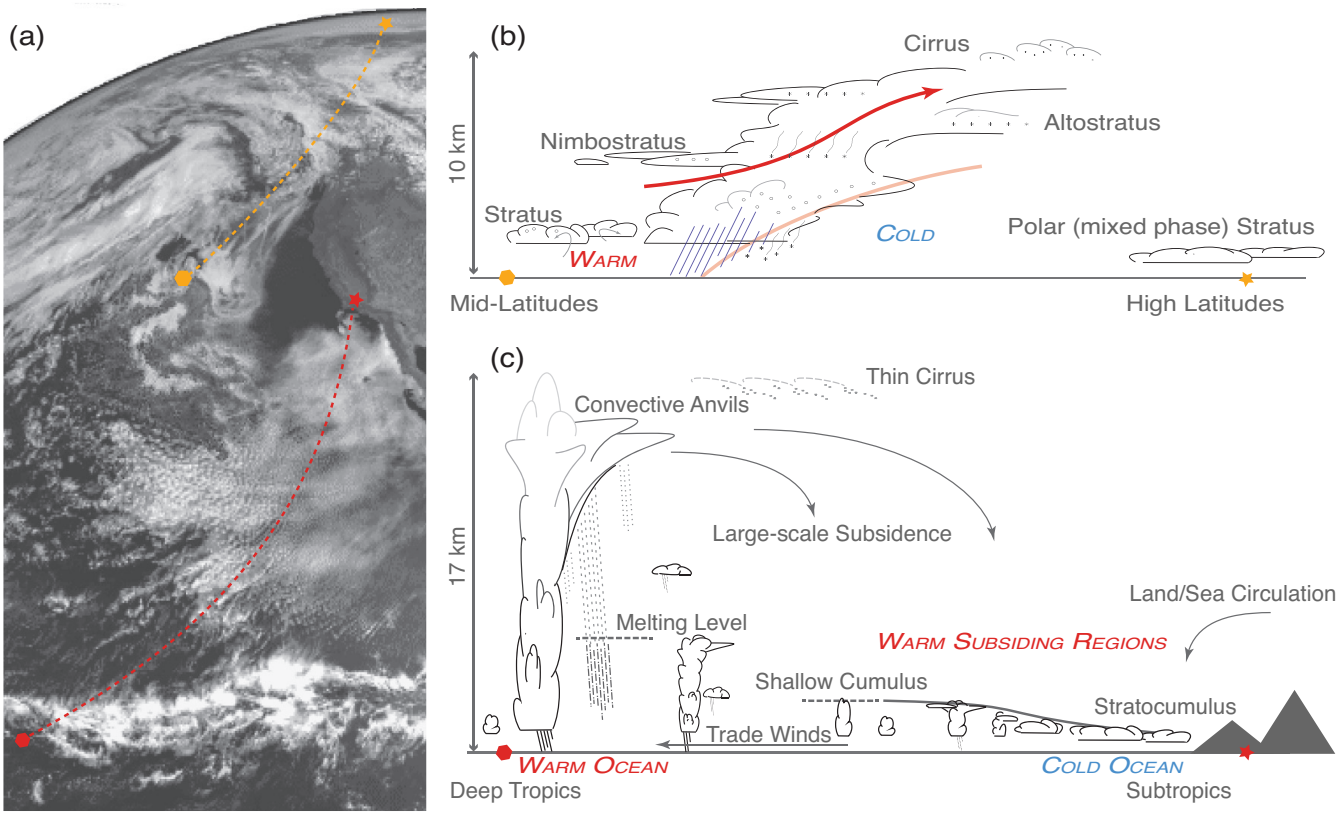

Figure 7.4 | Diverse cloud regimes reflect diverse meteorology. (a) A visible-wavelength geostationary satellite image shows (from top to bottom) expanses and long arcs of cloud associated with extratropical cyclones, subtropical coastal stratocumulus near Baja California breaking up into shallow cumulus clouds in the central Pacific and mesoscale convective systems outlining the Pacific Intertropical Convergence Zone (ITCZ). (b) A schematic section along the dashed line from the orange star to the orange circle in (a), through a typical warm front of an extratropical cyclone. It shows (from right to left) multiple layers of upper-tropospheric ice (cirrus) and mid-tropospheric water (altostratus) cloud in the upper-tropospheric outflow from the frontal zone, an extensive region of nimbostratus associated with frontal uplift and turbulence-driven boundary layer cloud in the warm sector. (c) A schematic section along the dashed line from the red star to the red circle in (a), along the low-level trade wind flow from a subtropical west coast of a continent to the ITCZ. It shows (from right to left) typical low-latitude cloud mixtures, shallow stratocumulus trapped under a strong subsidence inversion above the cool waters of the oceanic upwelling zone near the coast and shallow cumulus over warmer waters further offshore transitioning to precipitating cumulonimbus cloud systems with extensive cirrus anvils associated with rising air motions in the ITCZ.

cloud amounts are no less than those at high latitudes. At any given time, most clouds are not precipitating (Figure 7.5d).

In this chapter cloud above the 440 hPa pressure level is considered 'high', that below the 680 hPa level 'low', and that in-between is considered 'mid-level'. Most high cloud (mainly cirrus and deep cumulus outflows) occurs near the equator and over tropical continents, but can also be seen in the mid-latitude storm track regions and over mid-latitude continents in summer (Figure 7.6a, e); it is produced by the storms generating most of the global rainfall in regions where tropospheric air motion is upward, such that dynamical, rainfall and high-cloud fields closely resemble one another (Figure 7.6d, h). Mid-level cloud (Figure 7.6b, f), comprising a variety of types, is prominent in the storm tracks and some occurs in the Intertropical Convergence Zone (ITCZ). Low cloud (Figure 7.6c, g), including shallow cumulus and stratiform cloud, occurs over essentially all oceans but is most prevalent over cooler subtropical oceans and in polar regions. It is less common over land, except at night and in winter.

Overlap between cloud layers has long been an issue both for satellite (or ground-based) detection and for calculating cloud radiative effects. Active sensors show more clearly that low clouds are prevalent in nearly all types of convective systems, and are often underestimated by models (Chepfer et al., 2008; Naud et al., 2010; Haynes et al., 2011). Cloud layers at different levels overlap less often than typically assumed in General Circulation Models (GCMs), especially over high-latitude continents and subtropical oceans (Naud et al., 2008; Mace et al., 2009), and the common assumption that the radiative effects of precipitating ice can be neglected is not necessarily warranted (Waliser et al., 2011). New observations have led to revised treatments of overlap in some models, which significantly affects cloud radiative effects (Pincus et al., 2006; Shonk et al., 2012). Active sensors have also been useful in detecting low-lying Arctic clouds over sea ice (Kay et al., 2008), improving our ability to test climate model simulations of the interaction between sea ice loss and cloud cover (Kay et al., 2011).

7.2.1.2 Effects of Clouds on the Earth's Radiation Budget

The effect of clouds on the Earth's present-day top of the atmosphere (TOA) radiation budget, or cloud radiative effect (CRE), can be inferred from satellite data by comparing upwelling radiation in cloudy and non-cloudy conditions (Ramanathan et al., 1989). By enhancing the planetary albedo, cloudy conditions exert a global and annual shortwave cloud radiative effect (SWCRE) of approximately –50 W m^{-2} and, by contributing to the greenhouse effect, exert a mean longwave effect (LWCRE) of approximately +30 W m^{-2}, with a range of 10% or less between published satellite estimates (Loeb et al., 2009). Some of the apparent LWCRE comes from the enhanced water vapour coinciding with the natural cloud fluctuations used to measure the effect, so the true cloud LWCRE is about 10% smaller (Sohn et al., 2010). The net global mean CRE of approximately –20 W m^{-2} implies a net cooling

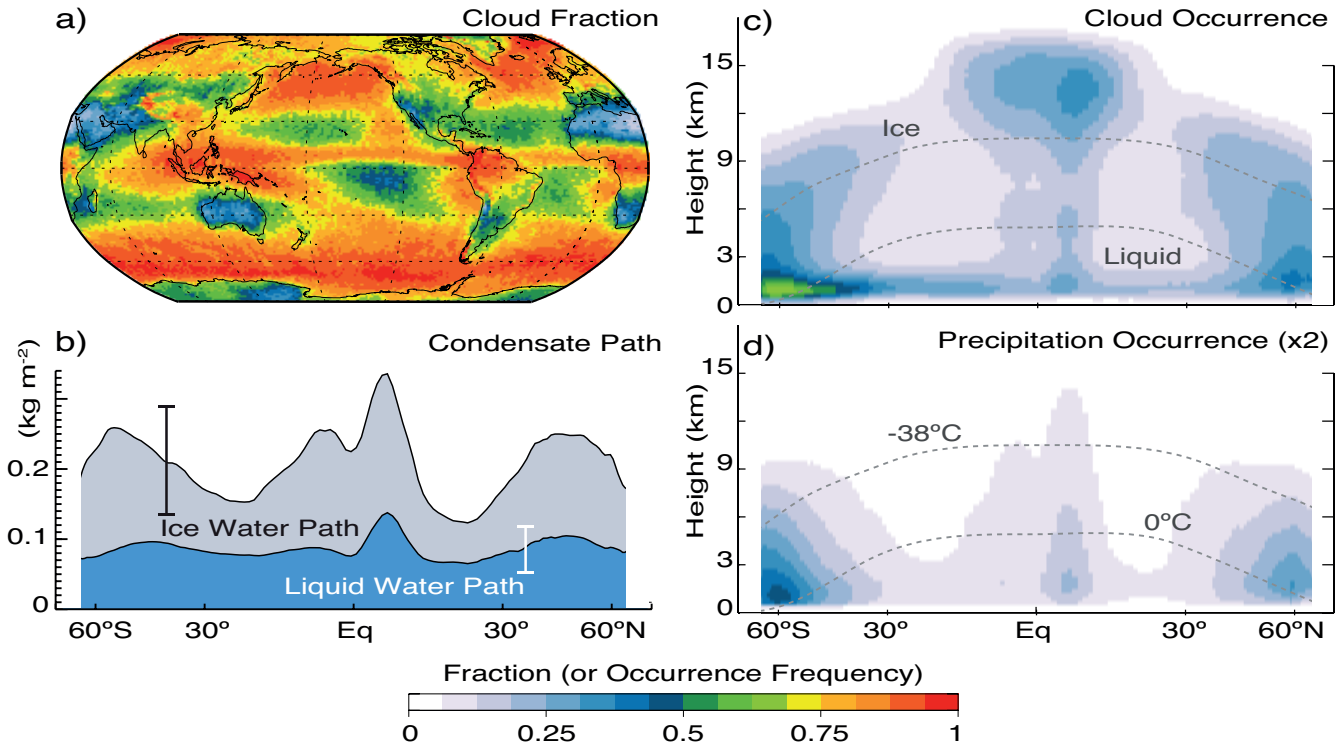

Figure 7.5 | (a) Annual mean cloud fractional occurrence (CloudSat/CALIPSO 2B-GEOPROF-LIDAR data set for 2006–2011; Mace et al., 2009). (b) Annual zonal mean liquid water path (blue shading, microwave radiometer data set for 1988–2005 from O'Dell et al. (2008)) and total water path (ice path shown with grey shading, from CloudSat 2C-ICE data set for 2006–2011 from Deng et al. (2010) over oceans). The 90% uncertainty ranges, assessed to be approximately 60 to 140% of the mean for the liquid and total water paths, are schematically indicated by the error bars. (c–d) latitude-height sections of annual zonal mean cloud (including precipitation falling from cloud) occurrence and precipitation (attenuation-corrected radar reflectivity >0 dBZ) occurrence; the latter has been doubled to make use of a common colour scale (2B-GEOPROF-LIDAR data set). The dashed curves show the annual mean 0°C and –38°C isotherms.

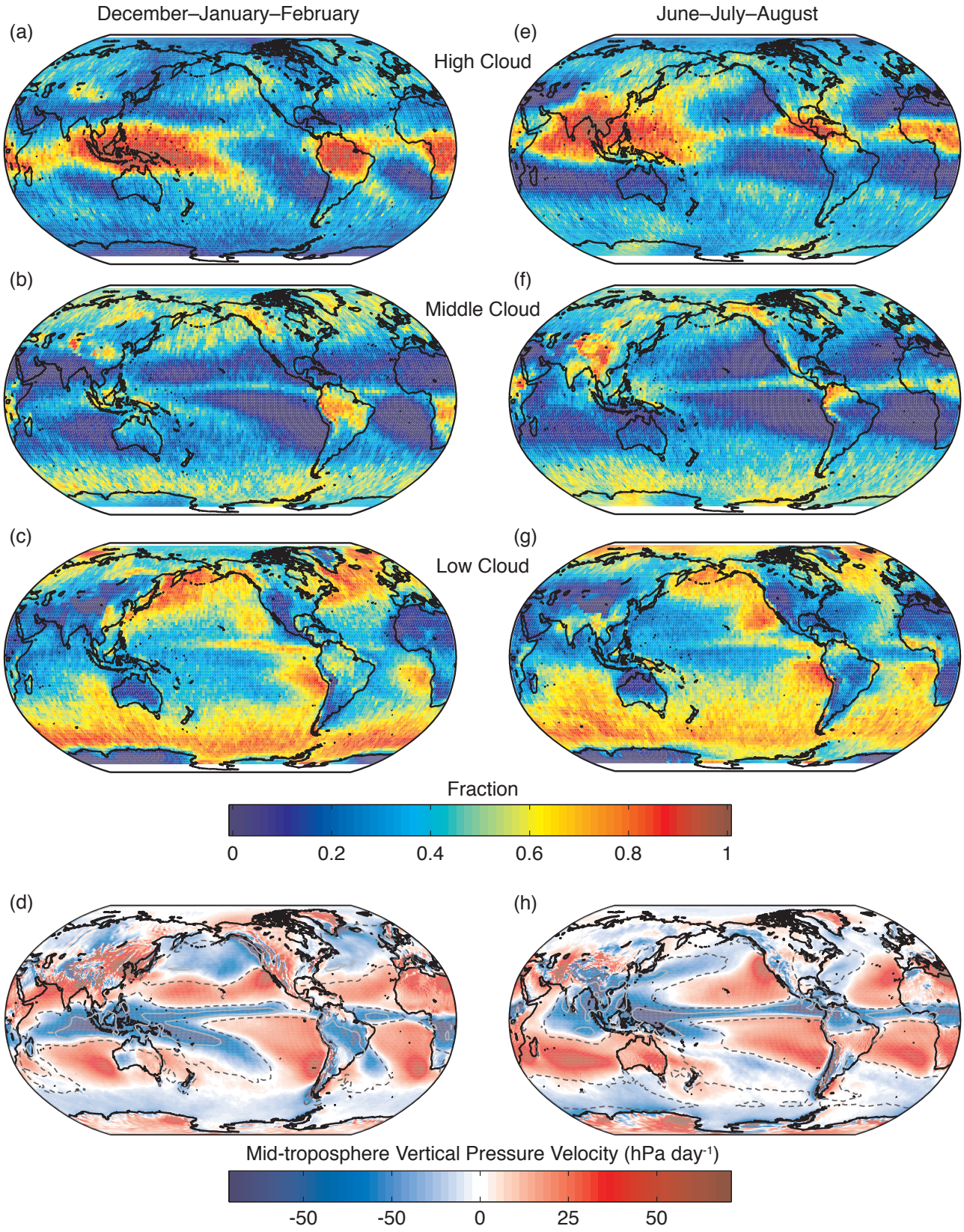

Figure 7.6 | (a–d) December–January–February mean high, middle and low cloud cover from CloudSat/CALIPSO 2B-GEOPROF R04 and 2B-GEOPROF-LIDAR P1.R04 data sets for 2006–2011 (Mace et al., 2009), 500 hPa vertical pressure velocity (colours, from ERA-Interim for 1979–2010; Dee et al., 2011), and Global Precipitation Climatology Project (GPCP) version 2.2 precipitation rate (1981–2010, grey contours at 3 mm day^{-1} in dash and 7 mm day^{-1} in solid); (e–h) same as (a–d), except for June–July–August. For low clouds, the GCM-Oriented CALIPSO Cloud Product (GOCCP) data set for 2007–2010 (Chepfer et al., 2010) is used at locations where it indicates a larger fractional cloud cover, because the GEOPROF data set removes some clouds with tops at altitudes below 750 m. Low cloud amounts are probably underrepresented in regions of high cloud (Chepfer et al., 2008), although not as severely as with earlier satellite instruments.

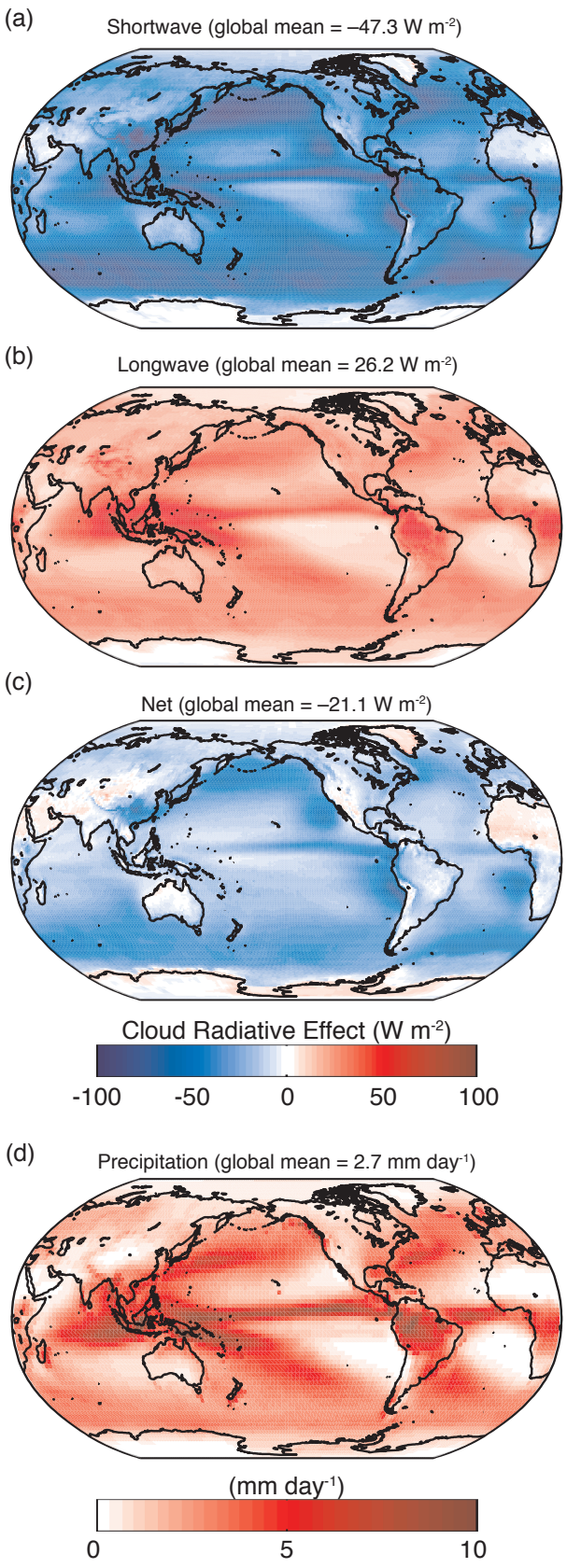

Figure 7.7 | Distribution of annual-mean top of the atmosphere (a) shortwave, (b) longwave, (c) net cloud radiative effects averaged over the period 2001–2011 from the Clouds and the Earth's Radiant Energy System (CERES) Energy Balanced and Filled (EBAF) Ed2.6r data set (Loeb et al., 2009) and (d) precipitation rate (1981–2000 average from the GPCP version 2.2 data set; Adler et al., 2003).

effect of clouds on the current climate. Owing to the large magnitudes of the SWCRE and LWCRE, clouds have the potential to cause significant climate feedback (Section 7.2.5). The sign of this feedback on climate change cannot be determined from the sign of CRE in the current climate, but depends instead on how climate-sensitive the properties are that govern the LWCRE and SWCRE.

The regional patterns of annual-mean TOA CRE (Figure 7.7a, b) reflect those of the altitude-dependent cloud distributions. High clouds, which are cold compared to the clear-sky radiating temperature, dominate patterns of LWCRE, while the SWCRE is sensitive to optically thick clouds at all altitudes. SWCRE also depends on the available sunlight, so for example is sensitive to the diurnal and seasonal cycles of cloudiness. Regions of deep, thick cloud with large positive LWCRE and large negative SWCRE tend to accompany precipitation (Figure 7.7d), showing their intimate connection with the hydrological cycle. The net CRE is negative over most of the globe and most negative in regions of very extensive low-lying reflective stratus and stratocumulus cloud such as the mid-latitude and eastern subtropical oceans, where SWCRE is strong but LWCRE is weak (Figure 7.7c). In these regions, the spatial distribution of net CRE on seasonal time scales correlates strongly with measures of low-level stability or inversion strength (Klein and Hartmann, 1993; Williams et al., 2006; Wood and Bretherton, 2006; Zhang et al., 2010).

Clouds also exert a CRE at the surface and within the troposphere, thus affecting the hydrological cycle and circulation (Section 7.6), though this aspect of CRE has received less attention. The net downward flux of radiation at the surface is sensitive to the vertical and horizontal distribution of clouds. It has been estimated more accurately through radiation budget measurements and cloud profiling (Kato et al., 2011). Based on these observations, the global mean surface downward longwave flux is about 10 W m^{-2} larger than the average in climate models, probably due to insufficient model-simulated cloud cover or lower tropospheric moisture (Stephens et al., 2012). This is consistent with a global mean precipitation rate in the real world somewhat larger than current observational estimates.

7.2.2 Cloud Process Modelling

Cloud formation processes span scales from the sub-micrometre scale of CCN, to cloud-system scales of up to thousands of kilometres. This range of scales is impossible to resolve with numerical simulations on computers, and this is not expected to change in the foreseeable future. Nonetheless progress has been made through a variety of modelling strategies, which are outlined briefly in this section, followed by a discussion in Section 7.2.3 of developments in representing clouds in global models. The implications of these discussions are synthesized in Section 7.2.3.5.

7.2.2.1 Explicit Simulations in Small Domains

High-resolution models in small domains have been widely used to simulate interactions of turbulence with various types of clouds. The grid spacing is chosen to be small enough to resolve explicitly the dominant turbulent eddies that drive cloud heterogeneity, with the effects of smaller-scale phenomena parameterized. Such models can be run in

idealized settings, or with boundary conditions for specific observed cases. This strategy is typically called large-eddy simulation (LES) when boundary-layer eddies are resolved, and cloud-resolving model (CRM) when only deep cumulus motions are well resolved. It is useful not only in simulating cloud and precipitation characteristics, but also in understanding how turbulent circulations within clouds transport and process aerosols and chemical constituents. It can be applied to any type of cloud system, on any part of the Earth. Direct numerical simulation (DNS) can be used to study turbulence and cloud microphysics on scales of a few metres or less (e.g., Andrejczuk et al., 2006) but cannot span crucial meteorological scales and is not further considered here.

Cloud microphysics, precipitation and aerosol interactions are treated with varying levels of sophistication, and remain a weak point in all models regardless of resolution. For example, recent comparisons to satellite data show that liquid water clouds in CRMs generally begin to rain too early in the day (Suzuki et al., 2011). Especially for ice clouds, and for interactions between aerosols and clouds, our understanding of the basic micro-scale physics is not yet adequate, although it is improving. Moreover, microphysical effects are quite sensitive to co-variations of velocity and composition down to very small scales. High-resolution models, such as those used for LES, explicitly calculate most of these variations, and so provide much more of the information needed for microphysical calculations, whereas in a GCM they are not explicitly available. For these reasons, low-resolution (e.g., climate) models will have even more trouble representing local aerosol–cloud interactions than will high-resolution models. Parameterizations are under development that could account for the small-scale variations statistically (e.g., Larson and Golaz, 2005) but have not been used in the Coupled Model Intercomparison Project Phase 5 (CMIP5) simulations.

High-resolution models have enhanced our understanding of cloud processes in several ways. First, they can help interpret *in situ* and high-resolution remote sensing observations (e.g., Stevens et al., 2005b; Blossey et al., 2007; Fridlind et al., 2007). Second, they have revealed important influences of small-scale interactions, turbulence, entrainment and precipitation on cloud dynamics that must eventually be accounted for in parameterizations (e.g., Krueger et al., 1995; Derbyshire et al., 2004; Kuang and Bretherton, 2006; Ackerman et al., 2009). Third, they can be used to predict how cloud system properties (such as cloud cover, depth, or radiative effect) may respond to climate changes (e.g., Tompkins and Craig, 1998; Bretherton et al., 2013). Fourth, they have become an important tool in testing and improving parameterizations of cloud-controlling processes such as cumulus convection, turbulent mixing, small-scale horizontal cloud variability and aerosol–cloud interactions (Randall et al., 2003; Rio and Hourdin, 2008; Stevens and Seifert, 2008; Lock, 2009; Del Genio and Wu, 2010; Fletcher and Bretherton, 2010), as well as the interplay between convection and large-scale circulations (Kuang, 2008).

Different aspects of clouds, and cloud types, require different grid resolutions. CRMs of deep convective cloud systems with horizontal resolutions of 2 km or finer (Bryan et al., 2003) can represent some statistical properties of the cloud system, including fractional area coverage of cloud (Xu et al., 2002), vertical thermodynamic structure (Blossey et al., 2007), the distribution of updraughts and downdraughts (Khairoutdinov et al., 2009) and organization into mesoscale convective systems (Grabowski et al., 1998). Modern high-order turbulence closure schemes may allow some statistics of boundary-layer cloud distributions, including cloud fractions and fluxes of moisture and energy, to be reasonably simulated even at horizontal resolution of 1 km or larger (Cheng and Xu, 2006, 2008). Finer grids (down to hundreds of metres) better resolve individual storm characteristics such as vertical velocity or tracer transport. Some cloud ensemble properties remain sensitive to CRM microphysical parameterization assumptions regardless of resolution, particularly the vertical distribution and optical depth of clouds containing ice.

Because of these requirements, it is computationally demanding to run a CRM in a domain large enough to capture convective organisation or perform regional forecasts. Some studies have created smaller regions of CRM-like resolution within realistically forced regional-scale models (e.g., Zhu et al., 2010; Boutle and Abel, 2012; Zhu et al., 2012), a special case of the common 'nesting' approach for regional downscaling (see Section 9.6). One application has been to orographic precipitation, associated both with extratropical cyclones (e.g., Garvert et al., 2005) and with explicitly simulated cumulus convection (e.g., Hohenegger et al., 2008); better resolution of the orography improves the simulation of precipitation initiation and wind drift of falling rain and snow between watersheds.

LES of shallow cumulus cloud fields with horizontal grid spacing of about 100 m and vertical grid spacing of about 40 m produces vertical profiles of cloud fraction, temperature, moisture and turbulent fluxes that agree well with available observations (Siebesma et al., 2003), though the simulated precipitation efficiency still shows some sensitivity to microphysical parameterizations (vanZanten et al., 2011). LES of stratocumulus-topped boundary layers reproduces the turbulence statistics and vertical thermodynamic structure well (e.g., Stevens et al., 2005b; Ackerman et al., 2009), and has been used to study the sensitivity of stratocumulus properties to aerosols (e.g., Savic-Jovcic and Stevens, 2008; Xue et al., 2008) and meteorological conditions. However, the simulated entrainment rate and cloud liquid water path are sensitive to the underlying numerical algorithms, even with vertical grid spacings as small as 5 m, due to poor resolution of the sharp capping inversion (Stevens et al., 2005a).

These grid requirements mean that low-cloud processes dominating the known uncertainty in cloud feedback cannot be explicitly simulated except in very small domains. Thus, notwithstanding all of the above benefits of explicit cloud modeling, these models cannot on their own quantify global cloud feedbacks or aerosol–cloud interactions definitively. They are important, however, in suggesting and testing feedback and adjustment mechanisms (see Sections 7.2.5 and 7.4).

7.2.2.2 Global Models with Explicit Clouds

Since AR4, increasing computer power has led to three types of developments in global atmospheric models. First, models have been run with resolution that is higher than in the past, but not sufficiently high that cumulus clouds can be resolved explicitly. Second, models have been run with resolution high enough to resolve (or 'permit') large individual cumulus clouds over the entire globe. In a third approach, the parameterizations of global models have been replaced by

embedded CRMs. The first approach is assessed in Chapter 9. The other two approaches are discussed below.

Global Cloud-Resolving Models (GCRMs) have been run with grid spacings as small as 3.5 km (Tomita et al., 2005; Putman and Suarez, 2011). At present GCRMs can be used only for relatively short simulations of a few simulated months to a year or two on the fastest supercomputers, but in the not-too distant future they may provide climate projections. GCRMs provide a consistent way to couple convective circulations to large-scale dynamics, but must still parameterize the effects of individual clouds, microphysics and boundary-layer circulations.

Because they avoid the use of uncertain cumulus parameterizations, GCRMs better simulate many properties of convective circulations that are very challenging for many current conventional GCMs, including the diurnal cycles of precipitation (Sato et al., 2009) and the Asian summer monsoon (Oouchi et al., 2009). Inoue et al. (2010) showed that the cloudiness simulated by a GCRM is in good agreement with observations from CloudSat and CALIPSO, but the results are sensitive to the parameterizations of turbulence and cloud microphysics (Satoh et al., 2010; Iga et al., 2011; Kodama et al., 2012).

Heterogeneous multiscale methods, in which CRMs are embedded in each grid cell of a larger scale model (Grabowski and Smolarkiewicz, 1999), have also been further developed as a way to realize some of the advantages of GCRMs but at less cost. This approach has come to be known as super-parameterization, because the CRM effectively replaces some of the existing GCM parameterizations (e.g., Khairoutdinov and Randall, 2001; Tao et al., 2009). Super-parameterized models, which are sometimes called multiscale modeling frameworks, occupy a middle ground between high-resolution 'process models' and 'climate models' (see Figure 7.8), in terms of both advantages and cost.

Like GCRMs, super-parameterized models give more realistic simulations of the diurnal cycle of precipitation (Khairoutdinov et al., 2005; Pritchard and Somerville, 2010) and the Madden-Julian Oscillation (Benedict and Randall, 2009) than most conventional GCMs; they can also improve aspects of the Asian monsoon and the El Niño–Southern Oscillation (ENSO; Stan et al., 2010; DeMott et al., 2011). Moreover, because they also begin to resolve cloud-scale circulations, both strategies provide a framework for studying aerosol–cloud interactions that conventional GCMs lack (Wang et al., 2011b). Thus both types of global model provide important insights, but because neither of them fully resolves cloud processes, especially for low clouds (see Section 7.2.2.1), their results must be treated with caution just as with conventional GCMs.

7.2.3 Parameterization of Clouds in Climate Models

7.2.3.1 Challenges of Parameterization

The representation of cloud microphysical processes in climate models is particularly challenging, in part because some of the fundamental details of these microphysical processes are poorly understood (particularly for ice- and mixed-phase clouds), and because spatial heterogeneity of key atmospheric properties occurs at scales significantly smaller than a GCM grid box. Such representation, however,

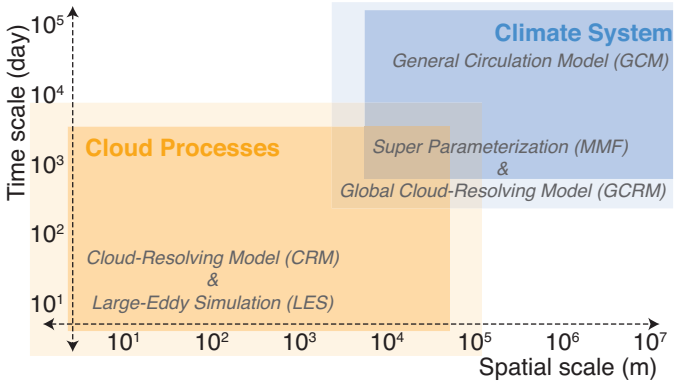

Figure 7.8 | Model and simulation strategy for representing the climate system and climate processes at different space and time scales. Also shown are the ranges of space and time scales usually associated with cloud processes (orange, lower left) and the climate system (blue, upper right). Classes of models are usually defined based on the range of spatial scales they represent, which in the figure is roughly spanned by the text for each model class. The temporal scales simulated by a particular type of model vary more widely. For instance, climate models are often run for a few time steps for diagnostic studies, or can simulate millennia. Hence the figure indicates the typical time scales for which a given model is used. Computational power prevents one model from covering all time and space scales. Since the AR4, the development of Global Cloud Resolving Models (GCRMs), and hybrid approaches such as General Circulation Models (GCMs) using the 'super-parameterization' approach (sometimes called the Multiscale Modelling Framework (MMF)), have helped fill the gap between climate system and cloud process models.

affects many aspects of a model's overall simulated climate including the Hadley circulation, precipitation patterns, and tropical variability. Therefore continuing weakness in these parameterizations affects not only modeled climate sensitivity, but also the fidelity with which these other variables can be simulated or projected.

Most CMIP5 climate model simulations use horizontal resolutions of 100 to 200 km in the atmosphere, with vertical layers varying between 100 m near the surface to more than 1000 m aloft. Within regions of this size in the real world, there is usually enormous small-scale variability in cloud properties, associated with variability in humidity, temperature and vertical motion (Figure 7.16). This variability must be accounted for to accurately simulate cloud–radiation interaction, condensation, evaporation and precipitation and other cloud processes that crucially depend on how cloud condensate is distributed across each grid box (Cahalan et al., 1994; Pincus and Klein, 2000; Larson et al., 2001; Barker et al., 2003).

The simulation of clouds in modern climate models involves several parameterizations that must work in unison. These include parameterization of turbulence, cumulus convection, microphysical processes, radiative transfer and the resulting cloud amount (including the vertical overlap between different grid levels), as well as sub-grid scale transport of aerosol and chemical species. The system of parameterizations must balance simplicity, realism, computational stability and efficiency. Many cloud processes are unrealistic in current GCMs, and as such their cloud response to climate change remains uncertain.

Cloud processes and/or turbulence parameterization are important not only for the GCMs used in climate projections but also for specialized chemistry–aerosol–climate models (see review by Zhang, 2008),

for regional climate models, and indeed for the cloud process models described in Section 7.2.2 which must still parameterize small-scale and microphysical effects. The nature of the parameterization problem, however, shifts as model scale decreases. Section 7.2.3.2 briefly assesses recent developments relevant to GCMs.

7.2.3.2 Recent Advances in Representing Cloud Microphysical Processes

7.2.3.2.1 Liquid clouds

Recent development efforts have been focused on the introduction of more complex representations of microphysical processes, with the dual goals of coupling them better to atmospheric aerosols and linking them more consistently to the sub-grid variability assumed by the model for other calculations. For example, most CMIP3 climate models predicted the average cloud and rain water mass in each grid cell only at a given time, diagnosing the droplet concentration using empirical relationships based on aerosol mass (e.g., Boucher and Lohmann, 1995; Menon et al., 2002), or altitude and proximity to land. Many were forced to employ an arbitrary lower bound on droplet concentration to reduce the aerosol RF (Hoose et al., 2009). Such formulations oversimplify microphysically mediated cloud variations.

By contrast, more models participating in CMIP5 predict both mass and number mixing ratios for liquid stratiform cloud. Some determine rain and snow number concentrations and mixing ratios (e.g., Morrison and Gettelman, 2008; Salzmann et al., 2010), allowing treatment of aerosol scavenging and the radiative effect of snow. Some models explicitly treat sub-grid cloud water variability for calculating microphysical process rates (e.g., Morrison and Gettelman, 2008). Cloud droplet activation schemes now account more realistically for particle composition, mixing and size (Abdul-Razzak and Ghan, 2000; Ghan et al., 2011; Liu et al., 2012). Despite such advances in internal consistency, a continuing weakness in GCMs (and to a much lesser extent GCRMs and super-parameterized models) is their inability to fully represent turbulent motions to which microphysical processes are highly sensitive.

7.2.3.2.2 Mixed-phase and ice clouds

Ice treatments are following a path similar to those for liquid water, and face similar but greater challenges because of the greater complexity of ice processes. Many CMIP3 models predicted the condensed water amount in just two categories—cloud and precipitation—with a temperature-dependent partitioning between liquid and ice within either category. Although supersaturation with respect to ice is commonly observed at low temperatures, only one CMIP3 GCM (ECHAM) allowed ice supersaturation (Lohmann and Kärcher, 2002).

Many climate models now include separate, physically based equations for cloud liquid versus cloud ice, and for rain versus snow, allowing a more realistic treatment of mixed-phase processes and ice supersaturation (Liu et al., 2007; Tompkins et al., 2007; Gettelman et al., 2010; Salzmann et al., 2010; see also Section 7.4.4). These new schemes are tested in a single-column model against cases observed in field campaigns (e.g., Klein et al., 2009) or against satellite observations (e.g., Kay et al., 2012), and provide superior simulations of cloud structure than typical CMIP3 parameterizations (Kay et al., 2012). However new observations reveal complexities not correctly captured by even relatively advanced schemes (Ma et al., 2012a). New representations of the Wegener–Bergeron–Findeisen process in mixed-phase clouds (Storelvmo et al., 2008b; Lohmann and Hoose, 2009) compare the rate at which the pre-existing ice crystals deplete the water vapour with the condensation rate for liquid water driven by vertical updraught speed (Korolev, 2007); these are not yet included in CMIP5 models. Climate models are increasingly representing detailed microphysics, including mixed-phase processes, inside convective clouds (Fowler and Randall, 2002; Lohmann, 2008; Song and Zhang, 2011). Such processes can influence storm characteristics like strength and electrification, and are crucial for fully representing aerosol–cloud interactions, but are still not included in most climate models; their representation is moreover subject to all the caveats noted in Section 7.2.3.1.

7.2.3.3 Recent Advances in Parameterizing Moist Turbulence and Convection

Both the mean state and variability in climate models are sensitive to the parameterization of cumulus convection. Since AR4, the development of convective parameterization has been driven largely by rapidly growing use of process models, in particular LES and CRMs, to inform parameterization development (e.g., Hourdin et al., 2013).

Accounting for greater or more state-dependent entrainment of air into deep cumulus updraughts has improved simulations of the Madden–Julian Oscillation, tropical convectively coupled waves and mean rainfall patterns in some models (Bechtold et al., 2008; Song and Zhang, 2009; Chikira and Sugiyama, 2010; Hohenegger and Bretherton, 2011; Mapes and Neale, 2011; Del Genio et al., 2012; Kim et al., 2012) but usually at the expense of a degraded simulation of the mean state. In another model, revised criteria for convective initiation and parameterizations of cumulus momentum fluxes improved ENSO and tropical vertical temperature profiles (Neale et al., 2008; Richter and Rasch, 2008). Since AR4, more climate models have adopted cumulus parameterizations that diagnose the expected vertical velocity in cumulus updraughts (e.g., Del Genio et al., 2007; Park and Bretherton, 2009; Chikira and Sugiyama, 2010; Donner et al., 2011), in principle allowing more complete representations of aerosol activation, cloud microphysical evolution and gravity wave generation by the convection.

Several new parameterizations couple shallow cumulus convection more closely to moist boundary layer turbulence (Siebesma et al., 2007; Neggers, 2009; Neggers et al., 2009; Couvreux et al., 2010) including cold pools generated by nearby deep convection (Grandpeix and Lafore, 2010). Many of these efforts have led to more accurate simulations of boundary-layer cloud radiative properties and vertical structure (e.g., Park and Bretherton, 2009; Köhler et al., 2011), and have ameliorated the common problem of premature deep convective initiation over land in one CMIP5 GCM (Rio et al., 2009).

7.2.3.4 Recent Advances in Parameterizing Cloud Radiative Effects

Some models have improved representation of sub-grid scale cloud variability, which has important effects on grid-mean radiative fluxes

and precipitation fluxes, for example, based on the use of probability density functions of thermodynamic variables (Sommeria and Deardorff, 1977; Watanabe et al., 2009). Stochastic approaches for radiative transfer can account for this variability in a computationally efficient way (Barker et al., 2008). New treatments of cloud overlap have been motivated by new observations (Section 7.2.1.1). Despite these advances, the CMIP5 models continue to exhibit the 'too few, too bright' low-cloud problem (Nam et al., 2012), with a systematic overestimation of cloud optical depth and underestimation of cloud cover.

7.2.3.5 Cloud Modelling Synthesis

Global climate models used in CMIP5 have improved their representation of cloud processes relative to CMIP3, but still face challenges and uncertainties, especially regarding details of small-scale variability that are crucial for aerosol–cloud interactions (see Section 7.4). Finer-scale LES and CRM models are much better able to represent this variability and are an important research tool, but still suffer from imperfect representations of aerosol and cloud microphysics and known biases. Most CRM and LES studies do not span the large space and time scales needed to fully determine the interactions among different cloud regimes and the resulting net planetary radiative effects. Thus our assessments in this chapter do not regard any model type on its own as definitive, but weigh the implications of process model studies in assessing the quantitative results of the global models.

7.2.4 Water Vapour and Lapse Rate Feedbacks

Climate feedbacks determine the sensitivity of global surface temperature to external forcing agents. Water vapour, lapse rate and cloud feedbacks each involve moist atmospheric processes closely linked to clouds, and in combination, produce most of the simulated climate feedback and most of its inter-model spread (Section 9.7). The radiative feedback from a given constituent can be quantified as its impact (other constituents remaining equal) on the TOA net downward radiative flux per degree of global surface (or near-surface) temperature increase, and may be compared with the basic 'black-body' response of -3.4 W m^{-2} °C^{-1} (Hansen et al., 1984). This definition assigns positive values to positive feedbacks, in keeping with the literature on this topic but contradictory to the conventions sometimes adopted in other climate research.

7.2.4.1 Water Vapour Response and Feedback

As pointed out in previous reports (Section 8.6.3.1 in Randall et al., 2007), physical arguments and models of all types suggest global water vapour amounts increase in a warmer climate, leading to a positive feedback via its enhanced greenhouse effect. The saturated water vapour mixing ratio (WVMR) increases nearly exponentially and very rapidly with temperature, at 6 to 10% °C^{-1} near the surface, and even more steeply aloft (up to 17% °C^{-1}) where air is colder. Mounting evidence indicates that any changes in relative humidity in warmer climates would have much less impact on specific humidity than the above increases, at least in a global and statistical sense. Hence the overall WVMR is expected to increase at a rate similar to the saturated WVMR.

Because global temperatures have been rising, the above arguments imply WVMR should be rising accordingly, and multiple observing systems indeed show this (Sections 2.5.4 and 2.5.5). A study challenging the water vapour increase (Paltridge et al., 2009) used an old reanalysis product, whose trends are contradicted by newer ones (Dessler and Davis, 2010) and by actual observations (Chapter 2). The study also reported decreasing relative humidity in data from Australian radiosondes, but more complete studies show Australia to be exceptional in this respect (Dai et al., 2011). Thus data remain consistent with the expected global feedback.

Some studies have proposed that the response of upper-level humidity to natural fluctuations in the global mean surface temperature is informative about the feedback. However, small changes to the global mean (primarily from ENSO) involve geographically heterogeneous temperature change patterns, the responses to which may be a poor analogue for global warming (Hurley and Galewsky, 2010a). Most climate models reproduce these natural responses reasonably well (Gettelman and Fu, 2008; Dessler and Wong, 2009), providing additional evidence that they at least represent the key processes.

The 'last-saturation' concept approximates the WVMR of air by its saturation value when it was last in a cloud (see Sherwood et al., 2010a for a review), which can be inferred from trajectory analysis. Studies since the AR4 using a variety of models and observations (including concentrations of water vapour isotopes) support this concept (Sherwood and Meyer, 2006; Galewsky and Hurley, 2010). The concept has clarified what determines relative humidity in the subtropical upper troposphere and placed the water vapour feedback on firmer theoretical footing by directly linking actual and saturation WVMR values (Hurley and Galewsky, 2010b). CRMs show that convection can adopt varying degrees of self-aggregation (e.g., Muller and Held, 2012), which could modify the water vapour or other feedbacks if this were climate sensitive, although observations do not suggest aggregation changes have a large net radiative effect (Tobin et al., 2012).

In a warmer climate, an upward shift of the tropopause and poleward shift of the jets and associated climate zones are expected (Sections 2.7.4 and 2.7.5) and simulated by most GCMs (Section 10.3.3). These changes account, at least qualitatively, for robust regional changes in the relative humidity simulated in warmer climate by GCMs, including decreases in the subtropical troposphere and tropical uppermost troposphere, and increases near the extratropical tropopause and high latitudes (Sherwood et al., 2010b). This pattern may be amplified, however, by non-uniform atmospheric temperature or wind changes (Hurley and Galewsky, 2010b). It is also the apparent cause of most model-predicted changes in mid- and upper-level cloudiness patterns (Wetherald and Manabe, 1980; Sherwood et al., 2010b; see also Section 7.2.5.2). Idealized CRM simulations of warming climates also show upward shifts of the humidity patterns with little change in the mean (e.g., Kuang and Hartmann, 2007; Romps, 2011).

It remains unclear whether stratospheric water vapour contributes significantly to climate feedback. Observations have shown decadal variations in stratospheric water vapour, which may have affected the planetary radiation budget somewhat (Solomon et al., 2010) but are not clearly linked to global temperature (Section 3.4.2.4 in Trenberth et

al., 2007). A strong positive feedback from stratospheric water vapour was reported in one GCM, but with parameter settings that produced an unrealistic present climate (Joshi et al., 2010).

7.2.4.2 Relationship Between Water Vapour and Lapse Rate Feedbacks

The lapse rate (decrease of temperature with altitude) should, in the tropics, change roughly as predicted by a moist adiabat, due to the strong restoring influence of convective heating. This restoring influence has now been directly inferred from satellite data (Lebsock et al., 2010), and the near-constancy of tropical atmospheric stability and deep-convective thresholds over recent decades is also now observable in SST and deep convective data (Johnson and Xie, 2010). The stronger warming of the atmosphere relative to the surface produces a negative feedback on global temperature because the warmed system radiates more thermal emission to space for a given increase in surface temperature than in the reference case where the lapse rate is fixed. This feedback varies somewhat among models because lapse rates in middle and high latitudes, which decrease less than in the tropics, do so differently among models (Dessler and Wong, 2009).

As shown by Cess (1975) and discussed in the AR4 (Randall et al., 2007), models with a more negative lapse rate feedback tend to have a more positive water vapour feedback. Cancellation between these is close enough that their sum has a 90% range in CMIP3 models of only +0.96 to +1.22 W m^{-2} °C^{-1} (based on a Gaussian fit to the data of Held and Shell (2012), see Figure 7.9) with essentially the same range in CMIP5 (Section 9.7). The physical reason for this cancellation is that as long as water vapour infrared absorption bands are nearly saturated, outgoing longwave radiation is determined by relative humidity (Ingram, 2010) which exhibits little global systematic change in any model (Section 7.2.4.1). In fact, Held and Shell (2012) and Ingram (2013a) argue that it makes more sense physically to redefine feedbacks in a different analysis framework in which relative humidity, rather than specific humidity, is the feedback variable. Analysed in that framework the inherent stabilization by the Planck response is weaker, but the water vapour and lapse rate feedbacks are also very small; thus the traditional view of large and partially compensating feedbacks has, arguably, arisen from arbitrary choices made when the analysis framework was originally set out, rather than being an intrinsic feature of climate or climate models.

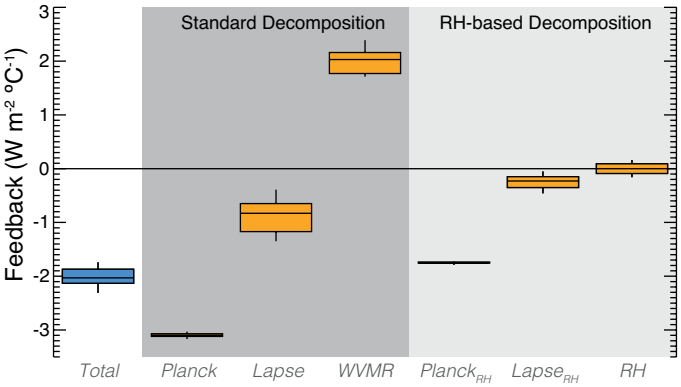

Figure 7.9 | Feedback parameters associated with water vapour or the lapse rate predicted by CMIP3 GCMs, with boxes showing interquartile range and whiskers showing extreme values. At left is shown the total radiative response including the Planck response. In the darker shaded region is shown the traditional breakdown of this into a Planck response and individual feedbacks from water vapour (labelled 'WVMR') and lapse rate (labelled 'Lapse'). In the lighter-shaded region at right are the equivalent three parameters calculated in an alternative, relative humidity-based framework. In this framework all three components are both weaker and more consistent among the models. (Data are from Held and Shell, 2012.)

There is some observational evidence (Section 2.4.4) suggesting tropical lapse rates might have increased in recent decades in a way not simulated by models (Section 9.4.1.4.2). Because the combined lapse rate and water vapour feedback depends on relative humidity change, however, the imputed lapse rate variations would have little influence on the total feedback or climate sensitivity even if they were a real warming response (Ingram, 2013b). In summary, there is increased evidence for a strong, positive feedback (measured in the traditional framework) from the combination of water vapour and lapse rate changes since AR4, with no reliable contradictory evidence.

7.2.5 Cloud Feedbacks and Rapid Adjustments to Carbon Dioxide

The dominant source of spread among GCM climate sensitivities in AR4 was due to diverging cloud feedbacks, particularly due to low clouds, and this continues to be true (Section 9.7). All global models continue to produce a near-zero to moderately strong positive net cloud feedback. Progress has been made since the AR4 in understanding the reasons for positive feedbacks in models and providing a stronger theoretical and observational basis for some mechanisms contributing to them. There has also been progress in quantifying feedbacks—including separating the effects of different cloud types, using radiative-kernel residual methods (Soden et al., 2008) and by computing cloud effects directly (e.g., Zelinka et al., 2012a)—and in distinguishing between feedback and adjustment responses (Section 7.2.5.6).

Until very recently cloud feedbacks have been diagnosed in models by differencing cloud radiative effects in doubled CO_2 and control climates, normalized by the change in global mean surface temperature. Different diagnosis methods do not always agree, and some simple methods can make positive cloud feedbacks look negative by failing to account for the nonlinear interaction between cloud and water vapour (Soden and Held, 2006). Moreover, it is now recognized that some of the cloud changes are induced directly by the atmospheric radiative effects of CO_2 independently of surface warming, and are therefore rapid adjustments rather than feedbacks (Section 7.2.5.6). Most of the published studies available for this assessment did not separate these effects, and only the total response is assessed here unless otherwise noted. It appears that the adjustments are sufficiently small in most models that general conclusions regarding feedbacks are not significantly affected.

Cloud changes cause both longwave (greenhouse warming) and shortwave (reflective cooling) effects, which combine to give the overall cloud feedback or forcing adjustment. Cloud feedback studies point to five aspects of the cloud response to climate change which are distinguished here: changes in high-level cloud altitude, effects of hydrological cycle and storm track changes on cloud systems, changes

in low-level cloud amount, microphysically induced opacity (optical depth) changes and changes in high-latitude clouds. Finally, recent research on the rapid cloud adjustments to CO_2 is assessed. Feedbacks involving aerosols (Section 7.3.5) are not considered here, and the discussion focuses only on mechanisms affecting the TOA radiation budget.

7.2.5.1 Feedback Mechanisms Involving the Altitude of High-Level Cloud

A dominant contributor of positive cloud feedback in models is the increase in the height of deep convective outflows tentatively attributed in AR4 to the so-called 'fixed anvil-temperature' mechanism (Hartmann and Larson, 2002). According to this mechanism, the average outflow level from tropical deep convective systems is determined in steady state by the highest point at which water vapour cools the atmosphere significantly through infrared emission; this occurs at a particular water vapour partial pressure, therefore at a similar temperature (higher altitude) as climate warms. A positive feedback results because, since the cloud top temperature does not keep pace with that of the troposphere, its emission to space does not increase at the rate expected for the no-feedback system. This occurs at all latitudes and has long been noted in model simulations (Hansen et al., 1984; Cess et al., 1990). This mechanism, with a small modification to account for lapse rate changes, predicts roughly +0.5 W m^{-2} $°C^{-1}$ of positive longwave feedback in GCMs (Zelinka and Hartmann, 2010), compared to an overall cloud-height feedback of +0.35 (+0.09 to +0.58) W m^{-2} $°C^{-1}$ (Figure 7.10). Importantly, CRMs also reproduce this increase in cloud height (Tompkins and Craig, 1998; Kuang and Hartmann, 2007; Romps, 2011; Harrop and Hartmann, 2012).

On average, natural fluctuations in tropical high cloud amount exert little net TOA radiative effect in the current climate due to near-compensation between their longwave and shortwave cloud radiative effects (Harrison et al., 1990; Figure 7.7). Similar compensation can be seen in the opposing variations of these two components of the high-cloud feedback across GCMs (Figure 7.10). This might suggest that the altitude feedback could be similarly compensated. However, GCMs can reproduce the observed compensation in the present climate (Sherwood et al., 1994) without producing one under global warming. In the above-noted cloud-resolving simulations, the entire cloud field (including the typical base) moved upward, in accord with a general upward shift of tropospheric fields (Singh and O'Gorman, 2012) and with drying at levels near cloud base (Minschwaner et al., 2006; Sherwood et al., 2010b). This supports the prediction of GCMs that the altitude feedback is not compensated by an increase in high-cloud thickness or albedo.

The observational record offers limited further support for the altitude increase. The global tropopause is rising as expected (Section 2.7.4). Observed cloud heights change roughly as predicted with regional, seasonal and interannual changes in near-tropopause temperature structure (Xu et al., 2007; Eitzen et al., 2009; Chae and Sherwood, 2010; Zelinka and Hartmann, 2011), although these tests may not be good analogues for global warming. Davies and Molloy (2012) report an apparent recent downward mean cloud height trend but this is probably an artefact (Evan and Norris, 2012); observed cloud height trends do not appear sufficiently reliable to test this cloud-height feedback mechanism (Section 2.5.6).

In summary, the consistency of GCM responses, basic understanding, strong support from process models, and weak further support from observations give us *high confidence* in a positive feedback contribution from increases in high-cloud altitude.

7.2.5.2 Feedback Mechanisms Involving the Amount of Middle and High Cloud

As noted in Section 7.2.5.1, models simulate a range of nearly compensating differences in shortwave and longwave high-cloud feedbacks, consistent with different changes in high-cloud amount, but also show a net positive offset consistent with higher cloud altitude (Figure 7.10). However, there is a tendency in most GCMs toward reduced middle and high cloud amount in warmer climates in low- and mid-latitudes, especially in the subtropics (Trenberth and Fasullo, 2009; Zelinka and Hartmann, 2010). This loss of cloud amount adds a positive shortwave and negative longwave feedback to the model average, which causes the average net positive feedback to appear to come from the shortwave part of the spectrum. The net effect of changes in amount of all cloud types averaged over models is a positive feedback of about +0.2 W m^{-2} $°C^{-1}$, but this roughly matches the contribution from low clouds (see the following section), implying a near-cancellation of longwave and shortwave effects for the mid- and high-level amount changes.

Changes in predicted cloud cover geographically correlate with simulated subtropical drying (Meehl et al., 2007), suggesting that they are partly tied to large-scale circulation changes including the poleward shifts found in most models (Wetherald and Manabe, 1980; Sherwood et al., 2010b; Section 2.7). Bender et al. (2012) and Eastman and Warren (2013) report poleward shifts in cloud since the 1970s

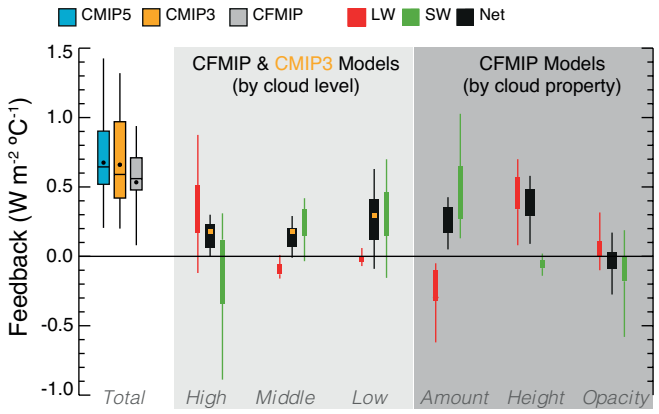

Figure 7.10 | Cloud feedback parameters as predicted by GCMs for responses to CO_2 increase including rapid adjustments. Total feedback shown at left, with centre light-shaded section showing components attributable to clouds in specific height ranges (see Section 7.2.1.1), and right dark-shaded panel those attributable to specific cloud property changes where available. The net feedback parameters are broken down in their longwave (LW) and shortwave (SW) components. Type attribution reported for CMIP3 does not conform exactly to the definition used in the Cloud Feedback Model Intercomparison Project (CFMIP) but is shown for comparison, with their 'mixed' category assigned to middle cloud. CFMIP data (original and CFMIP2) are from Zelinka et al. (2012a, 2012b; 2013); CMIP3 from Soden and Vecchi (2011); and CMIP5 from Tomassini et al. (2013).

consistent with those reported in other observables (Section 2.5.6) and simulated by most GCMs, albeit with weaker amplitude (Yin, 2005). This shift of clouds to latitudes of weaker sunlight decreases the planetary albedo and would imply a strong positive feedback if it were due to global warming (Bender et al., 2012), although it is probably partly driven by other factors (Section 10.3). The true amount of positive feedback coming from poleward shifts therefore remains highly uncertain, but is underestimated by GCMs if, as suggested by observational comparisons, the shifts are underestimated (Johanson and Fu, 2009; Allen et al., 2012).

The upward mass flux in deep clouds should decrease in a warmer climate (Section 7.6.2), which might contribute to cloudiness decreases in storm tracks or the ITCZ (Chou and Neelin, 2004; Held and Soden, 2006). Tselioudis and Rossow (2006) predict this within the storm tracks based on observed present-day relationships with meteorological variables combined with model-simulated changes to those driving variables but do not infer a large feedback. Most CMIP3 GCMs produce too little storm-track cloud cover in the southern hemisphere compared to nearly overcast conditions in reality, but clouds are also too bright. Arguments have been advanced that such biases could imply either model overestimation or underestimation of feedbacks (Trenberth and Fasullo, 2010; Brient and Bony, 2012).

The role of thin cirrus clouds for cloud feedback is not known and remains a source of possible systematic bias. Unlike high-cloud systems overall, these particular clouds exert a clear net warming effect (Jensen et al., 1994; Chen et al., 2000), making a significant cloud-cover feedback possible in principle (e.g., Rondanelli and Lindzen, 2010). While this does not seem to be important in recent GCMs (Zelinka et al., 2012b), and no specific mechanism has been suggested, the representation of cirrus in GCMs appears to be poor (Eliasson et al., 2011) and such clouds are microphysically complex (Section 7.4.4). This implies significant feedback uncertainty in addition to that already evident from model spread.

Model simulations, physical understanding and observations thus provide *medium confidence* that poleward shifts of cloud distributions will contribute to positive feedback, but by an uncertain amount. Feedbacks from thin cirrus amount cannot be ruled out and are an important source of uncertainty.

7.2.5.3 Feedback Mechanisms Involving Low Cloud

Differences in the response of low clouds to a warming are responsible for most of the spread in model-based estimates of equilibrium climate sensitivity (Randall et al., 2007). Since the AR4 this finding has withstood further scrutiny (e.g., Soden and Vecchi, 2011; Webb et al., 2013), holds in CMIP5 models (Vial et al., 2013) and has been shown to apply also to the transient climate response (e.g., Dufresne and Bony, 2008). This discrepancy in responses occurs over most oceans and cannot be clearly confined to any single region (Trenberth and Fasullo, 2010; Webb et al., 2013), but is usually associated with the representation of shallow cumulus or stratocumulus clouds (Williams and Tselioudis, 2007; Williams and Webb, 2009; Xu et al., 2010). Because the spread of responses emerges in a variety of idealized model formulations (Medeiros et al., 2008; Zhang and Bretherton, 2008; Brient and Bony, 2013), or conditioned on a particular dynamical state (Bony et al., 2004), and is similar in equilibrium or transient simulations (Yokohata et al., 2008), it appears to be attributable to how cloud, convective and boundary layer processes are parameterized in GCMs.

The modelled response of low clouds does not appear to be dominated by a single feedback mechanism, but rather the net effect of several potentially competing mechanisms as elucidated in LES and GCM sensitivity studies (e.g., Zhang and Bretherton, 2008; Blossey et al., 2013; Bretherton et al., 2013). Starting with some proposed negative feedback mechanisms, it has been argued that in a warmer climate, low clouds will be: (1) horizontally more extensive, because changes in the lapse rate of temperature also modify the lower-tropospheric stability (Miller, 1997); (2) optically thicker, because adiabatic ascent is accompanied by a larger condensation rate (Somerville and Remer, 1984); and (3) vertically more extensive, in response to a weakening of the tropical overturning circulation (Caldwell and Bretherton, 2009). While these mechanisms may play some role in subtropical low cloud feedbacks, none of them appears dominant. Regarding (1), dry static stability alone is a misleading predictor with respect to climate changes, as models with comparably good simulations of the current regional distribution and/or relationship to stability of low cloud can produce a broad range of cloud responses to climate perturbations (Wyant et al., 2006). Mechanism (2), discussed briefly in the next section, appears to have a small effect. Mechanism (3) cannot yet be ruled out but does not appear to be the dominant factor in determining subtropical cloud changes in GCMs (Bony and Dufresne, 2005; Zhang and Bretherton, 2008).

Since the AR4, several new positive feedback mechanisms have been proposed, most associated with the marine boundary layer clouds thought to be at the core of the spread in responses. These include the ideas that: warming-induced changes in the absolute humidity lapse rate change the energetics of mixing in ways that demand a reduction in cloud amount or thickness (Webb and Lock, 2013; Bretherton et al., 2013; Brient and Bony, 2013); energetic constraints prevent the surface evaporation from increasing with warming at a rate sufficient to balance expected changes in dry air entrainment, thereby reducing the supply of moisture to form clouds (Rieck et al., 2012; Webb and Lock, 2013); and that increased concentrations of GHGs reduce the radiative cooling that drives stratiform cloud layers and thereby the cloud amount (Caldwell and Bretherton, 2009; Stevens and Brenguier, 2009; Bretherton et al., 2013). These mechanisms, crudely operating through parameterized representations of cloud processes, could explain why climate models consistently produce positive low-cloud feedbacks. Among CFMIP GCMs, the low-cloud feedback ranges from –0.09 to +0.63 W m^{-2} $°C^{-1}$ (Figure 7.10), and is largely associated with a reduction in low-cloud amount, albeit with considerable spatial variability (e.g., Webb et al., 2013). One 'super-parameterized' GCM (Section 7.2.2.2) simulates a negative low-cloud feedback (Wyant et al., 2006, 2009), but that model's representation of low clouds was worse than some conventional GCMs.

The tendency of both GCMs and process models to produce these positive feedback effects suggests that the feedback contribution from changes in low clouds is positive. However, deficient representation of low clouds in GCMs, diverse model results, a lack of reliable

observational constraints, and the tentative nature of the suggested mechanisms leave us with *low confidence* in the sign of the low-cloud feedback contribution.

7.2.5.4 Feedbacks Involving Changes in Cloud Opacity

It has long been suggested that cloud water content could increase in a warmer climate simply due to the availability of more vapour for condensation in a warmer atmosphere, yielding a negative feedback (Paltridge, 1980; Somerville and Remer, 1984), but this argument ignores the physics of crucial cloud-regulating processes such as precipitation formation and turbulence. Observational evidence discounting a large effect of this kind was reported in AR4 (Randall et al., 2007).

The global mean net feedback from cloud opacity changes in CFMIP models (Figure 7.10) is approximately zero. Optical depths tend to reduce slightly at low and middle latitudes, but increase poleward of 50°, yielding a positive longwave feedback that roughly offsets the negative shortwave feedback. These latitude-dependent opacity changes may be attributed to phase changes at high latitudes and greater poleward moisture transport (Vavrus et al., 2009), and possibly to poleward shifts of the circulation.

Studies have reported warming-related changes in cloud opacity tied to cloud phase (e.g., Senior and Mitchell, 1993; Tsushima et al., 2006). This might be expected to cause negative feedback, because at mixed-phase temperatures of –38 to 0°C, cloud ice particles have typical diameters of 10 to 100 μm (e.g., Figure 8 in Donovan, 2003), several-fold larger than cloud water drops, so a given mass of cloud water would have less surface area and reflect less sunlight in ice form than in liquid form. As climate warms, a shift from ice to liquid at a given location could increase cloud opacity. An offsetting factor that may explain the absence of this in CFMIP, however, is that mixed-phase clouds may form at higher altitudes, and similar local temperatures, in warmer climates (Section 7.2.5.1). The key physics is in any case not adequately represented in climate models. Thus this particular feedback mechanism is highly uncertain.

7.2.5.5 Feedback from Arctic Cloud Interactions with Sea Ice

Arctic clouds, despite their low altitude, have a net heating effect at the surface in the present climate because their downward emission of infrared radiation over the year outweighs their reflection of sunlight during the short summer season. Their net effect on the atmosphere is cooling, however, so their effect on the energy balance of the whole system is ambiguous and depends on the details of the vertical cloud distribution and the impact of cloud radiative interactions on ice cover (Palm et al., 2010).

Low-cloud amount over the Arctic oceans varies inversely with sea ice amount (open water producing more cloud) as now confirmed since AR4 by visual cloud reports (Eastman and Warren, 2010) and lidar and radar observations (Kay and Gettelman, 2009; Palm et al., 2010). The observed effect is weak in boreal summer, when the melting sea ice is at a similar temperature to open water and stable boundary layers with extensive low cloud are common over both surfaces, and strongest in boreal autumn when cold air flowing over regions of open water stimulates cloud formation by boundary-layer convection (Kay and Gettelman, 2009; Vavrus et al., 2011). Kay et al. (2011) show that a GCM can represent this seasonal sensitivity of low cloud to open water, but doing so depends on the details of how boundary-layer clouds are parameterized. Vavrus et al. (2009) show that in a global warming scenario, GCMs simulate more Arctic low cloud in all seasons, but especially during autumn and the onset of winter when open water and very thin sea ice increase considerably, increasing upward moisture transport to the clouds.

A few studies in the literature suggest negative feedbacks from Arctic clouds, based on spatial correlations of observed warming and cloudiness (Liu et al., 2008) or tree-ring proxies of cloud shortwave effects over the last millenium (Gagen et al., 2011). However, the spatial correlations are not reliable indicators of feedback (Section 7.2.5.7), and the tree-ring evidence (assuming it is a good proxy) applies only to the shortwave effect of summertime cloud cover. The GCM studies would be consistent with warmer climates being cloudier, but have opposite radiative effects and positive feedback during the rest of the year. Even though a small positive feedback is suggested by models, there is overall little evidence for significant feedbacks from Arctic cloud.

7.2.5.6 Rapid Adjustments of Clouds to a Carbon Dioxide Change

It is possible to partition the response of TOA radiation in GCMs to an instantaneous doubling of CO_2 into a 'rapid adjustment' in which the land surface, atmospheric circulations and clouds respond to the radiative effect of the CO_2 increase, and an 'SST-mediated' response that develops more slowly as the oceans warm (see Section 7.1.3). This distinction is important not only to help understand model processes, but because the presence of rapid adjustments would cause clouds to respond slightly differently to a transient climate change (in which SST changes have not caught up to CO_2 changes) or to a climate change caused by other forcings, than they would to the same warming at equilibrium driven by CO_2. There is also a rapid adjustment of the hydrological cycle and precipitation field, discussed in Section 7.6.3.

Gregory and Webb (2008) reported that in some climate models, rapid adjustment of clouds can have TOA radiative effects comparable to those of the ensuing SST-mediated cloud changes, though Andrews and Forster (2008) found a smaller effect. Subsequent studies using more accurate kernel-based techniques find a cloud adjustment of roughly +0.4 to +0.5 W m^{-2} per doubling of CO_2, with standard deviation of about 0.3 W m^{-2} across models (Vial et al., 2013; Zelinka et al., 2013). This would account for about 20% of the overall cloud response in a model with average sensitivity; and because it is not strongly correlated with model sensitivity, it contributes perhaps 20% of the inter-model response spread (Andrews et al., 2012; Webb et al., 2013), which therefore remains dominated by feedbacks. The response occurs due to a general decrease in cloud cover caused by the slight stratification driven by CO_2 warming of the troposphere, which especially for middle and low clouds has a net warming effect (Colman and McAvaney, 2011; Zelinka et al., 2013). As explained at the beginning of Section 7.2.5, feedback numbers given in this report already account for these rapid adjustments.

7.2.5.7 Observational Constraints on Global Cloud Feedback

A number of studies since AR4 have attempted to constrain overall cloud feedback (or climate sensitivity) from observations of natural climate variability; here we discuss those using modern cloud, radiation or other measurements (see a complementary discussion in Section 12.5 based on past temperature data and forcing proxies).

One approach is to seek observable aspects of present-day cloud behaviour that reveal cloud feedback or some component thereof. Varying parameters in a GCM sometimes produces changes in cloud feedback that correlate with the properties of cloud simulated for the present day, but this depends on the GCM (Yokohata et al., 2010; Gettelman et al., 2013), and the resulting relationships do not hold across multiple models such as those from CMIP3 (Collins et al., 2011). Among the AR4 models, net cloud feedback correlates strongly with mid-latitude relative humidity (Volodin, 2008), with TOA radiation at high southern latitudes (Trenberth and Fasullo, 2010), and with humidity at certain latitudes during boreal summer (Fasullo and Trenberth, 2012); if valid each of these regression relations would imply a relatively strong positive cloud feedback in reality, but no mechanism has been proposed to explain or validate them and such apparent skill can arise fortuitously (Klocke et al., 2011). Likewise, Clement et al. (2009) found realistic decadal variations of cloud cover over the North Pacific in only one model (HadGEM1) and argued that the relatively strong cloud feedback in this model should therefore be regarded as more likely, but this finding lacks a mechanistic explanation and may depend on how model output is used (Broccoli and Klein, 2010). Chang and Coakley (2007) examined mid-latitude maritime clouds and found cloud thinning with increasing temperature, consistent with a positive feedback, whereas Gordon and Norris (2010) found the opposite result following a methodology that tried to isolate thermal and advective effects. In summary, there is no evidence of a robust link between any of the noted observables and the global feedback, though some apparent connections are tantalizing and are being studied further.

Several studies have attempted to derive global climate sensitivity from interannual relationships between global mean observations of TOA radiation and surface temperature (see also Section 10.8.2.2). One problem with this is the different spatial character of interannual and long-term warming; another is that the methodology can be confounded by cloud variations not caused by those of surface temperature (Spencer and Braswell, 2008). A range of climate sensitivities has been inferred based on such analyses (Forster and Gregory, 2006; Lindzen and Choi, 2011). Crucially, however, among different GCMs there is no correlation between the interannual and long-term cloud–temperature relationships (Dessler, 2010; Colman and Hanson, 2012), contradicting the basic assumption of these methods. Many but not all atmosphere–ocean GCMs predict relationships that are consistent with observations (Dessler, 2010, 2013). More recently there is interest in relating the time-lagged correlations of cloud and temperature to feedback processes (Spencer and Braswell, 2010) but again these relationships appear to reveal only a model's ability to simulate ENSO or other modes of interannual variability properly, which are not obviously informative about the cloud feedback on long-term global warming (Dessler, 2011).

For a putative observational constraint on climate sensitivity to be accepted, it should have a sound physical basis and its assumptions should be tested appropriately in climate models. No method yet proposed meets both conditions. Moreover, cloud responses to warming can be sensitive to relatively subtle details in the geographic warming pattern, such as the slight hemispheric asymmetry due to the lag of southern ocean warming relative to northern latitudes (Senior and Mitchell, 2000; Yokohata et al., 2008). Cloud responses to specified uniform ocean warming without CO_2 increases are not the same as those to CO_2-induced global warming simulated with more realistic oceans (Ringer et al., 2006), partly because of rapid adjustments (Section 7.2.5.6) and because low clouds also feed back tightly to the underlying surface (Caldwell and Bretherton, 2009). Simulated cloud feedbacks also differ significantly between colder and warmer climates in some models (Crucifix, 2006; Yoshimori et al., 2009) and between volcanic and other forcings (Yokohata et al., 2005). These sensitivities highlight the challenges facing any attempt to infer long-term cloud feedbacks from simple data analyses.

7.2.6 Feedback Synthesis

Together, the water vapour, lapse rate and cloud feedbacks are the principal determinants of equilibrium climate sensitivity. The water vapour and lapse rate feedbacks, as traditionally defined, should be thought of as a single phenomenon rather than in isolation (see Section 7.2.4.2). To estimate a 90% probability range for that feedback, we double the variance of GCM results about the mean to account for the possibility of errors common to all models, to arrive at +1.1 (+0.9 to +1.3) W m^{-2} $°C^{-1}$. Values in this range are supported by a steadily growing body of observational evidence, model tests, and physical reasoning. As a corollary, the net feedback from water vapour and lapse rate changes combined is *extremely likely* positive, allowing for the possibility of deep uncertainties or a fat-tailed error distribution. Key aspects of the responses of water vapour and clouds to climate warming now appear to be constrained by large-scale dynamical mechanisms that are not sensitive to poorly represented small-scale processes, and as such, are more credible. This feedback is thus known to be positive with *high confidence*, and contributes only a small part of the spread in GCM climate sensitivity (Section 9.7). An alternative framework has recently been proposed in which these feedbacks, and stabilization via thermal emission, are all significantly smaller and more consistent among models; thus the range given above may overstate the true uncertainty.

Several cloud feedback mechanisms now appear consistently in GCMs, summarized in Figure 7.11, most supported by other lines of evidence. Nearly all act in a positive direction. First, high clouds are expected to rise in altitude and thereby exert a stronger greenhouse effect in warmer climates. This altitude feedback mechanism is well understood, has theoretical and observational support, occurs consistently in GCMs and CRMs and explains about half of the mean positive cloud feedback in GCMs. Second, middle and high-level cloud cover tends to decrease in warmer climates even within the ITCZ, although the feedback effect of this is ambiguous and it cannot yet be tested observationally. Third, observations and most models suggest storm tracks shift poleward in a warmer climate, drying the subtropics and moistening the high latitudes, which causes further positive feedback via a net shift of cloud cover to latitudes that receive less sunshine. Finally, most GCMs also

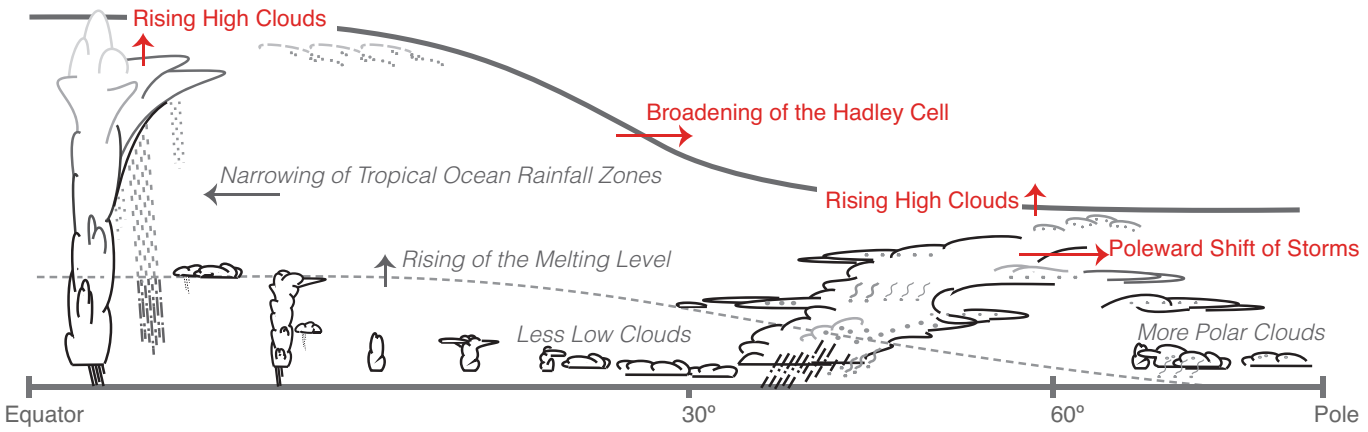

Figure 7.11 | Robust cloud responses to greenhouse warming (those simulated by most models and possessing some kind of independent support or understanding). The tropopause and melting level are shown by the thick solid and thin grey dashed lines, respectively. Changes anticipated in a warmer climate are shown by arrows, with red colour indicating those making a robust positive feedback contribution and grey indicating those where the feedback contribution is small and/or highly uncertain. No robust mechanisms contribute negative feedback. Changes include rising high cloud tops and melting level, and increased polar cloud cover and/or optical thickness (*high confidence*); broadening of the Hadley Cell and/or poleward migration of storm tracks, and narrowing of rainfall zones such as the Intertropical Convergence Zone (*medium confidence*); and reduced low-cloud amount and/or optical thickness (*low confidence*). Confidence assessments are based on degree of GCM consensus, strength of independent lines of evidence from observations or process models and degree of basic understanding.

predict that low cloud amount decreases, especially in the subtropics, another source of positive feedback though one that differs significantly among models and lacks a well-accepted theoretical basis. Over middle and high latitudes, GCMs suggest warming-induced transitions from ice to water clouds may cause clouds to become more opaque, but this appears to have a small systematic net radiative effect in models, possibly because it is offset by cloud altitude changes.

Currently, neither cloud process models (CRMs and LES) nor observations provide clear evidence to contradict or confirm feedback mechanisms involving low clouds. In some cases these models show stronger low-cloud feedbacks than GCMs, but each model type has limitations, and some studies suggest stronger positive feedbacks are more realistic (Section 7.2.5.7). Cloud process models suggest a variety of potentially opposing response mechanisms that may account for the current spread of GCM feedbacks. In summary we find no evidence to contradict either the cloud or water vapour–lapse rate feedback ranges shown by current GCMs, although the many uncertainties mean that true feedback could still lie outside these ranges. In particular, microphysical mechanisms affecting cloud opacity or cirrus amount may well be missing from GCMs. Missing feedbacks, if any, could act in either direction.

Based on the preceding synthesis of cloud behaviour, the net radiative feedback due to all cloud types is judged *likely* to be positive. This is reasoned probabilistically as follows. First, because evidence from observations and process models is mixed as to whether GCM cloud feedback is too strong or too weak overall, and because the positive feedback found in GCMs comes mostly from mechanisms now supported by other lines of evidence, the central (most likely) estimate of the total cloud feedback is taken as the mean from GCMs (+0.6 W m^{-2} $°C^{-1}$). Second, because there is no accepted basis to discredit individual GCMs *a priori*, the probability distribution of the true feedback cannot be any narrower than the distribution of GCM results. Third, since feedback mechanisms are probably missing from GCMs and some CRMs suggest feedbacks outside the range in GCMs, the probable range of the feedback must be broader than its spread in GCMs. We estimate a probability distribution for this feedback by doubling the spread about the mean of all model values in Figure 7.10 (in effect assuming an additional uncertainty about 1.7 times as large as that encapsulated in the GCM range, added to it in quadrature). This yields a 90% (*very likely*) range of –0.2 to +2.0 W m^{-2} $°C^{-1}$, with a 17% probability of a negative feedback.

Note that the assessment of feedbacks in this chapter is independent of constraints on climate sensitivity from observed trends or palaeoclimate information discussed in Box 12.2.

7.2.7 Anthropogenic Sources of Moisture and Cloudiness

Human activity can be a source of additional cloudiness through specific processes involving a source of water vapour in the atmosphere. We discuss here the impact of aviation and irrigation on water vapour and cloudiness. The impact of water vapour sources from combustion at the Earth's surface is thought to be negligible. Changes to the hydrological cycle because of land use change are briefly discussed in Section 12.4.8.

7.2.7.1 Contrails and Contrail-Induced Cirrus

Aviation jet engines emit hot moist air, which can form line shaped persistent condensation trails (contrails) in environments that are supersaturated with respect to ice and colder than about –40°C. The contrails are composed of ice crystals that are typically smaller than those of background cirrus (Heymsfield et al., 2010; Frömming et al., 2011). Their effect on longwave radiation dominates over their shortwave effect (Stuber and Forster, 2007; Rap et al., 2010b; Burkhardt and Kärcher, 2011) but models disagree on the relative importance of the two effects. Contrails have been observed to spread into large cirrus sheets that may persist for several hours, and observational studies confirm their overall positive net RF impact (Haywood et al., 2009).

Frequently Asked Questions

FAQ 7.1 | How Do Clouds Affect Climate and Climate Change?

Clouds strongly affect the current climate, but observations alone cannot yet tell us how they will affect a future, warmer climate. Comprehensive prediction of changes in cloudiness requires a global climate model. Such models simulate cloud fields that roughly resemble those observed, but important errors and uncertainties remain. Different climate models produce different projections of how clouds will change in a warmer climate. Based on all available evidence, it seems likely that the net cloud–climate feedback amplifies global warming. If so, the strength of this amplification remains uncertain.

Since the 1970s, scientists have recognized the critical importance of clouds for the climate system, and for climate change. Clouds affect the climate system in a variety of ways. They produce precipitation (rain and snow) that is necessary for most life on land. They warm the atmosphere as water vapour condenses. Although some of the condensed water re-evaporates, the precipitation that reaches the surface represents a net warming of the air. Clouds strongly affect the flows of both sunlight (warming the planet) and infrared light (cooling the planet as it is radiated to space) through the atmosphere. Finally, clouds contain powerful updraughts that can rapidly carry air from near the surface to great heights. The updraughts carry energy, moisture, momentum, trace gases, and aerosol particles. For decades, climate scientists have been using both observations and models to study how clouds change with the daily weather, with the seasonal cycle, and with year-to-year changes such as those associated with El Niño.

All cloud processes have the potential to change as the climate state changes. Cloud feedbacks are of intense interest in the context of climate change. Any change in a cloud process that is caused by climate change—and in turn influences climate—represents a cloud–climate feedback. Because clouds interact so strongly with both sunlight and infrared light, small changes in cloudiness can have a potent effect on the climate system.

Many possible types of cloud–climate feedbacks have been suggested, involving changes in cloud amount, cloud-top height and/or cloud reflectivity (see FAQ7.1, Figure 1). The literature shows consistently that high clouds amplify global warming as they interact with infrared light emitted by the atmosphere and surface. There is more uncertainty, however, about the feedbacks associated with low-altitude clouds, and about cloud feedbacks associated with amount and reflectivity in general.

Thick high clouds efficiently reflect sunlight, and both thick and thin high clouds strongly reduce the amount of infrared light that the atmosphere and surface emit to space. The compensation between these two effects makes

(continued on next page)

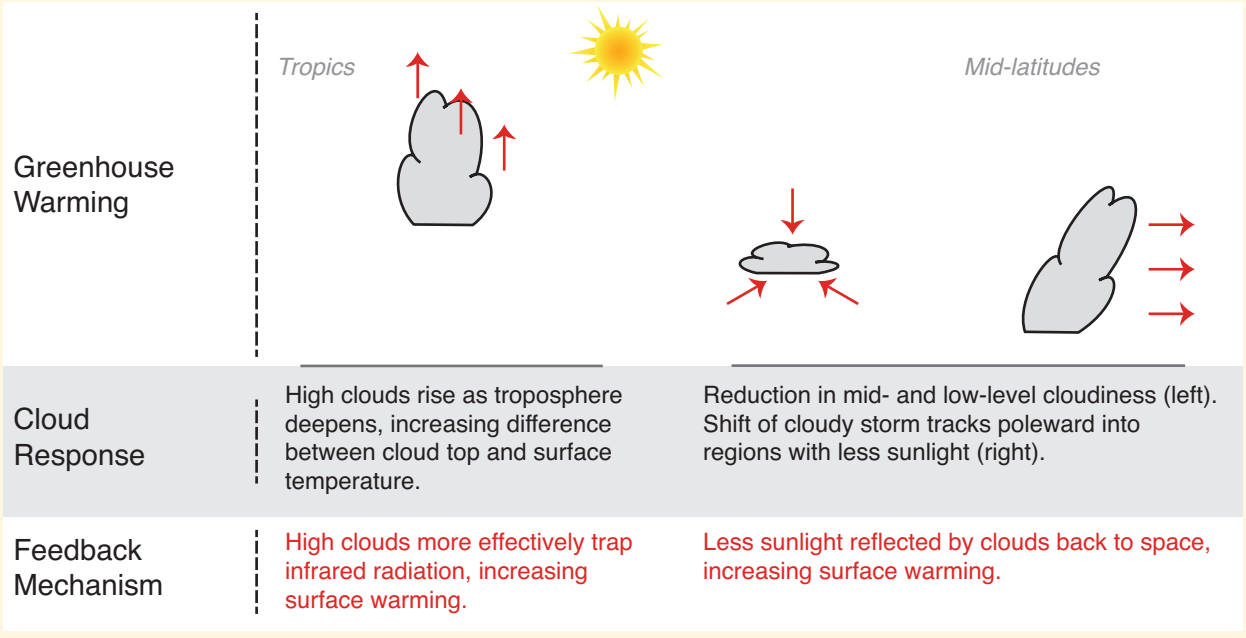

FAQ 7.1, Figure 1 | Schematic of important cloud feedback mechanisms.

FAQ 7.1 (continued)

the surface temperature somewhat less sensitive to changes in high cloud amount than to changes in low cloud amount. This compensation could be disturbed if there were a systematic shift from thick high cloud to thin cirrus cloud or vice versa; while this possibility cannot be ruled out, it is not currently supported by any evidence. On the other hand, changes in the altitude of high clouds (for a given high-cloud amount) can strongly affect surface temperature. An upward shift in high clouds reduces the infrared light that the surface and atmosphere emit to space, but has little effect on the reflected sunlight. There is strong evidence of such a shift in a warmer climate. This amplifies global warming by preventing some of the additional infrared light emitted by the atmosphere and surface from leaving the climate system.

Low clouds reflect a lot of sunlight back to space but, for a given state of the atmosphere and surface, they have only a weak effect on the infrared light that is emitted to space by the Earth. As a result, they have a net cooling effect on the present climate; to a lesser extent, the same holds for mid-level clouds. In a future climate warmed by increasing greenhouse gases, most IPCC-assessed climate models simulate a decrease in low and mid-level cloud amount, which would increase the absorption of sunlight and so tend to increase the warming. The extent of this decrease is quite model-dependent, however.

There are also other ways that clouds may change in a warmer climate. Changes in wind patterns and storm tracks could affect the regional and seasonal patterns of cloudiness and precipitation. Some studies suggest that the signal of one such trend seen in climate models—a poleward migration of the clouds associated with mid-latitude storm tracks—is already detectable in the observational record. By shifting clouds into regions receiving less sunlight, this could also amplify global warming. More clouds may be made of liquid drops, which are small but numerous and reflect more sunlight back to space than a cloud composed of the same mass of larger ice crystals. Thin cirrus cloud, which exerts a net warming effect and is very hard for climate models to simulate, could change in ways not simulated by models although there is no evidence for this. Other processes may be regionally important, for example, interactions between clouds and the surface can change over the ocean where sea ice melts, and over land where plant transpiration is reduced.

There is as yet no broadly accepted way to infer global cloud feedbacks from observations of long-term cloud trends or shorter-time scale variability. Nevertheless, all the models used for the current assessment (and the preceding two IPCC assessments) produce net cloud feedbacks that either enhance anthropogenic greenhouse warming or have little overall effect. Feedbacks are not 'put into' the models, but emerge from the functioning of the clouds in the simulated atmosphere and their effects on the flows and transformations of energy in the climate system. The differences in the strengths of the cloud feedbacks produced by the various models largely account for the different sensitivities of the models to changes in greenhouse gas concentrations.

Aerosol emitted within the aircraft exhaust may also affect high-level cloudiness. This last effect is classified as an aerosol–cloud interaction and is deemed too uncertain to be further assessed here (see also Section 7.4.4). Climate model experiments (Rap et al., 2010a) confirm earlier results (Kalkstein and Balling Jr, 2004; Ponater et al., 2005) that aviation contrails do not have, at current levels of coverage, an observable effect on the mean or diurnal range of surface temperature (*medium confidence*).

Estimates of the RF from persistent (linear) contrails often correspond to different years and need to be corrected for the continuous increase in air traffic. More recent estimates tend to indicate somewhat smaller RF than assessed in the AR4 (see Table 7.SM.1 and text in Supplementary Material). We adopt an RF estimate of +0.01 (+0.005 to +0.03) W m^{-2} for persistent (linear) contrails for 2011, with a *medium confidence* attached to this estimate. An additional RF of +0.003 W m^{-2} is due to emissions of water vapour in the stratosphere by aviation as estimated by Lee et al. (2009).

Forster et al. (2007) quoted Sausen et al. (2005) to update the 2000 forcing for aviation-induced cirrus (including linear contrails) to +0.03 (+0.01 to +0.08) W m^{-2} but did not consider this to be a best estimate because of large uncertainties. Schumann and Graf (2013) constrained their model with observations of the diurnal cycle of contrails and cirrus in a region with high air traffic relative to a region with little air traffic, and estimated a RF of +0.05 (+0.04 to +0.08) W m^{-2} for contrails and contrail-induced cirrus in 2006, but their model has a large shortwave contribution, and larger estimates are possible. An alternative approach was taken by Burkhardt and Kärcher (2011), who estimated a global RF for 2002 of +0.03 W m^{-2} from contrails and contrail cirrus within a climate model (Burkhardt and Kärcher, 2009), after compensating for reduced background cirrus cloudiness in the main traffic areas. Based on these two studies we assess the combined contrail and contrail-induced cirrus ERF for the year 2011 to be +0.05 (+0.02 to +0.15) W m^{-2} to take into uncertainties on spreading rate, optical depth, ice particle shape and radiative transfer and the ongoing increase in air traffic (see also Supplementary Material). A *low confidence* is attached to this estimate.

7.2.7.2 Irrigation-Induced Cloudiness

Boucher et al. (2004) estimated a global ERF due to water vapour from irrigation in the range of +0.03 to +0.10 W m^{-2} but the net climate effect was dominated by the evaporative cooling at the surface and by atmospheric thermal responses to low-level humidification. Regional surface cooling was confirmed by a number of more recent regional and global studies (Kueppers et al., 2007; Lobell et al., 2009). The resulting increase in water vapour may induce a small enhancement in precipitation downwind of the major irrigation areas (Puma and Cook, 2010), as well as some regional circulation patterns (Kueppers et al., 2007). Sacks et al. (2009) reported a 0.001 increase in cloud fraction over land (0.002 over irrigated land). This suggests an ERF no more negative than –0.1 W m^{-2} with *very low confidence*.

7.3 Aerosols

The section assesses the role of aerosols in the climate system, focusing on aerosol processes and properties, as well as other factors, that influence aerosol–radiation and aerosol–cloud interactions. Processes directly relevant to aerosol–cloud interactions are discussed in Section 7.4, and estimates of aerosol RFs and ERFs are assessed in Section 7.5. The time evolution of aerosols and their forcings are discussed in Chapters 2 and 8, with Chapter 8 also covering changes in natural volcanic aerosols.

7.3.1 Aerosols in the Present-Day Climate System

7.3.1.1 Aerosol Formation and Aerosol Types

Atmospheric aerosols, whether natural or anthropogenic, originate from two different pathways: emissions of primary particulate matter and formation of secondary particulate matter from gaseous precursors (Figure 7.12). The main constituents of the atmospheric aerosol are inorganic species (such as sulphate, nitrate, ammonium, sea salt), organic species (also termed organic aerosol or OA), black carbon (BC, a distinct type of carbonaceous material formed from the incomplete combustion of fossil and biomass based fuels under certain conditions), mineral species (mostly desert dust) and primary biological aerosol particles (PBAPs). Mineral dust, sea salt, BC and PBAPs are introduced into the atmosphere as primary particles, whereas non-sea-salt sulphate, nitrate and ammonium are predominantly from secondary aerosol formation processes. The OA has both significant primary and secondary sources. In the present-day atmosphere, the majority of BC, sulphate, nitrate and ammonium come from anthropogenic sources, whereas sea salt, most mineral dust and PBAPs are predominantly of natural origin. Primary and secondary organic aerosols (POA and SOA) are influenced by both natural and anthropogenic sources. Emission rates of aerosols and aerosol precursors are summarized in Table 7.1. The characteristics and role of the main aerosol species are listed in Table 7.2.

7.3.1.2 Aerosol Observations and Climatology

New and improved observational aerosol data sets have emerged since AR4. A number of field experiments have taken place such as the Intercontinental Chemical Transport Experiment (INTEX, Bergstrom et al., 2010; Logan et al., 2010), African Monsoon Multidisciplinary Analysis (AMMA; Jeong et al., 2008; Hansell et al., 2010), Integrated Campaign for Aerosols, gases and Radiation Budget (ICARB; Moorthy et al., 2008 and references therein), Megacity Impact on Regional and Global Environments field experiment (MILAGRO; Paredes-Miranda et al., 2009), Geostationary Earth Radiation Budget Inter-comparisons of Longwave and Shortwave (GERBILS, Christopher et al., 2009), Arctic Research of the Composition of the Troposphere from Aircraft and Satellites

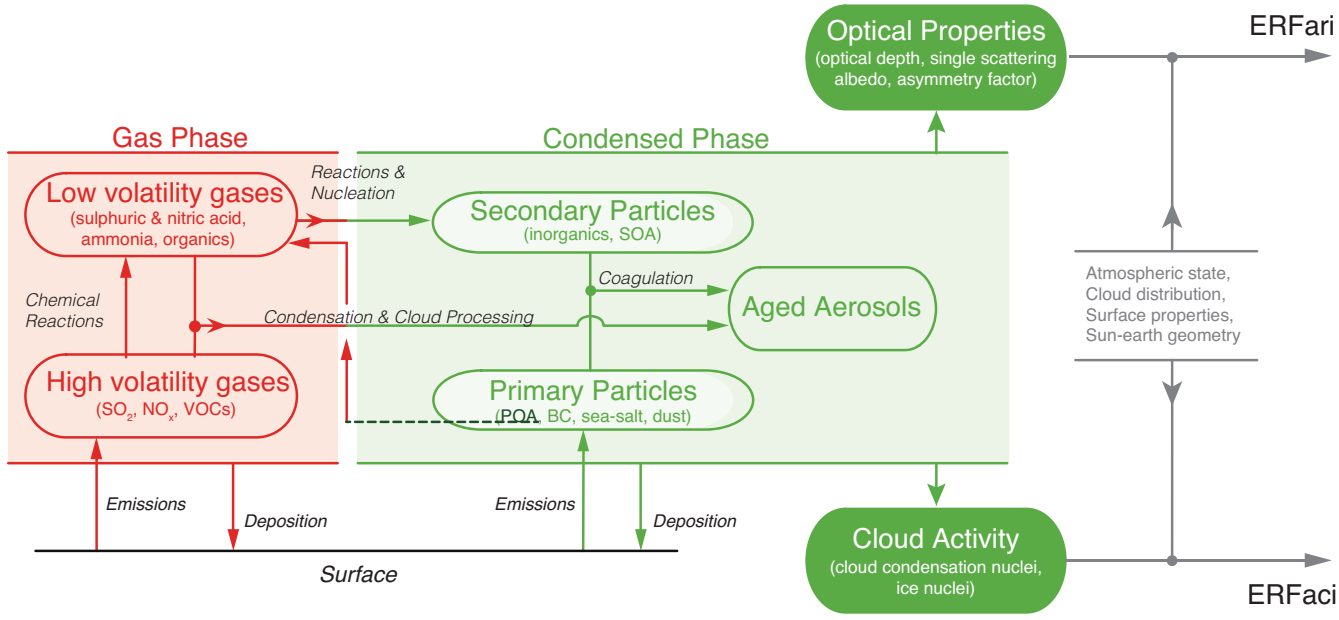

Figure 7.12 | Overview of atmospheric aerosol and environmental variables and processes influencing aerosol–radiation and aerosol–cloud interactions. Gas-phase variables and processes are highlighted in red while particulate-phase variables and processes appear in green. Although this figure shows a linear chain of processes from aerosols to forcings (ERFari and ERFaci), it is increasingly recognized that aerosols and clouds form a coupled system with two-way interactions (see Figure 7.16).

Table 7.1 | (a) Global and regional anthropogenic emissions of aerosols and aerosol precursors. The average, minimum and maximum values are from a range of available inventories (Cao et al., 2006; European Commission et al., 2009; Sofiev et al., 2009; Lu et al., 2010, 2011; Granier et al., 2011 and references therein; Knorr et al., 2012). It should be noted that the minimum to maximum range is not a measure of uncertainties which are often difficult to quantify. Units are Tg yr^{-1} and TgS yr^{-1} for sulphur dioxide (SO_2). NMVOCs stand for non-methane volatile organic compounds. (b) Global natural emissions of aerosols and aerosol precursors. Dust and sea-spray estimates span the range in the historical CMIP5 simulations. The ranges for monoterpenes and isoprene are from Arneth et al. (2008). There are other biogenic volatile organic compounds (BVOCs) such as sesquiterpenes, alcohols and aldehydes which are not listed here. Marine primary organic aerosol (POA) and terrestrial primary biological aerosol particle (PBAP) emission ranges are from Gantt et al. (2011) and Burrows et al. (2009), respectively. Note that emission fluxes from mineral dust, sea spray and terrestrial PBAPs are highly sensitive to the cut-off radius. The conversion rate of BVOCs to secondary organic aerosol (SOA) is also indicated using the range from Spracklen et al. (2011) and a lower bound from Kanakidou et al. (2005). Units are Tg yr^{-1} except for BVOCs (monoterpenes and isoprene), in TgC yr^{-1}, and dimethylsulphide (DMS), in TgS yr^{-1}.

(a)

Year 2000 Emissions Tg yr^{-1} or TgS yr^{-1}	Anthropogenic NMVOCs			Anthropogenic Black Carbon			Anthropogenic POA			Anthropogenic SO_2			Anthropogenic NH_3			Biomass Burning Aerosols		
	Avg	Min	Max	Avg	Min	Max	Avg	Min	Max	Avg	Min	Max	Avg	Min	Max	Avg	Min	Max
Total	126.9	98.2	157.9	4.8	3.6	6.0	10.5	6.3	15.3	55.2	43.3	77.9	41.6	34.5	49.6	49.1	29.0	85.3
Western Europe	11.0	9.2	14.3	0.4	0.3	0.4	0.4	0.3	0.4	4.0	3.0	7.0	4.2	3.4	4.5	0.4	0.1	0.8
Central Europe	2.9	2.3	3.5	0.1	0.1	0.2	0.3	0.2	0.4	3.0	2.3	5.0	1.2	1.1	1.2	0.3	0.1	0.4
Former Soviet Union	9.8	6.5	15.2	0.3	0.2	0.4	0.7	0.5	0.9	5.2	3.0	7.0	1.7	1.5	2.0	5.4	3.0	7.9
Middle East	13.0	9.9	15.0	0.1	0.1	0.2	0.2	0.2	0.3	3.6	3.2	4.1	1.4	1.4	1.4	0.3	0.0	1.3
North America	17.8	14.5	20.9	0.4	0.3	0.4	0.5	0.4	0.6	8.7	7.8	10.4	4.6	3.8	5.5	2.0	0.8	4.4
Central America	3.8	2.9	4.4	0.1	0.1	0.1	0.3	0.2	0.3	2.1	1.9	2.8	1.1	1.1	1.2	1.44	0.3	2.7
South America	8.6	8.2	9.2	0.3	0.2	0.3	0.6	0.3	0.8	2.5	1.9	3.6	3.4	3.4	3.5	5.9	2.6	10.9
Africa	13.2	9.9	15.0	0.5	0.4	0.6	1.4	1.0	1.9	3.1	2.6	4.4	2.4	2.3	2.4	23.9	18.5	35.3
China	16.4	11.5	24.5	1.2	0.7	1.5	2.4	1.1	3.1	11.7	9.6	17.0	10.9	8.9	12.7	1.1	0.3	2.3
India	8.9	7.3	10.8	0.7	0.5	1.0	1.9	1.0	3.3	2.9	2.6	3.9	5.8	3.7	8.5	0.5	0.1	0.9
Rest of Asia	18.1	14.1	23.9	0.6	0.5	0.7	1.7	0.8	3.0	3.9	2.2	5.7	4.1	3.2	5.9	2.0	0.4	3.4
Oceania	1.2	1.0	1.5	0.03	0.03	0.04	0.05	0.04	0.08	1.2	0.9	1.4	0.7	0.7	0.7	5.8	2.7	16.8
International Shipping	2.1	1.3	3.0	0.1	0.1	0.1	0.1	0.1	0.1	3.3	2.1	5.5						

(b)

Source	Natural Global	
	Min	Max
Sea spray	1400	6800
including marine POA	2	20
Mineral dust	1000	4000
Terrestrial PBAPs	50	1000
including spores		28
Dimethylsulphide (DMS)	10	40
Monoterpenes	30	120
Isoprene	410	600
SOA production from all BVOCs	20	380

(ARCTAS, Lyapustin et al., 2010), the Amazonian Aerosol Characterization Experiment 2008 (AMAZE-08, Martin et al., 2010b), the Integrated project on Aerosol Cloud Climate and Air Quality interactions (EUCAARI, Kulmala et al., 2011) and Atmospheric Brown Clouds (ABC, Nakajima et al., 2007), which have improved our understanding of regional aerosol properties.

Long-term aerosol mass concentrations are also measured more systematically at the surface by global and regional networks (see Section 2.2.3), and there are institutional efforts to improve the coordination and quality assurance of the measurements (e.g., GAW, 2011). A survey of the main aerosol types can be constructed from such measurements (e.g., Jimenez et al., 2009; Zhang et al., 2012b; Figure 7.13). Such analyses show a wide spatial variability in aerosol mass concentration, dominant aerosol type, and aerosol composition. Mineral dust dominates the aerosol mass over some continental regions with relatively higher concentrations especially in urban South Asia and China, accounting for about 35% of the total aerosol mass with diameter smaller than 10 μm. In the urban North America and South America, organic carbon (OC) contributes the largest mass fraction to the atmospheric aerosol (i.e., 20% or more), while in other areas of the world the OC fraction ranks second or third with a mean of about 16%. Sulphate normally accounts for about 10 to 30% by mass, except for the areas in rural Africa, urban Oceania and South America, where it is less than about 10%. The mass fractions of nitrate and ammonium are only around 6% and 4% on average, respectively. In most areas, elemental carbon (EC, which refers to a particular way of measuring BC) represents less than 5% of the aerosol mass, although this percentage may be larger (about 12%) in South America, urban Africa, urban Europe, South, Southeast and East Asia and urban Oceania due to the larger impact of combustion sources. Sea salt can be dominant at oceanic remote sites with 50 to 70% of aerosol mass.

Aerosol optical depth (AOD), which is related to the column-integrated aerosol amount, is measured by the Aerosol Robotic Network (AERONET, Holben et al., 1998), other ground-based networks (e.g.,

Table 7.2 | Key aerosol properties of the main aerosol species in the troposphere. Terrestrial primary biological aerosol particles (PBAPs), brown carbon and marine primary organic aerosols (POA) are particular types of organic aerosols (OA) but are treated here as separate components because of their specific properties. The estimated lifetimes in the troposphere are based on the AeroCom models, except for terrestrial PBAPs which are treated by analogy to other coarse mode aerosol types.

Aerosol Species	Size Distribution	Main Sources	Main Sinks	Tropospheric Lifetime	Key Climate Relevant Properties
Sulphate	Primary: Aitken, accumulation and coarse modes Secondary: Nucleation, Aitken, and accumulation modes	Primary: marine and volcanic emissions. Secondary: oxidation of SO_2 and other S gases from natural and anthropogenic sources	Wet deposition Dry deposition	~ 1 week	Light scattering. Very hygroscopic. Enhances absorption when deposited as a coating on black carbon. Cloud condensation nuclei (CCN) active.
Nitrate	Accumulation and coarse modes	Oxidation of NO_x	Wet deposition Dry deposition	~ 1 week	Light scattering. Hygroscopic. CCN active.
Black carbon	Freshly emitted: <100 nm Aged: accumulation mode	Combustion of fossil fuels, biofuels and biomass	Wet deposition Dry deposition	1 week to 10 days	Large mass absorption efficiency in the shortwave. CCN active when coated. May be ice nuclei (IN) active.
Organic aerosol	POA: Aitken and accumulation modes. SOA: nucleation, Aitken and mostly accumulation modes. Aged OA: accumulation mode	Combustion of fossil fuel, biofuel and biomass. Continental and marine ecosystems. Some anthropogenic and biogenic non-combustion sources	Wet deposition Dry deposition	~ 1 week	Light scattering. Enhances absorption when deposited as a coating on black carbon. CCN active (depending on aging time and size).
... of which brown carbon	Freshly emitted: 100–400 nm Aged: accumulation mode	Combustion of biofuels and biomass. Natural humic-like substances from the biosphere	Wet deposition Dry deposition	~ 1 week	Medium mass absorption efficiency in the UV and visible. Light scattering.
... of which terrestrial PBAP	Mostly coarse mode	Terrestrial ecosystems	Sedimentation Wet deposition Dry deposition	1 day to 1 week depending on size	May be IN active. May form giant CCN
Mineral dust	Coarse and super-coarse modes, with a small accumulation mode	Wind erosion, soil resuspension. Some agricultural practices and industrial activities (cement)	Sedimentation Dry deposition Wet deposition	1 day to 1 week depending on size	IN active. Light scattering and absorption. Greenhouse effect.
Sea spray	Coarse and accumulation modes	Breaking of air bubbles induced e.g., by wave breaking. Wind erosion.	Sedimentation Wet deposition Dry deposition	1 day to 1 week depending on size	Light scattering. Very hygroscopic. CCN active. Can include primary organic compounds in smaller size range
... of which marine POA	Preferentially Aitken and accumulation modes	Emitted with sea spray in biologically active oceanic regions	Sedimentation Wet deposition Dry deposition	~ 1 week	CCN active.

Bokoye et al., 2001; Che et al., 2009) and a number of satellite-based sensors. Instruments designed for aerosol retrievals such as Moderate Resolution Imaging Spectrometer (MODIS; Remer et al., 2005; Levy et al., 2010; Kleidman et al., 2012), Multi-angle Imaging Spectro-Radiometer (MISR; Kahn et al., 2005; Kahn et al., 2007) and Polarization and Directionality of the Earth's Reflectances (POLDER)/Polarization and Anisotropy of Reflectances for Atmospheric Sciences Coupled with Observations from Lidar (PARASOL) (Tanré et al., 2011) are used preferentially to less specialized instruments such as Advanced Very High Resolution Radiometer (AVHRR; e.g., Zhao et al., 2008a; Mishchenko et al., 2012), Total Ozone Mapping Spectrometer (TOMS; Torres et al., 2002) and Along Track Scanning Radiometer (ATSR)/Advanced Along Track Scanning Radiometer (AATSR) (Thomas et al., 2010) although the latter are useful for building aerosol climatologies because of their long measurement records (see Section 2.2.3). Although each AOD retrieval by satellite sensors shows some skill against more accurate sunphotometer measurements such as those of AERONET, there are still large differences among satellite products in regional and seasonal patterns because of differences and uncertainties in calibration, sampling, cloud screening, treatment of the surface reflectivity and aerosol microphysical properties (e.g., Li et al., 2009; Kokhanovsky et al., 2010). The global but incomplete sampling of satellite measurements can be combined with information from global aerosol models through data assimilation techniques (e.g., Benedetti et al., 2009; Figure 7.14a). Owing to the heterogeneity in their sources, their short lifetime and the dependence of sinks on the meteorology, aerosol distributions show large variations on daily, seasonal and interannual scales.

The CALIPSO spaceborne lidar (Winker et al., 2009) complements existing ground-based lidars. It now provides a climatology of the aerosol extinction coefficient (Figure 7.14b–e), highlighting that over most regions the majority of the optically active aerosol resides in the lowest 1 to 2 km. Yu et al. (2010) and Koffi et al. (2012) found that global aerosol models tend to have a positive bias in the aerosol extinction scale height in some (but not all) regions, due to an overestimate of aerosol concentrations above 6 km. There is less information available on the vertical profile of aerosol number and mass concentrations, although a number of field experiments involving research and commercial aircraft have measured aerosol concentrations (e.g., Heintzenberg et al., 2011). In particular vertical profiles of BC mixing ratios have been measured during the Aerosol Radiative Forcing over India (ARFI) aircraft/high altitude balloon campaigns (Satheesh et al., 2008), Arctic Research of the Composition of the Troposphere from Aircraft and Satellites (ARCTAS; Jacob et al., 2010), Aerosol, Radiation,

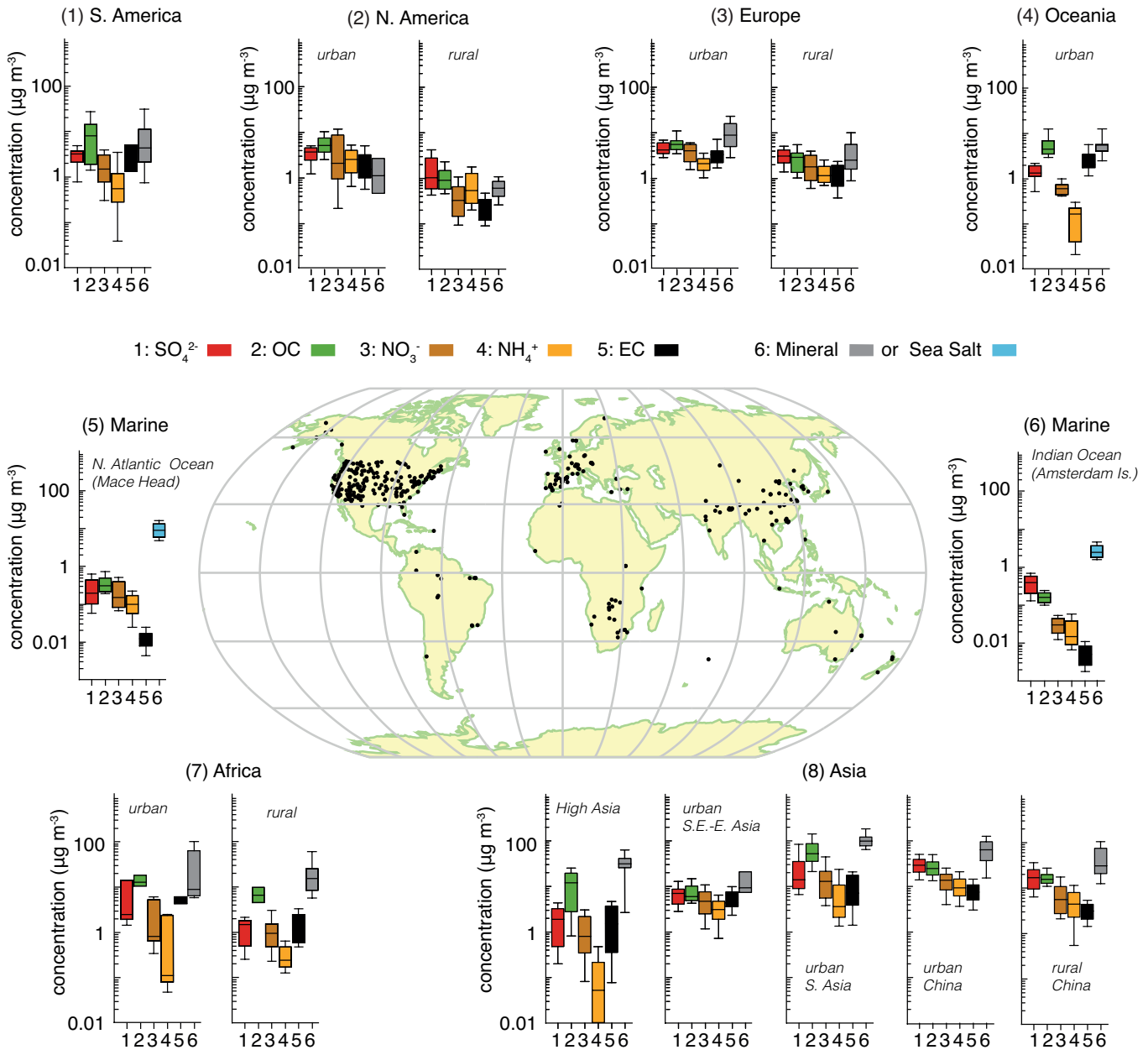

Figure 7.13 | Bar chart plots summarizing the mass concentration (µg m^{-3}) of seven major aerosol components for particles with diameter smaller than 10 µm, from various rural and urban sites (dots on the central world map) in six continental areas of the world with at least an entire year of data and two marine sites. The density of the sites is a qualitative measure of the spatial representativeness of the values for each area. The North Atlantic and Indian Oceans panels correspond to measurements from single sites (Mace Head and Amsterdam Island, respectively) that are not necessarily representative. The relative abundances of different aerosol compounds are considered to reflect the relative importance of emissions of these compounds or their precursors, either anthropogenic or natural, in the different areas. For consistency the mass of organic aerosol (OA) has been converted to that of organic carbon (OC), according to a conversion factor (typically 1.4 to 1.6), as provided in each study. For each area, the panels represent the median, the 25th to 75th percentiles (box), and the 10th to 90th percentiles (whiskers) for each aerosol component. These include: **(1) South America** (Artaxo et al., 1998; Morales et al., 1998; Artaxo et al., 2002; Celis et al., 2004; Bourotte et al., 2007; Fuzzi et al., 2007; Mariani and Mello, 2007; de Souza et al., 2010; Martin et al., 2010a; Gioda et al., 2011); **(2) North America** with **urban United States** (Chow et al., 1993; Kim et al., 2000; Ito et al., 2004; Malm and Schichtel, 2004; Sawant et al., 2004; Liu et al., 2005); and **rural United States** (Chow et al., 1993; Malm et al., 1994; Malm and Schichtel, 2004; Liu et al., 2005); **(3) Europe** with **urban Europe** (Lenschow et al., 2001; Querol et al., 2001, 2004, 2006, 2008; Roosli et al., 2001; Rodriguez et al., 2002, 2004; Putaud et al., 2004; Hueglin et al., 2005; Lonati et al., 2005; Viana et al., 2006, 2007; Perez et al., 2008; Yin and Harrison, 2008; Lodhi et al., 2009); and **rural Europe** (Gullu et al., 2000; Querol et al., 2001, 2004, 2009; Rodriguez et al., 2002; Putaud et al., 2004; Puxbaum et al., 2004;Rodrıguez et al., 2004; Hueglin et al., 2005; Kocak et al., 2007; Salvador et al., 2007; Yttri, 2007; Viana et al., 2008; Yin and Harrison, 2008;Theodosi et al., 2010); **(4) urban Oceania** (Chan et al., 1997; Maenhaut et al., 2000; Wang and Shooter, 2001; Wang et al., 2005a; Radhi et al., 2010); **(5) marine northern Atlantic Ocean** (Rinaldi et al., 2009; Ovadnevaite et al., 2011); **(6) marine Indian Ocea**n (Sciare et al., 2009; Rinaldi et al., 2011); **(7) Africa** with **urban Africa** (Favez et al., 2008; Mkoma, 2008; Mkoma et al., 2009a); and **rural Africa** (Maenhaut et al., 1996; Nyanganyura et al., 2007; Mkoma, 2008, 2009a, 2009b; Weinstein et al., 2010); **(8) Asia** with **high Asia**, with altitude larger than 1680 m (Shresth et al., 2000; Zhang et al., 2001, 2008, 2012b; Carrico et al., 2003; Rastogi and Sarin, 2005; Ming et al., 2007a; Rengarajan et al., 2007; Qu et al., 2008; Decesari et al., 2010; Ram et al., 2010); **urban Southeast and East Asia** (Lee and Kang, 2001; Oanh et al., 2006; Kim et al., 2007; Han et al., 2008; Khan et al., 2010); **urban South Asia** (Rastogi and Sarin, 2005; Kumar et al., 2007; Lodhi et al., 2009; Chakraborty and Gupta, 2010; Khare and Baruah, 2010; Raman et al., 2010; Safai et al., 2010; Stone et al., 2010; Sahu et al., 2011); **urban China** (Cheng et al., 2000; Yao et al., 2002; Zhang et al., 2002; Wang et al., 2003, 2005b, 2006; Ye et al., 2003; Xiao and Liu, 2004; Hagler et al., 2006; Oanh et al., 2006; Zhang et al., 2011, 2012b); and **rural China** (Hu et al., 2002; Zhang et al., 2002; Hagler et al., 2006; Zhang et al., 2012b).

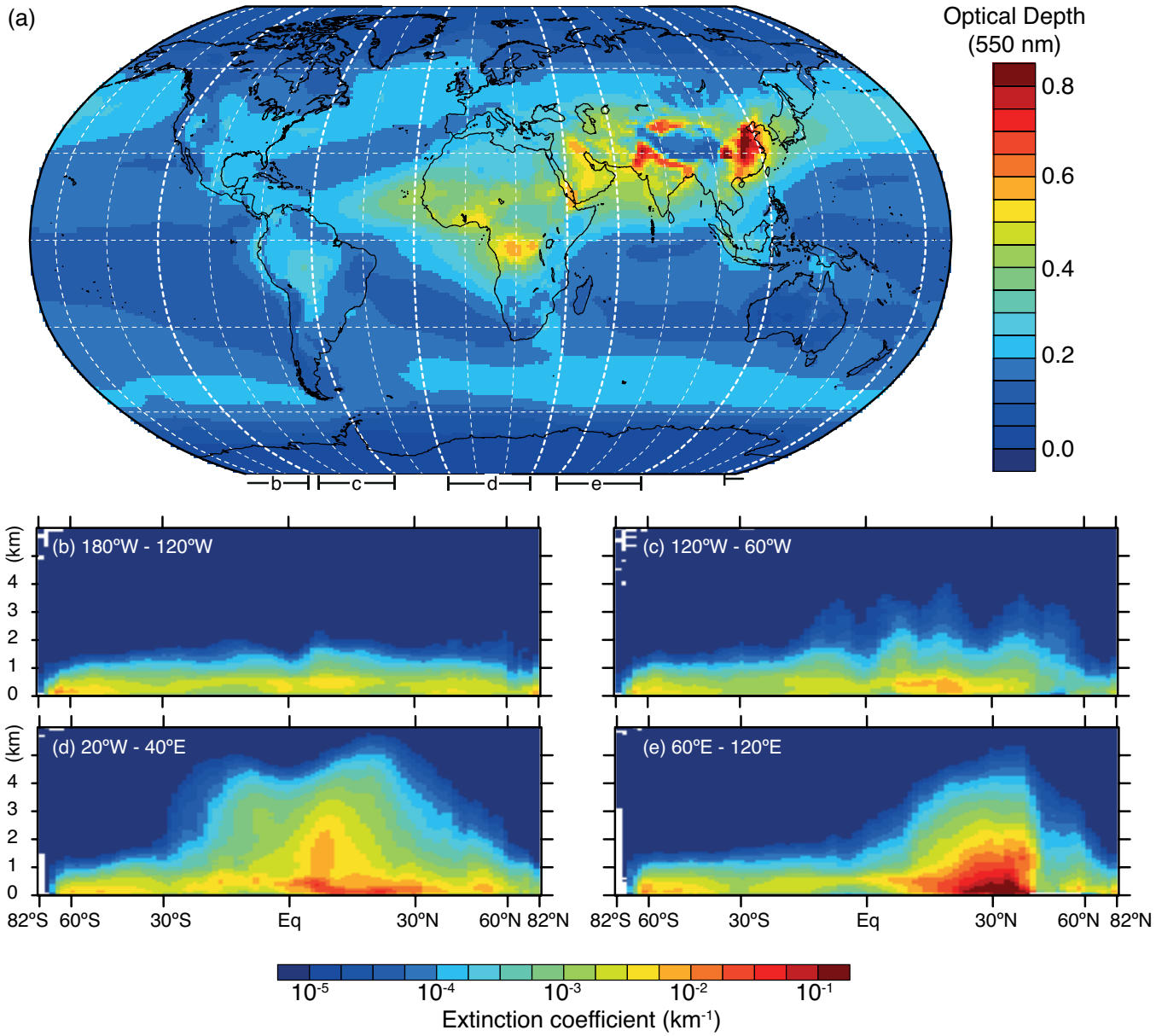

Figure 7.14 | (a) Spatial distribution of the 550 nm aerosol optical depth (AOD, unitless) from the European Centre for Medium Range Weather Forecasts (ECMWF) Integrated Forecast System model with assimilation of Moderate Resolution Imaging Spectrometer (MODIS) aerosol optical depth (Benedetti et al., 2009; Morcrette et al., 2009) averaged over the period 2003–2010; (b–e) latitudinal vertical cross sections of the 532 nm aerosol extinction coefficient (km^{-1}) for four longitudinal bands (180°W to 120°W, 120°W to 60°W, 20°W to 40°E, and 60°E to 120°E, respectively) from the Cloud–Aerosol Lidar with Orthogonal Polarization (CALIOP) instrument for the year 2010 (nighttime all-sky data, version 3; Winker et al., 2013).

and Cloud Processes affecting Arctic Climate (ARCPAC; Warneke et al., 2010), Aerosol Radiative Forcing in East Asia (A-FORCE; Oshima et al., 2012) and HIAPER Pole-to-Pole Observations (HIPPO1; Schwarz et al., 2010) campaigns. Comparison between models and observations have shown that aerosol models tend to underestimate BC mass concentrations in some outflow regions, especially in Asia, but overestimate concentrations in remote regions, especially at altitudes (Koch et al., 2009b; Figure 7.15), which make estimates of their RFari uncertain (see Section 7.5.2) given the large dependence of RFari on the vertical distribution of BC (Ban-Weiss et al., 2012). Absorption AOD can be retrieved from sun photometer measurements (Dubovik et al., 2002) or a combination of ground-based transmittance and satellite reflectance measurements (Lee et al., 2007) in situations where AOD is larger than about 0.4. Koch et al. (2009b) and Bond et al. (2013) used AERONET-based retrievals of absorption AOD to show that most AeroCom models underestimate absorption in many regions, but there remain representativeness issues when comparing point observations to a model climatology.

7.3.2 Aerosol Sources and Processes

7.3.2.1 Aerosol Sources

Sea spray is produced at the sea surface by bubble bursting induced mostly, but not exclusively, by breaking waves. The effective emission flux of sea spray particles to the atmosphere depends on the surface

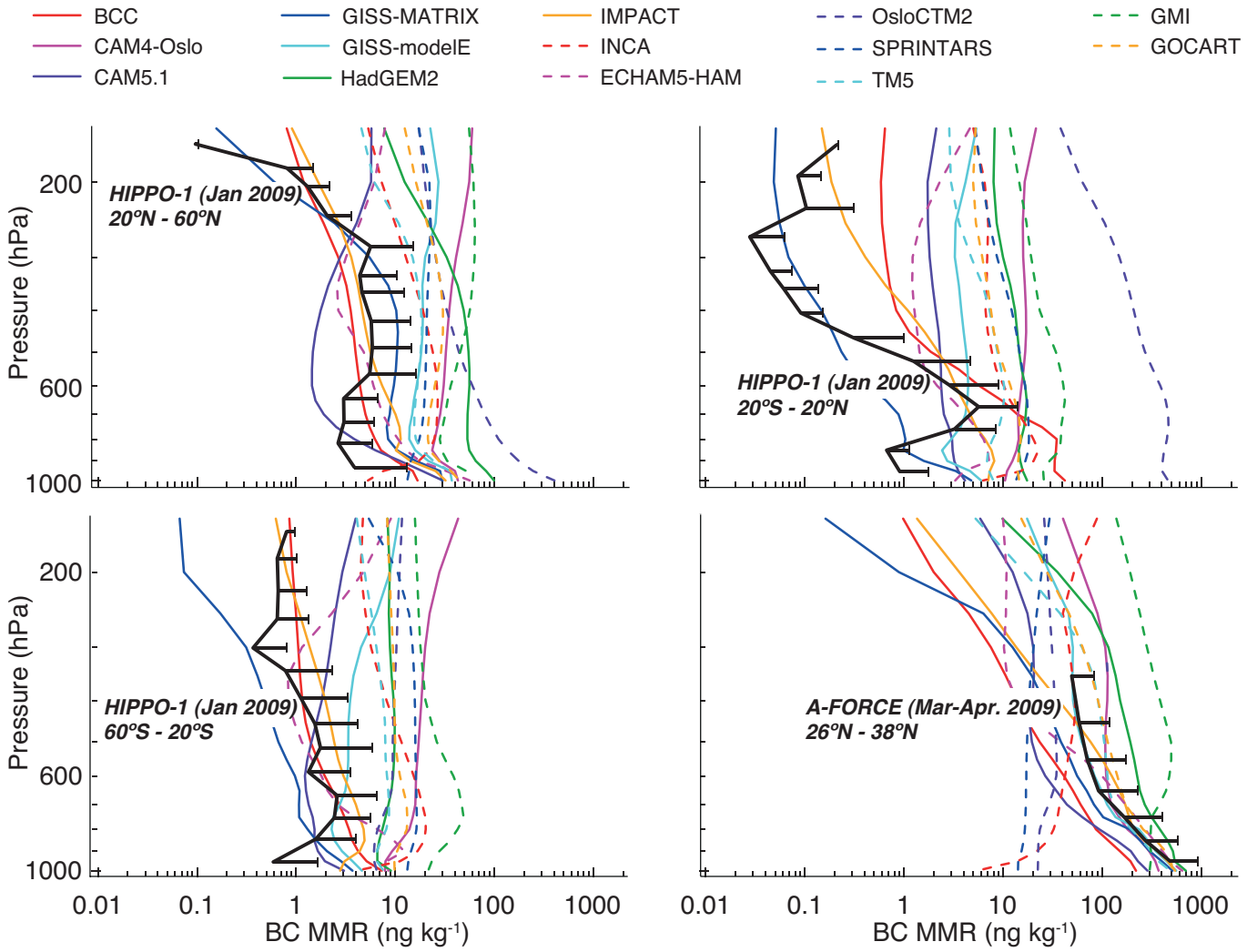

Figure 7.15 | Comparison of vertical profiles of black carbon (BC) mass mixing ratios (MMR, in ng kg^{-1}) as measured by airborne single particle soot photometer (SP2) instruments during the HIAPER Pole-to-Pole Observations (HIPPO1; Schwarz et al., 2010) and Aerosol Radiative Forcing in East Asia (A-FORCE; Oshima et al., 2012) aircraft campaigns and simulated by a range of AeroCom II models (Schulz et al., 2009). The black solid lines are averages of a number of vertical profiles in each latitude zone with the horizontal lines representing the standard deviation of the measurements at particular height ranges. Each HIPPO1 profile is the average of about 20 vertical profiles over the mid-Pacific in a two-week period in January 2009. The A-FORCE profile is the average of 120 vertical profiles measured over the East China Sea and Yellow Sea downstream of the Asian continent in March to April 2009. The model values (colour lines) are monthly averages corresponding to the measurement location and month, using meteorology and emissions corresponding to the year 2006.

wind speed, sea state and atmospheric stability, and to a lesser extent on the temperature and composition of the sea water. Our understanding of sea spray emissions has increased substantially since AR4; however, process-based estimates of the total mass and size distribution of emitted sea spray particles continue to have large uncertainties (de Leeuw et al., 2011; Table 7.1). Sea spray particles are composed of sea salt and marine primary organic matter, the latter being found preferentially in particles smaller than 200 nm in diameter (Leck and Bigg, 2008; Russell et al., 2010). The emission rate of marine POA depends on biological activity in ocean waters (Facchini et al., 2008) and its global emission rate has been estimated to be in the range 2 to 20 Tg yr^{-1} (Gantt et al., 2011). Uncertainty in the source and composition of sea spray translates into a significant uncertainty in the aerosol number concentration in the marine atmosphere that, unlike aerosol optical depth and mass concentrations, can only be constrained by *in situ* observations (Heintzenberg et al., 2000; Jaeglé et al., 2011).

Mineral dust particles are produced mainly by disintegration of aggregates following creeping and saltation of larger soil particles over desert and other arid surfaces (e.g., Zhao et al., 2006; Kok, 2011). The magnitude of dust emissions to the atmosphere depends on the surface wind speed and many soil-related factors such as its texture, moisture and vegetation cover. The range of estimates for the global dust emissions spans a factor of about five (Huneeus et al., 2011; Table 7.1). Anthropogenic sources, including road dust and mineral dust due to human land use change, remain ill quantified although some recent satellite observations suggest the fraction of mineral dust due to the latter source could be 20 to 25% of the total (Ginoux et al., 2012a, 2012b).

The sources of biomass burning aerosols at the global scale are usually inferred from satellite retrieval of burned areas and/or active fires, but inventories continue to suffer from the lack of sensitivity of satellite

data to small fires (Randerson et al., 2012) and uncertainties in emission factors. Terrestrial sources of PBAPs include bacteria, pollen, fungal spores, lichen, viruses and fragments of animals and plants (Després et al., 2012). Most of these particles are emitted in the coarse mode (Pöschl et al., 2010) and the contribution to the accumulation mode is thought to be small. There are only a few estimates of the global flux of PBAPs and these are poorly constrained (Burrows et al., 2009; Heald and Spracklen, 2009; see Table 7.1).

The main natural aerosol precursors are dimethylsulphide (DMS) emitted by the oceans and biogenic volatile organic compounds (BVOC) emitted mainly by the terrestrial biosphere. BVOC emissions depend on the amount and type of vegetation, temperature, radiation, the ambient CO_2 concentration and soil humidity (Grote and Niinemets, 2008; Pacifico et al., 2009; Peñuelas and Staudt, 2010). While speciated BVOC emission inventories have been derived for some continental regions, global emission inventories or schemes are available only for isoprene, monoterpenes and a few other compounds (Müller et al., 2008; Guenther et al., 2012). The total global BVOC emissions have large uncertainties, despite the apparent convergence in different model-based estimates (Arneth et al., 2008).

The ratio of secondary to primary organic aerosol is larger than previously thought, but has remained somewhat ambiguous due to atmospheric transformation processes affecting both these components (Robinson et al., 2007; Jimenez et al., 2009; Pye and Seinfeld, 2010). Globally, most of the atmospheric SOA is expected to originate from biogenic sources, even though anthropogenic sources could be equally important at northern mid-latitudes (de Gouw and Jimenez, 2009; Lin et al., 2012). Recent studies suggest that the SOA formation from BVOCs may be enhanced substantially by anthropogenic pollution due to (1) high concentrations of nitrogen oxides (NO_x) enhancing BVOC oxidation, and (2) high anthropogenic POA concentrations that facilitate transformation of oxidized volatile organic compounds (VOCs) to the particle phase (Carlton et al., 2010; Heald et al., 2011; Hoyle et al., 2011). The uncertainty range of atmospheric SOA formation is still large and estimated to be approximately 20 to 380 Tg yr^{-1} (Hallquist et al., 2009; Farina et al., 2010; Heald et al., 2010; Spracklen et al., 2011; Table 7.1).

Anthropogenic sources of aerosol particles (BC, POA) and aerosol precursors (sulphur dioxide, ammonia, NO_x and NMVOCs, hereafter also referred to as VOCs for simplicity) can be inferred from *a priori* emission inventories (Table 7.1). They are generally better constrained than natural sources, exceptions being anthropogenic sources of BC, which could be underestimated (Bond et al., 2013), and anthropogenic emissions of some VOCs, fly-ash and dust which are still poorly known. Since AR4, remote sensing by satellites has been increasingly used to constrain natural and anthropogenic aerosol and aerosol precursor emissions (e.g., Dubovik et al., 2008; Jaeglé et al., 2011; Huneeus et al., 2012).

7.3.2.2 Aerosol Processes

New particle formation is the process by which low-volatility vapours nucleate into stable molecular clusters, which under certain condensable vapour regimes can grow rapidly to produce nanometre-sized aerosol particles. Since AR4, substantial progress in our understanding of atmospheric nucleation and new particle formation has been made (e.g., Zhang et al., 2012a). Multiple lines of evidence indicate that while sulphuric acid is the main driver of nucleation (Kerminen et al., 2010; Sipilä et al., 2010), the nucleation rate is affected by ammonia and amines (Kurten et al., 2008; Smith et al., 2010; Kirkby et al., 2011; Yu et al., 2012) as well as low-volatility organic vapours (Metzger et al., 2010; Paasonen et al., 2010; Wang et al., 2010a). Nucleation pathways involving only uncharged molecules are expected to dominate over nucleation induced by ionization of atmospheric molecules in continental boundary layers, but the situation might be different in the free atmosphere (Kazil et al., 2010; Hirsikko et al., 2011).

Condensation is the main process transferring low-volatility vapours to aerosol particles, and also usually the dominant process for growth to larger sizes. The growth of the smallest particles depends crucially on the condensation of organic vapours (Donahue et al., 2011b; Riipinen et al., 2011; Yu, 2011) and is therefore tied strongly with atmospheric SOA formation discussed in Section 7.3.3.1. The treatment of condensation of semi-volatile compounds, such as ammonia, nitric acid and most organic vapours, remains a challenge in climate modeling. In addition, small aerosol particles collide with one another and stick (coagulate), one of the processes contributing to aerosol internal mixing. Coagulation is an important sink for sub-micrometre size particles, typically under high concentrations near sources and at lower concentrations in locations where the aerosol lifetime is long and amount of condensable vapours is low. It is the main sink for the smallest aerosol particles (Pierce and Adams, 2007).

Since AR4, observations of atmospheric nucleation and subsequent growth of nucleated particles to larger sizes have been increasingly reported in different atmospheric environments (Kulmala and Kerminen, 2008; Manninen et al., 2010; O'Dowd et al., 2010). Nucleation and growth enhance atmospheric CCN concentrations (Spracklen et al., 2008; Merikanto et al., 2009; Pierce and Adams, 2009a; Yu and Luo, 2009) and potentially affect aerosol–cloud interactions (Wang and Penner, 2009; Kazil et al., 2010; Makkonen et al., 2012a). However, CCN concentrations may be fairly insensitive to changes in nucleation rate because the growth of nucleated particles to larger sizes is limited by coagulation (see Sections 7.3.3.3 and 7.4.6.2).

Aerosols also evolve due to cloud processing, followed by the aerosol release upon evaporation of cloud particles, affecting the number concentration, composition, size and mixing state of atmospheric aerosol particles. This occurs via aqueous-phase chemistry taking place inside clouds, via altering aerosol precursor chemistry around and below clouds, and via different aerosol–hydrometeor interactions. These processes are discussed further in Section 7.4.1.2.

The understanding and modelling of aerosol sinks has seen less progress since AR4 in comparison to other aerosol processes. Improved dry deposition models, which depend on the particle size as well as the characteristics of the Earth's surface, have been developed and are increasingly being used in global aerosol models (Kerkweg et al., 2006; Feng, 2008; Petroff and Zhang, 2010). Sedimentation throughout the atmosphere and its role in dry deposition at the surface are important for the largest particles in the coarse mode. The uncertainty in

the estimate of wet deposition by nucleation and impaction scavenging is controlled by the uncertainties in the prediction of the amount, frequency and areal extent of precipitation, as well as the size and chemical composition of aerosol particles. For insoluble primary particles like BC and dust, nucleation scavenging also depends strongly on their degree of mixing with soluble compounds. Parameterization of aerosol wet deposition remains a key source of uncertainty in aerosol models, which affects the vertical and horizontal distributions of aerosols (Prospero et al., 2010; Vignati et al., 2010; Lee et al., 2011), with further impact on model estimates of aerosol forcings.

7.3.3 Progress and Gaps in Understanding Climate Relevant Aerosol Properties

The climate effects of atmospheric aerosol particles depend on their atmospheric distribution, along with their hygroscopicity, optical properties and ability to act as CCN and IN. Key quantities for aerosol optical and cloud forming properties are the particle number size distribution, chemical composition, mixing state and morphology. These properties are determined by a complex interplay between their sources, atmospheric transformation processes and their removal from the atmosphere (Section 7.3.2, Figures 7.12 and 7.16). Since AR4, measurement of some of the key aerosol properties has been greatly improved in laboratory and field experiments using advanced instrumentation, which allows for instance the analysis of individual particles. These experimental studies have in turn stimulated improvement in the model representations of the aerosol physical, chemical and optical properties (Ghan and Schwartz, 2007). We focus our assessment on some of the key issues where there has been progress since AR4.

7.3.3.1 Chemical Composition and Mixing State

Research on the climate impacts of aerosols has moved beyond the simple cases of externally mixed sulphate, BC emitted from fossil fuel combustion and biomass burning aerosols. Although the role of inorganic aerosols as an important anthropogenic contributor to aerosol–radiation and aerosol–cloud interactions has not been questioned, BC has received increasing attention because of its high absorption as has SOA because of its ubiquitous nature and ability to mix with other aerosol types.

The physical properties of BC (strongly light-absorbing, refractory with a vaporization temperature near 4000 K, aggregate in morphology, insoluble in most organic solvents) allow a strict definition in principle (Bond et al., 2013). Direct measurement of individual BC-containing particles is possible with laser-induced incandescence (single particle soot photometer, also called SP2; Gao et al., 2007; Schwarz et al., 2008a; Moteki and Kondo, 2010), which has enabled accurate measurements of the size of BC cores, as well as total BC mass concentrations. Condensation of gas-phase compounds on BC and coagulation with other particles alter the mixing state of BC (e.g., Li et al., 2003; Pósfai et al., 2003; Adachi et al., 2010), which can produce internally mixed BC in polluted urban air on a time scale of about 12 hours (Moteki et al., 2007; McMeeking et al., 2010). The resulting BC-containing particles can become hygroscopic, which can lead to reduced lifetime and atmospheric loading (Stier et al., 2006).

Formation processes of OA still remain highly uncertain, which is a major weakness in the present understanding and model representation of atmospheric aerosols (Kanakidou et al., 2005; Hallquist et al., 2009; Ziemann and Atkinson, 2012). Measurements by aerosol mass spectrometers have provided some insights into sources and atmospheric processing of OA (Zhang et al., 2005b; Lanz et al., 2007; Ulbrich et al., 2009). Observations at continental mid-latitudes including urban and rural/remote air suggest that the majority of SOA is probably oxygenated OA (Zhang et al., 2005a, 2007a). Experiments within and downstream of urban air indicate that under most circumstances SOA substantially contributes to the total OA mass (de Gouw et al., 2005; Volkamer et al., 2006; Zhang et al., 2007a).

There is a large range in the complexity with which OA is represented in global aerosol models. Some complex, yet still parameterized, chemical schemes have been developed recently that account for multigenerational oxidation (Robinson et al., 2007; Jimenez et al., 2009; Donahue et al., 2011a). Since AR4, some regional and global model have used a new scheme based on lumping VOCs into volatility bins (Robinson et al., 2007), which is an improved representation of the two-product absorptive partitioning scheme (Kroll and Seinfeld, 2008) for the formation and aging of SOA. This new framework includes organic compounds of different volatility, produced from parent VOCs by multi-generation oxidation processes and partitioned between the aerosol and gas phases (Farina et al., 2010; Tsimpidi et al., 2010; Yu, 2011), which improves the agreement between observed and modeled SOA in urban areas (Hodzic et al., 2010; Shrivastava et al., 2011). Field observations and laboratory studies suggest that OA is also formed efficiently in aerosol and cloud and liquid water contributing a substantial fraction of the organic aerosol mass (Sorooshian et al., 2007; Miyazaki et al., 2009; Lim et al., 2010; Ervens et al., 2011a). Chemical reactions in the aerosol phase (e.g., oligomerization) also make OA less volatile and more hygroscopic, influencing aerosol–radiation and aerosol–cloud interactions (Jimenez et al., 2009). As a consequence, OA concentrations are probably underestimated in many global aerosol models that do not include these chemical processes (Hallquist et al., 2009).

Some of the OA is light absorbing and can be referred to as brown carbon (BrC; Kirchstetter et al., 2004; Andreae and Gelencser, 2006). A fraction of the SOA formed in cloud and aerosol water is light-absorbing in the visible (e.g., Shapiro et al., 2009), while SOA produced from gas-phase oxidation of VOCs absorbs ultraviolet radiation (e.g., Nakayama et al., 2010).

Multiple observations show co-existence of external and internal mixtures relatively soon after emission (e.g., Hara et al., 2003; Schwarz et al., 2008b; Twohy and Anderson, 2008). In biomass burning aerosol, organic compounds and BC are frequently internally mixed with ammonium, nitrate, and sulphate (Deboudt et al., 2010; Pratt and Prather, 2010). Over urban locations, as much as 90% of the particles are internally mixed with secondary inorganic species (Bi et al., 2011). Likewise mineral dust and biomass burning aerosols can become internally mixed when these aerosol types age together (Hand et al., 2010). The aerosol mixing state can alter particle size distribution and hygroscopicity and hence the aerosol optical properties and ability to act as CCN (Wex et al., 2010). Global aerosol models can now approximate

the aerosol mixing state using size-resolving bin or modal schemes (e.g., Stier et al., 2005; Kim et al., 2008; Mann et al., 2010).

7.3.3.2 Size Distribution and Optical Properties

Aerosol size distribution is a key parameter determining both the aerosol optical and CCN properties. Since the AR4, much effort has been put into measuring and simulating the aerosol number rather than volume size distribution. For instance, number size distributions in the submicron range (30 to 500 nm) were measured at 24 sites in Europe for two years (Asmi et al., 2011), although systematic measurements are still limited in other regions. Although validation studies show agreement between column-averaged volume size distribution from sunphotometer measurements and direct *in situ* (surface as well as aircraft-based) measurements at some locations (Gerasopoulos et al., 2007; Radhi et al., 2010; Haywood et al., 2011), these inversion products have not been systematically validated. Satellite measurements produce valuable but more limited information on aerosol size.

The aerosol scattering, absorption and extinction coefficients depend on the aerosol size distribution, aerosol refractive index and mixing state. The humidification of internally mixed aerosols further influences their light scattering and absorption properties, through changes in particle shape, size and refractive index (Freney et al., 2010). Aerosol absorption is a key climate-relevant aerosol property and earlier *in situ* methods to measure it suffered from significant uncertainties (Moosmüller et al., 2009), partly due to the lack of proper reference material for instrument calibration and development (Baumgardner et al., 2012). Recent measurements using photo-acoustic methods and laser-induced incandescence methods are more accurate but remain sparse. The mass absorption cross sections for freshly generated BC were measured to be 7.5 ± 1.2 m^2 g^{-1} at 550 nm (Bond et al., 2013). Laboratory measurements conducted under well controlled conditions show that thick coating of soluble material over BC cores enhance the mass absorption cross section by a factor of 1.8 to 2 (Cross et al., 2010; Shiraiwa et al., 2010). It is more difficult to measure the enhancement factor in mass absorption cross sections for ambient BC, partly owing to the necessity of removing coatings of BC. Knox et al. (2009) observed enhancement by a factor 1.2 to 1.6 near source regions. A much lower enhancement factor was observed by Cappa et al. (2012) by a new measurement technique, in contradiction to the laboratory experiments and theoretical calculations. These results may not be representative and would require confirmation by independent measurement methods.

As discussed in Section 7.3.1.2, the global mean AOD is not well constrained from satellite-based measurements and remains a significant source of uncertainty when estimating aerosol–radiation interactions (Su et al., 2013). This is also true of the anthropogenic fraction of AOD which is more difficult to constrain from observations. AeroCom phase II models simulate an anthropogenic AOD at 550 nm of 0.03 ± 0.01 (with the range corresponding to one standard deviation) relative to 1850, which represents 24 ± 6% of the total AOD (Myhre et al., 2013). This is less than suggested by some satellite-based studies, i.e., 0.03 over the ocean only in Kaufman et al. (2005), and about 0.06 as a global average in Loeb and Su (2010) and Bellouin et al. (2013), but more than in the CMIP5 models (see Figure 9.29). Overall there is *medium confidence* that between 20 and 40% of the global mean AOD is of anthropogenic origin. There is agreement that the anthropogenic aerosol is smaller in size and more absorbing than the natural aerosol (Myhre, 2009; Loeb and Su, 2010), but there is disagreement on the anthropogenic absorption AOD and its contribution to the total absorption AOD, that is, 0.0015 ± 0.0007 (one standard deviation) relative to 1850 in Myhre et al. (2013) but about 0.004 and half of the total absorption AOD in Bellouin et al. (2013).

7.3.3.3 Cloud Condensation Nuclei

A subset of aerosol particles acts as CCN (see Table 7.2). The ability of an aerosol particle to take up water and subsequently activate, thereby acting as a CCN at a given supersaturation, is determined by its size and composition. Common CCN in the atmosphere are composed of sea salt, sulphates and sulphuric acid, nitrate and nitric acid and some organics. The uptake of water vapour by hygroscopic aerosols strongly affects their RFari.

CCN activity of inorganic aerosols is relatively well understood, and lately most attention has been paid to the CCN activity of mixed organic/inorganic aerosols (e.g., King et al., 2010; Prisle et al., 2010). Uncertainties in our current understanding of CCN properties are due primarily to SOA (Good et al., 2010), mainly because OA is still poorly characterized (Jimenez et al., 2009). The important effect of the formation of SOA is that internally mixed SOA contributes to the mass of aerosol particles, and therefore to their sizes. The size of the CCN has been found to be more important than their chemical composition at two continental locations as larger particles are more readily activated than smaller particles because they require a lower critical supersaturation (Dusek et al., 2006; Ervens et al., 2007). However, the chemical composition may be important in other locations such as the marine environment, where primary organic particles (hydrogels) have been shown to be exceptionally good CCN (Orellana et al., 2011; Ovadnevaite et al., 2011). For SOA it is not clear how important surface tension effects and bulk-to-surface partitioning of surfactants are, and if the water activity coefficient changes significantly as a function of the solute concentration (Prisle et al., 2008; Good et al., 2010).

The bulk hygroscopicity parameter κ has been introduced as a concise measure of how effectively an aerosol particle acts as a CCN (Rissler et al., 2004, 2010; Petters and Kreidenweis, 2007). It can be measured experimentally and is increasingly being used as a way to characterize aerosol properties. Pringle et al. (2010) used surface and aircraft measurements to evaluate the κ distributions simulated by a global aerosol model, and found generally good agreement. When the aerosol is dominated by organics, discrepancies between values of κ obtained directly from both CCN activity measurements and sub-saturated particle water uptake measurements have been observed in some instances (e.g., Prenni et al., 2007; Irwin et al., 2010; Roberts et al., 2010), whereas in other studies closure has been obtained (e.g., Duplissy et al., 2008; Kammermann et al., 2010; Rose et al., 2011). Adsorption theory (Kumar et al., 2011) replaces κ-theory for CCN activation for insoluble particles (e.g., mineral dust) while alternative theories are still required for explanation of marine POA that seem to have peculiar gel-like properties (Ovadnevaite et al., 2011).

Available modelling studies (Pierce and Adams, 2009a; Wang and Penner, 2009; Schmidt et al., 2012a) disagree on the anthropogenic fraction of CCN (taken here at 0.2% supersaturation). Based on these studies we assess this fraction to be between one fourth and two thirds in the global mean with *low confidence*, and highlight large interhemispheric and regional variations. Models that neglect or underestimate volcanic and natural organic aerosols would overestimate this fraction.

7.3.3.4 Ice Nuclei

Aerosols that act as IN are solid substances at atmospheric temperatures and supersaturations. Mineral dust, volcanic ash and primary bioaerosols such as bacteria, fungal spores and pollen, are typically known as good IN (Vali, 1985; Hoose and Möhler, 2012). Conflicting evidence has been presented for the ability of BC, organic, organic semi-solid/glassy organic and biomass burning particles to act as IN (Hoose and Möhler, 2012; Murray et al., 2012). The importance of biological particles acting as IN is unclear. A new study finds evidence of a large fraction of submicron particles in the middle-to-upper troposphere to be composed of biological particles (DeLeon-Rodriguez et al., 2013); however global modelling studies suggest that their concentrations are not sufficient to play an important role for ice formation (Hoose et al., 2010a; Sesartic et al., 2012). Because BC has anthropogenic sources, its increase since pre-industrial times may have caused changes to the lifetime of mixed-phase clouds (Section 7.4.4) and thus to RF (Lohmann, 2002b; Section 7.5).

Four heterogeneous ice-nucleation modes are distinguished in the literature: immersion freezing (initiated from within a cloud droplet), condensation freezing (freezing during droplet formation), contact freezing (due to collision with an IN) and deposition nucleation (that refers to the direct deposition of vapour onto IN). Lidar observations reveal that liquid cloud droplets are present before ice crystals form via heterogeneous freezing mechanisms (Ansmann et al., 2008; de Boer et al., 2011), indicating that deposition nucleation does not seem to be important for mixed-phase clouds. IN can either be bare or mixed with other substances. As bare particles age in the atmosphere, they acquire liquid surface coatings by condensing soluble species and water vapour or by coagulating with soluble particles, which may transform IN from deposition or contact nuclei into possible immersion nuclei. A change from contact to immersion freezing implies activation at colder temperatures, with consequences for the lifetime and radiative effect of mixed-phase clouds (Sections 7.4.4 and 7.5.3).

The atmospheric concentrations of IN are very uncertain because of the aforementioned uncertainties in freezing mechanisms and the difficulty of measuring IN in the upper troposphere. The anthropogenic fraction cannot be estimated at this point because of a lack of knowledge about the anthropogenic fractions of BC and mineral dust acting as IN and the contributions of PBAPs, other organic aerosols and other aerosols acting as IN.

7.3.4 Aerosol–Radiation Interactions

7.3.4.1 Radiative Effects due to Aerosol–Radiation Interactions

The radiative effect due to aerosol–radiation interactions (REari), formerly known as direct radiative effect, is the change in radiative flux caused by the combined scattering and absorption of radiation by anthropogenic and natural aerosols. The REari results from well-understood physics and is close to being an observable quantity, yet our knowledge of aerosol and environmental characteristics needed to quantify the REari at the global scale remains incomplete (Anderson et al., 2005; Satheesh and Moorthy, 2005; Jaeglé et al., 2011). The REari requires knowledge of the spectrally varying aerosol extinction coefficient, single scattering albedo, and phase function, which can in principle be estimated from the aerosol size distribution, shape, chemical composition and mixing state (Figure 7.12). Radiative properties of the surface, atmospheric trace gases and clouds also influence the REari. In the solar spectrum under cloud-free conditions the REari is typically negative at the TOA, but it weakens and can become positive with increasing aerosol absorption, decreasing upscatter fraction or increasing albedo of the underlying surface. REari is weaker in cloudy conditions, except when the cloud layer is thin or when absorbing aerosols are located above or between clouds (e.g., Chand et al., 2009). The REari at the surface is negative and can be much stronger than the REari at the TOA over regions where aerosols are absorbing (Li et al., 2010). In the longwave part of the spectrum, TOA REari is generally positive and mainly exerted by coarse-mode aerosols, such as sea spray and desert dust (Reddy et al., 2005), and by stratospheric aerosols (McCormick et al., 1995).

There have been many measurement-based estimates of shortwave REari (e.g., Yu et al., 2006; Bergamo et al., 2008; Di Biagio et al., 2010; Bauer et al., 2011) although some studies involve some degree of modelling. In contrast, estimates of longwave REari remain limited (e.g., Bharmal et al., 2009). Observed and calculated shortwave radiative fluxes agree within measurement uncertainty when aerosol properties are known (e.g., Osborne et al., 2011). Global observational estimates of the REari rely on satellite remote sensing of aerosol properties and/or measurements of the Earth's radiative budget (Chen et al., 2011; Kahn, 2012). Estimates of shortwave TOA REari annually averaged over cloud-free oceans range from –4 to –6 W m^{-2}, mainly contributed by sea spray (Bellouin et al., 2005; Loeb and Manalo-Smith, 2005; Yu et al., 2006; Myhre et al., 2007). However, REari can reach tens of W m^{-2} locally. Estimates over land are more difficult as the surface is less well characterized (Chen et al., 2009; Jethva et al., 2009) despite recent progress in aerosol inversion algorithms (e.g., Dubovik et al., 2011). Attempts to estimate the REari in cloudy sky remain elusive (e.g., Peters et al., 2011b), although passive and active remote sensing of aerosols over clouds is now possible (Torres et al., 2007; Omar et al., 2009; Waquet et al., 2009; de Graaf et al., 2012). Notable areas of positive TOA REari exerted by absorbing aerosols include the Arctic over ice surfaces (Stone et al., 2008) and seasonally over southeastern Atlantic stratocumulus clouds (Chand et al., 2009; de Graaf et al., 2012). While AOD and aerosol size are relatively well constrained, uncertainties in the aerosol single-scattering albedo (McComiskey et al., 2008; Loeb and Su, 2010) and vertical profile (e.g., Zarzycki and Bond, 2010) contribute significantly to the overall uncertainties in REari. Consequently,

diversity in large-scale numerical model estimates of REari increases with aerosol absorption and between cloud-free and cloudy conditions (Stier et al., 2013).

7.3.4.2 Rapid Adjustments to Aerosol–Radiation Interactions

Aerosol–radiation interactions give rise to rapid adjustments (see Section 7.1), which are particularly pronounced for absorbing aerosols such as BC. Associated cloud changes are often referred to as the semi-direct aerosol effect (see Figure 7.3). The ERF from aerosol–radiation interactions is quantified in Section 7.5.2; only the corresponding processes governing rapid adjustments are discussed here. Impacts on precipitation are discussed in Section 7.6.3.

Since AR4, additional observational studies have found correlations between cloud cover and absorbing aerosols (e.g., Brioude et al., 2009; Wilcox, 2010), and eddy-resolving, regional and global scale modelling studies have helped confirm a causal link. Relationships between cloud and aerosol reveal a more complicated picture than initially anticipated (e.g., Hill and Dobbie, 2008; Koch and Del Genio, 2010; Zhuang et al., 2010; Sakaeda et al., 2011; Ghan et al., 2012).

Absorbing aerosols modify atmospheric stability in the boundary layer and free troposphere (e.g., Wendisch et al., 2008; Babu et al., 2011). The effect of this on cloud cover depends on the height of the aerosol relative to the cloud and the type of cloud (e.g., Yoshimori and Broccoli, 2008; Allen and Sherwood, 2010; Koch and Del Genio, 2010; Persad et al., 2012). Aerosol also reduces the downwelling solar radiation at the surface. Together the changes in atmospheric stability and reduction in surface fluxes provide a means for aerosols to significantly modify the fraction of surface-forced clouds (Feingold et al., 2005; Sakaeda et al., 2011). These changes may also affect precipitation as discussed in Section 7.6.3.

Cloud cover is expected to decrease if absorbing aerosol is embedded in the cloud layer. This has been observed (Koren et al., 2004) and simulated (e.g., Feingold et al., 2005) for clouds over the Amazon forest in the presence of smoke aerosols. In the stratocumulus regime, absorbing aerosol above cloud top strengthens the temperature inversion, reduces entrainment and tends to enhance cloudiness. Satellite observations (Wilcox, 2010) and modelling (Johnson et al., 2004) of marine stratocumulus show a thickening of the cloud layer beneath layers of absorbing smoke aerosol, which induces a local negative forcing. The responses of other cloud types, such as those associated with deep convection, are not well determined.

Absorbing aerosols embedded in cloud drops enhance their absorption, which can affect the dissipation of cloud. The contribution to RFari is small (Stier et al., 2007; Ghan et al., 2012), and there is contradictory evidence regarding the magnitude of the cloud dissipation effect influencing ERFari (Feingold et al., 2005; Ghan et al., 2012; Jacobson, 2012; Bond et al., 2013). Global forcing estimates are necessarily based on global models (see Section 7.5.2), although the accuracy of GCMs in this regard is limited by their ability to represent low cloud processes accurately. This is an area of concern as discussed in Section 7.2 and limits confidence in these estimates.

7.3.5 Aerosol Responses to Climate Change and Feedback

The climate drivers of changes in aerosols can be split into physical changes (temperature, humidity, precipitation, soil moisture, solar radiation, wind speed, sea ice extent, etc.), chemical changes (availability of oxidants) and biological changes (vegetation cover and properties, plankton abundance and speciation, etc). The response of aerosols to climate change may constitute a feedback loop whereby climate processes amplify or dampen the initial perturbation (Carslaw et al., 2010; Raes et al., 2010). We assess here the relevance and strength of aerosol–climate feedbacks in the context of future climate change scenarios.

7.3.5.1 Changes in Sea Spray and Mineral Dust

Concentrations of sea spray will respond to changes in surface wind speed, atmospheric stability, precipitation and sea ice cover (Struthers et al., 2011). Climate models disagree about the balance of effects, with estimates ranging from an overall 19% reduction in global sea salt burden from the present-day to year 2100 (Liao et al., 2006), to little sensitivity (Mahowald et al., 2006a), to a sizeable increase (Jones et al., 2007; Bellouin et al., 2011). In particular there is little understanding of how surface wind speed may change over the ocean in a warmer climate, and observed recent changes (e.g., Young et al., 2011; Section 2.7.2) may not be indicative of future changes. Given that sea spray particles comprise a significant fraction of CCN concentrations over the oceans, such large changes will feed back on climate through changes in cloud droplet number (Korhonen et al., 2010b).

Studies of the effects of climate change on dust loadings also give a wide range of results. Woodward et al. (2005) found a tripling of the dust burden in 2100 relative to present-day because of a large increase in bare soil fraction. A few studies projected moderate (10 to 20%) increases, or decreases (e.g., Tegen et al., 2004; Jacobson and Streets, 2009; Liao et al., 2009). Mahowald et al. (2006b) found a 60% decrease under a doubled CO_2 concentration due to the effect of CO_2 fertilization on vegetation. The large range reflects different responses of the atmosphere and vegetation cover to climate change forcings, and results in *low confidence* in these predictions.

7.3.5.2 Changes in Sulphate, Ammonium and Nitrate Aerosols

The DMS–sulphate–cloud–climate feedback loop could operate in numerous ways through changes in temperature, absorbed solar radiation, ocean mixed layer depth and nutrient recycling, sea ice extent, wind speed, shift in marine ecosystems due to ocean acidification and climate change, and atmospheric processing of DMS into CCN. Although no study has included all the relevant effects, two decades of research have questioned the original formulation of the feedback loop (Leck and Bigg, 2007) and have provided important insights into this complex, coupled system (Ayers and Cainey, 2007; Kloster et al., 2007; Carslaw et al., 2010). There is now *medium confidence* for a weak feedback due to a weak sensitivity of the CCN population to changes in DMS emissions, based on converging evidence from observations and Earth System model simulations (Carslaw et al., 2010; Woodhouse et al., 2010; Quinn and Bates, 2011). Parameterizations of oceanic DMS

production nevertheless lack robust mechanistic justification (Halloran et al., 2010) and as a result the sensitivity to ocean acidification and climate change remains uncertain (Bopp et al., 2004; Kim et al., 2010; Cameron-Smith et al., 2011).

Chemical production of sulphate increases with atmospheric temperature (Aw and Kleeman, 2003; Dawson et al., 2007; Kleeman, 2008), but future changes in sulphate are found to be more sensitive to simulated future changes in precipitation removal. Under fixed anthropogenic emissions, most studies to date predict a small (0 to 9%) reduction in global sulphate burden mainly because of future increases in precipitation (Liao et al., 2006; Racherla and Adams, 2006; Unger et al., 2006; Pye et al., 2009). However, Rae et al. (2007) found a small increase in global sulphate burden from 2000 to 2100 because the simulated future precipitation was reduced in regions of high sulphate abundance.

Changes in temperature have a large impact on nitrate aerosol formation through shifting gas–particle equilibria. There is some agreement among global aerosol models that climate change alone will contribute to a decrease in the nitrate concentrations (Liao et al., 2006; Racherla and Adams, 2006; Pye et al., 2009; Bellouin et al., 2011) with the exception of Bauer et al. (2007) who found little change in nitrate for year 2030. It should be noted however that these modeling studies have reported that changes in precursor emissions are expected to increase nitrate concentrations in the future (Section 11.3.5). Besides the changes in meteorological parameters, climate change can also influence ammonium formation by changing concentrations of sulphate and nitrate, but the effect of climate change alone was found to be small (Pye et al., 2009).

7.3.5.3 Changes in Carbonaceous Aerosols

There is evidence that future climate change could lead to increases in the occurrence of wildfires because of changes in fuel availability, readiness of the fuel to burn and ignition sources (Mouillot et al., 2006; Marlon et al., 2008; Spracklen et al., 2009; Kloster et al., 2010; Pechony and Shindell, 2010). However, vegetation dynamics may also play a role that is not well understood. Increased fire occurrence would increase aerosol emissions, but decrease BVOC emissions. This could lead to a small positive or negative net radiative effect and feedback (Carslaw et al., 2010).

A large fraction of SOA forms from the oxidation of isoprene, monoterpenes and sesquiterpenes from biogenic sources (Section 7.3.3.1). Emissions from vegetation can increase in a warmer atmosphere, everything else being constant (Guenther et al., 2006). Global aerosol models simulate an increase in isoprene emissions of 22 to 55% by 2100 in response to temperature change (Sanderson et al., 2003; Liao et al., 2006; Heald et al., 2008) and a change in global SOA burden of –6% to +100% through climate-induced changes in aerosol processes and removal rates (Liao et al., 2006; Tsigaridis and Kanakidou, 2007; Heald et al., 2008). An observationally based study suggest a small global feedback parameter of –0.01 W m^{-2} $°C^{-1}$ despite larger regional effects (Paasonen et al., 2013). Increasing CO_2 concentrations, drought and surface ozone also affect BVOC emissions (Arneth et al., 2007; Peñuelas and Staudt, 2010), which adds significant uncertainty to future global emissions (Makkonen et al., 2012b). Future changes in vegetation cover, whether they are natural or anthropogenic, also introduce large uncertainty in emissions (Lathière et al., 2010; Wu et al., 2012). There is little understanding on how the marine source of organic aerosol may change with climate, notwithstanding the large range of emission estimates for the present day (Carslaw et al., 2010).

7.3.5.4 Synthesis

The emissions, properties and concentrations of aerosols or aerosol precursors could respond significantly to climate change, but there is little consistency across studies in the magnitude or sign of this response. The lack of consistency arises mostly from our limited understanding of processes governing the source of natural aerosols and the complex interplay of aerosols with the hydrological cycle. The feedback parameter as a result of the future changes in emissions of natural aerosols is mostly bracketed within ±0.1 W m^{-2} $°C^{-1}$ (Carslaw et al., 2010). With respect to anthropogenic aerosols, Liao et al. (2009) showed a significant positive feedback (feedback parameter of +0.04 to +0.15 W m^{-2} $°C^{-1}$ on a global mean basis) while Bellouin et al. (2011) simulated a smaller negative feedback of –0.08 to –0.02 W m^{-2} $°C^{-1}$. Overall we assess that models simulate relatively small feedback parameters (i.e., within ±0.2 W m^{-2} $°C^{-1}$) with *low confidence,* however regional effects on the aerosol may be important.

7.4 Aerosol–Cloud Interactions

7.4.1 Introduction and Overview of Progress Since AR4

This section assesses our understanding of aerosol–cloud interactions, emphasizing the ways in which anthropogenic aerosol may be affecting the distribution and radiative properties of non- and weakly precipitating clouds. The idea that anthropogenic aerosol is changing cloud properties, thus contributing a substantial forcing to the climate system, has been addressed to varying degrees in all of the previous IPCC assessment reports.

Since AR4, research has continued to articulate new pathways through which the aerosol may affect the radiative properties of clouds, as well as the intensity and spatial patterns of precipitation (e.g., Rosenfeld et al., 2008). Progress can be identified on four fronts: (1) global-scale modelling now represents a greater diversity of aerosol–cloud interactions, and with greater internal consistency; (2) observational studies continue to document strong local correlations between aerosol and cloud properties or precipitation, but have become more quantitative and are increasingly identifying and addressing the methodological challenges associated with such correlations; (3) regional-scale modelling is increasingly being used to assess regional influences of aerosol on cloud field properties and precipitation; (4) fine-scale process models have begun to be used more widely, and among other things have shown how turbulent mixing, cloud and meso-scale circulations may buffer the effects of aerosol perturbations.

This section focuses on the microphysics of aerosol–cloud interactions in liquid, mixed-phase and pure ice clouds. Their radiative implications are quantified in Section 7.5. This section also includes a discussion of

aerosol influences on light precipitation in shallow clouds but defers discussion of aerosol effects on more substantial precipitation from mixed-phase clouds to Section 7.6.4.

7.4.1.1 Classification of Hypothesized Aerosol–Cloud Interactions

Denman et al. (2007) catalogued several possible pathways via which the aerosol might affect clouds. Given the number of possible aerosol–cloud interactions, and the difficulty of isolating them individually, there is little value in attempting to assess each effect in isolation, especially because modelling studies suggest that the effects may interact and compensate (Stevens and Feingold, 2009; Morrison and Grabowski, 2011). Instead, all radiative consequences of aerosol–cloud interactions are grouped into an 'effective radiative forcing due to aerosol–cloud interactions', or ERFaci (Figure 7.3). ERFaci accounts for aerosol-related microphysical modifications to the cloud albedo (Twomey, 1977), as well as any secondary effects that result from clouds adjusting rapidly to changes in their environment (i.e., 'lifetime effects'; Albrecht, 1989; Liou and Ou, 1989; Pincus and Baker, 1994). We do assess the physical underpinnings of the cloud albedo effect, but in contrast to previous assessments, no longer distinguish the resultant forcing. Note that ERFaci includes potential radiative adjustments to the cloud system associated with aerosol–cloud interactions but does not include adjustments originating from aerosol–radiation interactions (ERFari). Possible contributions to ERFaci from warm (liquid) clouds are discussed in Section 7.4.3, separately from those associated with adjustments by cold (ice or mixed-phase) clouds (Section 7.4.4). Figure 7.16 shows a schematic of many of the processes to be discussed in Sections 7.4, 7.5 and 7.6.

7.4.1.2 Advances and Challenges in Observing Aerosol–Cloud Interactions

Since AR4, numerous field studies (e.g., Rauber et al., 2007; Wood et al., 2011b; Vogelmann et al., 2012) and laboratory investigations (e.g., Stratmann et al., 2009) of aerosol–cloud interactions have highlighted the numerous ways that the aerosol impacts cloud processes, and how clouds in turn modify the aerosol. The latter occurs along a number of pathways including aqueous chemistry, which adds aerosol mass to droplets (e.g., Schwartz and Freiberg, 1981; Ervens et al., 2011a); coalescence scavenging, whereby drop collision–coalescence diminishes the droplet (and aerosol) number concentration (Hudson, 1993) and changes the mixing state of the aerosol; new particle formation in the vicinity of clouds (Clarke et al., 1999); and aerosol removal by precipitation (see also Section 7.3.2.2).

Satellite-based remote sensing continues to be the primary source of global data for aerosol–cloud interactions but concerns persist regarding how measurement artefacts affect retrievals of both aerosol (Tanré et al., 1996; Tanré et al., 1997; Kahn et al., 2005; Jeong and Li, 2010) and cloud properties (Platnick et al., 2003; Yuekui and Di Girolamo, 2008) in broken cloud fields. Two key issues are that measurements classified as 'cloud-free' may not be, and that aerosol measured in the vicinity of clouds is significantly different than it would be were the cloud field, and its proximate cause (high humidity), not present (e.g., Loeb and Schuster, 2008). The latter results from humidification effects on aerosol optical properties (Charlson et al., 2007; Su et al., 2008; Tackett and Di Girolamo, 2009; Twohy et al., 2009; Chand et al., 2012), contamination by undetectable cloud fragments (Koren et al., 2007) and the remote effects of radiation scattered by cloud edges on aerosol retrieval (Wen et al., 2007; Várnai and Marshak, 2009).

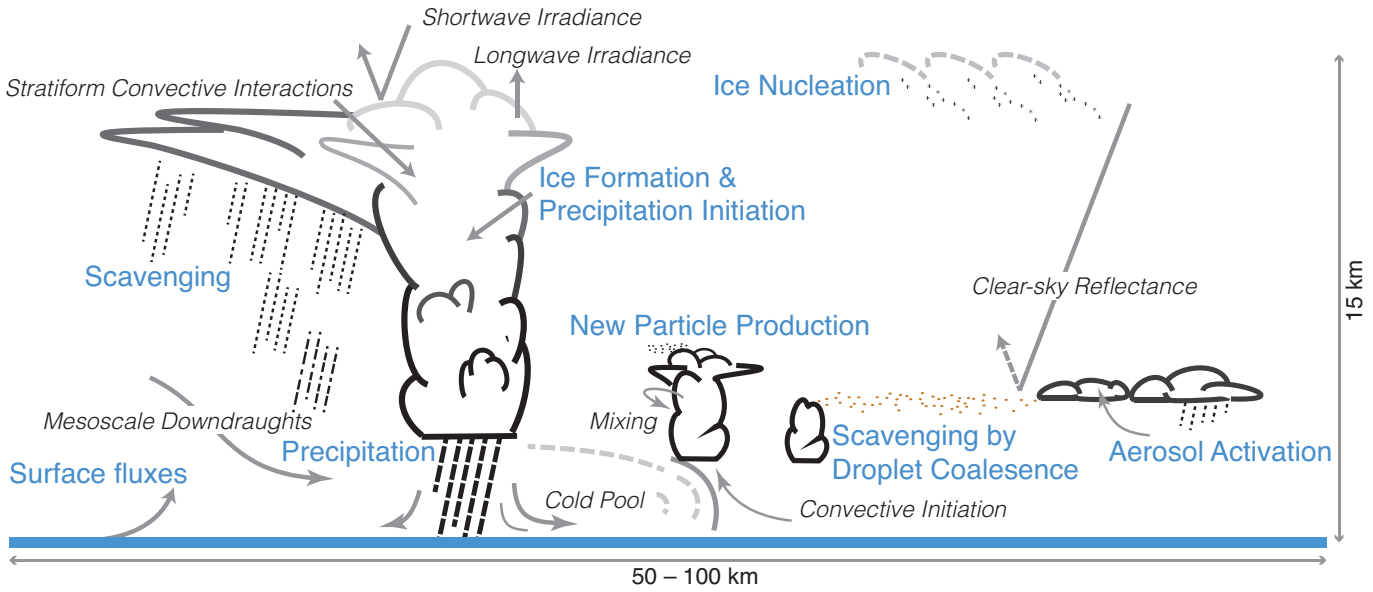

Figure 7.16 | Schematic depicting the myriad aerosol–cloud–precipitation related processes occurring within a typical GCM grid box. The schematic conveys the importance of considering aerosol–cloud–precipitation processes as part of an interactive system encompassing a large range of spatiotemporal scales. Cloud types include low-level stratocumulus and cumulus where research focuses on aerosol activation, mixing between cloudy and environmental air, droplet coalescence and scavenging which results in cloud processing of aerosol particles, and new particle production near clouds; cirrus clouds where a key issue is ice nucleation through homogeneous and heterogeneous freezing; and deep convective clouds where some of the key questions relate to aerosol influences on liquid, ice, and liquid–ice pathways for precipitation formation, cold pool formation and scavenging. These processes influence the shortwave and longwave cloud radiative effect and hence climate. Primary processes that affect aerosol–cloud interactions are labelled in blue while secondary processes that result from and influence aerosol–cloud interactions are in grey.

While most passive satellite retrievals are unable to distinguish aerosol layers above or below clouds from those intermingling with the cloud field, active space-based remote sensing (L'Ecuyer and Jiang, 2010) has begun to address this problem (Stephens et al., 2002; Anderson et al., 2005; Huffman et al., 2007; Chand et al., 2008; Winker et al., 2010). Spectral polarization and multi-angular measurements can discriminate between cloud droplets and aerosol particles and thus improve estimates of aerosol loading and absorption (Deuzé et al., 2001; Chowdhary et al., 2005; Mishchenko et al., 2007; Hasekamp, 2010).

Use of active remote sensing, both from monitoring ground stations (e.g., McComiskey et al., 2009; Li et al., 2011) and satellites (Costantino and Bréon, 2010), as well as aerosol proxies not influenced by cloud contamination of retrievals (Jiang et al., 2008; Berg et al., 2011) have emerged as a particular effective way of identifying whether aerosol and cloud perturbations are intermingled.

Because the aerosol is a strong function of air-mass history and origin, and is strongly influenced by cloud and precipitation processes (Clarke et al., 1999; Petters et al., 2006; Anderson et al., 2009), and both are affected by meteorology (Engström and Ekman, 2010; Boucher and Quaas, 2013), correlations between the aerosol and cloud, or precipitation, should not be taken as generally indicating a cloud response to the aerosol (e.g., Painemal and Zuidema, 2010). Furthermore, attempts to control for other important factors (air-mass history or cloud dynamical processes) are limited by a lack of understanding of large-scale cloud controlling factors in the first place (Anderson et al., 2009; Siebesma et al., 2009; Stevens and Brenguier, 2009). These problems are increasingly being considered in observationally based inferences of aerosol effects on clouds and precipitation, but ascribing changes in cloud properties to changes in the aerosol remains a fundamental challenge.

7.4.1.3 Advances and Challenges in Modelling Aerosol–Cloud Interactions

Modelling of aerosol–cloud interactions must contend with the fact that the key physical processes are fundamentally occurring at the fine scale and cannot be represented adequately based on large-scale fields. There exist two distinct challenges: fundamental understanding of processes and their representation in large-scale models.

Fine-scale LES and CRM models (Section 7.2.2.1) have greatly advanced as a tool for testing the physical mechanisms proposed to govern aerosol–cloud–precipitation interactions (e.g., Ackerman et al., 2009; vanZanten et al., 2011). Their main limitation is that they are idealized, for example, they do not resolve synoptic scale circulations or allow for representation of orography. A general finding from explicit numerical simulations of warm (liquid) clouds is that various aerosol impact mechanisms tend to be mediated (and often buffered) by interactions across scales not included in the idealized albedo and lifetime effects (Stevens and Feingold, 2009). Specific examples involve the interplay between the drop-size distribution and mixing processes that determine cloud macrostructure (Stevens et al., 1998; Ackerman et al., 2004; Bretherton et al., 2007; Wood, 2007; Small et al., 2009), or the dependence of precipitation development in stratiform clouds on details of the vertical structure of the cloud (Wood, 2007). Thus warm clouds may typically be less sensitive to aerosol perturbations in nature than in large-scale models, which do not represent all of these compensating processes. Hints of similar behaviour in mixed-phase (liquid and ice) stratus are beginning to be documented (Section 7.4.4.3) but process-level understanding and representation in models are less advanced.

Regional models include realism in the form of non-idealized meteorology, synoptic scale forcing, variability in land surface, and diurnal/monthly cycles (e.g., Iguchi et al., 2008; Bangert et al., 2011; Seifert et al., 2012; Tao et al., 2012), however, at the expense of resolving fine-scale cloud processes. Regional models have brought to light the possibility of aerosol spatial inhomogeneity causing changes in circulation patterns via numerous mechanisms including changes in the radiative properties of cloud anvils (van den Heever et al., 2011), changes in the spatial distribution of precipitation (Lee, 2012; Section 7.6.2) or gradients in heating rates associated with aerosol–radiation interactions (Lau et al., 2006; Section 7.3.4.2).

GCMs, our primary tool for quantifying global mean forcings, now represent an increasing number of hypothesized aerosol–cloud interactions, but at poor resolution. GCMs are being more closely scrutinized through comparisons to observations and to other models (Quaas et al., 2009; Penner et al., 2012). Historically, aerosol–cloud interactions in GCMs have been based on simple constructs (e.g., Twomey, 1977; Albrecht, 1989; Pincus and Baker, 1994). There has been significant progress on parameterizing aerosol activation (e.g., Ghan et al., 2011) and ice nucleation (Liu and Penner, 2005; Barahona and Nenes, 2008; DeMott et al., 2010; Hoose et al., 2010b); however, these still depend heavily on unresolved quantities such as updraught velocity. Similarly, parameterizations of aerosol influences on cloud usually do not account for known non-monotonic responses of cloud amount and properties to aerosols (Section 7.4.3.2). Global models are now beginning to represent aerosol effects in convective, ice and mixed-phase clouds (e.g., Lohmann, 2008; Song and Zhang, 2011; Section 7.6.4). Nevertheless, for both liquid-only and mixed-phase clouds, these parameterizations are severely limited by the need to parameterize cloud-scale motions over a huge range of spatio-temporal scales (Section 7.2.3).

Although advances have been considerable, the challenges remain daunting. The response of cloud systems to aerosol is nuanced (e.g., vanZanten et al., 2011) and the representation of both clouds and aerosol–cloud interactions in large-scale models remains primitive (Section 7.2.3). Thus it is not surprising that large-scale models exhibit a range of manifestations of aerosol–cloud interactions, which limits quantitative inference (Quaas et al., 2009). This highlights the need to incorporate into GCMs the lessons learned from cloud-scale models, in a physically-consistent way. New 'super-parameterization' and probability distribution function approaches (Golaz et al., 2002; Rio and Hourdin, 2008; Section 7.2.2.2) hold promise, with recent results supporting the notion that aerosol forcing is smaller than simulated by standard climate models (Wang et al., 2011b; see Section 7.5.3).

7.4.1.4 Combined Modelling and Observational Approaches

Combined approaches, which attempt to maximize the respective advantage of models and observations, are beginning to add to understanding of aerosol–cloud interactions. These include inversions

of the observed historical record using simplified climate models (e.g., Forest et al., 2006; Aldrin et al., 2012) but also the use of reanalysis and chemical transport models to help interpret satellite records (Chameides et al., 2002; Koren et al., 2010a; Mauger and Norris, 2010), field study data to help constrain fine-scale modelling studies (e.g., Ackerman et al., 2009; vanZanten et al., 2011), or satellite/surface-based climatologies to constrain large-scale modelling (Wang et al., 2012).

7.4.2 Microphysical Underpinnings of Aerosol–Cloud Interactions

7.4.2.1 The Physical Basis

The cloud albedo effect (Twomey, 1977) is the mechanism by which an increase in aerosol number concentration leads to an increase in the albedo of liquid clouds (reflectance of incoming solar radiation) by increasing the cloud droplet number concentration, decreasing the droplet size, and hence increasing total droplet surface area, with the liquid water content and cloud geometrical thickness hypothetically held fixed. Although only the change in the droplet concentration is considered in the original concept of the cloud albedo effect, a change in the shape of the droplet size distribution that is directly induced by the aerosols may also play a role (e.g., Feingold et al., 1997; Liu and Daum, 2002). In the Arctic, anthropogenic aerosol may influence the longwave emissivity of optically thin liquid clouds and generate a positive forcing at the surface (Garrett and Zhao, 2006; Lubin and Vogelmann, 2006; Mauritsen et al., 2011), but TOA forcing is thought to be negligible.

7.4.2.2 Observational Evidence for Aerosol–Cloud Interactions

The physical basis of the albedo effect is fairly well understood, with research since AR4 generally reinforcing earlier work. Detailed *in situ* aircraft observations show that droplet concentrations observed just above the cloud base generally agree with those predicted based on the aerosol properties and updraught velocity observed below the cloud (e.g., Fountoukis et al., 2007). Vertical profiles of cloud droplet effective radius also agree with those predicted by models that take into account the effect of entrainment (Lu et al., 2008), although uncertainties still remain in estimating the shape of the droplet size distribution (Brenguier et al., 2011), and the degree of entrainment mixing within clouds.

At relatively low aerosol loading (AOD less than about 0.3) there is ample observational evidence for increases in aerosol resulting in an increase in droplet concentration and decrease in droplet size (for constant liquid water) but uncertainties remain regarding the magnitude of this effect, and its sensitivity to spatial averaging. Based on simple metrics, there is a large range of physically plausible responses, with aircraft measurements (e.g., Twohy et al., 2005; Lu et al., 2007, 2008;; Hegg et al., 2012) tending to show stronger responses than satellite-derived responses (McComiskey and Feingold, 2008; Nakajima and Schulz, 2009; Grandey and Stier, 2010). At high AOD and high aerosol concentration, droplet concentration tends to saturate (e.g., Verheggen et al., 2007) and, if the aerosol is absorbing, there may be reductions in droplet concentration and cloudiness (Koren et al., 2008). This absorbing effect originates from aerosol–radiation interactions and is therefore part of ERFari (Section 7.3.4.2). Negative correlation between AOD and ice particle size has also been documented in deep convective clouds (e.g., Sherwood, 2002; Jiang et al., 2008).

7.4.2.3 Advances in Process Level Understanding

At the heart of the albedo effect lie two fundamental issues. The first is aerosol activation and its sensitivity to aerosol and dynamical parameters. The primary controls on droplet concentration are the aerosol number concentration (particularly at diameters greater than about 60 nm) and cooling rate (proportional to updraught velocity). Aerosol size distribution can play an important role under high aerosol loadings, whereas aerosol composition tends to be much less important, except perhaps under very polluted conditions and low updraught velocities (e.g., Ervens et al., 2005; McFiggans et al., 2006). This is partially because aging tends to make particles more hygroscopic regardless of their initial composition, but also because more hygroscopic particles lead to faster water vapour uptake, which then lowers supersaturation, limiting the initial increase in activation.

The second issue is that the amount of energy reflected by a cloud system is a strong function of the amount of condensate. Simple arguments show that in a relative sense the amount of reflected energy is approximately two-and-a-half times more sensitive to changes in the liquid water path than to changes in droplet concentration (Boers and Mitchell, 1994). Because both of these parameters experience similar ranges of relative variability, the magnitude of aerosol–cloud related forcing rests mostly on dynamical factors such as turbulent strength and entrainment that control cloud condensate, and a few key aerosol parameters such as aerosol number concentration and size distribution, and to a much lesser extent, composition.

7.4.3 Forcing Associated with Adjustments in Liquid Clouds

7.4.3.1 The Physical Basis for Adjustments in Liquid Clouds

The adjustments giving rise to ERFaci are multi-faceted and are associated with both albedo and so-called 'lifetime' effects (Figure 7.3). However, this old nomenclature is misleading because it assumes a relationship between cloud lifetime and cloud amount or water content. Moreover, the effect of the aerosol on cloud amount may have nothing to do with cloud lifetime *per se* (e.g., Pincus and Baker, 1994).

The traditional view (Albrecht, 1989; Liou and Ou, 1989) has been that adjustment effects associated with aerosol–cloud–precipitation interactions will add to the initial albedo increase by increasing cloud amount. The chain of reasoning involves three steps: that droplet concentrations depend on the number of available CCN; that precipitation development is regulated by the droplet concentration; and that the development of precipitation reduces cloud amount (Stevens and Feingold, 2009). Of the three steps, the first has ample support in both observations and theory (Section 7.4.2.2). More problematic are the last two links in the chain of reasoning. Although increased droplet concentrations inhibit the initial development of precipitation (see Section 7.4.3.2.1), it is not clear that such an effect is sustained in an evolving cloud field. In the trade-cumulus regime, some modelling

studies suggest the opposite, with increased aerosol concentrations actually promoting the development of deeper clouds and invigorating precipitation (Stevens and Seifert, 2008; see discussion of similar responses in deep convective clouds in Section 7.6.4). Others have shown alternating cycles of larger *and* smaller cloud water in both aerosol-perturbed stratocumulus (Sandu et al., 2008) and trade cumulus (Lee et al., 2012), pointing to the important role of environmental adjustment. There exists limited unambiguous observational evidence (exceptions to be given below) to support the original hypothesised cloud-amount effects, which are often assumed to hold universally and have dominated GCM parameterization of aerosol–cloud interactions. GCMs lack the more nuanced responses suggested by recent work, which influences their ERFaci estimates.

7.4.3.2 Observational Evidence of Adjustments in Liquid Clouds

Since observed effects generally include both the albedo effect and the adjustments, with few if any means of observing only one or the other in isolation, in this section we discuss and interpret observational findings that reflect both effects. Stratocumulus and trade cumulus regimes are discussed separately.

7.4.3.2.1 Stratocumulus

The cloud albedo effect is best manifested in so-called ship tracks, which are bright lines of clouds behind ships. Many ship tracks are characterized by an increase in the droplet concentration resulting from the increase in aerosol number concentration and an absence of drizzle size drops, which leads to a decrease in the droplet radius and an increase in the cloud albedo (Durkee et al., 2000), all else equal. However, liquid water changes are the primary determinant of albedo changes (Section 7.4.2.3; Chen et al., 2012), therefore adjustments are key to understanding radiative response. Coakley and Walsh (2002) showed that cloud water responses can be either positive or negative. This is supported by more recent shiptrack analyses based on new satellite sensors (Christensen and Stephens, 2011): aerosol intrusions result in weak decreases in liquid water (–6%) in overcast clouds, but significant increases in liquid water (+39%) and increases in cloud fraction in precipitating, broken stratocumulus clouds. The global ERFaci of visible ship tracks has been estimated from satellite and found to be insignificant at about –0.5 mW m^{-2} (Schreier et al., 2007), although this analysis may not have identified all shiptracks. Some observational studies downwind of ship tracks have been unable to distinguish aerosol influences from meteorological influences on cloud microphysical or macrophysical properties (Peters et al., 2011a), although it is not clear whether their methodology had sufficient sensitivity to detect the aerosol effects. Notwithstanding evidence of shiptracks locally increasing the cloud fraction and albedo of broken cloud scenes quite significantly (e.g., Christensen and Stephens, 2011; Goren and Rosenfeld, 2012), their contribution to global ERFaci is thought to be small. These ship track results are consistent with satellite studies of the influence of long-term degassing of low-lying volcanic aerosol on stratocumulus, which point to smaller droplet sizes but ambiguous changes in cloud fraction and cloud water (Gasso, 2008). The lack of clear evidence for a global increase in cloud albedo from shiptracks and volcanic plumes should be borne in mind when considering geoengineering methods that rely on cloud modification (Section 7.7.2.2).

The development of precipitation in stratocumulus, whether due to aerosol or meteorological influence can, in some instances, change a highly reflective closed-cellular cloud field to a weakly reflective broken open-cellular field (Comstock et al., 2005; Stevens et al., 2005a; vanZanten et al., 2005; Sharon et al., 2006; Savic-Jovcic and Stevens, 2008; Wang and Feingold, 2009a). In some cases, compact regions (pockets) of open-cellular convection become surrounded by regions of closed-cellular convection. It is, however, noteworthy that observed precipitation rates can be similar in both open and closed-cell environments (Wood et al., 2011a). The lack of any apparent difference in the large-scale environment of the open cells, versus the surrounding closed cellular convection, suggests the potential for multiple equilibria (Baker and Charlson, 1990; Feingold et al., 2010). Therefore in the stratocumulus regime, the onset of precipitation due to a dearth of aerosol may lead to a chain of events that leads to a large-scale reduction of cloudiness in agreement with Liou and Ou (1989) and Albrecht (1989). The transition may be bidirectional: ship tracks passing through open-cell regions also appear to revert the cloud field to a closed-cell regime inducing a potentially strong ERFaci locally (Christensen and Stephens, 2011; Wang et al., 2011a; Goren and Rosenfeld, 2012).

7.4.3.2.2 Trade-cumulus

Precipitation from trade cumuli proves difficult to observe, as the clouds are small, and not easily observed by space-based remote sensing techniques (Stephens et al., 2008). Satellite remote sensing of trade cumuli influenced by aerosol associated with slow volcanic degassing points to smaller droplet size, decreased precipitation efficiency, increased cloud amount and higher cloud tops (Yuan et al., 2011). Other studies show that in the trade cumulus regime cloud amount tends to increase with precipitation amount: for example, processes that favour precipitation development also favour cloud development (Nuijens et al., 2009); precipitation-driven colliding outflows tend to regenerate clouds; and trade cumuli that support precipitation reach heights where wind shear increases cloud fraction (Zuidema et al., 2012).

While observationally based study of the microphysical aspects of aerosol–cloud interactions has a long history, more recent assessment of the ability of detailed models to reproduce the associated radiative effect in cumulus cloud fields is beginning to provide the important link between aerosol–cloud interactions and total RF (Schmidt et al., 2009).

7.4.3.3 Advances in Process Level Understanding

Central to ERFaci is the question of how susceptible is precipitation to droplet concentration, and by inference, to the available aerosol. Some studies point to the droplet effective radius as a threshold indicator of the onset of drizzle (Rosenfeld and Gutman, 1994; Gerber, 1996; Rosenfeld et al., 2012). Others focus on the sensitivity of the conversion of cloud water to rain water (i.e., autoconversion) to droplet concentration, which is usually in the form of (droplet concentration) to the power $-\alpha$. Both approaches indicate that from the microphysical standpoint, an increase in the aerosol suppresses rainfall. Models and theory show α ranging from ½ (Kostinski, 2008; Seifert and Stevens, 2010) to 2 (Khairoutdinov and Kogan, 2000), while observational studies suggest $\alpha = 1$ (approximately the inverse of drop concentration;

Pawlowska and Brenguier, 2003; Comstock et al., 2005; vanZanten et al., 2005). Note that thicker liquid clouds amplify rain via accretion of cloud droplets by raindrops, a process that is relatively insensitive to droplet concentration, and therefore to aerosol perturbations (e.g., Khairoutdinov and Kogan, 2000). The balance of evidence suggests that $\alpha = ½$ is more likely and that liquid water path (or cloud depth) has significantly more leverage over precipitation than does droplet concentration. Many GCMs assume a much stronger relationship between precipitation and cloud droplet number concentration (i.e., $\alpha = 2$) (Quaas et al., 2009).

Small-scale studies (Ackerman et al., 2004; Xue et al., 2008; Small et al., 2009) and satellite observations (Lebsock et al., 2008; Christensen and Stephens, 2011) tend to confirm two responses of the cloud liquid water to increasing aerosol. Under clean conditions when clouds are prone to precipitation, an increase in the aerosol tends to increase cloud amount as a result of aerosol suppression of precipitation. Under non-precipitating conditions, clouds tend to thin in response to increasing aerosol through a combination of droplet sedimentation (Bretherton et al., 2007) and evaporation–entrainment adjustments (e.g., Hill et al., 2009). Treatment of the subtlety of these responses and associated detail in small-scale cloud processes is not currently feasible in GCMs, although probability distribution function approaches are promising (Guo et al., 2010).

Since AR4, cloud resolving model simulation has begun to stress the importance of scale interactions when addressing aerosol–cloud interactions. Model domains on the order of 100 km allow mesoscale circulations to develop in response to changes in the aerosol. These dynamical responses may have a significant impact on cloud morphology and RF. Examples include the significant changes in cloud albedo associated with transitions between closed and open cellular states discussed above, and the cloud-free, downdraught 'shadows' that appear alongside ship tracks (Wang and Feingold, 2009b). Similar examples of large-scale changes in circulation associated with aerosol and associated influence on precipitation are discussed in Section 7.6.4. These underscore the large gap between our process level understanding of aerosol–cloud–precipitation interactions and the ability of GCMs to represent them.

7.4.3.4 Advances in and Insights Gained from Large-Scale Modelling Studies

Regional models are increasingly including representation of aerosol–cloud interactions using sophisticated microphysical models (Bangert et al., 2011; Yang et al., 2011; Seifert et al., 2012). Some of these regional models are operational weather forecast models that undergo routine evaluation. Yang et al. (2011) show improved simulations of stratocumulus fields when aerosol–cloud interactions are introduced. Regional models are increasingly being used to provide the meteorological context for satellite observations of aerosol–cloud interactions (see Section 7.4.1.4), with some (e.g., Painemal and Zuidema, 2010) suggesting that droplet concentration differences are driven primarily by synoptic scale influences rather than aerosol.

GCM studies that have explored sensitivity to autoconversion parameterization (Golaz et al., 2011) show that ERFaci can vary by 1 W m^{-2} depending on the parameterization. Elimination of the sensitivity of rain formation to the autoconversion process has begun to be considered in GCMs (Posselt and Lohmann, 2009). Wang et al. (2012) have used satellite observations to constrain autoconversion and find a reduction in ERFaci of about 33% relative to a standard GCM autoconversion parameterization. It is worth reiterating that these uncertainties are not necessarily associated with uncertainties in the physical process itself, but more so by the ability of a GCM to resolve the processes (see Section 7.4.1.3).

7.4.4 Adjustments in Cold Clouds

7.4.4.1 The Physical Basis for Adjustments in Cold Clouds

Mixed-phase clouds, containing both liquid water and ice particles, exist at temperatures between 0°C and –38°C. At warmer temperatures ice melts rapidly, whereas at colder temperatures liquid water freezes homogeneously. The formation of ice in mixed-phase clouds depends on heterogeneous freezing, initiated by IN (Section 7.3.3.4), which are typically solid or crystalline aerosol particles. In spite of their very low concentrations (on the order of 1 per litre), IN have an important influence on mixed-phase clouds. Mineral dust particles have been identified as good IN but far less is known about the IN ability of other aerosol types, and their preferred modes of nucleation. For example, the ice nucleating ability of BC particles remains controversial (Hoose and Möhler, 2012). Soluble matter can hinder glaciation by depressing the freezing temperature of supercooled drops to the point where homogeneous freezing occurs (e.g., Girard et al., 2004; Baker and Peter, 2008). Hence anthropogenic perturbations to the aerosol have the potential to affect glaciation, water and ice optical properties, and their radiative effect.

Because the equilibrium vapour pressure with respect to ice is lower than that with respect to liquid, the initiation of ice in a supercooled liquid cloud will cause vapour to diffuse rapidly toward ice particles at the expense of the liquid water (Wegener–Bergeron–Findeisen process; e.g., Schwarzenbock et al., 2001; Verheggen et al., 2007; Hudson et al., 2010). This favours the depositional growth of ice crystals, the largest of which may sediment away from the water-saturated region of the atmosphere, influencing the subsequent evolution of the cloud. Hence anthropogenic perturbations to the IN can influence the rate at which ice forms, which in turn may regulate cloud amount (Lohmann, 2002b; Storelvmo et al., 2011; see also Section 7.2.3.2.2), cloud optical properties and humidity near the tropopause.

Finally, formation of the ice phase releases latent heat to the environment (influencing cloud dynamics), and provides alternate, complex pathways for precipitation to develop (e.g., Zubler et al., 2011, and Section 7.6.4).

7.4.4.2 Observations of ERFaci in Deep Convective Clouds

As noted in Section 7.4.2.2, observations have demonstrated correlations between aerosol loading and ice crystal size but influence on cloud optical depth is unclear (e.g., Koren et al., 2005). Satellite remote sensing suggests that aerosol-related invigoration of deep convective clouds may generate more extensive anvils that radiate at cooler

temperatures, are optically thinner, and generate a positive contribution to ERFaci (Koren et al., 2010b). The global influence on ERFaci is unclear.

7.4.4.3 Observations of Aerosol Effects on Arctic Ice and Mixed-Phase Stratiform Clouds

Arctic mixed-phase clouds have received a great deal of attention since AR4, with major field programs conducted in 2004 (Verlinde et al., 2007) and 2008 (Jacob et al., 2010; Brock et al., 2011; McFarquhar et al., 2011), in addition to long-term monitoring at high northern latitude stations (e.g., Shupe et al., 2008) and analysis of earlier field experiments (Uttal et al., 2002). Mixed-phase Arctic clouds persist for extended periods of time (days and even weeks; Zuidema et al., 2005), in spite of the inherent instability of the ice–water mix (see also Section 7.2.3.2.2). In spite of their low concentrations, IN have an important influence on cloud persistence, with clouds tending to glaciate and disappear rapidly when IN concentrations are relatively high and/or updraught velocities too small to sustain a liquid water layer (e.g., Ovchinnikov et al., 2011). The details of the heterogeneous ice-nucleation mechanism remain controversial but there is increasing evidence that ice forms in Arctic stratus via the liquid phase (immersion freezing) so that the CCN population also plays an important role (de Boer et al., 2011; Lance et al., 2011). If ice indeed forms via the liquid phase this represents a self-regulating feedback that helps sustain the mixed-phase clouds: as ice forms, liquid water (the source of the ice) is depleted, which restricts further ice formation and competition for water vapour via the Wegener–Bergeron–Findeisen process (Morrison et al., 2012).

7.4.4.4 Advances in Process Level Understanding

Since AR4, research on ice-microphysical processes has been very active as evidenced by the abovementioned field experiments (Section 7.4.4.3). The persistence of some mixed-phase stratiform clouds has prompted efforts to explain this phenomenon in a theoretical framework (Korolev and Field, 2008). Predicting cloud persistence may require a high level of understanding of very detailed processes. For example, ice particle growth by vapour diffusion depends strongly on crystal shape (Harrington et al., 2009), the details of which may have similar relative influence on glaciation times to the representation of ice nucleation mechanism (Ervens et al., 2011b). A recent review (Morrison et al., 2012) discusses the myriad processes that create a resilient mixed-phase cloud system, invoking the ideas of 'buffering' seen in liquid clouds (Stevens and Feingold, 2009). Importantly, the Wegener–Bergeron–Findeisen process does not necessarily destabilize the cloud system, unless sufficient ice exists (Korolev, 2007). Bistability has also been observed in the mixed-phase Arctic cloud system; the resilient cloud state is sometimes interrupted by a cloud-free state (Stramler et al., 2011), but there is much uncertainty regarding the meteorological and microphysical conditions determining which of these states is preferred.

Significant effort has been expended on heterogeneous freezing parameterizations employed in cloud or larger-scale models. Some parameterizations are empirical (e.g., Lohmann and Diehl, 2006; Hoose et al., 2008; Phillips et al., 2008; Storelvmo et al., 2008a; DeMott et al., 2010; Gettelman et al., 2010; Salzmann et al., 2010), whereas others attempt to represent the processes explicitly (Jacobson, 2003) or ground the development of parameterizations in concepts derived from classical nucleation theory (Chen et al., 2008; Hoose et al., 2010b). The details of how these processes are treated have important implications for tropical anvils (Ekman et al., 2007; Fan et al., 2010).

Homogeneous ice nucleation in cirrus clouds (at temperatures lower than about –38°C) depends crucially on the cloud updraught velocity and hence the supersaturation with respect to ice. The onset relative humidities for nucleation have been parameterized using results of parcel model simulations (e.g., Sassen and Dodd, 1988; Barahona and Nenes, 2009), airborne measurements in cirrus or wave clouds (Heymsfield and Miloshevich, 1995; Heymsfield et al., 1998), extensions of classical homogeneous ice nucleation theory (Khvorostyanov and Sassen, 1998; Khvorostyanov and Curry, 2009) and data from laboratory measurements (e.g., Bertram et al., 2000; Koop et al., 2000; Mohler et al., 2003; Magee et al., 2006; Friedman et al., 2011). There is new evidence that although ice nucleation in cirrus has traditionally been regarded as homogeneous, the preferred freezing pathway may be heterogeneous because it occurs at lower onset relative humidities (or higher onset temperatures) than homogeneous nucleation (Jensen et al., 2010). The onset relative humidities (or temperatures) for heterogeneous nucleation depend on the type and size of the IN (Section 7.3.3.4).

Cloud resolving modeling of deep convective clouds points to the potential for aerosol-related changes in cirrus anvils (e.g., Morrison and Grabowski, 2011; van den Heever et al., 2011; Storer and van den Heever, 2013), but the physical mechanisms involved and their influence on ERFaci are poorly understood, and their global impact is unclear.

7.4.4.5 Advances in and Insights Gained from Large-Scale Modelling Studies

Since the AR4, mixed-phase and ice clouds have received significant attention, with effort on representation of both heterogeneous (mixed-phase clouds) and homogeneous (cirrus) freezing processes in GCMs (e.g., Lohmann and Kärcher, 2002; Storelvmo et al., 2008a). In GCMs the physics of cirrus clouds usually involves only ice-phase microphysical processes and is somewhat simpler than that of mixed-phase clouds. Nevertheless, representation of aerosol–cloud interactions in mixed-phase and ice clouds is considerably less advanced than that involving liquid-only clouds.

Our poor understanding of the climatology and lifecycle of aerosol particles that can serve as IN complicates attempts to assess what constitutes an anthropogenic perturbation to the IN population, let alone the effect of such a perturbation. BC can impact background (i.e., non contrail) cirrus by affecting ice nucleation properties but the effect remains uncertain (Kärcher et al., 2007). The numerous GCM studies that have evaluated ERFaci for ice clouds are summarised in Section 7.5.4.

7.4.5 Synthesis on Aerosol–Cloud Interactions

Earlier assessments considered the radiative implications of aerosol–cloud interactions as two complementary processes—albedo and lifetime effects—that together amplify forcing. Since then the complexity

of cloud system responses to aerosol perturbations has become more fully appreciated. Recent work at the process scale has identified compensating adjustments that make the system less susceptible to perturbation than might have been expected based on the earlier albedo and lifetime effects. Increases in the aerosol can therefore result in either an increase or a decrease in aerosol–cloud related forcing depending on the particular environmental conditions. Because many current GCMs do not include the possibility of compensating effects that are not mediated by the large-scale state, there are grounds for expecting these models to overestimate the magnitude of ERFaci. Nevertheless it is also possible that poorly understood and unrepresented interactions could cause real ERFaci to differ in either direction from that predicted by current models. Forcing estimates are discussed in Section 7.5.3.

7.4.6 Impact of Cosmic Rays on Aerosols and Clouds

Many studies have reported observations that link solar activity to particular aspects of the climate system (e.g., Bond et al., 2001; Dengel et al., 2009; Eichler et al., 2009). Various mechanisms have been proposed that could amplify relatively small variations in total solar irradiance, such as changes in stratospheric and tropospheric circulation induced by changes in the spectral solar irradiance or an effect of the flux of cosmic rays on clouds. We focus in this subsection on the latter hypothesis while Box 10.2 discusses solar influences on the climate system more generally.

Solar activity variations influence the strength and three-dimensional structure of the heliosphere. High solar activity increases the deflection of low energy cosmic rays, which reduces the flux of cosmic rays impinging upon the Earth's atmosphere. It has been suggested that the ionization caused by cosmic rays in the troposphere has an impact on aerosols and clouds (e.g., Dickinson, 1975; Kirkby, 2007). This subsection assesses studies that either seek to establish a causal relationship between cosmic rays and aerosols or clouds by examining empirical correlations, or test one of the physical mechanisms that have been put forward to account for such a relationship.

7.4.6.1 Observed Correlations Between Cosmic Rays and Properties of Aerosols and Clouds

Correlation between the cosmic ray flux and cloud properties has been examined for decadal variations induced by the 11-year solar cycle, shorter variations associated with the quasi-periodic oscillation in solar activity centred on 1.68 years, or sudden and large variations known as Forbush decrease events. It should be noted that long-term variations in cloud properties are difficult to detect (Section 2.5.6) while short-term variations may be difficult to attribute to a particular cause. Moreover, the cosmic ray flux co-varies with other solar parameters such as solar and UV irradiance. This makes any attribution of cloud changes to the cosmic ray flux problematic (Laken et al., 2011).

Some studies have shown co-variation between the cosmic ray flux and low-level cloud cover using global satellite data over periods of typically 5 to 10 years (Marsh and Svensmark, 2000; Pallé Bagó and Butler, 2000). Such correlations have not proved to be robust when extending the time period under consideration (Agee et al., 2012), and restricting the analysis to particular cloud types (Kernthaler et al., 1999) or locations (Udelhofen and Cess, 2001; Usoskin and Kovaltsov, 2008). The purported correlations have also been attributed to ENSO variability (Farrar, 2000; Laken et al., 2012) and artefacts of the satellite data cannot be ruled out (Pallé, 2005). Statistically significant (but weak) correlations between the diffuse fraction of surface solar radiation and the cosmic ray flux have been found at some locations in the UK over the 1951–2000 period (Harrison and Stephenson, 2006). Harrison (2008) also found a unique 1.68-year periodicity in surface radiation for two different UK sites between 1978 and 1990, potentially indicative of a cosmic ray effect of the same periodicity. Svensmark et al. (2009) found large global reductions in the aerosol Ångström exponent, liquid water path, and cloud cover after large Forbush decreases, but these results were not corroborated by other studies that found no statistically significant links between the cosmic ray flux and clouds at the global scale (Čalogović et al., 2010; Laken and Čalogović, 2011). Although some studies found statistically significant correlations between the cosmic ray flux and cloudiness at the regional scale (Laken et al., 2010; Rohs et al., 2010), these correlations were generally weak, cloud changes were small, and the results were sensitive to how the Forbush events were selected and composited (Kristjánsson et al., 2008; Laken et al., 2009).

7.4.6.2 Physical Mechanisms Linking Cosmic Rays to Cloudiness

The most widely studied mechanism proposed to explain the possible influence of the cosmic ray flux on cloudiness is the 'ion-aerosol clear air' mechanism, in which atmospheric ions produced by cosmic rays facilitate aerosol nucleation and growth ultimately impacting CCN concentrations and cloud properties (Carslaw et al., 2002; Usoskin and Kovaltsov, 2008). The variability in atmospheric ionization rates due to changes in cosmic ray flux can be considered relatively well quantified (Bazilevskaya et al., 2008), whereas resulting changes in aerosol nucleation rates are very poorly known (Enghoff and Svensmark, 2008; Kazil et al., 2008). Laboratory experiments indicate that ionization induced by cosmic rays enhances nucleation rates under middle and upper tropospheric conditions, but not necessarily so in the continental boundary layer (Kirkby et al., 2011). Field measurements qualitatively support this view but cannot provide any firm conclusion due to the scarcity and other limitations of free-troposphere measurements (Arnold, 2006; Mirme et al., 2010), and due to difficulties in separating nucleation induced by cosmic rays from other nucleation pathways in the continental boundary layer (Hirsikko et al., 2011). Based on surface aerosol measurements at one site, Kulmala et al. (2010) found no connection between the cosmic ray flux and new particle formation or any other aerosol property over a solar cycle (1996–2008), although particles nucleated in the free troposphere are known to contribute to particle number and CCN concentrations in the boundary layer (Merikanto et al., 2009). Our understanding of the 'ion-aerosol clear air' mechanism as a whole relies on a few model investigations that simulate changes in cosmic ray flux over a solar cycle (Pierce and Adams, 2009b; Snow-Kropla et al., 2011; Kazil et al., 2012) or during strong Forbush decreases (Bondo et al., 2010; Snow-Kropla et al., 2011; Dunne et al., 2012). Changes in CCN concentrations due to variations in the cosmic ray flux appear too weak to cause a significant radiative effect because the aerosol system is insensitive to a small change in the nucleation rate in the presence of pre-existing aerosols (see also Section 7.3.2.2).

A second pathway linking the cosmic ray flux to cloudiness has been proposed through the global electric circuit. A small direct current is able to flow vertically between the ionosphere and the Earth's surface over fair-weather regions because of cosmic-ray-induced atmospheric ionization. Charge can accumulate at the upper and lower cloud boundaries as a result of the effective scavenging of ions by cloud droplets (Tinsley, 2008). This creates conductivity gradients at the cloud edges (Nicoll and Harrison, 2010), and may influence droplet–droplet collisions (Khain et al., 2004), cloud droplet–particle collisions (Tinsley, 2008) and cloud droplet formation processes (Harrison and Ambaum, 2008). These microphysical effects may potentially influence cloud properties both directly and indirectly. Although Harrison and Ambaum (2010) observed a small reduction in downward longwave radiation that they associated with variations in surface current density, supporting observations are extremely limited. Our current understanding of the relationship between cloud properties and the global electric circuit remains very low, and there is no evidence yet that associated cloud processes could be of climatic significance.

7.4.6.3 Synthesis

Correlations between cosmic ray flux and observed aerosol or cloud properties are weak and local at best, and do not prove to be robust on the regional or global scale. Although there is some evidence that ionization from cosmic rays may enhance aerosol nucleation in the free troposphere, there is *medium evidence* and *high agreement* that the cosmic ray-ionization mechanism is too weak to influence global concentrations of CCN or droplets or their change over the last century or during a solar cycle in any climatically significant way.

7.5 Radiative Forcing and Effective Radiative Forcing by Anthropogenic Aerosols

7.5.1 Introduction and Summary of AR4

In this section, aerosol forcing estimates are synthesized and updated from AR4. As depicted in Figure 7.3, RF refers to the radiative forcing due to either aerosol–radiation interactions (ari), formerly known as the direct aerosol forcing, or aerosol–cloud interactions (aci), formerly known as the first indirect aerosol forcing or cloud albedo effect in AR4. ERF refers to the effective radiative forcing and is typically estimated from experiments with fixed SSTs (see Sections 7.1.3 and 8.1). It includes rapid adjustments, such as changes to the cloud lifetime, cloud altitude, changes in lapse rate due to absorbing aerosols and aerosol microphysical effects on mixed-phase, ice and convective clouds.

Chapter 2 of AR4 (Forster et al., 2007) assessed RFari to be –0.5 ± 0.4 W m^{-2} and broke this down into components associated with several species. Land albedo changes associated with BC on snow were assessed to be +0.1 ± 0.1 W m^{-2}. The RFaci was assessed to be –0.70 W m^{-2} with a –1.8 to –0.3 W m^{-2} uncertainty range. These uncertainty estimates were based on a combination of model results and observations from remote sensing. The semi-direct effect and other aerosol indirect effects were assessed in Chapter 7 of AR4 (Denman et al., 2007) to contribute additional uncertainty. The combined total aerosol forcing was given as two distinct ranges: –2.3 to –0.2 W m^{-2} from models and a –1.7 to –0.1 W m^{-2} range from inverse estimates.

As discussed in Section 7.4, it is inherently difficult to separate RFaci from subsequent rapid cloud adjustments either in observations or model calculations (e.g., George and Wood, 2010; Lohmann et al., 2010; Mauger and Norris, 2010; Painemal and Zuidema, 2010). For this reason estimates of RFaci are of limited interest and are not assessed in this report. This chapter estimates RFari, ERFari, and ERFari+aci based purely on *a priori* approaches, and calculates ERFaci as the residual between ERFari+aci and ERFari assuming the two effects are additive. Inverse studies that estimate ERFari+aci from the observed rate of planetary energy uptake and estimates of climate feedbacks and other RFs are discussed in Section 10.8.

For consistency with AR4 and Chapter 8 of this Report, all quoted ranges represent a 5 to 95% uncertainty range unless otherwise stated, and we evaluate the forcings between 1750 and approximately 2010. The reference year of 1750 is chosen to represent pre-industrial times, so changes since then broadly represent the anthropogenic effect on climate, although for several aerosol species (such as biomass burning) this does not quite equate to the anthropogenic effect as emissions started to be influenced by humans before the Industrial Revolution. Many studies estimate aerosol forcings between 1850 and the present day and any conversion to a forcing between 1750 and the present day increases the uncertainty (Bellouin et al., 2008). This section principally discusses global forcing estimates and attributes them to aerosol species. Chapter 8 discusses regional forcings and additionally attributes aerosol forcing to emission sources.

7.5.2 Estimates of Radiative Forcing and Effective Radiative Forcing from Aerosol–Radiation Interactions

Building on our understanding of aerosol processes and their radiative effects (Section 7.3), this subsection assesses RFari and ERFari, but also the forcings from absorbing aerosol (BC and dust) on snow and ice.

7.5.2.1 Radiative Forcing and Effective Radiative Forcing from All Aerosols

Observations can give useful constraints to aspects of the global RFari but cannot measure it directly (Section 7.3.4; Anderson et al., 2005; Kahn, 2012). Remote sensing observations, *in situ* measurements of fine-mode aerosol properties and a better knowledge of bulk aerosol optical properties make the estimate of total RFari more robust than the RF for individual species (see Forster et al., 2007). Estimates of RFari are either taken from global aerosol models directly (Schulz et al., 2009; Myhre et al., 2013) or based mostly on observations, but using supplemental information from models (e.g., Myhre, 2009; Loeb and Su, 2010; Su et al., 2013). A number of studies (Bellouin et al., 2008; Zhao et al., 2008b, 2011; Myhre, 2009) have improved aspects of the satellite-based RFari estimate over those quoted in AR4. Of these, only Myhre (2009) make the necessary adjustments to the observations to account for forcing in cloudy regions and pre-industrial concentrations to estimate a RFari of –0.3 ± 0.2 W m^{-2}.

A second phase of AeroCom model results gives an RFari estimate of –0.35 W m^{-2}, with a model range of about –0.60 to –0.13 W m^{-2}, after their forcings for 1850–2000 have been scaled by emissions to represent 1750–2010 changes (Myhre et al., 2013). Figure 7.17 shows the zonal mean total RFari for AeroCom phase II models for 1850–2000. Robust features are the maximum negative RF around 10°N to 50°N, at latitudes of highest aerosol concentrations, and a positive RF at higher latitudes due to the higher surface albedo there.

For observationally based estimates, a variety of factors are important in constraining the radiative effect of aerosols (McComiskey et al., 2008; Loeb and Su, 2010; Kahn, 2012). Particularly important are the single scattering albedo (especially over land or above clouds) and the AOD (see Section 7.3.4.1). Errors in remotely sensed, retrieved AOD can be 0.05 or larger over land (Remer et al., 2005; Kahn et al., 2010; Levy et al., 2010; Kahn, 2012). Loeb and Su (2010) found that the total uncertainty in forcing was dominated by the uncertainty in single scattering albedo, using single scattering albedo errors of ± 0.06 over ocean and ± 0.03 over land from Dubovik et al. (2000), and assuming errors can be added in quadrature. These retrieval uncertainties could lead to a 0.5 to 1.0 W m^{-2} uncertainty in RFari (Loeb and Su, 2010). However, model sensitivity studies and reanalyses can provide additional constraints leading to a reduced error estimate. Ma et al. (2012b) performed a sensitivity study in one model, finding a best estimate of RFari of –0.41 W m^{-2} with an asymmetrical uncertainty range of –0.61 to –0.08 W m^{-2}, with BC particle size and mixing state having the largest effect of the parameters investigated. In models, assumptions about surface albedo, background cloud distribution and radiative transfer contribute a relative standard deviation of 39% (Stier et al., 2013). Bellouin et al. (2013) quantified uncertainties in RFari using reanalysis data that combined MODIS satellite data over oceans with the global coverage of their model. This approach broke down the uncertainty in aerosol properties into a local and a regional error to find a RFari standard deviation of 0.3 W m^{-2}, not accounting for uncertainty in the pre-industrial reference. When cloudy-sky and pre-industrial corrections were applied an RFari best estimate of –0.4 W m^{-2} was suggested.

The overall forcing uncertainty in RFari consists of the uncertainty in the distribution of aerosol amount, composition and radiative properties (Loeb and Su, 2010; Myhre et al., 2013), the uncertainty in radiative transfer (Randles et al., 2013) and the uncertainty owing to the dependence of the forcing calculation on other uncertain parameters, such as clouds or surface albedos (Stier et al., 2013). To derive a best estimate and range for RFari we combine modelling and observationally based studies. The best estimate is taken as –0.35 W m^{-2}. This is the same as the AeroCom II model estimate, and also the average of the Myhre (2009) observationally based estimate (–0.3 W m^{-2}) and the Bellouin et al. (2013) reanalysis estimate (–0.4 W m^{-2}). Models probably underestimate the positive RFari from BC and the negative forcing from OA aerosol (see Section 7.5.2.2), and currently there is no evidence that one of these opposing biases dominates over the other. The 5 to 95% range of RFari adopted in this assessment employs the Bellouin et al. (2013) uncertainty to account for retrieval error in observational quantities when constrained by global models, giving an uncertainty estimate of ±0.49 W m^{-2}. This is at the low end of the uncertainty analysis of Loeb and Su (2010). However, our uncertainty is partly based on models, and to account for this aspect, it is combined in quadrature with a ±0.1 W m^{-2} uncertainty from non-aerosol related parameters following Stier et al. (2013). This gives an assessed RFari of –0.35 ± 0.5 W m^{-2}. This is a larger range than that exhibited by the AeroCom II models. It is also a smaller magnitude but slightly larger range than in AR4, with a more positive upper bound. This more positive upper bound can be justified by the sensitivity to BC aerosol (Ma et al., 2012b and Section 7.5.2.3). Despite the larger range, there is increased confidence in this assessment due to dedicated modelling sensitivity studies, more robust observationally based estimates and their better agreement with models.

ERFari adds the radiative effects from rapid adjustments onto RFari. Studies have evaluated the rapid adjustments separately as a semi-direct effect (see Section 7.3.4.2) and/or the ERFari has been directly evaluated. Rapid adjustments are caused principally by cloud changes. There is *high confidence* that the local heating caused by absorbing aerosols can alter clouds. However, there is *low confidence* in determining the sign and magnitude of the rapid adjustments at the global scale as current models differ in their responses and are known to inadequately represent some of the important relevant cloud processes (see Section 7.3.4). Existing estimates of ERFari nevertheless rely on such global models. Five GCMs were analysed for RFari and ERFari in Lohmann et al. (2010). Their rapid adjustments ranged from –0.3 to +0.1 W m^{-2}. In a further study, Takemura and Uchida (2011) found a rapid adjustment of +0.06 W m^{-2}. The sensitivity analysis of Ghan et al. (2012) found a –0.1 to +0.1 W m^{-2} range over model variants, where an improved aging of the mixing state led to small negative rapid adjustment of around –0.1 W m^{-2}. Bond et al. (2013) assessed scaled RF and efficacy estimates from seven earlier studies focusing on

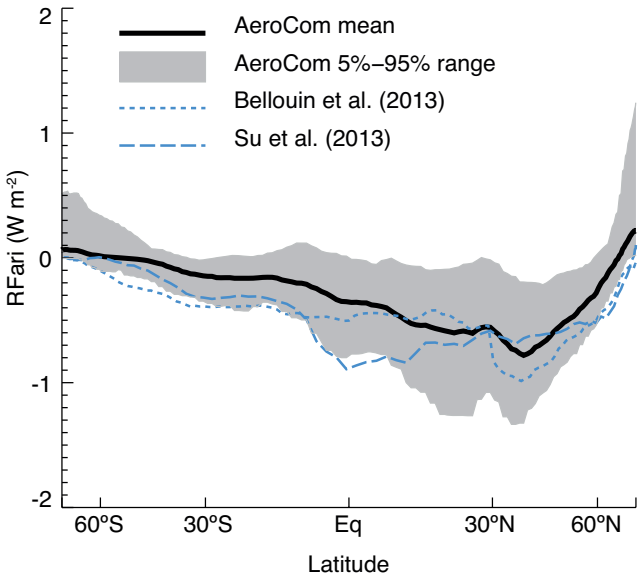

Figure 7.17 | Annual zonal mean top of the atmosphere radiative forcing due to aerosol–radiation interactions (RFari, in W m^{-2}) due to all anthropogenic aerosols from the different AeroCom II models. No adjustment for missing species in certain models has been applied. The multi-model mean and 5th to 95th percentile range from AeroCom II models (Myhre et al., 2013) are shown with a black solid line and grey envelope. The estimates from Bellouin et al. (2013) and Su et al. (2013) are shown with dotted and dashed lines, respectively. The forcings are for the 1850 to 2000 period. See Supplementary Material for a figure with labelled individual AeroCom II model estimates.

BC and found a range of rapid adjustments between –0.2 and –0.01 W m^{-2}. There is a potential additional rapid adjustment term from the effect of cloud drop inclusions (see Section 7.3.4.2). Based on Ghan et al. (2012) and Jacobson (2012), Bond et al. (2013) estimate an additional ERFari term of +0.2 W m^{-2}, with an uncertainty range of –0.1 to +0.9 W m^{-2}; however there is *very low confidence* in the sign or magnitude of this effect and we do not include it in our assessment. Overall a best estimate for the rapid adjustment is taken to be –0.1 W m^{-2}, with a 5 to 95% uncertainty range of –0.3 to +0.1 W m^{-2}. The best estimate is based on Ghan et al. (2012) and the range on Lohmann et al. (2010). The uncertainties are added in quadrature to the estimate of RFari and rounded to give an overall assessment for ERFari of –0.45 ± 0.5 W m^{-2}.

7.5.2.2 Radiative Forcing by Species

AeroCom II studies have calculated aerosol distributions using 1850 and 2000 simulations with the same meteorology to isolate RFari for individual aerosol types (sulphate, BC fossil-fuel plus biofuel, OA fossil-fuel and biofuel, biomass burning or BB, SOA, nitrate). Many of these models account for internal mixing, so that partitioning RFari by species is not straightforward, and different modelling groups adopt different techniques (Myhre et al., 2013). Note also that due to internal mixing of aerosol types the total RFari is not necessarily the sum of the RFari from different types (Ocko et al., 2012). Unless otherwise noted in the text below, the best estimate and 5 to 95% ranges for individual types quoted in Figure 7.18 are solely based on the AeroCom II range (Myhre et al., 2013) and the estimates have been scaled by emissions to derive 1750–2010 RFari values. Note that although global numbers are presented here, these RF estimates all exhibit large regional variations, and individual aerosol species can contribute significantly to regional climate change despite rather small RF estimates (e.g., Wang et al., 2010b).

For sulphate, AeroCom II models give a RF median and 5 to 95% uncertainty range of –0.31 (–0.58 to –0.11) W m^{-2} for the 1850–2000 period, and –0.34 (–0.61 to –0.13) W m^{-2} for the 1750–2010 period. This estimate and uncertainty range are consistent with the AR4 estimate of –0.4 ± 0.2 W m^{-2}, which is retained as the best estimate for AR5.

RF from BC is evaluated in different ways in the literature. The BC RF in this report is from fossil fuel and biofuel sources, while open burning sources are attributed separately to the biomass-burning aerosol, which also includes other organic species (see Section 7.3.2). BC can also affect clouds and surface albedo (see Sections 7.5.2.3 and Chapter 8). Here we only isolate the fossil fuel and biofuel RFari attributable to BC over 1750–2010. Two comprehensive studies have quantified the BC RFari and derive different central estimates and uncertainty ranges. Myhre et al. (2013) quantify RF over 1850–2000 in the AeroCom II generation of models and scale these up using emissions to derive an RF estimate over 1750–2010 of +0.23 (+0.06 to +0.48) W m^{-2} for fossil fuel and biofuel emissions. Bond et al. (2013) employ an observationally weighted scaling of an earlier generation of AeroCom models, regionally scaling BC absorption to match absorption AOD as retrieved at available AERONET sites. They derive a RF of +0.51 (+0.06 to +0.91) W m^{-2} for fossil fuel and biofuel sources. There are known biases in BC RF estimates from aerosol models. BC concentrations are underestimated near source regions, especially in Asia, but overestimated in remote regions and at altitude (Figure 7.15). Models also probably underestimate the mass absorption cross-section probably because enhanced absorption due to internal mixing is insufficiently accounted for (see Section 7.3.3.2). Together these biases are expected to cause the modelled BC RF to be underestimated. The Bond et al. estimate accounted for these biases by scaling model results. However, there are a number of methodological difficulties associated with the absorption AOD retrieval from sunphotometer retrievals (see Section 7.3.3.2), the attribution of absorption AOD to BC, and the distribution and representativeness of AERONET stations for constraining global and relatively coarse-resolution models. Absorption by OA (see Section 7.3.3), which may amount to 20% of fine-mode aerosol absorption (Chung et al., 2012), is included into the BC RF estimate in Bond et al. but is now treated separately in most AeroCom II models, some of which have a global absorption AOD close to the Bond et al. estimate. We use our expert judgement here to adopt a BC RF estimate that is halfway between the two estimates and has a wider uncertainty range from combining distributions. This gives a BC RF estimate from fossil fuel and biofuel of +0.4 (+0.05 to +0.8) W m^{-2}.

The AeroCom II estimate of the SOA RFari is –0.03 (–0.27 to –0.02) W m^{-2} and the primary OA from fossil fuel and biofuel estimate is –0.05 (–0.09 to –0.02) W m^{-2}. An intercomparison of current chemistry–climate models found two models outside of this range for SOA RFari, with one model exhibiting a significant positive forcing from land use and cover changes influencing biogenic emissions (Shindell et al., 2013). We therefore adjust the upper end of the range to account for this, giving an SOA RFari estimate of –0.03 (–0.27 to +0.20) W m^{-2}. Our assessment also scales the AeroComII estimate of the primary OA from fossil fuel and biofuel by 1.74 to –0.09 (–0.16 to –0.03) W m^{-2} to allow for the underestimate of emissions identified in Bond et al. (2013). For OA from natural burning, and for SOA, the natural radiative effects can be an order of magnitude larger than the RF (see Sections 7.3.2 and 7.3.4, and O'Donnell et al., 2011) and they could thus contribute to climate feedback (see Section 7.3.5).

The RFari from biomass burning includes both BC and OA species that contribute RFari of opposite sign, giving a net RFari close to zero (Bond et al., 2013; Myhre et al., 2013). The AeroCom II models give a 1750–2010 RFari of 0.00 (–0.08 to +0.07) W m^{-2}, and an estimate of +0.0 (–0.2 to +0.2) W m^{-2} is adopted in this assessment, doubling the model uncertainty range to account for a probable underestimate of their emissions (Bond et al., 2013). Combining information in Samset et al. (2013) and Myhre et al. (2013) would give a BC RFari contribution from biomass burning of slightly less than +0.1 W m^{-2} over 1850–2000 from the models. However, this ignores a significant contribution expected before 1850 and the probable underestimate in emissions. Our assessment therefore solely relies on Bond et al. (2013), giving an estimate of +0.2 (+0.03 to +0.4) W m^{-2} for the 1750–2010 BC contribution to the biomass burning RFari. This is a 50% larger forcing than the earlier generation of AeroCom models found (Schulz et al., 2006). Note that we also expect an OA RFari of the same magnitude with opposite sign.

The AeroCom II RF estimate for nitrate aerosol gives an RFari of –0.11 (–0.17 to –0.03) W m^{-2}, but comprises a relatively large 1850 to 1750 correction term. In these models ammonium aerosol is included within the sulphate and nitrate estimates. An intercomparison of current

chemistry–climate models found an RF range of –0.41 to –0.03 W m^{-2} over 1850–2000. Some of the models with strong RF did not exhibit obvious biases, whereas others did (Shindell et al., 2013). These sets of estimates are in good agreement with earlier estimates (e.g., Adams et al., 2001; Bauer et al., 2007; Myhre et al., 2009). Our assessment of the RFari from nitrate aerosol is –0.11 (–0.3 to –0.03) W m^{-2}. This is based on AeroCom II with an increased lower bound.

Anthropogenic sources of mineral aerosols can result from changes in land use and water use or climate change. Estimates of the RF from anthropogenic mineral aerosols are highly uncertain, because natural and anthropogenic sources of mineral aerosols are often located close to each other (Mahowald et al., 2009; Ginoux et al., 2012b). Using a compilation of observations of dust records over the 20th century with model simulations, Mahowald et al. (2010) deduced a 1750–2000 change in mineral aerosol RFari including both natural and anthropogenic changes of –0.14 ± 0.11 W m^{-2}. This is consistent within the AR4 estimate of –0.1 ± 0.2 W m^{-2} (Forster et al., 2007) which is retained here. Note that part of the dust RF could be due to feedback processes (see Section 7.3.5).

Overall the species breakdown of RFari is less certain than the total RFari. Fossil fuel and biofuel emissions contribute to RFari via sulphate aerosol –0.4 (–0.6 to –0.2) W m^{-2}; black carbon aerosol +0.4 (+0.05 to +0.8) W m^{-2}; and primary and secondary organic aerosol –0.12 (–0.4 to +0.1) W m^{-2} (adding uncertainties in quadrature). Additional RFari contributions are via biomass burning emissions, where black carbon and organic aerosol changes offset each other to give an estimate of +0.0 (–0.2 to +0.2) W m^{-2}; nitrate aerosol –0.11 (–0.3 to –0.03) W m^{-2}; and a contribution from mineral dust of –0.1 (–0.3 to +0.1) W m^{-2} that may not be entirely anthropogenic in origin. The sum of the RFari from these species agrees with, but is slightly weaker than, the best estimate of the better-constrained total RFari.

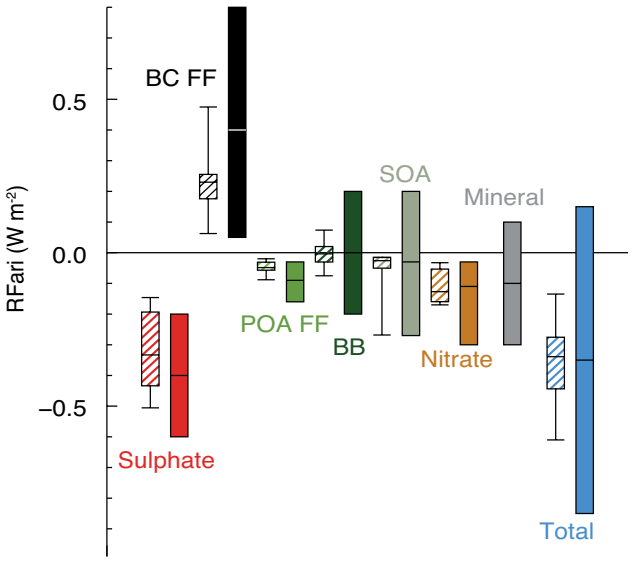

Figure 7.18 | Annual mean top of the atmosphere radiative forcing due to aerosol–radiation interactions (RFari, in W m^{-2}) due to different anthropogenic aerosol types, for the 1750–2010 period. Hatched whisker boxes show median (line), 5th to 95th percentile ranges (box) and min/max values (whiskers) from AeroCom II models (Myhre et al., 2013) corrected for the 1750–2010 period. Solid coloured boxes show the AR5 best estimates and 90% uncertainty ranges. BC FF is for black carbon from fossil fuel and biofuel, POA FF is for primary organic aerosol from fossil fuel and biofuel, BB is for biomass burning aerosols and SOA is for secondary organic aerosols.

7.5.2.3 Absorbing Aerosol on Snow and Sea Ice

Forster et al. (2007) estimated the RF for surface albedo changes from BC deposited on snow to be +0.10 ± 0.10 W m^{-2}, with a low level of understanding, based largely on studies from Hansen and Nazarenko (2004) and Jacobson (2004). Since AR4, observations of BC in snow have been conducted using several different measurement techniques (e.g., McConnell et al., 2007; Forsström et al., 2009; Ming et al., 2009; Xu et al., 2009; Doherty et al., 2010; Huang et al., 2011; Kaspari et al., 2011), providing data with which to constrain models. Laboratory measurements have confirmed the albedo reduction due to BC in snow (Hadley and Kirchstetter, 2012). The albedo effects of non-BC constituents have also been investigated but not rigorously quantified. Remote sensing can inform on snow impurity content in some highly polluted regions. However, it cannot be used to infer global anthropogenic RF because of numerous detection challenges (Warren, 2013).

Global modelling studies since AR4 have quantified present-day radiative effects from BC on snow of +0.01 to +0.08 W m^{-2} (Flanner et al., 2007, 2009; Hansen et al., 2007; Koch et al., 2009a; Rypdal et al., 2009; Skeie et al., 2011; Wang et al., 2011c; Lee et al., 2013). These studies apply different BC emission inventories and atmospheric aerosol representations, include forcing from different combinations of terrestrial snow, sea ice, and snow on sea ice, and some include different rapid adjustment effects such as snow grain size evolution and melt-induced accumulation of impurities at the snow surface, observed on Tibetan glaciers (Xu et al., 2012) and in Arctic snow (Doherty et al., 2013). The forcing operates mostly on terrestrial snow and is largest during March to May, when boreal snow and ice are exposed to strong insolation (Flanner et al., 2007).

All climate modelling studies find that the Arctic warms in response to snow and sea ice forcing. In addition, estimates of the change in global mean surface temperature per unit forcing are 1.7 to 4.5 times greater for snow and sea ice forcing than for CO_2 forcing (Hansen and Nazarenko, 2004; Hansen et al., 2005; Flanner et al., 2007; Flanner et al., 2009; Bellouin and Boucher, 2010). The Koch et al. (2009a) estimate is not included in this range owing to the lack of a clear signal in their study. The greater response of global mean temperature occurs primarily because all of the forcing energy is deposited directly into the cryosphere, whose evolution drives a positive albedo feedback on climate. Key sources of forcing uncertainty include BC concentrations in snow and ice, BC mixing state and optical properties, snow and ice coverage and patchiness, co-presence of other light-absorbing particles in the snow pack, snow effective grain size and its influence on albedo perturbation, the masking of snow surfaces by clouds and vegetation and the accumulation of BC at the top of snowpack caused by melting and sublimation. Bond et al. (2013) derive a 1750–2010 snow and sea ice RF estimate of +0.046 (+0.015 to +0.094) W m^{-2} for BC by (1) considering forcing ranges from all relevant global studies, (2) accounting for biases caused by (a) modelled Arctic BC-in-snow concentrations using measurements from Doherty et al. (2010), and (b) excluding mineral dust, which reduces BC forcing by approximately 20%, (3) combining in quadrature individual uncertainty terms from Flanner et al. (2007)

plus that originating from the co-presence of dust, and (4) scaling the present-day radiative contributions from BB, biofuel and fossil fuel BC emissions according to their 1750–2010 changes. Note that this RF estimate allows for some rapid adjustments in the snowpack but is not a full ERF as it does not account for adjustments in the atmosphere. For this RF, we adopt an estimate of +0.04 (+0.02 to +0.09) W m^{-2} and note that the surface temperature change is roughly three (two to four) times more responsive to this RF relative to CO_2.

7.5.3 Estimate of Effective Radiative Forcing from Combined Aerosol–Radiation and Aerosol–Cloud Interactions

In addition to ERFari, there are changes due to aerosol–cloud interactions (ERFaci). Because of nonlinearities in forcings and rapid adjustments, the total effective forcing ERFari+aci does not necessarily equal the sum of the ERFari and ERFaci calculated separately. Moreover a strict separation is often difficult in either state of the art models or observations. Therefore we first assess ERFari+aci and postpone our assessment of ERFaci to Section 7.5.4. For similar reasons, we focus primarily on ERF rather than RF.

ERFari+aci is defined as the change in the net radiation at the TOA from pre-industrial to present day. Climate model estimates of ERFari+aci in the literature differ for a number of reasons. (1) The reference years for pre-industrial and present-day conditions vary between estimates. Studies can use 1750, 1850, or 1890 for pre-industrial; early estimates of ERFari+aci used present-day emissions for 1985, whereas most newer estimates use emissions for the year 2000. (2) The processes they include also differ: aerosol–cloud interactions in large-scale liquid stratiform clouds are typically included, but studies can also include aerosol–cloud interactions for mixed-phase, convective clouds and/or cirrus clouds. (3) The way in which ERFari+aci is calculated can also differ between models, with some earlier studies only reporting the change in shortwave radiation. Changes in longwave radiation arise from rapid adjustments, or from aerosol–cloud interactions involving mixed-phase or ice clouds (e.g., Storelvmo et al., 2008b, 2010; Ghan et al., 2012), and tend to partially offset changes in shortwave radiation. In the estimates discussed below and those shown in Figure 7.19, we refer to estimates of the change in net (shortwave plus longwave) TOA radiation whenever possible, but report changes in shortwave radiation when changes in net radiation are not available. While this mostly affects earlier studies, the subset of models that we concentrate on all include both shortwave and longwave radiative effects. However, for the sake of comparison, the satellite studies must be adjusted to account for missing longwave contributions as explained below.

Early GCM estimates of ERFari+aci only included aerosol–cloud interactions in liquid phase stratiform clouds; some of these were already considered in AR4. Grouping these early estimates with similar (liquid phase only) estimates from publications since the AR4 yields a median value of ERFari+aci of –1.5 W m^{-2} with a 5 to 95% range between –2.4 and –0.6 W m^{-2} (Figure 7.19). In those studies that attempt a more complete representation of aerosol–cloud interactions, by including aerosol–cloud interactions in mixed-phase and/or convective cloud, the magnitude of the ERF tends to be somewhat smaller (see Figure 7.19). The physical explanation for the mixed-phase reduction in the magnitude of the ERF is that some aerosols also act as IN causing supercooled clouds to glaciate and precipitate more readily. This reduction in cloud cover leads to less reflected shortwave radiation and a less negative ERFari+aci. This effect can however be offset if the IN become coated with soluble material, making them less effective at nucleating ice, leading to less efficient precipitation production and more reflected shortwave radiation (Hoose et al., 2008; Storelvmo et al., 2008a). Models that have begun to incorporate aerosol–cloud interactions in convective clouds also have a tendency to reduce the magnitude of the ERF, but this effect is less systematic (Jacobson, 2003; Lohmann, 2008; Suzuki et al., 2008) and reasons for differences among the models in this category are less well understood.

For our expert judgment of ERFari+aci a subset of GCM studies, which strived for a more complete and consistent treatment of aerosol–cloud interactions (by incorporating either convective or mixed-phase processes) was identified and scrutinized. The ERFari+aci derived from these models is somewhat less negative than in the full suite of models, and ranges from –1.68 and –0.81 W m^{-2} with a median value of –1.38 W m^{-2}. Because in some cases a number of studies have been performed with the same GCM, in what might be described as an evolving effort, our assessment is further restricted to the best (usually most recent) estimate by each modelling group (see black symbols in Figure 7.19 and Table 7.4). This ensures that no single GCM is given a disproportionate weight. Further, we consider only simulations not constrained by the historical temperature rise, motivated by the desire to emphasize a process-based estimate. Although it may be argued that greater uncertainty is introduced by giving special weight to models that only incorporate more comprehensive treatments of aerosol–cloud interactions, and for processes that (as Section 7.4 emphasizes) are on the frontier of understanding, it should be remembered that aerosol–cloud interactions for liquid-phase clouds remain very uncertain. Although the understanding and treatment of aerosol–cloud interactions in convective or mixed-phase clouds are also very uncertain, as discussed in Section 7.4.4, we exercise our best judgment of their influence.

A less negative ERFari+aci (–0.93 to –0.45 W m^{-2} with a median of –0.85 W m^{-2}, Figure 7.19 and Table 7.4) is found in studies that use variability in the present day satellite record to infer aerosol–cloud interactions, or that constrain GCM parameterizations to optimize agreement with satellite observations. Because some groups have published multiple estimates as better information became available, only their latest study was incorporated into this assessment. Moreover, if a study did not report ERFari+aci but only evaluated changes in ERFaci, their individual estimate was combined with the average ERFari of –0.45 W m^{-2} from Section 7.5.2. Likewise, those (all but one) studies that only accounted for changes in shortwave radiation when computing ERFaci were corrected by adding a constant factor of +0.2 W m^{-2}, taken from the lower range of the modeled longwave effects which varied from +0.2 to +0.6 W m^{-2} in the assessed models. These procedures result in the final estimates of ERFari+aci shown as black symbols in Figure 7.19 and in Table 7.4. This resulted in a median ERFari+aci of –0.85 W m^{-2} for satellite-based ERFari+aci estimates. Results of pure satellite-based studies are sensitive to the spatial scale of measurements (Grandey and Stier, 2010; McComiskey and Feingold, 2012; Section 7.4.2.2), as well as to how pre-industrial conditions and variations between pre-industrial and present-day conditions are inferred from the observed

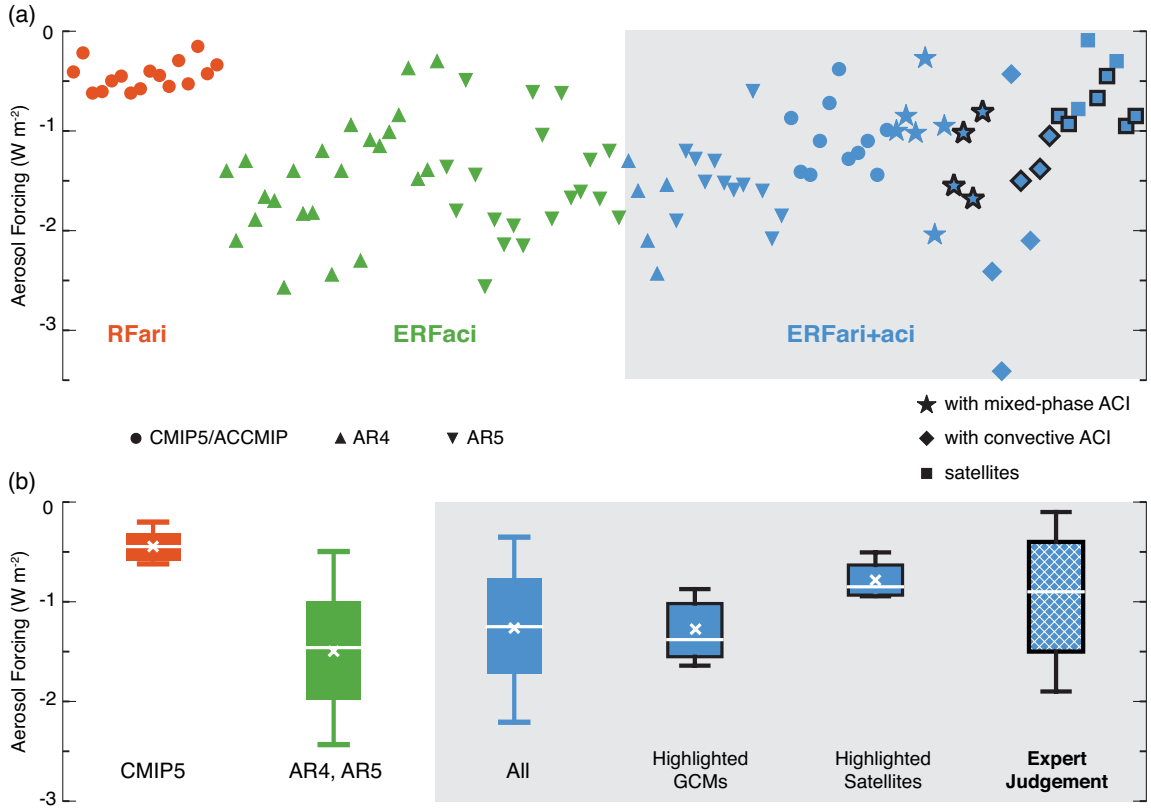

Figure 7.19 | (a) GCM studies and studies involving satellite estimates of RFari (red), ERFaci (green) and ERFari+aci (blue in grey-shaded box). Each symbol represents the best estimate per model and paper (see Table 7.3 for references). The values for RFari are obtained from the CMIP5 models. ERFaci and ERFari+aci studies from GCMs on liquid phase stratiform clouds are divided into those published prior to and included in AR4 (labelled AR4, triangles up), studies published after AR4 (labelled AR5, triangles down) and from the CMIP5/ACCMIP models (filled circles). GCM estimates that include adjustments beyond aerosol–cloud interactions in liquid phase stratiform clouds are divided into those including aerosol–cloud interactions in mixed-phase clouds (stars) and those including aerosol–cloud interactions in convective clouds (diamonds). Studies that take satellite data into account are labelled as 'satellites'. Studies highlighted in black are considered for our expert judgement of ERFari+aci. (b) Whisker boxes from GCM studies and studies involving satellite data of RFari, ERFaci and ERFari+aci. They are grouped into RFari from CMIP5/ACCMIP GCMs (labelled CMIP5 in red), ERFaci from GCMs (labelled AR4, AR5 in green), all estimates of ERFari+aci shown in the upper panel (labelled 'All' in blue), ERFari+aci from GCMs highlighted in the upper panel (labelled 'Highlighted GCMs' in blue), ERFari+aci from satellites highlighted in the upper panel (labelled 'Highlighted Satellites' in blue), and our expert judgement based on estimates of ERFari+aci from these GCM and satellite studies (labelled 'Expert Judgement' in blue). Displayed are the averages (cross sign), median values (middle line), 17th and 83th percentiles (*likely* range shown as box boundaries) and 5th and 95th percentiles (whiskers). References for the individual estimates are provided in Table 7.3. Table 7.4 includes the values of the GCM and satellite studies considered for the expert judgement of ERFari+aci that are highlighted in black.

Table 7.3 | List of references for each category of estimates displayed in Figure 7.19.

Estimate	Acronym	References
Effective radiative forcing due to aerosol–cloud interactions (ERFaci) published prior to and considered in AR4	AR4	Lohmann and Feichter (1997); Rotstayn (1999); Lohmann et al., (2000); Ghan et al. (2001); Jones et al. (2001); Rotstayn and Penner (2001); Williams et al. (2001); Kristjánsson (2002); Lohmann (2002a); Menon et al. (2002); Peng and Lohmann (2003); Penner et al. (2003); Easter et al. (2004); Kristjánsson et al. (2005); Ming et al. (2005); Rotstayn and Liu (2005); Takemura et al. (2005); Johns et al. (2006); Penner et al. (2006); Quaas et al. (2006); Storelvmo et al. (2006)
ERFaci published since AR4	AR5	Menon and Del Genio (2007); Ming et al. (2007b); Kirkevåg et al. (2008); Seland et al. (2008); Storelvmo et al. (2008a); Hoose et al. (2009); Quaas et al. (2009); Rotstayn and Liu (2009); Chen et al. (2010); Ghan et al. (2011); Penner et al. (2011); Makkonen et al. (2012a); Takemura (2012); Kirkevåg et al. (2013)
Effective radiative forcing due to aerosol–radiation and aerosol–cloud interactions (ERFari+aci) in liquid phase stratiform clouds published prior to AR4	AR4	Lohmann and Feichter (2001); Quaas et al. (2004); Menon and Rotstayn (2006); Quaas et al. (2006)
ERFari+aci in liquid phase stratiform clouds published since AR4	AR5	Lohmann et al. (2007); Rotstayn et al. (2007); Posselt and Lohmann (2008); Posselt and Lohmann (2009); Quaas et al. (2009); Salzmann et al. (2010); Bauer and Menon (2012); Gettelman et al. (2012); Ghan et al. (2012); Makkonen et al. (2012a); Takemura (2012); Kirkevåg et al. (2013)
ERFari+aci in liquid and mixed-phase stratiform clouds	with mixed-phase clouds	Lohmann (2004); Jacobson (2006); Lohmann and Diehl (2006); Hoose et al. (2008); Storelvmo et al. (2008a); Lohmann and Hoose (2009); Hoose et al. (2010b); Lohmann and Ferrachat (2010); Salzmann et al. (2010); Storelvmo et al. (2010)
ERFari+aci in stratiform and convective clouds	with convective clouds	Menon and Rotstayn (2006); Menon and Del Genio (2007); Lohmann (2008); Koch et al. (2009a); Unger et al. (2009); Wang et al. (2011b)
ERFari+aci including satellite observations	Satellites	Lohmann and Lesins (2002); Sekiguchi et al. (2003); Quaas et al. (2006); Lebsock et al. (2008); Quaas et al. (2008); Quaas et al. (2009); Bellouin et al. (2013)

Table 7.4 | List of ERFari+aci values (W m^{-2}) considered for the expert judgement of ERFari+aci (black symbols in Figure 7.19). For the GCM studies only the best estimate per modelling group is used. For satellite studies the estimates are corrected for the ERFari and for the longwave component of ERFari+aci when these are not included (see text).

Category	Best Estimate	Climate Model and/or Satellite Instrument	Reference
with mixed-phase clouds	–1.55	CAM Oslo	Hoose et al. (2010b)
with mixed-phase clouds	–1.02	ECHAM	Lohmann and Ferrachat (2010)
with mixed-phase clouds	–1.68	GFDL	Salzmann et al. (2010)
with mixed-phase clouds	–0.81	CAM Oslo	Storelvmo et al. (2008b; 2010)
with convective clouds	–1.50	ECHAM	Lohmann (2008)
with convective clouds	–1.38	GISS	Koch et al. (2009a)
with convective clouds	–1.05	PNNL-MMF	Wang et al. (2011b)
Satellite-based	–0.85	ECHAM + POLDER	Lohmann and Lesins (2002)
Satellite-based	–0.93	AVHRR	Sekiguchi et al. (2003)
Satellite-based	–0.67	CERES / MODIS	Lebsock et al. (2008)
Satellite-based	–0.45	CERES / MODIS	Quaas et al. (2008)
Satellite-based	–0.95	Model mean + MODIS	Quaas et al. (2009)
Satellite-based	–0.85	MACC + MODIS	Bellouin et al. (2013)

AVHRR = Advanced Very High Resolution Radiometer. MACC = Monitoring Atmospheric Composition and Climate. POLDER = Polarization and Directionality of the Earth's Reflectances.
CERES = Clouds and the Earth's Radiant Energy System. MODIS = Moderate Resolution Imaging Spectrometer.

variability in present-day aerosol and cloud properties (Quaas et al., 2011; Penner et al., 2012). In addition, all (model- and satellite-based) estimates of ERFari+aci are very sensitive to the assumed pre-industrial or natural cloud droplet concentration (Hoose et al., 2009). The large spatial scales of satellite measurements relative to *in situ* measurements generally suggest smaller responses in cloud droplet number increases for a given aerosol increase (Section 7.4.2.2). Satellite studies, however, show a strong effect of aerosol on cloud amount, which could be a methodological artefact as GCMs associate clouds with humidity and aerosol swelling (Quaas et al., 2010). There are thus possible biases in both directions, so the sign and magnitude of any net bias is not clear.

In large-scale models for which cloud-scale circulations are not explicitly represented, it is difficult to capture all relevant cloud controlling processes (Section 7.2.2). Because the response of clouds to aerosol perturbations depends critically on the interplay of poorly understood physical processes, global model-based estimates of aerosol–cloud interactions remain uncertain (Section 7.4). Moreover, the connection between the aerosol amount and cloud properties is too direct in the large-scale modelling studies (as it relies heavily on the autoconversion rate). Because of this, GCMs tend to overestimate the magnitude of the aerosol effect on cloud properties (Section 7.4.5; see also discussion in Section 7.5.4). This view has some support from studies that begin to incorporate some cloud, or cloud-system scale responses to aerosol–cloud interactions. For instance, in an attempt to circumvent some of difficulties of parameterizing clouds, some groups (e.g., Wang et al., 2011b) have begun developing modelling frameworks that can explicitly represent cloud-scale circulations, and hence the spatio-temporal covariances of cloud-controlling processes. Another group (Khairoutdinov and Yang, 2013) has used the same cloud-resolving model in a radiative convective equilibrium approach, and compared the relative contribution of aerosol–cloud interactions to warming from the doubling of atmospheric CO_2. In both studies a smaller (–1.1 and –0.8 W m^{-2}, respectively) ERFari+aci than for the average GCM was found. Furthermore, the study best resolving the cloud-scale circulations (Wang et al., 2011b) found little change in cloud amount in response to changes in aerosol, consistent with other fine-scale modelling studies discussed in Section 7.4.

Based on the above considerations, we assess ERFari+aci using expert judgement to be –0.9 W m^{-2} with a 5 to 95% uncertainty range of –1.9 to –0.1 W m^{-2} (*medium confidence*), and a *likely* range of –1.5 to –0.4 W m^{-2}. These ranges account for the GCM results by allowing for an ERFari+aci somewhat stronger than what is estimated by the satellite studies with a longer tail in the direction of stronger effects, but (for reasons given above) give less weight to the early GCM estimates shown in Figure 7.19. The ERFari+aci can be much larger regionally but the global value is consistent with several new lines of evidence suggesting less negative estimates of aerosol–cloud interactions than the corresponding estimate in Chapter 7 of AR4 of –1.2 W m^{-2}. The AR4 estimate was based mainly on GCM studies that did not take secondary processes (such as aerosol effects on mixed-phase and/or convective clouds) into account, did not benefit as much from the use of the recent satellite record, and did not account for the effect of rapid adjustments on the longwave radiative budget. This uncertainty range is slightly smaller than the –2.3 to –0.2 W m^{-2} in AR4, with a less negative upper bound due to the reasons outlined above. The best estimate of ERFari+aci is not only consistent with the studies allowing cloud-scale responses (Wang et al., 2011b; Khairoutdinov and Yang, 2013) but also is in line with the average ERFari+aci from the CMIP5/ACCMIP models (about –1 W m^{-2}, see Table 7.5), which as a whole reproduce the observed warming of the 20th century (see Chapter 10). Studies that infer ERFari+aci from the historical temperature rise are discussed in Section 10.8.

7.5.4 Estimate of Effective Radiative Forcing from Aerosol–Cloud Interactions Alone

ERFaci refers to changes in TOA radiation since pre-industrial times due only to aerosol–cloud interactions, i.e., albedo effects augmented by possible changes in cloud amount and lifetime. As stated in Section 7.5.1, we do not discuss RFaci by itself because it is an academic

Table 7.5 | Estimates of aerosol 1850–2000 effective radiative forcing (ERF, in W m^{-2}) in some of the CMIP5 and ACCMIP models. The ERFs are estimated from fixed-sea-surface temperature (SST) experiments using atmosphere-only version of the models listed. Different models include different aerosol effects. The CMIP5 and ACCMIP protocols differ, hence differences in forcing estimates for one model.

Modelling Group	Model Name	ERFari+aci from All Anthropogenic Aerosols	ERFari+aci from Sulphate Aerosols Only
CCCma	CanESM2	–0.87	–0.90
CSIRO-QCCCE	CSIRO-Mk3-6-0[b]	–1.41	–1.10
GFDL	GFDL-AM3	–1.60 (–1.44[a])	–1.62
GISS	GISS-E2-R[b]	–1.10[a]	–0.61
GISS	GISS-E2-R-TOMAS[b]	–0.76[a]	
IPSL	IPSL-CM5A-LR	–0.72	–0.71
LASG-IAP	FGOALS-s2[c]	–0.38	–0.34
MIROC	MIROC-CHEM[b]	–1.24[a]	
MIROC	MIROC5	–1.28	–1.05
MOHC	HadGEM2-A	–1.22	–1.16
MRI	MRI-CGM3	–1.10	–0.48
NCAR	NCAR-CAM5.1[b]	–1.44[a]	
NCC	NorESM1-M	–0.99	
Ensemble mean		–1.08	
Standard deviation		+0.32	

Notes:

[a] From ACCMIP (Shindell et al., 2013).

[b] These models include the black carbon on snow effect.

[c] This model does not include the ERF from aerosol–cloud interactions.

ACCMIP = Atmospheric Chemistry and Climate Model Intercomparison Project.

CMIP5 = Coupled Model Intercomparison Project Phase 5.

construct. However, processes in GCMs that tend to affect RFaci such as changes to the droplet size distribution breadth (e.g., Rotstayn and Liu, 2005) will also affect ERFaci. Early studies evaluated just the change in shortwave radiation or cloud radiative effect for ERFaci, but lately the emphasis has changed to report changes in net TOA radiation for ERFaci. As discussed in Section 7.5.3, evaluating ERFaci from changes in net TOA radiation is the only correct method, and therefore this is used whenever possible also in this section. However some earlier estimates of ERFaci only reported changes in cloud radiative effect, which we show in Figure 7.19 as the last resort. However, estimates of changes in cloud radiative effect can differ quite substantially from those in net radiation if rapid adjustments to aerosol–cloud interactions induce changes in clear-sky radiation.

Cloud amount and lifetime effects manifest themselves in GCMs via their representation of autoconversion of cloud droplets to rain, a process that is inversely dependent on droplet concentration. Thus, ERFaci and ERFari+aci have been found to be very sensitive to the autoconversion parameterization (Rotstayn, 2000; Golaz et al., 2011; Wang et al., 2012). GCMs probably underestimate the extent to which precipitation is formed via raindrop accretion of cloud droplets (Wood, 2005), a process that is insensitive to aerosol and droplet concentration. Indeed, models that remedy this imbalance in precipitation formation between autoconversion and accretion (Posselt and Lohmann, 2009; Wang et al., 2012) exhibit weaker ERFaci in agreement with small-scale studies that typically do not show a systematic increase in cloud lifetime because of entrainment and because smaller droplets also evaporate more readily (Jiang et al., 2006; Bretherton et al., 2007). Bottom-up estimates of ERFaci are shown in Figure 7.19. Their median estimate of –1.4 W m^{-2} is more negative than our expert judgement of ERFari+aci because of the limitations of these studies discussed above.

There is conflicting evidence for the importance of ERFaci associated with cirrus, ranging from a statistically significant impact on cirrus coverage (Hendricks et al., 2005) to a very small effect (Liu et al., 2009). Penner et al. (2009) obtained a rather large negative RFaci of anthropogenic ice-forming aerosol on upper tropospheric clouds of –0.67 to –0.53 W m^{-2}; however, they ignored potential compensating effects on lower lying clouds. A new study based on two GCMs and different ways to deduce ERFaci on cirrus clouds estimates ERFaci to be +0.27 ± 0.1 W m^{-2} (Gettelman et al., 2012), thus rendering aerosol effects on cirrus clouds smaller than previously estimated and of opposite sign.

One reason for having switched to providing an expert judgment estimate of ERFari+aci rather than of ERFaci is that the individual contributions are very difficult to disentangle. The individual components can be isolated only if linearity of ERFari and ERFaci is assumed but there is no *a priori* reason why the ERFs should be additive because by definition they occur in a system that is constantly readjusting to multiple nonlinear forcings. Nevertheless assuming additivity, ERFaci could be obtained as the difference between ERFari+aci and ERFari. This yields an ERFaci estimate of –0.45 W m^{-2}, that is, much smaller than the median ERFaci value of –1.4 W m^{-2} (see above and Figure 7.19). This discrepancy arises because the GCM estimates of ERFaci do not consider secondary processes and because these studies are not necessarily conducted with the same GCMs that estimate ERFari+aci. This difference could also be a measure of the non-linearity of the ERFs. A 90% uncertainty range of –1.2 to 0 W m^{-2} is adopted for ERFaci, which accounts for the error covariance between ERFari and ERFaci and the larger uncertainty on the lower bound. In summary, there is much less confidence associated with the estimate of ERFaci than with the estimate of ERFari+aci.

Frequently Asked Questions

FAQ 7.2 | How Do Aerosols Affect Climate and Climate Change?

Atmospheric aerosols are composed of small liquid or solid particles suspended in the atmosphere, other than larger cloud and precipitation particles. They come from natural and anthropogenic sources, and can affect the climate in multiple and complex ways through their interactions with radiation and clouds. Overall, models and observations indicate that anthropogenic aerosols have exerted a cooling influence on the Earth since pre-industrial times, which has masked some of the global mean warming from greenhouse gases that would have occurred in their absence. The projected decrease in emissions of anthropogenic aerosols in the future, in response to air quality policies, would eventually unmask this warming.

Atmospheric aerosols have a typical lifetime of one day to two weeks in the troposphere, and about one year in the stratosphere. They vary greatly in size, chemical composition and shape. Some aerosols, such as dust and sea spray, are mostly or entirely of natural origin, while other aerosols, such as sulphates and smoke, come from both natural and anthropogenic sources.

Aerosols affect climate in many ways. First, they scatter and absorb sunlight, which modifies the Earth's radiative balance (see FAQ.7.2, Figure 1). Aerosol scattering generally makes the planet more reflective, and tends to cool the climate, while aerosol absorption has the opposite effect, and tends to warm the climate system. The balance between cooling and warming depends on aerosol properties and environmental conditions. Many observational studies have quantified local radiative effects from anthropogenic and natural aerosols, but determining their

(continued on next page)

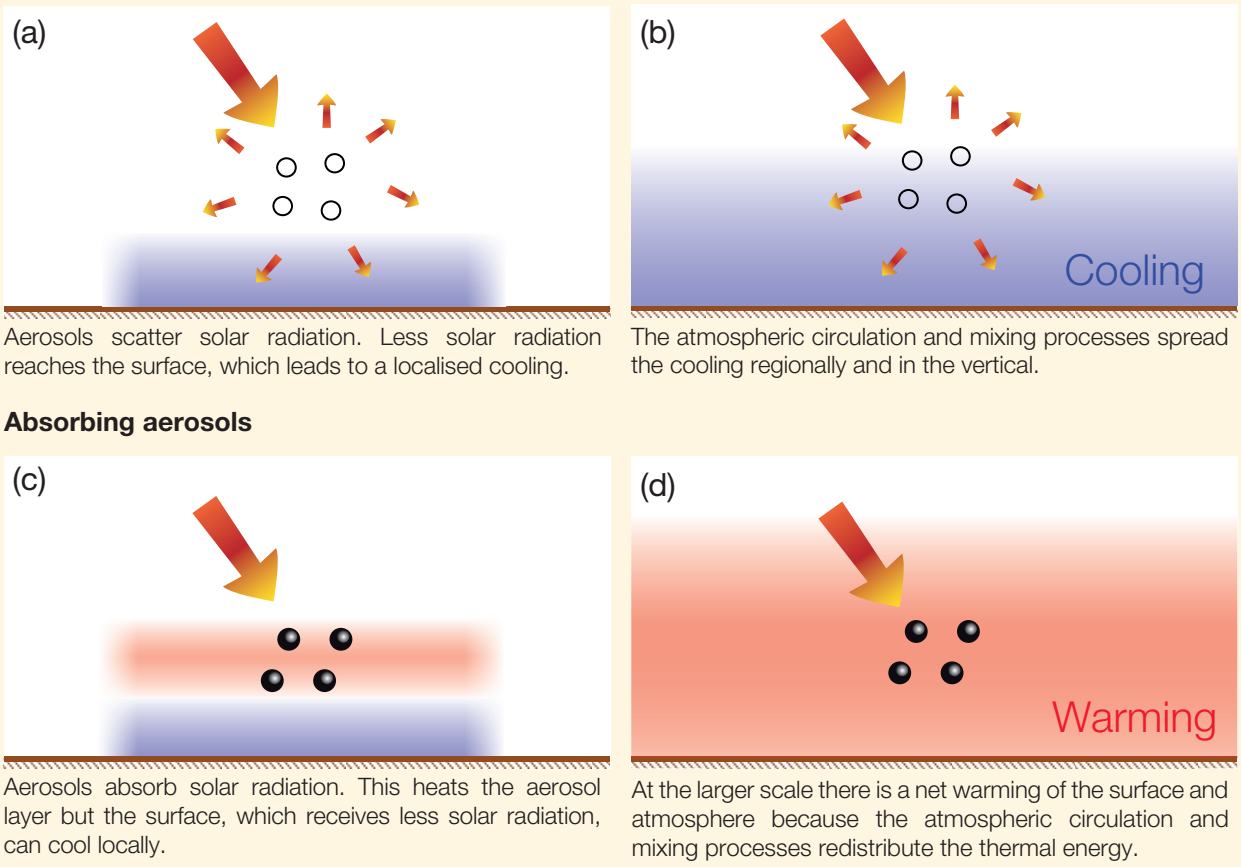

FAQ 7.2, Figure 1 | Overview of interactions between aerosols and solar radiation and their impact on climate. The left panels show the instantaneous radiative effects of aerosols, while the right panels show their overall impact after the climate system has responded to their radiative effects.

FAQ 7.2 (continued)

global impact requires satellite data and models. One of the remaining uncertainties comes from black carbon, an absorbing aerosol that not only is more difficult to measure than scattering aerosols, but also induces a complicated cloud response. Most studies agree, however, that the overall radiative effect from anthropogenic aerosols is to cool the planet.

Aerosols also serve as condensation and ice nucleation sites, on which cloud droplets and ice particles can form (see FAQ.7.2, Figure 2). When influenced by more aerosol particles, clouds of liquid water droplets tend to have more, but smaller droplets, which causes these clouds to reflect more solar radiation. There are however many other pathways for aerosol–cloud interactions, particularly in ice—or mixed liquid and ice—clouds, where phase changes between liquid and ice water are sensitive to aerosol concentrations and properties. The initial view that an increase in aerosol concentration will also increase the amount of low clouds has been challenged because a number of counteracting processes come into play. Quantifying the overall impact of aerosols on cloud amounts and properties is understandably difficult. Available studies, based on climate models and satellite observations, generally indicate that the net effect of anthropogenic aerosols on clouds is to cool the climate system.

Because aerosols are distributed unevenly in the atmosphere, they can heat and cool the climate system in patterns that can drive changes in the weather. These effects are complex, and hard to simulate with current models, but several studies suggest significant effects on precipitation in certain regions.

Aerosol-cloud interactions

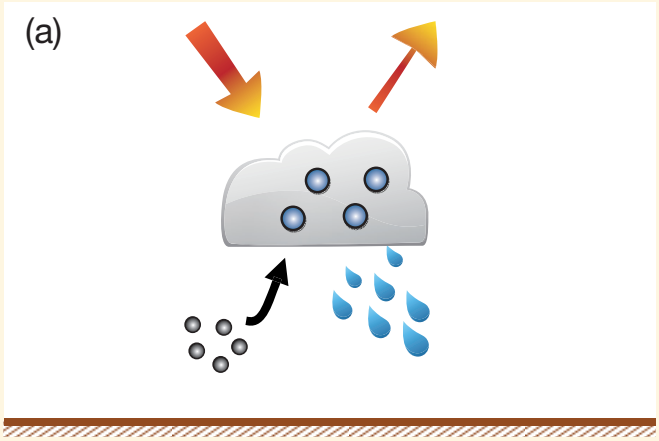

FAQ 7.2, Figure 2 | Overview of aerosol–cloud interactions and their impact on climate. Panels (a) and (b) represent a clean and a polluted low-level cloud, respectively.

Because of their short lifetime, the abundance of aerosols—and their climate effects—have varied over time, in rough concert with anthropogenic emissions of aerosols and their precursors in the gas phase such as sulphur dioxide (SO_2) and some volatile organic compounds. Because anthropogenic aerosol emissions have increased substantially over the industrial period, this has counteracted some of the warming that would otherwise have occurred from increased concentrations of well mixed greenhouse gases. Aerosols from large volcanic eruptions that enter the stratosphere, such as those of El Chichón and Pinatubo, have also caused cooling periods that typically last a year or two.

Over the last two decades, anthropogenic aerosol emissions have decreased in some developed countries, but increased in many developing countries. The impact of aerosols on the global mean surface temperature over this particular period is therefore thought to be small. It is projected, however, that emissions of anthropogenic aerosols will ultimately decrease in response to air quality policies, which would suppress their cooling influence on the Earth's surface, thus leading to increased warming.

7.6 Processes Underlying Precipitation Changes

7.6.1 Introduction

In this section we outline some of the main processes thought to control the climatological distribution of precipitation and precipitation extremes. Emphasis is placed on large-scale constraints that relate to processes, such as changes in the water vapour mixing ratio that accompany warming, or changes in atmospheric heating rates that accompany changing GHG and aerosol concentrations, which are discussed earlier in this chapter. The fidelity with which large-scale models represent different aspects of precipitation, ranging from the diurnal cycle to extremes, is discussed in Section 9.4.1. Building on, and adding to, concepts developed here, Section 11.3.2 presents near term projections of changes in regional precipitation features. Projections of changes on longer time scales, again with more emphasis on regionally specific features and the coupling to the land surface, are presented in Section 12.4.5. The effect of processes discussed in this section on specific precipitation systems, such as the monsoon, the intertropical convergence zones, or tropical cyclones are presented in Chapter 14.

Precipitation is sustained by the availability of moisture and energy. In a globally averaged sense the oceans provide an unlimited supply of moisture, so that precipitation formation is energetically limited (Mitchell et al., 1987). Locally precipitation can be greatly modified by limitations in the availability of moisture (for instance over land) and the effect of circulation systems, although these too are subject to local energetic constraints (Neelin and Held, 1987; Raymond et al., 2009). There are many ways to satisfy these constraints, and climate models still exhibit substantial biases in their representation of the spatio-temporal distribution of precipitation (Stephens et al., 2010; Liepert and Previdi, 2012; Section 9.5). Nonetheless, through careful analysis, it is possible to identify robust features in the simulated response of precipitation to changes in precipitation drivers. In almost every case these can be related to well understood processes, as described below.

7.6.2 The Effects of Global Warming on Large-Scale Precipitation Trends

The atmospheric water vapour mixing ratio is expected to increase with temperature roughly following the saturation value (e.g., with increases in surface values ranging from 6 to 10% $°C^{-1}$ and larger increases aloft, see Section 7.2.4.1). Increases in global mean precipitation are, however, constrained by changes in the net radiative cooling rate of the troposphere. GCMs, whose detailed treatment of radiative transfer provides a basis for calculating these energetic limitations, suggest that for the CO_2 forcing, globally-averaged precipitation increases with global mean surface temperature at about 1 to 3% $°C^{-1}$ (Mitchell et al., 1987; Held and Soden, 2006; Richter and Xie, 2008). Precipitation changes evince considerable regional variability about the globally averaged value; generally speaking precipitation is expected to increase in the wettest latitudes, whereas dry latitudes may even see a precipitation decrease (Mitchell et al., 1987; Allen and Ingram, 2002; Held and Soden, 2006). On smaller scales, or near precipitation margins, the response is less clear due to model-specific, and less well understood, regional circulation shifts (Neelin et al., 2006), but there is some evidence that the sub-tropical dry zones are expanding (Section 7.2.5.2 and Section 2.7.5), both as a result of the tropical convergence zones narrowing (Neelin et al., 2006; Chou et al., 2009), and the storm tracks moving poleward (Allen et al., 2012) and strengthening (O'Gorman and Schneider, 2008).

The 'wet-get-wetter' and 'dry-get-drier' response that is evident at large scales over oceans can be understood as a simple consequence of a change in the water vapour content carried by circulations, which otherwise are little changed (Mitchell et al., 1987; Held and Soden, 2006). Wet regions are wet because they import moisture from dry regions, increasingly so with warmer temperatures. These ideas have withstood additional analysis and scrutiny since AR4 (Chou et al., 2009; Seager et al., 2010; Muller and O'Gorman, 2011), are evident in 20th century precipitation trends (Allan and Soden, 2007; Zhang et al., 2007b; see Section 2.5.1) and are assessed on different time scales in Chapters 11 and 12. Because the wet-get-wetter argument implies that precipitation changes associated with warming correlate with the present-day pattern of precipitation, biases in the simulation of present-day precipitation will lead to biases in the projections of future precipitation change (Bony et al., 2013).

The wet-get-wetter and dry-get-drier response pattern is mitigated, particularly in the dry regions, by the anticipated slowdown of the atmospheric circulation (as also discussed in Section 7.2.5.3), as well as by gains from local surface evaporation. The slowdown within the descent regions can be partly understood as a consequence of the change in the dry static stability of the atmosphere with warming. And although this line of argument is most effective for explaining changes over the ocean (Chou et al., 2009; Bony et al., 2013), it can also be used to understand the GCM land responses to some extent (Muller and O'Gorman, 2011).

The non-uniform nature of surface warming induces regional circulation shifts that affect precipitation trends. In the tropics SSTs warm more where winds are weak and thus are less effective in damping surface temperature anomalies, and precipitation systematically shifts to regions that warm more (Xie et al., 2010). The greater warming over land, and its regional variations, also affect the regional distributions of precipitation (Joshi et al., 2008). However, low understanding of soil moisture–precipitation feedbacks complicates interpretations of local responses to warming over land (Hohenegger et al., 2009), so that the effect of warming on precipitation at the scale of individual catchments is not well understood. Some broad-scale responses, particularly over the ocean, are more robust and relatively well understood.

7.6.3 Radiative Forcing of the Hydrological Cycle

In the absence of a compensating temperature change, an increase in well-mixed GHG concentrations tends to reduce the net radiative cooling of the troposphere. This reduces the rainfall rate and the strength of the overturning circulation (Andrews et al., 2009; Bony et al., 2013), such that the increase in global mean precipitation would be 1.5 to 3.5% $°C^{-1}$ due to temperature alone but is reduced by about 0.5% $°C^{-1}$ due to the effect of CO_2 (Lambert and Webb, 2008). The dynamic effects are similar to those that result from the effect of atmospheric warming on the lapse rate, which also reduces the strength of the atmospheric

overturning circulation (e.g., Section 7.6.2), and are robustly evident over a wide range of models and model configurations (Bony et al., 2013; see also Figure 7.20). These circulation changes influence the regional response, and are more pronounced over the ocean, because asymmetries in the land-sea response to changing concentrations of GHGs (Joshi et al., 2008) amplify the maritime and dampen or even reverse the terrestrial signal (Wyant et al., 2012; Bony et al., 2013).

The dependence of the intensity of the hydrological cycle on the tropospheric cooling rate helps to explain why perturbations having the same RF do not produce the same precipitation responses. Apart from the relatively small increase in absorption by atmospheric water vapour, increased solar forcing does not directly affect the net tropospheric cooling rate. As a result the hydrological cycle mostly feels the subsequent warming through its influence on the rate of tropospheric cooling (Takahashi, 2009). This is why modeling studies suggest that solar radiation management (geoengineering) methods that maintain a constant surface temperature will lead to a reduction in globally averaged precipitation as well as different regional distributions of precipitation (Schmidt et al., 2012b; Section 7.7.3).

Changes in cloud radiative effects, and aerosol RF can also be effective in changing the net radiative heating rate within the troposphere (Lambert and Webb, 2008; Pendergrass and Hartmann, 2012). Most prominently, absorption of solar radiation by atmospheric aerosols is understood to reduce the globally averaged precipitation. But this effect may be offset by the tendency of absorbing aerosols to reduce the planetary albedo, thereby raising surface temperature, leading to more precipitation (Andrews et al., 2009). Heterogeneously distributed precipitation drivers such as clouds, aerosols and tropospheric ozone will also induce circulations that may amplify or dampen their local impact on the hydrological cycle (Ming et al., 2010; Allen et al., 2012; Shindell et al., 2012). Such regional effects are discussed further in Chapter 14 for the case of aerosols.

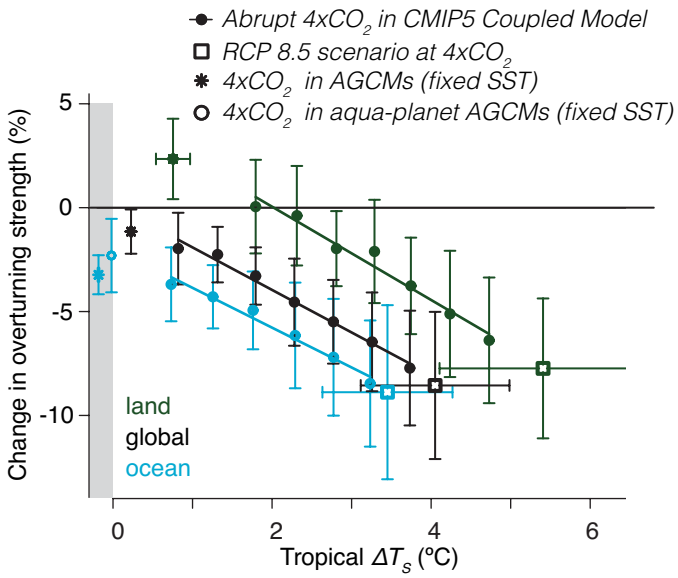

Figure 7.20 | Illustration of the response of the large-scale atmospheric overturning to warming (adapted from Bony et al., 2013). The overturning intensity is shown on the *y*-axis and is measured by the difference between the mean motion in upward moving air and the mean motion in downward moving air. The warming is shown on the *x*-axis and is measured by the change in surface temperature averaged over the Tropics, ΔT_s, after an abrupt quadrupling of atmospheric CO_2. The grey region delineates responses for which ΔT_s is zero by definition. Nearly one half of the final reduction in the intensity of the overturning is evident before any warming is felt, and can be associated with a rapid adjustment of the hydrological cycle to changes in the atmospheric cooling rate accompanying a change in CO_2. With warming the circulation intensity is further reduced. The rapid adjustment, as measured by the change in circulation intensity for zero warming, is different over land and ocean. Over land the increase in CO_2 initially causes an intensification of the circulation. The result is robust in the sense that it is apparent in all of the 15 CMIP5 models analysed, irrespective of the details of their configuration.

7.6.4 Effects of Aerosol–Cloud Interactions on Precipitation

Aerosol–cloud interactions directly influence the cloud microphysical structure, and only indirectly (if at all) the net atmospheric heating rate, and for this reason have mostly been explored in terms of their effect on the character and spatio-temporal distribution of precipitation, rather than on the globally-averaged amount of precipitation.

The sensitivity of simulated clouds to their microphysical development (e.g., Fovell et al., 2009; Parodi and Emanuel, 2009) suggests that they may be susceptible to the availability of CCN and IN. For instance, an increase in CCN favours smaller cloud droplets, which delays the onset of precipitation and the formation of ice particles in convective clouds (Rosenfeld and Woodley, 2001; Khain et al., 2005). It has been hypothesized that such changes may affect the vertical distribution and total amount of latent heating in ways that would intensify or invigorate convective storms, as measured by the strength and vertical extent of the convective updraughts (Andreae et al., 2004; Rosenfeld et al., 2008; Rosenfeld and Bell, 2011; Tao et al., 2012). Support for the idea that the availability of CCN influences the vigour of convective systems can be found in some modelling studies, but the strength, and even sign, of such an effect has been shown to be contingent on a variety of environmental factors (Seifert and Beheng, 2006; Fan et al., 2009; Khain, 2009; Seifert et al., 2012) as well as on modelling assumptions (Ekman et al., 2011).

Observational studies, based on large data sets that sample many convective systems, report systematic correlations between aerosol amount and cloud-top temperatures (Devasthale et al., 2005; Koren et al., 2010a; Li et al., 2011). Weekly cycles in cloud properties and precipitation, wherein convective intensity, cloud cover or precipitation increases during that part of the week when aerosol concentrations are largest, have also been reported (Bäumer and Vogel, 2007; Bell et al., 2008; Rosenfeld and Bell, 2011). Both types of studies have been interpreted in terms of an aerosol influence on convective cloud systems. However, whether or not these findings demonstrate that a greater availability of CCN systematically invigorates, or otherwise affects, convection remains controversial. Many of the weekly cycle studies are disputed on statistical or other methodological grounds (Barmet et al., 2009; Stjern, 2011; Tuttle and Carbone, 2011; Sanchez-Lorenzo et al., 2012; Yuter et al., 2013). Even in cases where relationships between aerosol amount and some measure of convective intensity appear to be unambiguous, the interpretation that this reflects an aerosol effect on the convection is less clear, as both aerosol properties and convection are strongly influenced by meteorological factors that

are not well controlled for (e.g., Boucher and Quaas, 2013). Studies that have used CRMs to consider the net effect of aerosol–cloud interactions integrated over many storms, or in more of a climate context wherein convective heating must balance radiative cooling within the atmosphere, also do not support a strong and systematic invigoration effect resulting from very large (many fold) changes in the ambient aerosol (Morrison and Grabowski, 2011; van den Heever et al., 2011; Seifert et al., 2012; Khairoutdinov and Yang, 2013). Locally in space or time, however, radiative processes are less constraining, leaving open the possibility of stronger effects from localized or transient aerosol perturbations.

Because precipitation development in clouds is a time-dependent process, which proceeds at rates that are partly determined by the cloud microphysical structure (Seifert and Zängl, 2010), aerosol–cloud interactions may lead to shifts in topographic precipitation to the leeward side of mountains when precipitation is suppressed, or to the windward side in cases when it is more readily initiated. Orographic clouds show a reduction in the annual precipitation over topographical barriers downwind of major urban areas in some studies (Givati and Rosenfeld, 2004; Jirak and Cotton, 2006) but not in others (Halfon et al., 2009). Even in cases where effects are reported, the results have proven sensitive to how the data are analysed (Alpert et al., 2008; Levin and Cotton, 2009).

In summary, it is unclear whether changes in aerosol–cloud interactions arising from changes in the availability of CCN or IN can affect, and possibly intensify, the evolution of individual precipitating cloud systems. Some observational and modelling studies suggest such an effect, but are undermined by alternative interpretations of the observational evidence, and a lack of robustness in the modelling studies. The evidence for systematic effects over larger areas and long time periods is, if anything, more limited and ambiguous.

7.6.5 The Physical Basis for Changes in Precipitation Extremes

The physical basis for aerosol microphysical effects on convective intensity was discussed in the previous section. Here we briefly discuss process understanding of the effect of warming on precipitation extremes; observed trends supporting these conclusions are presented in Section 2.6.2.

Precipitation within individual storms is expected to increase with the available moisture content in the atmosphere or near the surface rather than with the global precipitation (Allen and Ingram, 2002; Held and Soden, 2006), which leads to a 6 to 10% °C^{-1} increase, but with longer intervals between storms (O'Gorman and Schneider, 2009). Because GCMs are generally poor at simulating precipitation extremes (Stephens et al., 2010) and predicted changes in a warmer climate vary (Kharin et al., 2007; Sugiyama et al., 2010), they are not usually thought of as a source of reliable information regarding extremes. However, a recent study (O'Gorman, 2012) shows that GCM predictions of extremes can be constrained by observable relationships in the present day climate, and upon doing so become broadly consistent with the idea that extreme precipitation increases by 6 to 10% per °C of warming. Central estimates of sensitivity of extreme (99.9th percentile)

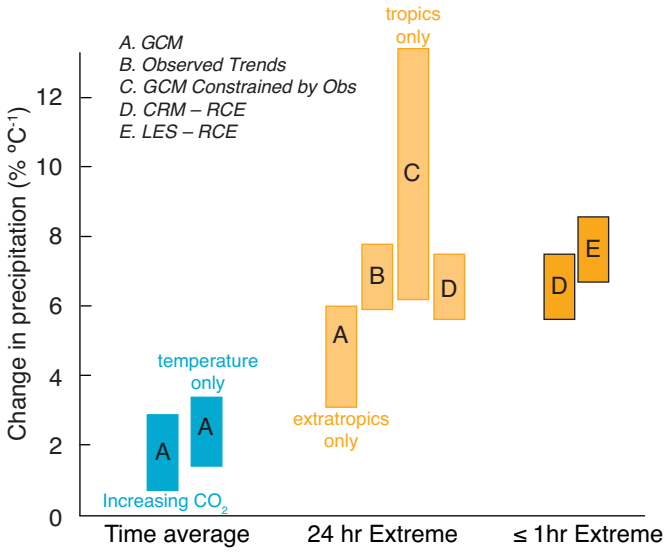

Figure 7.21 | Estimate (5 to 95% range) of the increase in precipitation amount per degree Celsius of global mean surface temperature change. At left (blue) are climate model predictions of changes in time-averaged global precipitation; at centre and right (orange) are predictions or estimates of the typical or average increase in local 99.9th percentile extremes, over 24 hours (centre) and over one hour or less (right). Data are adapted from (A) GCM studies (Allen and Ingram, 2002; and Lambert and Webb, 2008, for time average; O'Gorman and Schneider, 2009 for extremes), (B) long-term trends at many sites globally (Westra et al., 2013), (C) GCMs constrained by present-day observations of extremes (O'Gorman, 2012), (D, E) cloud-resolving model (CRM) and large-eddy simulation (LES) studies of radiative convective equilibrium (Muller et al., 2011; Romps, 2011).

daily rainfall to global temperature from this study were 10% °C^{-1} in the tropics (O'Gorman, 2012), compared to 5% °C^{-1} predicted by the models in the extratropics, where they may be more reliable (O'Gorman and Schneider, 2009). How precipitation extremes depend on temperature has also been explored using cloud resolving simulations (but only for tropical conditions) which produce similar increases in extreme instantaneous rain rate (Romps, 2011) and daily or hourly rain totals (Muller et al., 2011) within storms (Figure 7.21). Because these latter studies are confined to small domains, they may exclude important synoptic or larger-scale dynamical changes such as increases in flow convergence (Chou et al., 2009; Sugiyama et al., 2010).

By taking advantage of natural variability in the present day climate, a number of studies have correlated observed rainfall extremes with local temperature variations. In the extratropics, these studies document sensitivities of extreme precipitation to temperature much higher than those reported above (Lenderink and Van Meijgaard, 2008), but sensitivities vary with temperature (Lenderink et al., 2011), are often negative in the tropics (Hardwick Jones et al., 2010) and usually strengthen at the shortest (e.g., hourly or less) time scales (e.g., Haerter et al., 2010; Hardwick Jones et al., 2010). However, local temperature changes may not be a good proxy for global warming because they tend to co-vary with other meteorological factors (such as humidity, atmospheric stability, or wind direction) in ways that are uncharacteristic of changes in the mean temperature (see Section 7.2.5.7), and these other meteorological factors may dominate the observed signal (e.g., Haerter and Berg, 2009). Thus, the idea that precipitation extremes depend much more strongly on temperature than the 5 to

10% increase per degree Celsius attributable to water vapour changes, remains controversial.

Following the AR4, studies have also continued to show that extremes in precipitation are associated with the coincidence of particular weather patterns (e.g., Lavers et al., 2011). We currently lack an adequate understanding of what controls the return time and persistence of such rare events.

From the aforementioned model and observational evidence, there is *high confidence* that the intensity of extreme precipitation events will increase with warming, at a rate well exceeding that of the mean precipitation. There is *medium confidence* that the increase is roughly 5 to 10% $°C^{-1}$ warming but may vary with time scale, location and season.

7.7 Solar Radiation Management and Related Methods

7.7.1 Introduction

Geoengineering—also called climate engineering—is defined as a broad set of methods and technologies that aim to deliberately alter the climate system in order to alleviate impacts of climate change (Keith, 2000; Izrael et al., 2009; Royal Society, 2009; IPCC, 2011). Two main classes of geoengineering are often considered. Solar Radiation Management (SRM) proposes to counter the warming associated with increasing GHG concentrations by reducing the amount of sunlight absorbed at the surface. A related method seeks to alter high-altitude cirrus clouds to reduce their greenhouse effect. Another class of geoengineering called Carbon Dioxide Removal (CDR) is discussed in Section 6.5. This section assesses how the climate system might respond to some proposed SRM methods and related methods thought to have the potential to influence the global energy budget by at least a few tenths of a W m^{-2} but it does not assess technological or economical feasibility, or consider methods targeting specific climate impacts (MacCracken, 2009). Geoengineering is quite a new field of research, and there are relatively few studies focussed on it. Assessment of SRM is limited by (1) gaps in understanding of some important processes; (2) a relative scarcity of studies; and (3) a scarcity of studies using similar experimental design. This section discusses some aspects of SRM potential to mitigate global warming, outlines robust conclusions where they are apparent, and evaluates uncertainties and potential side effects. Additional impacts of SRM are assessed in Section 19.5.4 of the WGII report, while some of the socio-economic issues are assessed in Chapters 3, 6 and 13 of the WGIII report.

7.7.2 Assessment of Proposed Solar Radiation Management Methods

A number of studies have suggested reducing the amount of sunlight reaching the Earth by placing solid or refractive disks, or dust particles, in outer space (Early, 1989; Mautner, 1991; Angel, 2006; Bewick et al., 2012). Although we do not assess the feasibility of these methods, they provide an easily described mechanism for reducing sunlight reaching the planet, and motivate the idealized studies discussed in Section 7.7.3.

7.7.2.1 Stratospheric Aerosols

Some SRM methods propose increasing the amount of stratospheric aerosol to produce a cooling effect like that observed after strong explosive volcanic eruptions (Budyko, 1974; Crutzen, 2006). Recent studies have used numerical simulations and/or natural analogues to explore the possibility of forming sulphuric acid aerosols by injecting sulphur-containing gases into the stratosphere (Rasch et al., 2008b). Because aerosols eventually sediment out of the stratosphere (within roughly a year or less), these methods require replenishment to maintain a given level of RF. Research has also begun to explore the efficacy of other types of aerosol particles (Crutzen, 2006; Keith, 2010; Ferraro et al., 2011; Kravitz et al., 2012) but the literature is much more limited and not assessed here.

The RF depends on the choice of chemical species (gaseous sulphur dioxide (SO_2), sulphuric acid (H_2SO_4) or sprayed aerosols), location(s), rate and frequency of injection. The injection strategy affects particle size (Rasch et al., 2008a; Heckendorn et al., 2009; Pierce et al., 2010; English et al., 2012), with larger particles producing less RF (per unit mass) and more rapid sedimentation than smaller particles, affecting the efficacy of the method. The aerosol size distribution is controlled by an evolving balance between new particle formation, condensation of vapour on pre-existing particles, evaporation of particles, coagulation and sedimentation. Models that more fully account for aerosol processes (Heckendorn et al., 2009; Pierce et al., 2010; English et al., 2012) found smaller aerosol burdens, larger particles and weaker RF than earlier studies that prescribed the particle size over the particle lifetime. Current modeling studies indicate that injection of sulphate aerosol precursors of at least 10 Mt S (approximately the amount of sulphur injected by the Mount Pinatubo eruption) would be needed annually to maintain a RF of –4 W m^{-2}, roughly equal but opposite to that associated with a doubling of atmospheric CO_2 (Heckendorn et al., 2009; Pierce et al., 2010; Niemeier et al., 2011). Stratospheric aerosols may affect high clouds in the tropopause region, and one study (Kuebbeler et al., 2012) suggests significant negative forcing would result, but this is uncertain given limited understanding of ice nucleation in high clouds (Section 7.4.4.4).

Along with its potential to mitigate some aspects of global warming, the potential side effects of SRM must also be considered. Tilmes et al. (2008; 2009) estimated that stratospheric aerosols SRM might increase chemical ozone loss at high latitudes and delay recovery of the Antarctic ozone hole (expected at the end of this century) by 30 to 70 years, with changes in column ozone of –3 to –10% in polar latitudes and +3 to +5% in the tropics. A high latitude ozone loss is expected to increase UV radiation reaching the surface there, although the effect would be partially compensated by the increase in attenuation by the aerosol itself (Vogelmann et al., 1992; Tilmes et al., 2012). A decrease in direct radiation and increase in diffuse radiation reaching the Earth's surface would occur and would be expected to increase photosynthesis in terrestrial ecosystems (Mercado et al., 2009; see Section 6.5.4) and decrease the efficiency of some solar energy technologies (see WGII AR5, Section 19.5.4). Models indicate that stratospheric aerosol SRM would not pose a surface acidification threat with maximum acid deposition rates estimated to be at least 500 times less than the threshold of concern for the most sensitive land ecosystems (Kuylenstierna et al.,

2001; Kravitz et al., 2009); contributions to ocean acidification are also estimated to represent a very small fraction of that induced by anthropogenic CO_2 emissions (Kravitz et al., 2009). There are other known side effects that remain unquantified, and limited understanding (and limited study) make additional impacts difficult to anticipate.

7.7.2.2 Cloud Brightening

Boundary layer clouds act to cool the planet, and relatively small changes in albedo or areal extent of low cloud can have profound effects on the Earth's radiation budget (Section 7.2.1). Theoretical, modelling and observational studies show that the albedo of these types of cloud systems are susceptible to changes in their droplet concentrations, but the detection and quantification of RF attributable to such effects is difficult to separate from meteorological variability (Section 7.4.3.2). Nonetheless, by systematically introducing CCN into the marine boundary layer, it should be possible to locally increase boundary layer cloud albedo as discussed in Section 7.4.2. These ideas underpin the method of cloud brightening, for instance through the direct injection (seeding) of sea-spray particles into cloud-forming air masses (Latham, 1990). An indirect cloud brightening mechanism through enhanced DMS production has also been proposed (Wingenter et al., 2007) but the efficacy of the DMS mechanism is disputed (Vogt et al., 2008; Woodhouse et al., 2008).

The seeding of cloud layers with a propensity to precipitate may change cloud structure (e.g., from open to closed cells) and/or increase liquid water content (Section 7.4.3.2.1), in either case changing albedo and producing strong negative forcing. A variety of methods have been used to identify which cloud regions are most susceptible to an aerosol change (Oreopoulos and Platnick, 2008; Salter et al., 2008; Alterskjær et al., 2012). Marine stratocumulus clouds with relatively weak precipitation are thought to be an optimal cloud type for brightening because of their relatively low droplet concentrations, their expected increase in cloud water in response to seeding (Section 7.4.3.2.1), and the longer lifetime of sea salt particles in non- or weakly precipitating environments. Relatively strong local ERFaci (–30 to –100 W m^{-2}) would be required to produce a global forcing of –1 to –5 W m^{-2} if only the more susceptible clouds were seeded.

Simple modelling studies suggest that increasing droplet concentrations in marine boundary layer clouds by a factor of five or so (to concentrations of 375 to 1000 cm^{-3}) could produce an ERFaci of about –1 W m^{-2} if 5% of the ocean surface area were seeded, and an ERFaci as strong as –4 W m^{-2} if that fraction were increased to 75% (Latham et al., 2008; Jones et al., 2009; Rasch et al., 2009). Subsequent studies with more complete treatments of aerosol–cloud interactions have produced both stronger (Alterskjær et al., 2012; Partanen et al., 2012) and weaker (Korhonen et al., 2010a) changes. Because the initial response to cloud seeding is local, high-resolution, limited-domain simulations are especially useful to explore the efficacy of seeding. One recent study of this type (Wang et al., 2011a) found that cloud brightening is sensitive to cloud dynamical adjustments that are difficult to treat in current GCMs (Sections 7.4.3 and 7.5.3) and concluded that the seeding rates initially proposed for cloud seeding may be insufficient to produce the desired cloud brightening. Recent studies accounting for clear-sky brightening from increased aerosol concentrations (i.e., ERFari) also found an increase in the amplitude of the ERF by 30 to 50% (Hill and Ming, 2012; Partanen et al., 2012), thereby making the aerosol seeding more effective than previous estimates that neglected that effect.

In summary, evidence that cloud brightening methods are effective and feasible in changing cloud reflectivity is ambiguous and subject to many of the uncertainties associated with aerosol–cloud interactions more broadly. If cloud brightening were to produce large local changes in ERF, those changes would affect the local energy budget, with further impacts on larger-scale oceanic and atmospheric circulations. Possible side effects accompanying such large and spatially heterogeneous changes in ERF have not been systematically studied.

7.7.2.3 Surface Albedo Changes

A few studies have explored how planetary albedo might be increased by engineering local changes to the albedo of urban areas, croplands, grasslands, deserts and the ocean surface. Effects from whitening of urban areas have been estimated to yield a potential RF of –0.17 W m^{-2} (Hamwey, 2007) although subsequent studies (Lenton and Vaughan, 2009; Oleson et al., 2010; Jacobson and Ten Hoeve, 2012) suggest that this estimate may be at the upper end of what is achievable. Larger effects might be achievable by replacing native grassland or cropland with natural or bioengineered species with a larger albedo. A hypothetical 25% increase in grassland albedo could yield a RF as large as –0.5 W m^{-2} (Lenton and Vaughan, 2009), with the maximum effect in the mid-latitudes during summer (Ridgwell et al., 2009; Doughty et al., 2011). The feasibility of increasing crop and grassland albedo remains unknown, and there could be side effects on photosynthetic activity, carbon uptake and biodiversity. The low albedo and large extent of oceanic surfaces mean that only a small increase in albedo, for example, by increasing the concentration of microbubbles in the surface layer of the ocean (Evans et al., 2010; Seitz, 2011), could be sufficient to offset several W m^{-2} of RF by GHGs. Neither the extent of microbubble generation and persistence required for a significant climate impact, nor the potential side effects on the ocean circulation, air-sea fluxes and marine ecosystems have been assessed.

7.7.2.4 Cirrus Thinning

Although not strictly a form of SRM, proposals have been made to cool the planet by reducing the coverage or longwave opacity of high thin cirrus clouds, which act to warm the surface through their greenhouse effect (see Section 7.2.1.2). A proposal for doing so involves adding efficient IN in regions prone to forming thin cirrus cloud (Mitchell and Finnegan, 2009). To the extent such a proposal is feasible, one modelling study suggests that an ERFaci of as strong as –2 W m^{-2} could be achieved (Storelvmo et al., 2013), with further negative forcing caused by a reduction in humidity of the upper troposphere associated with the cloud changes. However, lack of understanding of cirrus cloud formation processes, as well as ice microphysical processes (Section 7.4.4), makes it difficult to judge the feasibility of such a method, particularly in light of the fact that increasing ice nucleation can also increase cirrus opacity, under some circumstances producing an opposite, positive forcing (Storelvmo et al., 2013). Side effects specific to the 'cirrus thinning' method have not been investigated.

7.7.3 Climate Response to Solar Radiation Management Methods

As discussed elsewhere in this and other chapters of this assessment, significant gaps remain in our understanding of the climate response to forcing mechanisms. Geoengineering is also a relatively new field of research. The gaps in understanding, scarcity of studies and diversity in the model experimental design make quantitative model evaluation and intercomparison difficult, hindering an assessment of the efficacy and side effects of SRM. This motivates dividing the discussion into two sections, one that assesses idealized studies that focus on conceptual issues and searches for robust responses to simple changes in the balance between solar irradiance and CO_2 forcing, and another discussing studies that more closely emulate specific SRM methods.

7.7.3.1 Climate Response in Idealized Studies

Perhaps the simplest SRM experiment that can be performed in a climate model consists of a specified reduction of the total solar irradiance, which could approximate the radiative impact of space reflectors. Reductions in solar irradiance in particular regions (over land or ocean, or in polar or tropical regions) could also provide useful information. Idealized simulations often focus on the effects of a complete cancellation of the warming from GHGs, but the rate of warming is occasionally explored by producing a negative RF that partially cancels the anthropogenic forcing (e.g., Eliseev et al., 2009). They can also provide insight into the climate response to other SRM methods, and can provide a simple baseline for examining other SRM techniques.

The most comprehensive and systematic evaluation of idealized SRM to date is the Geoengineering Model Intercomparison Project (Kravitz et al., 2011). Together with earlier model studies, this project found robust surface temperature reductions when the total solar irradiance is reduced: when this reduction compensates for CO_2 RF, residual effects appear regionally, but they are much smaller than the warming due to the CO_2 RF alone (Kravitz et al., 2011; Schmidt et al., 2012b; Figures 7.22a, b and 7.23a–d) The substantial warming from 4 × CO_2 at high latitudes (4°C to 18°C) is reduced to a warming of 0°C to 3°C near

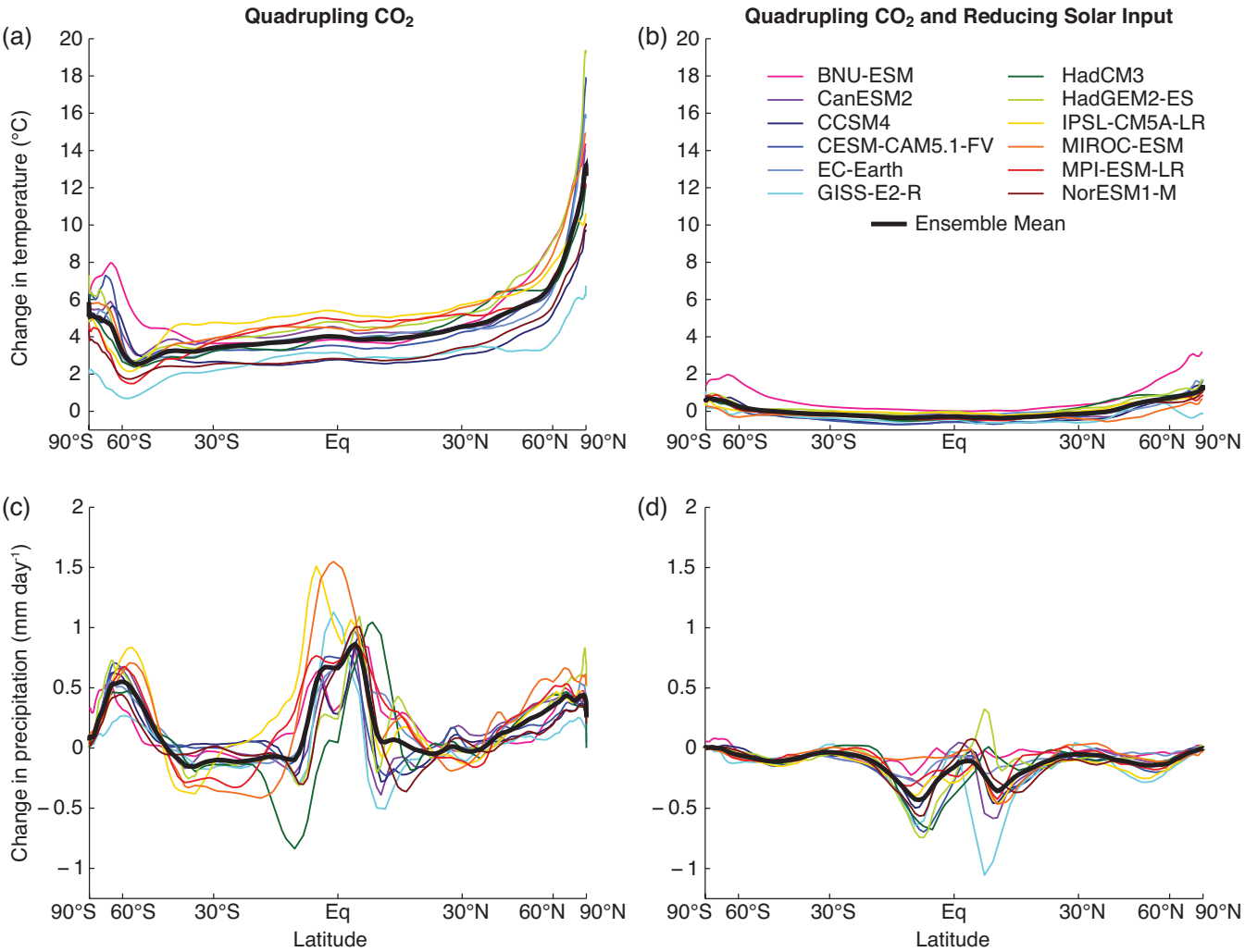

Figure 7.22 | Zonally and annually averaged change in surface air temperature (°C) for (a) an abrupt 4 × CO_2 experiment and (b) an experiment where the 4 × CO_2 forcing is balanced by a reduction in the total solar irradiance to produce a global top of the atmosphere flux imbalance of less than ±0.1 W m^{-2} during the first 10 years of the simulation (Geoengineering Model Intercomparison Project (GeoMIP) G1 experiment; Kravitz et al., 2011). (c, d) Same as (a) and (b) but for the change in precipitation (mm day^{-1}). The multi-model ensemble mean is shown with a thick black solid line. All changes are relative to the pre-industrial control experiment and averaged over years 11 to 50. The figure extends the results from Schmidt et al. (2012b) and shows the results from an ensemble of 12 coupled ocean–atmosphere general circulation models.

the winter pole. The residual surface temperature changes are generally positive at mid- and high-latitudes, especially over continents, and generally negative in the tropics (Bala et al., 2008; Lunt et al., 2008; Schmidt et al., 2012b). These anomalies can be understood in terms of the difference between the more uniform longwave forcing associated with changes in long-lived GHGs and the less uniform shortwave forcing from SRM that has a stronger variation in latitude and season. The compensation between SRM and CO_2 forcing is inexact in other ways. For example, SRM will change heating rates only during daytime, but increasing greenhouse effect changes temperatures during both day and night, influencing the diurnal cycle of surface temperature even if compensation for the diurnally averaged surface temperature is correct.

Although increasing CO_2 concentrations lead to a positive RF that warms the entire troposphere, SRM produces a negative RF that tends to cool the surface. The combination of RFs produces an increase in

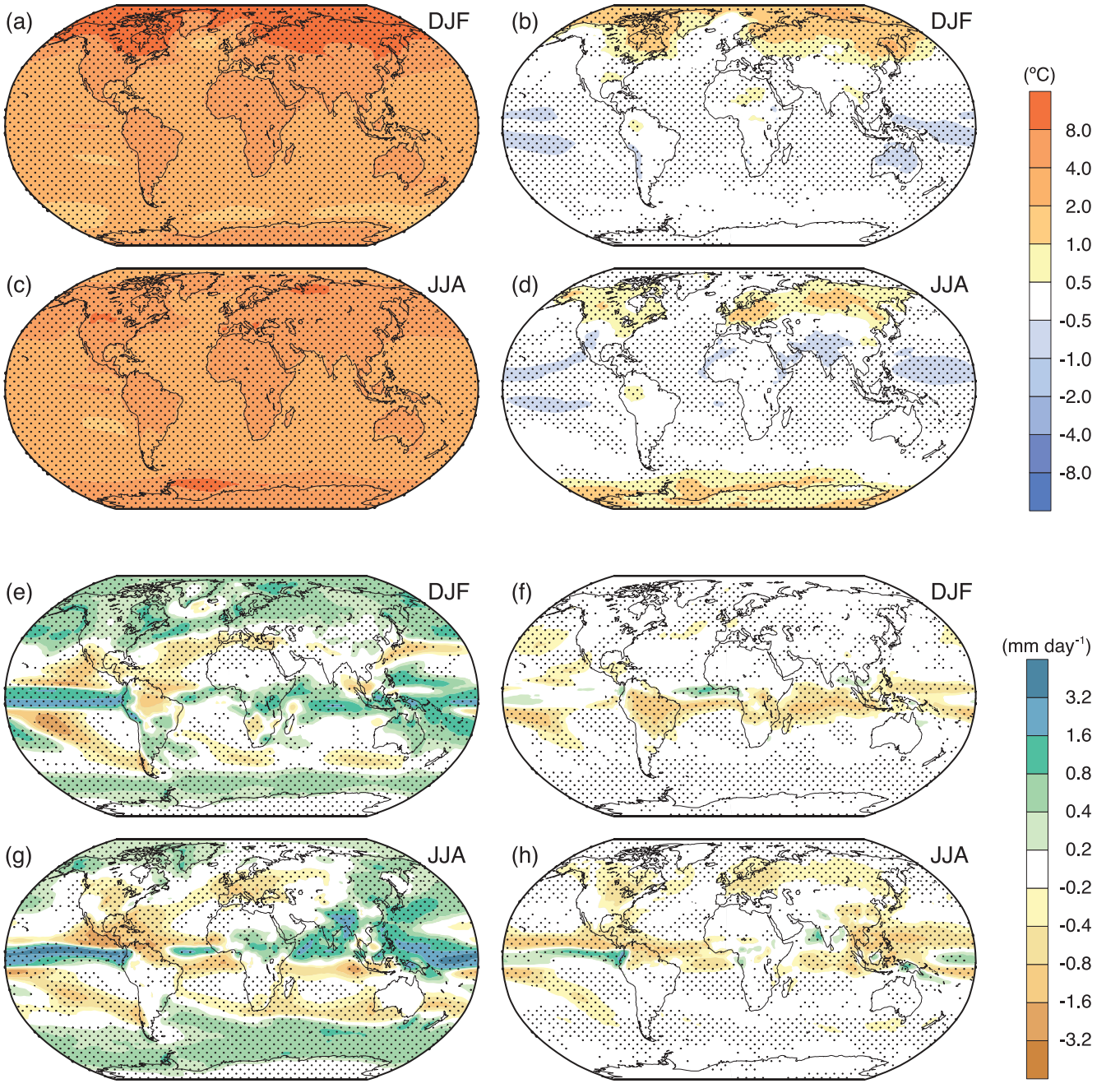

Figure 7.23 | Multi-model mean of the change in surface air temperature (°C) averaged over December, January and February (DJF) for (a) an abrupt 4 × CO_2 simulation and (b) an experiment where the 4 × CO_2 forcing is balanced by a reduction in the total solar irradiance to produce a global top of the atmosphere flux imbalance of less than ±0.1 W m^{-2} during the first 10 years of the simulation (Geoengineering Model Intercomparison Project (GeoMIP) G1 experiment; Kravitz et al., 2011). (c, d) Same as (a-b) but for June, July and August (JJA). (e–h) same as (a–d) but for the change in precipitation (mm day^{-1}). All changes are relative to the pre-industrial control experiment and averaged over years 11 to 50. The figure extends the results from Schmidt et al. (2012b) and shows the results from an ensemble of 12 coupled ocean–atmosphere general circulation models. Stippling denotes agreement on the sign of the anomaly in at least 9 out of the 12 models.

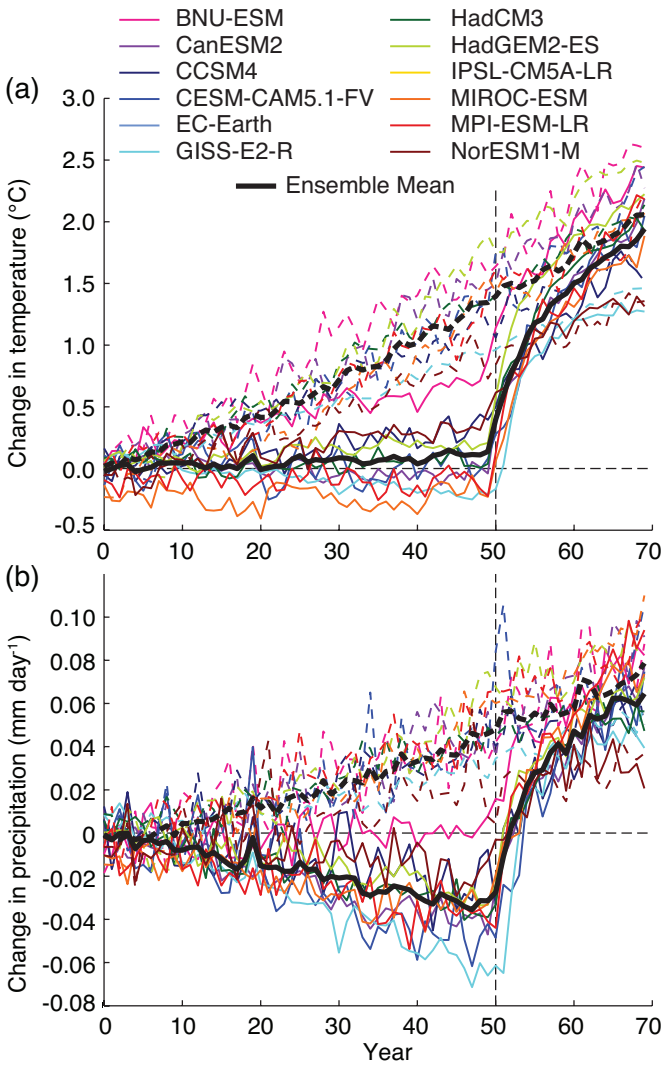

Figure 7.24 | Time series of globally averaged (a) surface temperature (°C) and (b) precipitation (mm day^{-1}) changes relative to each model's 1 × CO_2 reference simulation. Solid lines are for simulations using solar radiation management (SRM) through an increasing reduction of the total solar irradiance to balance a 1% yr^{-1} increase in CO_2 concentration until year 50, after which SRM is stopped for the next 20 years (Geoengineering Model Intercomparison Project (GeoMIP) G2 experiment; Kravitz et al., 2011). Dashed lines are for 1% CO_2 increase simulations with no SRM. The multi-model ensemble mean is shown with thick black lines.

stability that leads to less global precipitation as seen in Figures 7.22c, d and 7.23e–g (Bala et al., 2008; Andrews et al., 2010; Schmidt et al., 2012b) and discussed in Section 7.6.3. The reduction in precipitation shows similarities to the climate response induced by the Pinatubo eruption (Trenberth and Dai, 2007). Although the impact of changes in the total solar irradiance on global mean precipitation is well understood and robust in models, there is less understanding and agreement among models in the spatial pattern of the precipitation changes. Modelling studies suggest that some residual patterns may be robust (e.g., approximately 5% reduction in precipitation over Southeast Asia and the Pacific Warm Pool in June, July and August), but a physical explanation for these changes is lacking. Some model results indicate that an asymmetric hemispheric SRM forcing would induce changes in some regional precipitation patterns (Haywood et al., 2013).

High CO_2 concentrations from anthropogenic emissions will persist in the atmosphere for more than a thousand years in the absence of active efforts to remove atmospheric CO_2 (see Chapter 6). If SRM were used to counter positive forcing, it would be needed as long as the CO_2 concentrations remained high (Boucher et al., 2009). If GHG concentrations continued to increase, then the scale of SRM to offset the resulting warming would need to increase proportionally, amplifying residual effects from increasingly imperfect compensation. Figure 7.24 shows projections of the globally averaged surface temperature and precipitation changes associated with a 1% yr^{-1} CO_2 increase, with and without SRM. The scenario includes a hypothetical, abrupt termination of SRM at year 50, which could happen due to any number of unforeseeable circumstances. After this event, all the simulations predict a return to temperature levels consistent with the CO_2 forcing within one to two decades (*high confidence*), and with a large rate of temperature change (see also Irvine et al., 2012). Precipitation, which drops by 1% over the SRM period, rapidly returns to levels consistent with the CO_2 forcing upon SRM termination. The very rapid warming would probably affect ecosystem and human adaptation, and would also weaken carbon sinks, accelerating atmospheric CO_2 accumulation and contributing to further warming (Matthews and Caldeira, 2007).

Research suggests that this 'termination effect' might be avoided if SRM were used at a modest level and for a relatively short period of time (less than a century) when combined with aggressive CO_2 removal efforts to minimize the probability that the global mean temperature might exceed some threshold (Matthews, 2010; Smith and Rasch, 2012).

7.7.3.2 Climate Response to Specific Solar Radiation Management Methods

Several studies examined the model response to more realistic stratospheric aerosol SRM (Rasch et al., 2008b; Robock et al., 2008; Jones et al., 2010; Fyfe et al., 2013). These studies produced varying aerosol burdens, and RF and model responses also varied more strongly than in idealized experiments. Although these studies differ in details, their climate responses were generally consistent with the idealized experiments described in Section 7.7.3.1.

Studies treating the interaction between the carbon cycle, the hydrologic cycle, and SRM indicate that SRM could affect the temperature-driven suppression of some carbon sinks, and that the increased stomatal resistance with increased CO_2 concentrations combined with less warming, may further affect the hydrological cycle over land (Matthews and Caldeira, 2007; Fyfe et al., 2013), with larger impacts on precipitation for stratospheric aerosol SRM than for a uniform reduction in incoming sunlight.

Coupled ocean–atmosphere–sea ice models have also been used to assess the climate impacts of cloud brightening due to droplet concentration changes (Jones et al., 2009; Rasch et al., 2009; Baughman et al., 2012; Hill and Ming, 2012). The patterns of temperature and precipitation change differ substantially between models. These studies showed larger residual temperature changes than the idealized SRM studies, with more pronounced cooling over the regions of enhanced albedo. The cooling over the seeded regions (the marine stratocumulus regions)

Frequently Asked Questions

FAQ 7.3 | Could Geoengineering Counteract Climate Change and What Side Effects Might Occur?

Geoengineering—also called climate engineering—is defined as a broad set of methods and technologies that aim to deliberately alter the climate system in order to alleviate impacts of climate change. Two distinct categories of geoengineering methods are usually considered: Solar Radiation Management (SRM, assessed in Section 7.7) aims to offset the warming from anthropogenic greenhouse gases by making the planet more reflective while Carbon Dioxide Removal (CDR, assessed in Section 6.5) aims at reducing the atmospheric CO_2 concentration. The two categories operate on different physical principles and on different time scales. Models suggest that if SRM methods were realizable they would be effective in countering increasing temperatures, and would be less, but still, effective in countering some other climate changes. SRM would not counter all effects of climate change, and all proposed geoengineering methods also carry risks and side effects. Additional consequences cannot yet be anticipated as the level of scientific understanding about both SRM and CDR is low. There are also many (political, ethical, and practical) issues involving geoengineering that are beyond the scope of this report.

Carbon Dioxide Removal Methods

CDR methods aim at removing CO_2 from the atmosphere by deliberately modifying carbon cycle processes, or by industrial (e.g., chemical) approaches. The carbon withdrawn from the atmosphere would then be stored in land, ocean or in geological reservoirs. Some CDR methods rely on biological processes, such as large-scale afforestation/reforestation, carbon sequestration in soils through biochar, bioenergy with carbon capture and storage (BECCS) and ocean fertilization. Others would rely on geological processes, such as accelerated weathering of silicate and carbonate rocks—on land or in the ocean (see FAQ.7.3, Figure 1). The CO_2 removed from the atmosphere would

(continued on next page)

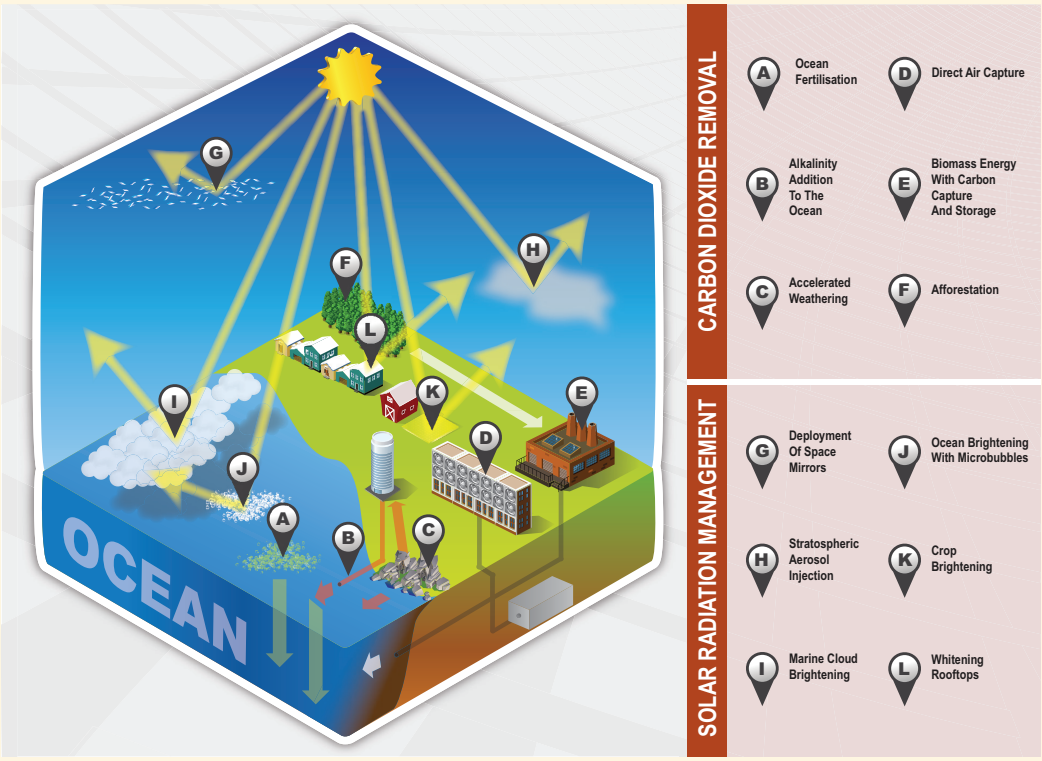

FAQ 7.3, Figure 1 | Overview of some proposed geoengineering methods as they have been suggested. Carbon Dioxide Removal methods (see Section 6.5 for details): (A) nutrients are added to the ocean (ocean fertilization), which increases oceanic productivity in the surface ocean and transports a fraction of the resulting biogenic carbon downward; (B) alkalinity from solid minerals is added to the ocean, which causes more atmospheric CO_2 to dissolve in the ocean; (C) the weathering rate of silicate rocks is increased, and the dissolved carbonate minerals are transported to the ocean; (D) atmospheric CO_2 is captured chemically, and stored either underground or in the ocean; (E) biomass is burned at an electric power plant with carbon capture, and the captured CO_2 is stored either underground or in the ocean; and (F) CO_2 is captured through afforestation and reforestation to be stored in land ecosystems. Solar Radiation Management methods (see Section 7.7 for details): (G) reflectors are placed in space to reflect solar radiation; (H) aerosols are injected in the stratosphere; (I) marine clouds are seeded in order to be made more reflective; (J) microbubbles are produced at the ocean surface to make it more reflective; (K) more reflective crops are grown; and (L) roofs and other built structures are whitened.

FAQ 7.3 (continued)

then be stored in organic form in land reservoirs, or in inorganic form in oceanic and geological reservoirs, where it would have to be stored for at least hundreds of years for CDR to be effective.

CDR methods would reduce the radiative forcing of CO_2 inasmuch as they are effective at removing CO_2 from the atmosphere and keeping the removed carbon away from the atmosphere. Some methods would also reduce ocean acidification (see FAQ 3.2), but other methods involving oceanic storage might instead increase ocean acidification if the carbon is sequestered as dissolved CO_2. A major uncertainty related to the effectiveness of CDR methods is the storage capacity and the permanence of stored carbon. Permanent carbon removal and storage by CDR would decrease climate warming in the long term. However, non-permanent storage strategies would allow CO_2 to return back to the atmosphere where it would once again contribute to warming. An intentional removal of CO_2 by CDR methods will be partially offset by the response of the oceanic and terrestrial carbon reservoirs if the CO_2 atmospheric concentration is reduced. This is because some oceanic and terrestrial carbon reservoirs will outgas to the atmosphere the anthropogenic CO_2 that had previously been stored. To completely offset past anthropogenic CO_2 emissions, CDR techniques would therefore need to remove not just the CO_2 that has accumulated in the atmosphere since pre-industrial times, but also the anthropogenic carbon previously taken up by the terrestrial biosphere and the ocean.

Biological and most chemical weathering CDR methods cannot be scaled up indefinitely and are necessarily limited by various physical or environmental constraints such as competing demands for land. Assuming a maximum CDR sequestration rate of 200 PgC per century from a combination of CDR methods, it would take about one and half centuries to remove the CO_2 emitted in the last 50 years, making it difficult—even for a suite of additive CDR methods—to mitigate climate change rapidly. Direct air capture methods could in principle operate much more rapidly, but may be limited by large-scale implementation, including energy use and environmental constraints.

CDR could also have climatic and environmental side effects. For instance, enhanced vegetation productivity may increase emissions of N_2O, which is a more potent greenhouse gas than CO_2. A large-scale increase in vegetation coverage, for instance through afforestation or energy crops, could alter surface characteristics, such as surface reflectivity and turbulent fluxes. Some modelling studies have shown that afforestation in seasonally snow-covered boreal regions could in fact accelerate global warming, whereas afforestation in the tropics may be more effective at slowing global warming. Ocean-based CDR methods that rely on biological production (i.e., ocean fertilization) would have numerous side effects on ocean ecosystems, ocean acidity and may produce emissions of non-CO_2 greenhouse gases.

Solar Radiation Management Methods

The globally averaged surface temperature of the planet is strongly influenced by the amount of sunlight absorbed by the Earth's atmosphere and surface, which warms the planet, and by the existence of the greenhouse effect, the process by which greenhouse gases and clouds affect the way energy is eventually radiated back to space. An increase in the greenhouse effect leads to a surface temperature rise until a new equilibrium is found. If less incoming sunlight is absorbed because the planet has been made more reflective, or if energy can be emitted to space more effectively because the greenhouse effect is reduced, the average global surface temperature will be reduced.

Suggested geoengineering methods that aim at managing the Earth's incoming and outgoing energy flows are based on this fundamental physical principle. Most of these methods propose to either reduce sunlight reaching the Earth or increase the reflectivity of the planet by making the atmosphere, clouds or the surface brighter (see FAQ 7.3, Figure 1). Another technique proposes to suppress high-level clouds called cirrus, as these clouds have a strong greenhouse effect. Basic physics tells us that if any of these methods change energy flows as expected, then the planet will cool. The picture is complicated, however, because of the many and complex physical processes which govern the interactions between the flow of energy, the atmospheric circulation, weather and the resulting climate.

While the globally averaged surface temperature of the planet will respond to a change in the amount of sunlight reaching the surface or a change in the greenhouse effect, the temperature at any given location and time is influenced by many other factors and the amount of cooling from SRM will not in general equal the amount of warming caused by greenhouse gases. For example, SRM will change heating rates only during daytime, but increasing greenhouse gases can change temperatures during both day and night. This inexact compensation can influence

(continued on next page)

FAQ 7.3 (continued)

the diurnal cycle of surface temperature, even if the average surface temperature is unchanged. As another example, model calculations suggest that a uniform decrease in sunlight reaching the surface might offset global mean CO_2-induced warming, but some regions will cool less than others. Models suggest that if anthropogenic greenhouse warming were completely compensated by stratospheric aerosols, then polar regions would be left with a small residual warming, while tropical regions would become a little cooler than in pre-industrial times.

SRM could theoretically counteract anthropogenic climate change rapidly, cooling the Earth to pre-industrial levels within one or two decades. This is known from climate models but also from the climate records of large volcanic eruptions. The well-observed eruption of Mt Pinatubo in 1991 caused a temporary increase in stratospheric aerosols and a rapid decrease in surface temperature of about 0.5°C.

Climate consists of many factors besides surface temperature. Consequences for other climate features, such as rainfall, soil moisture, river flow, snowpack and sea ice, and ecosystems may also be important. Both models and theory show that compensating an increased greenhouse effect with SRM to stabilize surface temperature would somewhat lower the globally averaged rainfall (see FAQ 7.3, Figure 2 for an idealized model result), and there also could be regional changes. Such imprecise compensation in regional and global climate patterns makes it improbable that SRM will produce a future climate that is 'just like' the one we experience today, or have experienced in the past. However, available climate models indicate that a geoengineered climate with SRM and high atmospheric CO_2 levels would be generally closer to 20th century climate than a future climate with elevated CO_2 concentrations and no SRM.

SRM techniques would probably have other side effects. For example, theory, observation and models suggest that stratospheric sulphate aerosols from volcanic eruptions and natural emissions deplete stratospheric ozone, especially while chlorine from chlorofluorocarbon emissions resides in the atmosphere. Stratospheric aerosols introduced for SRM are expected to have the same effect. Ozone depletion would increase the amount of ultraviolet light reaching the surface damaging terrestrial and marine ecosystems. Stratospheric aerosols would also increase the ratio of direct to diffuse sunlight reaching the surface, which generally increases plant productivity. There has also been some concern that sulphate aerosol SRM would increase acid rain, but model studies suggest that acid rain is probably not a major concern since the rate of acid rain production from stratospheric aerosol SRM would be much smaller than values currently produced by pollution sources. SRM will also not address the ocean acidification associated with increasing atmospheric CO_2 concentrations and its impacts on marine ecosystems.

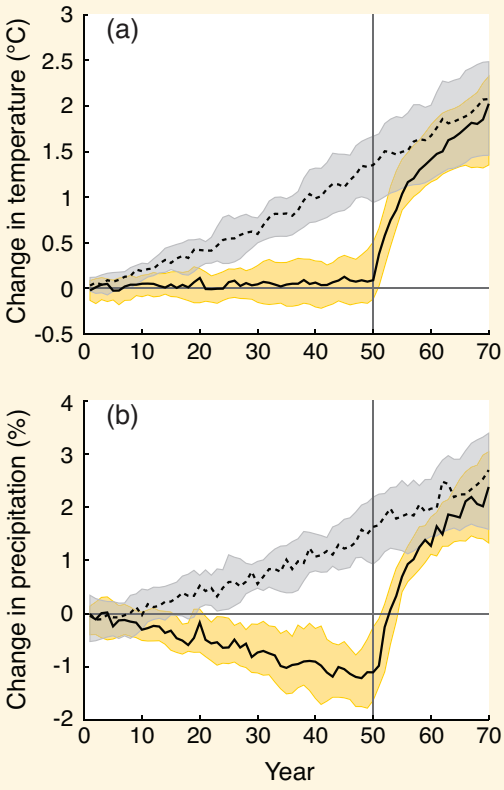

FAQ 7.3, Figure 2 | Change in globally averaged (a) surface temperature (°C) and (b) precipitation (%) in two idealized experiments. Solid lines are for simulations using Solar Radiation Management (SRM) to balance a 1% yr^{-1} increase in CO_2 concentration until year 50, after which SRM is stopped. Dashed lines are for simulations with a 1% yr^{-1} increase in CO_2 concentration and no SRM. The yellow and grey envelopes show the 25th to 75th percentiles from eight different models.

Without conventional mitigation efforts or potential CDR methods, high CO_2 concentrations from anthropogenic emissions will persist in the atmosphere for as long as a thousand years, and SRM would have to be maintained as long as CO_2 concentrations were high. Stopping SRM while CO_2 concentrations are still high would lead to a very rapid warming over one or two decades (see FAQ7.3, Figure 2), severely stressing ecosystem and human adaptation.

If SRM were used to avoid some consequences of increasing CO_2 concentrations, the risks, side effects and shortcomings would clearly increase as the scale of SRM increase. Approaches have been proposed to use a time-limited amount of SRM along with aggressive strategies for reducing CO_2 concentrations to help avoid transitions across climate thresholds or tipping points that would be unavoidable otherwise; assessment of such approaches would require a very careful risk benefit analysis that goes much beyond this Report.

and a warmer North Pacific adjacent to a cooler northwestern Canada, produced a SST response with a La Niña-like pattern. One study has noted regional shifts in the potential hurricane intensity and hurricane genesis potential index in the Atlantic Ocean and South China Sea in response to cloud brightening (Baughman et al., 2012), due primarily to decreases in vertical wind shear, but overall the investigation and identification of robust side effects has not been extensively explored.

Irvine et al. (2011) tested the impact of increasing desert albedo up to 0.80 in a climate model. This cooled surface temperature by –1.1°C (versus –0.22°C and –0.11°C for their largest crop and urban albedo change) and produced very significant changes in regional precipitation patterns.

7.7.4 Synthesis on Solar Radiation Management Methods

Theory, model studies and observations suggest that some SRM methods may be able to counteract a portion of global warming effects (on temperature, sea ice and precipitation) due to high concentrations of anthropogenic GHGs (*high confidence*). But the level of understanding about SRM is low, and it is difficult to assess feasibility and efficacy because of remaining uncertainties in important climate processes and the interactions among those processes. Although SRM research is still in its infancy, enough is known to identify some potential benefits, which must be weighed against known side effects (there could also be side effects that have not yet been identified). All studies suggest there would be a small but measurable decrease in global precipitation from SRM. Other side effects are specific to specific methods, and a number of research areas remain largely unexplored. There are also features that develop as a consequence of the combination of high CO_2 and SRM (e.g., effects on evapotranspiration and precipitation). SRM counters only some consequences of elevated CO_2 concentrations; it does not in particular address ocean acidification.

Many model studies indicate that stratospheric aerosol SRM could counteract some changes resulting from GHG increases that produce a RF as strong as 4 W m^{-2} (*medium confidence*), but they disagree on details. Marine cloud brightening SRM has received less attention, and there is no consensus on its efficacy, in large part due to the high level of uncertainty about cloud radiative responses to aerosol changes. There have been fewer studies and much less attention focused on all other SRM methods, and it is not currently possible to provide a general assessment of their specific efficacy, scalability, side effects and risks.

There is robust agreement among models and *high confidence* that the compensation between GHG warming and SRM cooling is imprecise. SRM would not produce a future climate identical to the present (or pre-industrial) climate. Nonetheless, although models disagree on details, they consistently suggest that a climate with SRM and high atmospheric CO_2 levels would be closer to that of the last century than a world with elevated CO_2 concentrations and no SRM (Lunt et al., 2008; Ricke et al., 2010; Moreno-Cruz et al., 2011), as long as the SRM could be continuously sustained and calibrated to offset the forcing by GHGs. Aerosol-based methods would, however, require a continuous program of replenishment to achieve this. If CO_2 concentrations and SRM were increased in concert, the risks and residual climate change produced by the imprecise compensation between SRM and CO_2 forcing would also increase. If SRM were terminated for any reason, a rapid increase in surface temperatures (within a decade or two) to values consistent with the high GHG forcing would result (*high confidence*). This rate of climate change would far exceed what would have occurred without geoengineering, causing any impacts related to the rate of change to be correspondingly greater than they would have been without geoengineering. In contrast, SRM in concert with aggressive CO_2 mitigation might conceivably help avoid transitions across climate thresholds or tipping points that would be unavoidable otherwise.

Acknowledgements

Thanks go to Anne-Lise Barbanes (IPSL/CNRS, Paris), Bénédicte Fisset (IPSL/CNRS, Paris) and Edwina Berry for their help in assembling the list of references. Sylvaine Ferrachat (ETH Zürich) is acknowledged for her contribution to drafting Figure 7.19.

References

Abdul-Razzak, H., and S. Ghan, 2000: A parameterization of aerosol activation 2. Multiple aerosol types. *J. Geophys. Res.*, **105**, 6837–6844.

Ackerman, A. S., M. P. Kirkpatrick, D. E. Stevens, and O. B. Toon, 2004: The impact of humidity above stratiform clouds on indirect aerosol climate forcing. *Nature*, **432**, 1014–1017.

Ackerman, A. S., et al., 2009: Large-eddy simulations of a drizzling, stratocumulus-topped marine boundary layer. *Mon. Weather Rev.*, **137**, 1083–1110.

Adachi, K., S. H. Chung, and P. R. Buseck, 2010: Shapes of soot aerosol particles and implications for their effects on climate. *J. Geophys. Res.*, **115**, D15206.

Adams, P. J., J. H. Seinfeld, D. Koch, L. Mickley, and D. Jacob, 2001: General circulation model assessment of direct radiative forcing by the sulfate-nitrate-ammonium-water inorganic aerosol system. *J. Geophys. Res.*, **106**, 1097–1111.

Adler, R. F., et al., 2003: The Version 2 Global Precipitation Climatology Project (GPCP) Monthly Precipitation Analysis (1979–Present). *J. Hydrometeor.*, **4**, 1147–1167.

Agee, E. M., K. Kiefer, and E. Cornett, 2012: Relationship of lower troposphere cloud cover and cosmic rays: An updated perspective. *J. Clim.*, **25**, 1057–1060.

Albrecht, B. A., 1989: Aerosols, cloud microphysics, and fractional cloudiness. *Science*, **245**, 1227–1230.

Aldrin, M., M. Holden, P. Guttorp, R. B. Skeie, G. Myhre, and T. K. Berntsen, 2012: Bayesian estimation of climate sensitivity based on a simple climate model fitted to observations of hemispheric temperatures and global ocean heat content. *Environmetrics*, **23**, 253–271.

Allan, R. P., and B. J. Soden, 2007: Large discrepancy between observed and simulated precipitation trends in the ascending and descending branches of the tropical circulation. *Geophys. Res. Lett.*, **34**, L18705.

Allen, M. R., and W. J. Ingram, 2002: Constraints on future changes in climate and the hydrologic cycle. *Nature*, **419**, 224–232.

Allen, R. J., and S. C. Sherwood, 2010: Aerosol-cloud semi-direct effect and land-sea temperature contrast in a GCM. *Geophys. Res. Lett.*, **37**, L07702.

Allen, R. J., S. C. Sherwood, J. R. Norris, and C. S. Zender, 2012: Recent Northern Hemisphere tropical expansion primarily driven by black carbon and tropospheric ozone. *Nature*, **485**, 350–354.

Alpert, P., N. Halfon, and Z. Levin, 2008: Does air pollution really suppress precipitation in Israel? *J. Appl. Meteor. Climatol.*, **47**, 933–943.

Alterskjær, K., J. E. Kristjánsson, and Ø. Seland, 2012: Sensitivity to deliberate sea salt seeding of marine clouds - observations and model simulations. *Atmos. Chem. Phys.*, **12**, 2795–2807.

Anderson, T. L., et al., 2005: An "A-Train" strategy for quantifying direct climate forcing by anthropogenic aerosols. *Bull. Am. Meteor. Soc.*, **86**, 1795–1809.

Anderson, T. L., et al., 2009: Temporal and spatial variability of clouds and related aerosol. In: *Clouds in the Perturbed Climate System: Their Relationship to Energy Balance, Atmospheric Dynamics, and Precipitation* [R. J. Charlson, and J. Heintzenberg (eds.)]. MIT Press, Cambridge, MA, USA, pp. 127–148.

Andreae, M. O., and A. Gelencser, 2006: Black carbon or brown carbon? The nature of light-absorbing carbonaceous aerosols. *Atmos. Chem. Phys.*, **6**, 3131–3148.

Andreae, M. O., C. D. Jones, and P. M. Cox, 2005: Strong present-day aerosol cooling implies a hot future. *Nature*, **435**, 1187–1190.

Andreae, M. O., D. Rosenfeld, P. Artaxo, A. A. Costa, G. P. Frank, K. M. Longo, and M. A. F. Silva-Dias, 2004: Smoking rain clouds over the Amazon. *Science*, **303**, 1337–1342.

Andrejczuk, M., W. W. Grabowski, S. P. Malinowski, and P. K. Smolarkiewicz, 2006: Numerical simulation of cloud-clear air interfacial mixing: Effects on cloud microphysics. *J. Atmos. Sci.*, **63**, 3204–3225.

Andrews, T., and P. M. Forster, 2008: CO_2 forcing induces semi-direct effects with consequences for climate feedback interpretations. *Geophys. Res. Lett.*, **35**, L04802.

Andrews, T., P. M. Forster, and J. M. Gregory, 2009: A surface energy perspective on climate change. *J. Clim.*, **22**, 2557–2570.

Andrews, T., J. M. Gregory, M. J. Webb, and K. E. Taylor, 2012: Forcing, feedbacks and climate sensitivity in CMIP5 coupled atmosphere-ocean climate models. *Geophys. Res. Lett.*, **39**, L09712.

Andrews, T., P. M. Forster, O. Boucher, N. Bellouin, and A. Jones, 2010: Precipitation, radiative forcing and global temperature change. *Geophys. Res. Lett.*, **37**, L14701.

Angel, R., 2006: Feasibility of cooling the Earth with a cloud of small spacecraft near the inner Lagrange Point (L1). *Proc. Natl. Acad. Sci. U.S.A.*, **103**, 17184–17189.

Ansmann, A., et al., 2008: Influence of Saharan dust on cloud glaciation in southern Morocco during the Saharan Mineral Dust Experiment. *J. Geophys. Res.*, **113**, D04210.

Arakawa, A., 1975: Modeling clouds and cloud processes for use in climate models. In: *The Physical Basis of Climate and Climate Modelling*. ICSU/WMO, GARP Publications Series N° 16, Geneva, Switzerland, pp. 181–197.

Arakawa, A., 2004: The cumulus parameterization problem: Past, present, and future. *J. Clim.*, **17**, 2493–2525.

Arneth, A., R. K. Monson, G. Schurgers, U. Niinemets, and P. I. Palmer, 2008: Why are estimates of global terrestrial isoprene emissions so similar (and why is this not so for monoterpenes)? *Atmos. Chem. Phys.*, **8**, 4605–4620.

Arneth, A., P. A. Miller, M. Scholze, T. Hickler, G. Schurgers, B. Smith, and I. C. Prentice, 2007: CO_2 inhibition of global terrestrial isoprene emissions: Potential implications for atmospheric chemistry. *Geophys. Res. Lett.*, **34**, L18813.

Arnold, F., 2006: Atmospheric aerosol and cloud condensation nuclei formation: A possible influence of cosmic rays? *Space Sci. Rev.*, **125**, 169–186.

Artaxo, P., et al., 1998: Large-scale aerosol source apportionment in Amazonia. *J. Geophys. Res.*, **103**, 31837–31847.

Artaxo, P., et al., 2002: Physical and chemical properties of aerosols in the wet and dry seasons in Rondônia, Amazonia. *J. Geophys. Res.*, **107**, 8081.

Asmi, A., et al., 2011: Number size distributions and seasonality of submicron particles in Europe 2008–2009. *Atmos. Chem. Phys.*, **11**, 5505–5538.

Aw, J., and M. J. Kleeman, 2003: Evaluating the first-order effect of intraannual temperature variability on urban air pollution. *J. Geophys. Res.*, **108**, 4365.

Ayers, G. P., and J. M. Cainey, 2007: The CLAW hypothesis: A review of the major developments. *Environ. Chem.*, **4**, 366–374.

Babu, S. S., et al., 2011: Free tropospheric black carbon aerosol measurements using high altitude balloon: Do BC layers build "their own homes" up in the atmosphere? *Geophys. Res. Lett.*, **38**, L08803.

Baker, M. B., and R. J. Charlson, 1990: Bistability of CCN concentrations and thermodynamics in the cloud-topped boundary-layer. *Nature*, **345**, 142–145.

Baker, M. B., and T. Peter, 2008: Small-scale cloud processes and climate. *Nature*, **451**, 299–300.

Bala, G., P. B. Duffy, and K. E. Taylor, 2008: Impact of geoengineering schemes on the global hydrological cycle. *Proc. Natl. Acad. Sci. U.S.A.*, **105**, 7664–7669.

Ban-Weiss, G., L. Cao, G. Bala, and K. Caldeira, 2012: Dependence of climate forcing and response on the altitude of black carbon aerosols. *Clim. Dyn.*, **38**, 897–911.

Bangert, M., C. Kottmeier, B. Vogel, and H. Vogel, 2011: Regional scale effects of the aerosol cloud interaction simulated with an online coupled comprehensive chemistry model. *Atmos. Chem. Phys.*, **11**, 4411–4423.

Barahona, D., and A. Nenes, 2008: Parameterization of cirrus cloud formation in large-scale models: Homogeneous nucleation. *J. Geophys. Res.*, **113**, D11211.

Barahona, D., and A. Nenes, 2009: Parameterizing the competition between homogeneous and heterogeneous freezing in ice cloud formation—polydisperse ice nuclei. *Atmos. Chem. Phys.*, **9**, 5933–5948.

Barker, H. W., J. N. S. Cole, J.-J. Morcrette, R. Pincus, P. Raisaenen, K. von Salzen, and P. A. Vaillancourt, 2008: The Monte Carlo Independent Column Approximation: An assessment using several global atmospheric models. *Q. J. R. Meteorol. Soc.*, **134**, 1463–1478.

Barker, H. W., et al., 2003: Assessing 1D atmospheric solar radiative transfer models: Interpretation and handling of unresolved clouds. *J. Clim.*, **16**, 2676–2699.

Barmet, P., T. Kuster, A. Muhlbauer, and U. Lohmann, 2009: Weekly cycle in particulate matter versus weekly cycle in precipitation over Switzerland. *J. Geophys. Res.*, **114**, D05206.

Bauer, S., E. Bierwirth, M. Esselborn, A. Petzold, A. Macke, T. Trautmann, and M. Wendisch, 2011: Airborne spectral radiation measurements to derive solar radiative forcing of Saharan dust mixed with biomass burning smoke particles. *Tellus B*, **63**, 742–750.

Bauer, S. E., and S. Menon, 2012: Aerosol direct, indirect, semidirect, and surface albedo effects from sector contributions based on the IPCC AR5 emissions for preindustrial and present-day conditions. *J. Geophys. Res.*, **117**, D01206.

Bauer, S. E., D. Koch, N. Unger, S. M. Metzger, D. T. Shindell, and D. G. Streets, 2007: Nitrate aerosols today and in 2030: |A global simulation including aerosols and tropospheric ozone. *Atmos. Chem. Phys.*, **7**, 5043–5059.

Baughman, E., A. Gnanadesikan, A. Degaetano, and A. Adcroft, 2012: Investigation of the surface and circulation impacts of cloud-brightening geoengineering. *J. Clim.*, **25**, 7527–7543.

Bäumer, D., and B. Vogel, 2007: An unexpected pattern of distinct weekly periodicities in climatological variables in Germany. *Geophys. Res. Lett.*, **34**, L03819.

Baumgardner, D., et al., 2012: Soot reference materials for instrument calibration and intercomparisons: A workshop summary with recommendations. *Atmos. Meas. Tech.*, **5**, 1869–1887.

Bazilevskaya, G. A., et al., 2008: Cosmic ray induced ion production in the atmosphere. *Space Sci. Rev.*, **137**, 149–173.

Bechtold, P., et al., 2008: Advances in simulating atmospheric variability with the ECMWF model: From synoptic to decadal time-scales. *Q. J. R. Meteorol. Soc.*, **134**, 1337–1351.

Bell, T. L., D. Rosenfeld, K.-M. Kim, J.-M. Yoo, M.-I. Lee, and M. Hahnenberger, 2008: Midweek increase in US summer rain and storm heights suggests air pollution invigorates rainstorms. *J. Geophys. Res.*, **113**, D02209.

Bellouin, N., and O. Boucher, 2010: Climate response and efficacy of snow forcing in the HadGEM2–AML climate model. Hadley Centre Technical Note N°82. Met Office, Exeter, Devon, UK.

Bellouin, N., O. Boucher, J. Haywood, and M. S. Reddy, 2005: Global estimate of aerosol direct radiative forcing from satellite measurements. *Nature*, **438**, 1138–1141.

Bellouin, N., A. Jones, J. Haywood, and S. A. Christopher, 2008: Updated estimate of aerosol direct radiative forcing from satellite observations and comparison against the Hadley Centre climate model. *J. Geophys. Res.*, **113**, D10205.

Bellouin, N., J. Quaas, J.-J. Morcrette, and O. Boucher, 2013: Estimates of aerosol radiative forcing from the MACC re-analysis. *Atmos. Chem. Phys.*, **13**, 2045–2062.

Bellouin, N., J. Rae, C. Johnson, J. Haywood, A. Jones, and O. Boucher, 2011: Aerosol forcing in the Climate Model Intercomparison Project (CMIP5) simulations by HadGEM2–ES and the role of ammonium nitrate. *J. Geophys. Res.*, **116**, D20206.

Bender, F. A.-M., V. Ramanathan, and G. Tselioudis, 2012: Changes in extratropical storm track cloudiness 1983–2008: Observational support for a poleward shift. *Clim. Dyn.*, **38**, 2037–2053.

Benedetti, A., et al., 2009: Aerosol analysis and forecast in the ECMWF Integrated Forecast System. Part II : Data assimilation. *J. Geophys. Res.*, **114**, D13205.

Benedict, J. J., and D. A. Randall, 2009: Structure of the Madden-Julian Oscillation in the Superparameterized CAM. *J. Atmos. Sci.*, **66**, 3277–3296.

Berg, L. K., C. M. Berkowitz, J. C. Barnard, G. Senum, and S. R. Springston, 2011: Observations of the first aerosol indirect effect in shallow cumuli. *Geophys. Res. Lett.*, **38**, L03809.

Bergamo, A., A. M. Tafuro, S. Kinne, F. De Tomasi, and M. R. Perrone, 2008: Monthly-averaged anthropogenic aerosol direct radiative forcing over the Mediterranian based on AERONET aerosol properties. *Atmos. Chem. Phys.*, **8**, 6995–7014.

Bergstrom, R. W., et al., 2010: Aerosol spectral absorption in the Mexico City area: Results from airborne measurements during MILAGRO/INTEX B. *Atmos. Chem. Phys.*, **10**, 6333–6343.

Bertram, A. K., T. Koop, L. T. Molina, and M. J. Molina, 2000: Ice formation in $(NH_4)_2SO_4$–H_2O particles. *J. Phys. Chem. A*, **104**, 584–588.

Bewick, R., J. P. Sanchez, and C. R. McInnes, 2012: Gravitationally bound geoengineering dust shade at the inner Lagrange point. *Adv. Space Res.*, **50**, 1405–1410.

Bharmal, N. A., A. Slingo, G. J. Robinson, and J. J. Settle, 2009: Simulation of surface and top of atmosphere thermal fluxes and radiances from the radiative atmospheric divergence using the ARM Mobile Facility, GERB data, and AMMA Stations experiment. *J. Geophys. Res.*, **114**, D00E07.

Bi, X., et al., 2011: Mixing state of biomass burning particles by single particle aerosol mass spectrometer in the urban area of PRD, China. *Atmos. Environ.*, **45**, 3447–3453.

Blossey, P. N., C. S. Bretherton, J. Cetrone, and M. Kharoutdinov, 2007: Cloud-resolving model simulations of KWAJEX: Model sensitivities and comparisons with satellite and radar observations. *J. Atmos. Sci.*, **64**, 1488–1508.

Blossey, P. N., et al., 2013: Marine low cloud sensitivity to an idealized climate change: The CGILS LES intercomparison. *J. Adv. Model. Earth Syst.*, **5**, 234–258.

Bodenschatz, E., S. P. Malinowski, R. A. Shaw, and F. Stratmann, 2010: Can we understand clouds without turbulence? *Science*, **327**, 970–971.

Boers, R., and R. M. Mitchell, 1994: Absorption feedback in stratocumulus clouds—Influence on cloud-top albedo. *Tellus A*, **46**, 229–241.

Bokoye, A. I., A. Royer, N. T. O'Neil, P. Cliche, G. Fedosejevs, P. M. Teillet, and L. J. B. McArthur, 2001: Characterization of atmospheric aerosols across Canada from a ground-based sunphotometer network: AEROCAN. *Atmos. Ocean*, **39**, 429–456.

Bond, G., et al., 2001: Persistent solar influence on North Atlantic climate during the Holocene. *Science*, **294**, 2130–2136.

Bond, T. C., et al., 2013: Bounding the role of black carbon in the climate system: A scientific assessment. *J. Geophys. Res. Atmos.*, **118**, 5380–5552.

Bondo, T., M. B. Enghoff, and H. Svensmark, 2010: Model of optical response of marine aerosols to Forbush decreases. *Atmos. Chem. Phys.*, **10**, 2765–2776.

Bony, S., and J.-L. Dufresne, 2005: Marine boundary layer clouds at the heart of tropical cloud feedback uncertainties in climate models. *Geophys. Res. Lett.*, **32**, L20806.

Bony, S., J.-L. Dufresne, H. Le Treut, J.-J. Morcrette, and C. Senior, 2004: On dynamic and thermodynamic components of cloud changes. *Clim. Dyn.*, **22**, 71–86.

Bony, S., G. Bellon, D. Klocke, S. Sherwood, S. Fermapin, and S. Denvil, 2013: Robust direct effect of carbon dioxide on tropical circulation and regional precipitation. *Nature Geosci.*, **6**, 447–451.

Bony, S., et al., 2006: How well do we understand and evaluate climate change feedback processes? *J. Clim.*, **19**, 3445–3482.

Bopp, L., O. Boucher, O. Aumont, S. Belviso, J.-L. Dufresne, M. Pham, and P. Monfray, 2004: Will marine dimethylsulfide emissions amplify or alleviate global warming? A model study. *Can. J. Fish. Aquat. Sci.*, **61**, 826–835.

Boucher, O., and U. Lohmann, 1995: The sulfate-CCN-cloud albedo effect—A sensitivity study with two general circulation models. *Tellus B*, **47**, 281–300.

Boucher, O., and J. Quaas, 2013: Water vapour affects both rain and aerosol optical depth. *Nature Geosci.*, **6**, 4–5.

Boucher, O., G. Myhre, and A. Myhre, 2004: Direct influence of irrigation on atmospheric water vapour and climate. *Clim. Dyn.*, **22**, 597–603.

Boucher, O., J. Lowe, and C. D. Jones, 2009: Constraints of the carbon cycle on timescales of climate-engineering options. *Clim. Change*, **92**, 261–273.

Bourotte, C., A.-P. Curi-Amarante, M.-C. Forti, L. A. A. Pereira, A. L. Braga, and P. A. Lotufo, 2007: Association between ionic composition of fine and coarse aerosol soluble fraction and peak expiratory flow of asthmatic patients in Sao Paulo city (Brazil). *Atmos. Environ.*, **41**, 2036–2048.

Boutle, I. A., and S. J. Abel, 2012: Microphysical controls on the stratocumulus topped boundary-layer structure during VOCALS-REx. *Atmos. Chem. Phys.*, **12**, 2849–2863.

Brenguier, J.-L., F. Burnet, and O. Geoffroy, 2011: Cloud optical thickness and liquid water path—does the *k* coefficient vary with droplet concentration? *Atmos. Chem. Phys.*, **11**, 9771–9786.

Bretherton, C. S., P. N. Blossey, and J. Uchida, 2007: Cloud droplet sedimentation, entrainment efficiency, and subtropical stratocumulus albedo. *Geophys. Res. Lett.*, **34**, L03813.

Bretherton, C. S., P. N. Blossey, and C. R. Jones, 2013: A large-eddy simulation of mechanisms of boundary layer cloud response to climate change. *J. Adv. Model. Earth Syst.*, **5**, 316–337.

Brient, F., and S. Bony, 2012: How may low-cloud radiative properties simulated in the current climate influence low-cloud feedbacks under global warming? *Geophys. Res. Lett.*, **39**, L20807.

Brient, F., and S. Bony, 2013: Interpretation of the positive low-cloud feedback predicted by a climate model under global warming. *Clim. Dyn.*, **40**, 2415–2431.

Brioude, J., et al., 2009: Effect of biomass burning on marine stratocumulus clouds off the California coast. *Atmos. Chem. Phys.*, **9**, 8841–8856.

Broccoli, A. J., and S. A. Klein, 2010: Comment on "Observational and model evidence for positive low-level cloud feedback". *Science*, **329**, 277–a.

Brock, C. A., et al., 2011: Characteristics, sources, and transport of aerosols measured in spring 2008 during the aerosol, radiation, and cloud processes affecting Arctic Climate (ARCPAC) Project. *Atmos. Chem. Phys.*, **11**, 2423–2453.

Bryan, G. H., J. C. Wyngaard, and J. M. Fritsch, 2003: Resolution requirements for the simulation of deep moist convection. *Mon. Weather Rev.*, **131**, 2394–2416.

Budyko, M. I., 1974: *Izmeniya Klimata.* Gidrometeoroizdat, Leningrad.

Burkhardt, U., and B. Kärcher, 2009: Process-based simulation of contrail cirrus in a global climate model. *J. Geophys. Res.*, **114**, D16201.

Burkhardt, U., and B. Kärcher, 2011: Global radiative forcing from contrail cirrus. *Nature Clim. Change*, **1**, 54–58.

Burrows, S. M., T. Butler, P. Jöckel, H. Tost, A. Kerkweg, U. Pöschl, and M. G. Lawrence, 2009: Bacteria in the global atmosphere—Part 2: Modeling of emissions and transport between different ecosystems. *Atmos. Chem. Phys.*, **9**, 9281–9297.

Cahalan, R. F., W. Ridgway, W. J. Wiscombe, T. L. Bell, and J. B. Snider, 1994: The albedo of fractal stratocumulus clouds. *J. Atmos. Sci.*, **51**, 2434–2455.

Caldwell, P., and C. S. Bretherton, 2009: Response of a subtropical stratocumulus-capped mixed layer to climate and aerosol changes. *J. Clim.*, **22**, 20–38

Čalogović, J., C. Albert, F. Arnold, J. Beer, L. Desorgher, and E. O. Flueckiger, 2010: Sudden cosmic ray decreases: No change of global cloud cover. *Geophys. Res. Lett.*, **37**, L03802.

Cameron-Smith, P., S. Elliott, M. Maltrud, D. Erickson, and O. Wingenter, 2011: Changes in dimethyl sulfide oceanic distribution due to climate change. *Geophys. Res. Lett.*, **38**, L07704.

Cao, G., X. Zhang, and F. Zheng, 2006: Inventory of black carbon and organic carbon emissions from China. *Atmos. Environ.*, **40**, 6516–6527.

Cappa, C. D., et al., 2012: Radiative absorption enhancements due to the mixing state of atmospheric black carbon. *Science*, **337**, 1078–1081.

Carlton, A. G., R. W. Pinder, P. V. Bhave, and G. A. Pouliot, 2010: To what extent can biogenic SOA be controlled? *Environ. Sci. Technol.*, **44**, 3376–3380.

Carrico, C. M., M. H. Bergin, A. B. Shrestha, J. E. Dibb, L. Gomes, and J. M. Harris, 2003: The importance of carbon and mineral dust to seasonal aerosol properties in the Nepal Himalaya. *Atmos. Environ.*, **37**, 2811–2824.

Carslaw, K. S., R. G. Harrison, and J. Kirkby, 2002: Cosmic rays, clouds, and climate. *Science*, **298**, 1732–1737.

Carslaw, K. S., O. Boucher, D. V. Spracklen, G. W. Mann, J. G. L. Rae, S. Woodward, and M. Kulmala, 2010: A review of natural aerosol interactions and feedbacks within the Earth system. *Atmos. Chem. Phys.*, **10**, 1701–1737.

Celis, J. E., J. R. Morales, C. A. Zarorc, and J. C. Inzunza, 2004: A study of the particulate matter PM_{10} composition in the atmosphere of Chillán, Chile. *Chemosphere*, **54**, 541–550.

Cess, R. D., 1975: Global climate change—Investigation of atmospheric feedback mechanisms. *Tellus*, **27**, 193–198.

Cess, R. D., et al., 1989: Interpretation of cloud-climate feedbacks as produced by 14 atmospheric general circulation models. *Science*, **245**, 513–516.

Cess, R. D., et al., 1990: Intercomparison and interpretation of climate feedback processes in 19 atmospheric general circulation models. *J. Geophys. Res.*, **95**, 16601–16615.

Chae, J. H., and S. C. Sherwood, 2010: Insights into cloud-top height and dynamics from the seasonal cycle of cloud-top heights observed by MISR in the West Pacific region. *J. Atmos. Sci.*, **67**, 248–261.

Chakraborty, A., and T. Gupta, 2010: Chemical characterization and source apportionment of submicron (PM1) aerosol in Kanpur region, India. *Aeros. Air Qual. Res.*, **10**, 433–445.

Chameides, W. L., C. Luo, R. Saylor, D. Streets, Y. Huang, M. Bergin, and F. Giorgi, 2002: Correlation between model-calculated anthropogenic aerosols and satellite-derived cloud optical depths: Indication of indirect effect? *J. Geophys. Res.*, **107**, 4085.

Chan, M. A., and J. C. Comiso, 2011: Cloud features detected by MODIS but not by CloudSat and CALIOP. *Geophys. Res. Lett.*, **38**, L24813.

Chan, Y. C., R. W. Simpson, G. H. Mctainsh, P. D. Vowles, D. D. Cohen, and G. M. Bailey, 1997: Characterisation of chemical species in $PM_{2.5}$ and PM_{10} aerosols in Brisbane, Australia. *Atmos. Environ.*, **31**, 3773–3785.

Chand, D., R. Wood, T. L. Anderson, S. K. Satheesh, and R. J. Charlson, 2009: Satellite-derived direct radiative effect of aerosols dependent on cloud cover. *Nature Geosci.*, **2**, 181–184.

Chand, D., T. L. Anderson, R. Wood, R. J. Charlson, Y. Hu, Z. Liu, and M. Vaughan, 2008: Quantifying above-cloud aerosol using spaceborne lidar for improved understanding of cloudy-sky direct climate forcing. *J. Geophys. Res.*, **113**, D13206.

Chand, D., et al., 2012: Aerosol optical depth increase in partly cloudy conditions. *J. Geophys. Res.*, **117**, D17207.

Chang, F. L., and J. A. Coakley, 2007: Relationships between marine stratus cloud optical depth and temperature: Inferences from AVHRR observations. *J. Clim.*, **20**, 2022–2036.

Charlson, R. J., A. S. Ackerman, F. A. M. Bender, T. L. Anderson, and Z. Liu, 2007: On the climate forcing consequences of the albedo continuum between cloudy and clear air. *Tellus B*, **59**, 715–727.

Charney, J. G., et al., 1979: Carbon dioxide and climate: A scientific assessment. Report of an Ad-Hoc Group on Carbon Dioxide and Climate, National Academy of Sciences, Washington D.C., USA, 33 pp.

Che, H., et al., 2009: Instrument calibration and aerosol optical depth validation of the China Aerosol Remote Sensing Network. *J. Geophys. Res.*, **114**, D03206.

Chen, J. P., A. Hazra, and Z. Levin, 2008: Parameterizing ice nucleation rates using contact angle and activation energy derived from laboratory data. *Atmos. Chem. Phys.*, **8**, 7431–7449.

Chen, L., G. Shi, S. Qin, S. Yang, and P. Zhang, 2011: Direct radiative forcing of anthropogenic aerosols over oceans from satellite observations. *Adv. Atmos. Sci.*, **28**, 973–984.

Chen, T., W. B. Rossow, and Y. Zhang, 2000: Radiative effects of cloud-type variations. *J. Clim.*, **13**, 264–286.

Chen, W. T., Y. H. Lee, P. J. Adams, A. Nenes, and J. H. Seinfeld, 2010: Will black carbon mitigation dampen aerosol indirect forcing? *Geophys. Res. Lett.*, **37**, L09801.

Chen, Y., Q. Li, R. A. Kahn, J. T. Randerson, and D. J. Diner, 2009: Quantifying aerosol direct radiative effect with Multiangle Imaging Spectroradiometer observations: Top-of-atmosphere albedo change by aerosols based on land surface types. *J. Geophys. Res.*, **114**, D02109.

Chen, Y. C., M. W. Christensen, L. Xue, A. Sorooshian, G. L. Stephens, R. M. Rasmussen, and J. H. Seinfeld, 2012: Occurrence of lower cloud albedo in ship tracks. *Atmos. Chem. Phys.*, **12**, 8223–8235.

Cheng, A., and K. M. Xu, 2006: Simulation of shallow cumuli and their transition to deep convective clouds by cloud-resolving models with different third-order turbulence closures. *Q. J. R. Meteorol. Soc.*, **132**, 359–382.

Cheng, A., and K.-M. Xu, 2008: Simulation of boundary-layer cumulus and stratocumulus clouds using a cloud-resolving model with low- and third-order turbulence closures. *J. Meteorol. Soc. Jpn*, **86**, 67–86.

Cheng, Z. L., K. S. Lam, L. Y. Chan, and K. K. Cheng, 2000: Chemical characteristics of aerosols at coastal station in Hong Kong. I. Seasonal variation of major ions, halogens and mineral dusts between 1995 and 1996. *Atmos. Environ.*, **34**, 2771–2783.

Chepfer, H., S. Bony, D. Winker, M. Chiriaco, J.-L. Dufresne, and G. Sèze, 2008: Use of CALIPSO lidar observations to evaluate the cloudiness simulated by a climate model. *Geophys. Res. Lett.*, **35**, L15704.

Chepfer, H., et al., 2010: The GCM-Oriented CALIPSO Cloud Product (CALIPSO-GOCCP). *J. Geophys. Res.*, **115**, D00H16.

Chikira, M., and M. Sugiyama, 2010: A cumulus parameterization with state-dependent entrainment rate. Part I: Description and sensitivity to temperature and humidity profiles. *J. Atmos. Sci.*, **67**, 2171–2193.

Chou, C., and J. D. Neelin, 2004: Mechanisms of global warming impacts on regional tropical precipitation. *J. Clim.*, **17**, 2688–2701.

Chou, C., J. D. Neelin, C. A. Chen, and J. Y. Tu, 2009: Evaluating the "Rich-Get-Richer" mechanism in tropical precipitation change under global warming. *J. Clim.*, **22**, 1982–2005.

Chow, J. C., J. G. Waston, D. H. Lowenthal, P. A. Solomon, K. L. Magliano, S. D. Ziman, and L. W. Richards, 1993: PM_{10} and $PM_{2.5}$ compositions in California's San Joaquin Valley. *Aer. Sci. Technol.*, **18**, 105–128.

Chowdhary, J., et al., 2005: Retrieval of aerosol scattering and absorption properties from photopolarimetric observations over the ocean during the CLAMS experiment. *J. Atmos. Sci.*, **62**, 1093–1117.

Christensen, M. W., and G. L. Stephens, 2011: Microphysical and macrophysical responses of marine stratocumulus polluted by underlying ships: Evidence of cloud deepening. *J. Geophys. Res.*, **116**, D03201.

Christopher, S. A., B. Johnson, T. A. Jones, and J. Haywood, 2009: Vertical and spatial distribution of dust from aircraft and satellite measurements during the GERBILS field campaign. *Geophys. Res. Lett.*, **36**, L06806.

Chung, C. E., V. Ramanathan, and D. Decremer, 2012: Observationally constrained estimates of carbonaceous aerosol radiative forcing. *Proc. Natl. Acad. Sci. U.S.A.*, **109**, 11624–11629.

Clarke, A. D., V. N. Kapustin, F. L. Eisele, R. J. Weber, and P. H. McMurry, 1999: Particle production near marine clouds: Sulfuric acid and predictions from classical binary nucleation. *Geophys. Res. Lett.*, **26**, 2425–2428.

Clement, A. C., R. Burgman, and J. R. Norris, 2009: Observational and model evidence for positive low-level cloud feedback. *Science*, **325**, 460–464.

Coakley, J. A., and C. D. Walsh, 2002: Limits to the aerosol indirect radiative effect derived from observations of ship tracks. *J. Atmos. Sci.*, **59**, 668–680.

Collins, M., B. B. Booth, B. Bhaskaran, G. R. Harris, J. M. Murphy, D. M. H. Sexton, and M. J. Webb, 2011: Climate model errors, feedbacks and forcings: A comparison of perturbed physics and multi-model ensembles. *Clim. Dyn.*, **36**, 1737–1766.

Colman, R. A., and B. J. McAvaney, 2011: On tropospheric adjustment to forcing and climate feedbacks. *Clim. Dyn.*, **36**, 1649–1658.

Colman, R. A., and L. I. Hanson, 2012: On atmospheric radiative feedbacks associated with climate variability and change. *Clim. Dyn.*, **40**, 475–492.

Comstock, K. K., C. S. Bretherton, and S. E. Yuter, 2005: Mesoscale variability and drizzle in Southeast Pacific stratocumulus. *J. Atmos. Sci.*, **62**, 3792–3807.

Costantino, L., and F.-M. Bréon, 2010: Analysis of aerosol-cloud interaction from multi-sensor satellite observations. *Geophys. Res. Lett.*, **37**, L11801.

Couvreux, F., F. Hourdin, and C. Rio, 2010: Resolved versus parametrized boundary-layer plumes. Part I: A parametrization-oriented conditional sampling in large-eddy simulations. *Bound. Layer Meteor.*, **134**, 441–458.

Cross, E. S., et al., 2010: Soot Particle Studies—Instrument Inter-Comparison—Project Overview. *Aer. Sci. Technol.*, **44**, 592–611.

Crucifix, M., 2006: Does the Last Glacial Maximum constrain climate sensitivity? *Geophys. Res. Lett.*, **33**, L18701.

Crutzen, P. J., 2006: Albedo enhancement by stratospheric sulfur injections: A contribution to resolve a policy dilemma? *Clim. Change*, **77**, 211–220.

Dai, A. G., J. H. Wang, P. W. Thorne, D. E. Parker, L. Haimberger, and X. L. L. Wang, 2011: A new approach to homogenize daily radiosonde humidity data. *J. Clim.*, **24**, 965–991.

Davies, R., and M. Molloy, 2012: Global cloud height fluctuations measured by MISR on Terra from 2000 to 2010. *Geophys. Res. Lett.*, **39**, L03701.

Davis, A. B., A. Marshak, H. Gerber, and W. J. Wiscombe, 1999: Horizontal structure of marine boundary layer clouds from centimeter to kilometer scales. *J. Geophys. Res.*, **104**, 6123–6144.

Dawson, J. P., P. J. Adams, and S. N. Pandis, 2007: Sensitivity of PM2.5 to climate in the Eastern US: A modeling case study. *Atmos. Chem. Phys.*, **7**, 4295–4309.

de Boer, G., H. Morrison, M. D. Shupe, and R. Hildner, 2011: Evidence of liquid dependent ice nucleation in high-latitude stratiform clouds from surface remote sensors. *Geophys. Res. Lett.*, **38**, L01803.

de Gouw, J., and J. L. Jimenez, 2009: Organic aerosols in the Earth's atmosphere. *Environ. Sci. Technol.*, **43**, 7614–7618.

de Gouw, J. A., et al., 2005: Budget of organic carbon in a polluted atmosphere: Results from the New England Air Quality Study in 2002. *J. Geophys. Res.*, **110**, D16305.

de Graaf, M., L. G. Tilstra, P. Wang, and P. Stammes, 2012: Retrieval of the aerosol direct radiative effect over clouds from spaceborne spectrometry. *J. Geophys. Res.*, **117**, D07207.

de Leeuw, G., et al., 2011: Production flux of sea spray aerosol. *Rev. Geophys.*, **49**, RG2001.

de Souza, P. A., W. Z. de Mello, L. M. Rauda, and S. M. Sella, 2010: Caracterização do material particulado fino e grosso e composição da fração inorgânica solúvel em água em São José Dos Campos (SP). *Química Nova*, **33**, 1247–1253.

Deboudt, K., P. Flament, M. Choel, A. Gloter, S. Sobanska, and C. Colliex, 2010: Mixing state of aerosols and direct observation of carbonaceous and marine coatings on African dust by individual particle analysis. *J. Geophys. Res.*, **115**, D24207.

Decesari, S., et al., 2010: Chemical composition of PM_{10} and PM_1 at the high-altitude Himalayan station Nepal Climate Observatory-Pyramid (NCO-P) (5079 m.a.s.l.). *Atmos. Chem. Phys.*, **10**, 4583–4596.

Dee, D. P., et al., 2011: The ERA-Interim reanalysis: Configuration and performance of the data assimilation system. *Q. J. R. Meteorol. Soc.*, **137**, 553–597.

Del Genio, A. D., and J. B. Wu, 2010: The role of entrainment in the diurnal cycle of continental convection. *J. Clim.*, **23**, 2722–2738.

Del Genio, A. D., M.-S. Yao, and J. Jonas, 2007: Will moist convection be stronger in a warmer climate? *Geophys. Res. Lett.*, **34**, L16703.

Del Genio, A. D., Y.-H. Chen, D. Kim, and M.-S. Yao, 2012: The MJO transition from shallow to deep convection in CloudSat/CALIPSO data and GISS GCM simulations. *J. Clim.*, **25**, 3755–3770.

DeLeon-Rodriguez, N., et al., 2013: Microbiome of the upper troposphere: Species composition and prevalence, effects of tropical storms, and atmospheric implications. *Proc. Natl. Acad. Sci. U.S.A.*, **110**, 2575–2580.

DeMott, C. A., C. Stan, D. A. Randall, J. L. Kinter III, and M. Khairoutdinov, 2011: The Asian Monsoon in the super-parameterized CCSM and its relation to tropical wave activity. *J. Clim.*, **24**, 5134–5156.

DeMott, P. J., et al., 2010: Predicting global atmospheric ice nuclei distributions and their impacts on climate. *Proc. Natl. Acad. Sci. U.S.A.*, **107**, 11217–11222.

Deng, M., G. G. Mace, Z. E. Wang, and H. Okamoto, 2010: Tropical Composition, Cloud and Climate Coupling Experiment validation for cirrus cloud profiling retrieval using CloudSat radar and CALIPSO lidar. *J. Geophys. Res.*, **115**, D00J15.

Dengel, S., D. Aeby, and J. Grace, 2009: A relationship between galactic cosmic radiation and tree rings. *New Phytologist*, **184**, 545–551.

Denman, K. L., et al., 2007: Couplings between changes in the climate system and biogeochemistry. In: *Climate Change 2007: The Physical Science Basis. Contribution of Working Group I to the Fourth Assessment Report of the Intergovernmental Panel on Climate Change* [Solomon, S., D. Qin, M. Manning, Z. Chen, M. Marquis, K. B. Averyt, M. Tignor and H. L. Miller (eds.)] Cambridge University Press, Cambridge, United Kingdom and New York, NY, USA, pp. 499-587.

Derbyshire, S. H., I. Beau, P. Bechtold, J.-Y. Grandpeix, J.-M. Piriou, J.-L. Redelsperger, and P. M. M. Soares, 2004: Sensitivity of moist convection to environmental humidity. *Q. J. R. Meteorol. Soc.*, **130**, 3055–3079.

Després, V. R., et al., 2012: Primary biological aerosol particles in the atmosphere: A review. *Tellus B*, **64**, 15598.

Dessler, A. E., 2010: A determination of the cloud feedback from climate variations over the past decade. *Science*, **330**, 1523–1527.

Dessler, A. E., 2011: Cloud variations and the Earth's energy budget. *Geophys. Res. Lett.*, **38**, L19701.

Dessler, A. E., 2013: Observations of climate feedbacks over 2000–10 and comparisons to climate models. *J. Clim.*, **26**, 333–342.

Dessler, A. E., and S. Wong, 2009: Estimates of the water vapor climate feedback during El Niño-Southern Oscillation. *J. Clim.*, **22**, 6404–6412.

Dessler, A. E., and S. M. Davis, 2010: Trends in tropospheric humidity from reanalysis systems. *J. Geophys. Res.*, **115**, D19127.

Deuzé, J.-L., et al., 2001: Remote sensing of aerosols over land surfaces from POLDER-ADEOS-1 polarized measurements. *J. Geophys. Res.*, **106**, 4913–4926.

Devasthale, A., O. Kruger, and H. Graßl, 2005: Change in cloud-top temperatures over Europe. *IEEE Geosci. Remote Sens. Lett.*, **2**, 333–336.

Di Biagio, C., A. di Sarra, and D. Meloni, 2010: Large atmospheric shortwave radiative forcing by Mediterranean aerosols derived from simultaneous ground-based and spaceborne observations and dependence on the aerosol type and single scattering albedo. *J. Geophys. Res.*, **115**, D10209.

Dickinson, R., 1975: Solar variability and the lower atmosphere. *Bull. Am. Meteor. Soc.*, **56**, 1240–1248.

Doherty, S. J., S. G. Warren, T. C. Grenfell, A. D. Clarke, and R. E. Brandt, 2010: Light-absorbing impurities in Arctic snow. *Atmos. Chem. Phys.*, **10**, 11647–11680.

Doherty, S. J., T. C. Grenfell, S. Forsström, D. L. Hegg, R. E. Brandt, and S. G. Warren, 2013: Observed vertical redistribution of black carbon and other insoluble light-absorbing particles in melting snow. *J. Geophys. Res. Atmos.*, **118**, 5553–5569.

Donahue, N. M., S. A. Epstein, S. N. Pandis, and A. L. Robinson, 2011a: A two-dimensional volatility basis set: 1. Organic-aerosol mixing thermodynamics. *Atmos. Chem. Phys.*, **11**, 3303–3318.

Donahue, N. M., E. R. Trump, J. R. Pierce, and I. Riipinen, 2011b: Theoretical constraints on pure vapor-pressure driven condensation of organics to ultrafine particles. *Geophys. Res. Lett.*, **38**, L16801.

Dong, B.-W., J. M. Gregory, and R. T. Sutton, 2009: Understanding land-sea warming contrast in response to increasing greenhouse gases. Part I: Transient adjustment. *J. Clim.*, **22**, 3079–3097.

Donner, L. J., et al., 2011: The dynamical core, physical parameterizations, and basic simulation characteristics of the atmospheric component AM3 of the GFDL global coupled model CM3. *J. Clim.*, **24**, 3484–3519

Donovan, D. P., 2003: Ice-cloud effective particle size parameterization based on combined lidar, radar reflectivity, and mean Doppler velocity measurements. *J. Geophys. Res.*, **108**, 4573.

Doughty, C. E., C. B. Field, and A. M. S. McMillan, 2011: Can crop albedo be increased through the modification of leaf trichomes, and could this cool regional climate? *Clim. Change*, **104**, 379–387.

Dubovik, O., A. Smirnov, B. N. Holben, M. D. King, Y. J. Kaufman, T. F. Eck, and I. Slutsker, 2000: Accuracy assessments of aerosol optical properties retrieved from Aerosol Robotic Network (AERONET) Sun and sky radiance measurements. *J. Geophys. Res.*, **105**, 9791–9806.

Dubovik, O., T. Lapyonok, Y. J. Kaufman, M. Chin, P. Ginoux, R. A. Kahn, and A. Sinyuk, 2008: Retrieving global aerosol sources from satellites using inverse modeling. *Atmos. Chem. Phys.*, **8**, 209–250.

Dubovik, O., et al., 2002: Variability of absorption and optical properties of key aerosol types observed in worldwide locations. *J. Atmos. Sci.*, **59**, 590–608.

Dubovik, O., et al., 2011: Statistically optimized inversion algorithm for enhanced retrieval of aerosol properties from spectral multi-angle polarimetric satellite observations. *Atmos. Meas. Tech.*, **4**, 975–1018.

Dufresne, J.-L., and S. Bony, 2008: An assessment of the primary sources of spread of global warming estimates from coupled atmosphere-ocean models. *J. Clim.*, **21**, 5135–5144.

Dunne, E. M., L. A. Lee, C. L. Reddington, and K. S. Carslaw, 2012: No statistically significant effect of a short-term decrease in the nucleation rate on atmospheric aerosols. *Atmos. Chem. Phys.*, **12**, 11573–11587.

Duplissy, J., et al., 2008: Cloud forming potential of secondary organic aerosol under near atmospheric conditions. *Geophys. Res. Lett.*, **35**, L03818.

Durkee, P. A., K. J. Noone, and R. T. Bluth, 2000: The Monterey Area Ship Track experiment. *J. Atmos. Sci.*, **57**, 2523–2541.

Dusek, U., et al., 2006: Size matters more than chemistry for cloud-nucleating ability of aerosol particles. *Science*, **312**, 1375–1378.

Early, J. T., 1989: Space-based solar shield to offset greenhouse effect. *J. Br. Interplanet. Soc.*, **42**, 567–569.

Easter, R. C., et al., 2004: MIRAGE: Model description and evaluation of aerosols and trace gases. *J. Geophys. Res.*, **109**, D20210.

Eastman, R., and S. G. Warren, 2010: Interannual variations of Arctic cloud types in relation to sea ice. *J. Clim.*, **23**, 4216–4232.

Eastman, R., and S. G. Warren, 2013: A 39–yr survey of cloud changes from land stations worldwide 1971–2009: Long-term trends, relation to aerosols, and expansion of the tropical belt. *J. Clim.*, **26**, 1286–1303.

Eichler, A., et al., 2009: Temperature response in the Altai region lags solar forcing. *Geophys. Res. Lett.*, **36**, L01808.

Eitzen, Z. A., K. M. Xu, and T. Wong, 2009: Cloud and radiative characteristics of tropical deep convective systems in extended cloud objects from CERES observations. *J. Clim.*, **22**, 5983–6000.

Ekman, A. M. L., A. Engström, and C. Wang, 2007: The effect of aerosol composition and concentration on the development and anvil properties of a continental deep convective cloud. *Q. J. R. Meteorol. Soc.*, **133**, 1439–1452.

Ekman, A. M. L., A. Engström, and A. Söderberg, 2011: Impact of two-way aerosol–cloud interaction and changes in aerosol size distribution on simulated aerosol-induced deep convective cloud sensitivity. *J. Atmos. Sci.*, **68**, 685–698.

Eliasson, S., S. A. Buehler, M. Milz, P. Eriksson, and V. O. John, 2011: Assessing observed and modelled spatial distributions of ice water path using satellite data. *Atmos. Chem. Phys.*, **11**, 375–391.

Eliseev, A. V., A. V. Chernokulsky, A. A. Karpenko, and I. I. Mokhov, 2009: Global warming mitigation by sulphur loading in the stratosphere: Dependence of required emissions on allowable residual warming rate. *Theor. Appl. Climatol.*, **101**, 67–81.

Enghoff, M. B., and H. Svensmark, 2008: The role of atmospheric ions in aerosol nucleation—a review. *Atmos. Chem. Phys.*, **8**, 4911–4923.

English, J. T., O. B. Toon, and M. J. Mills, 2012: Microphysical simulations of sulfur burdens from stratospheric sulfur geoengineering. *Atmos. Phys. Chem.*, **12**, 4775–4793.

Engström, A., and A. M. L. Ekman, 2010: Impact of meteorological factors on the correlation between aerosol optical depth and cloud fraction. *Geophys. Res. Lett.*, **37**, L18814.

Ervens, B., G. Feingold, and S. M. Kreidenweis, 2005: Influence of water-soluble organic carbon on cloud drop number concentration. *J. Geophys. Res.*, **110**, D18211.

Ervens, B., B. J. Turpin, and R. J. Weber, 2011a: Secondary organic aerosol formation in cloud droplets and aqueous particles (aqSOA): A review of laboratory, field and model studies. *Atmos. Chem. Phys.*, **11**, 11069–11102.

Ervens, B., G. Feingold, K. Sulia, and J. Harrington, 2011b: The impact of microphysical parameters, ice nucleation mode, and habit growth on the ice/liquid partitioning in mixed-phase Arctic clouds. *J. Geophys. Res.*, **116**, D17205.

Ervens, B., et al., 2007: Prediction of cloud condensation nucleus number concentration using measurements of aerosol size distributions and composition and light scattering enhancement due to humidity. *J. Geophys. Res.*, **112**, D10S32.

European Commission, Joint Research Centre, and Netherlands Environmental Assessment Agency (PBL), 2009: Emission Database for Global Atmospheric Research (EDGAR), release version 4.0. http://edgar.jrc.ec.europa.eu, last accessed 7 June 2013.

Evan, A. T., and J. R. Norris, 2012: On global changes in effective cloud height. *Geophys. Res. Lett.*, **39**, L19710.

Evans, J. R. G., E. P. J. Stride, M. J. Edirisinghe, D. J. Andrews, and R. R. Simons, 2010: Can oceanic foams limit global warming? *Clim. Res.*, **42**, 155–160.

Facchini, M. C., et al., 2008: Primary submicron marine aerosol dominated by insoluble organic colloids and aggregates. *Geophys. Res. Lett.*, **35**, L17814.

Fan, J., et al., 2009: Dominant role by vertical wind shear in regulating aerosol effects on deep convective clouds. *J. Geophys. Res.*, **114**, D22206.

Fan, J. W., J. M. Comstock, and M. Ovchinnikov, 2010: The cloud condensation nuclei and ice nuclei effects on tropical anvil characteristics and water vapor of the tropical tropopause layer. *Environ. Res. Lett.*, **5**, 6.

Farina, S. C., P. J. Adams, and S. N. Pandis, 2010: Modeling global secondary organic aerosol formation and processing with the volatility basis set: Implications for anthropogenic secondary organic aerosol. *J. Geophys. Res.*, **115**, D09202.

Farrar, P. D., 2000: Are cosmic rays influencing oceanic cloud coverage – or is it only El Niño? *Clim. Change*, **47**, 7–15.

Fasullo, J. T., and K. E. Trenberth, 2012: A less cloudy future: The role of subtropical subsidence in climate sensitivity. *Science*, **338**, 792–794.

Favez, O., H. Cachier, J. Sciarea, S. C. Alfaro, T. M. El-Araby, M. A. Harhash, and Magdy M. Abdelwahab, 2008: Seasonality of major aerosol species and their transformations in Cairo megacity. *Atmos. Environ.*, **42**, 1503–1516.

Feingold, G., H. L. Jiang, and J. Y. Harrington, 2005: On smoke suppression of clouds in Amazonia. *Geophys. Res. Lett.*, **32**, L02804.

Feingold, G., R. Boers, B. Stevens, and W. R. Cotton, 1997: A modeling study of the effect of drizzle on cloud optical depth and susceptibility. *J. Geophys. Res.*, **102**, 13527–13534.

Feingold, G., I. Koren, H. Wang, H. Xue, and W. A. Brewer, 2010: Precipitation-generated oscillations in open cellular cloud fields. *Nature*, **466**, 849–852.

Feng, J., 2008: A size-resolved model and a four-mode parameterization of dry deposition of atmospheric aerosols. *J. Geophys. Res.*, **113**, D12201.

Ferraro, A. J., E. J. Highwood, and A. J. Charlton-Perez, 2011: Stratospheric heating by potential geoengineering aerosols. *Geophys. Res. Lett.*, **38**, L24706.

Flanner, M. G., C. S. Zender, J. T. Randerson, and P. J. Rasch, 2007: Present-day climate forcing and response from black carbon in snow. *J. Geophys. Res.*, **112**, D11202.

Flanner, M. G., C. S. Zender, P. G. Hess, N. M. Mahowald, T. H. Painter, V. Ramanathan, and P. J. Rasch, 2009: Springtime warming and reduced snow cover from carbonaceous particles. *Atmos. Chem. Phys.*, **9**, 2481–2497.

Fletcher, J. K., and C. S. Bretherton, 2010: Evaluating boundary layer-based mass flux closures using cloud-resolving model simulations of deep convection. *J. Atmos. Sci.*, **67**, 2212–2225.

Forest, C. E., P. H. Stone, and A. P. Sokolov, 2006: Estimated PDFs of climate system properties including natural and anthropogenic forcings. *Geophys. Res. Lett.*, **33**, L01705.

Forsström, S., J. Ström, C. A. Pedersen, E. Isaksson, and S. Gerland, 2009: Elemental carbon distribution in Svalbard snow. *J. Geophys. Res.*, **114**, D19112.

Forster, P., et al., 2007: Changes in Atmospheric Constituents and in Radiative Forcing. In: *Climate Change 2007: The Physical Science Basis. Contribution of Working Group I to the Fourth Assessment Report of the Intergovernmental Panel on Climate Change* [Solomon, S., D. Qin, M. Manning, Z. Chen, M. Marquis, K. B. Averyt, M. Tignor and H. L. Miller (eds.)] Cambridge University Press, Cambridge, United Kingdom and New York, NY, USA, pp. 129–234.

Forster, P. M. D., and J. M. Gregory, 2006: The climate sensitivity and its components diagnosed from Earth Radiation Budget data. *J. Clim.*, **19**, 39–52.

Fountoukis, C., et al., 2007: Aerosol-cloud drop concentration closure for clouds sampled during the International Consortium for Atmospheric Research on Transport and Transformation 2004 campaign. *J. Geophys. Res.*, **112**, D10S30.

Fovell, R. G., K. L. Corbosiero, and H.-C. Kuo, 2009: Cloud microphysics impact on hurricane track as revealed in idealized experiments. *J. Atmos. Sci.*, **66**, 1764–1778.

Fowler, L. D., and D. A. Randall, 2002: Interactions between cloud microphysics and cumulus convection in a general circulation model. *J. Atmos. Sci.*, **59**, 3074–3098.

Freney, E. J., K. Adachi, and P. R. Buseck, 2010: Internally mixed atmospheric aerosol particles: Hygroscopic growth and light scattering. *J. Geophys. Res.*, **115**, D19210.

Fridlind, A. M., et al., 2007: Ice properties of single-layer stratocumulus during the Mixed-Phase Arctic Cloud Experiment: 2. Model results. *J. Geophys. Res.*, **112**, D24202.

Friedman, B., G. Kulkarni, J. Beranek, A. Zelenyuk, J. A. Thornton, and D. J. Cziczo, 2011: Ice nucleation and droplet formation by bare and coated soot particles. *J. Geophys. Res.*, **116**, D17203.

Frömming, C., M. Ponater, U. Burkhardt, A. Stenke, S. Pechtl, and R. Sausen, 2011: Sensitivity of contrail coverage and contrail radiative forcing to selected key parameters. *Atmos. Environ.*, **45**, 1483–1490.

Fuzzi, S., et al., 2007: Overview of the inorganic and organic composition of size-segregated aerosol in Rondonia, Brazil, from the biomass-burning period to the onset of the wet season. *J. Geophys. Res.*, **112**, D01201.

Fyfe, J. C., J. N. S. Cole, V. K. Arora, and J. F. Scinocca, 2013: Biogeochemical carbon coupling influences global precipitation in geoengineering experiments. *Geophys. Res. Lett.*, **40**, 651–655.

Gagen, M., et al., 2011: Cloud response to summer temperatures in Fennoscandia over the last thousand years. *Geophys. Res. Lett.*, **38**, L05701.

Galewsky, J., and J. V. Hurley, 2010: An advection-condensation model for subtropical water vapor isotopic ratios. *J. Geophys. Res.*, **115**, D16116.

Gantt, B., N. Meskhidze, M. C. Facchini, M. Rinaldi, D. Ceburnis, and C. D. O'Dowd, 2011: Wind speed dependent size-resolved parameterization for the organic mass fraction of sea spray aerosol. *Atmos. Chem. Phys.*, **11**, 8777–8790.

Gao, R. S., et al., 2007: A novel method for estimating light-scattering properties of soot aerosols using a modified single-particle soot photometer. *Aer. Sci. Technol.*, **41**, 125–135.

Garrett, T. J., and C. F. Zhao, 2006: Increased Arctic cloud longwave emissivity associated with pollution from mid-latitudes. *Nature*, **440**, 787–789.

Garvert, M. F., C. P. Woods, B. A. Colle, C. F. Mass, P. V. Hobbs, M. T. Stoelinga, and J. B. Wolfe, 2005: The 13–14 December 2001 IMPROVE-2 event. Part II: Comparisons of MM5 model simulations of clouds and precipitation with observations. *J. Atmos. Sci.*, **62**, 3520–3534.

Gasso, S., 2008: Satellite observations of the impact of weak volcanic activity on marine clouds. *J. Geophys. Res.*, **113**, D14S19.

GAW, 2011: WMO/GAW Standard Operating Procedures for In-situ Measurements of Aerosol Mass Concentration, Light Scattering and Light Absorption. GAW Report No. 200, World Meteorological Organization, Geneva, Switzerland, 130 pp.

George, R. C., and R. Wood, 2010: Subseasonal variability of low cloud radiative properties over the southeast Pacific Ocean. *Atmos. Chem. Phys.*, **10**, 4047–4063.

Gerasopoulos, E., et al., 2007: Size-segregated mass distributions of aerosols over Eastern Mediterranean: Seasonal variability and comparison with AERONET columnar size-distributions. *Atmos. Chem. Phys.*, **7**, 2551–2561.

Gerber, H., 1996: Microphysics of marine stratocumulus clouds with two drizzle modes. *J. Atmos. Sci.*, **53**, 1649–1662.

Gettelman, A., and Q. Fu, 2008: Observed and simulated upper-tropospheric water vapor feedback. *J. Clim.*, **21**, 3282–3289.

Gettelman, A., J. E. Kay, and J. T. Fasullo, 2013: Spatial decomposition of climate feedbacks in the Community Earth System Model. *J. Clim.*, **26**, 3544–3561.

Gettelman, A., X. Liu, D. Barahona, U. Lohmann, and C.-C. Chen, 2012: Climate impacts of ice nucleation. *J. Geophys. Res.*, **117**, D20201.

Gettelman, A., et al., 2010: Global simulations of ice nucleation and ice supersaturation with an improved cloud scheme in the Community Atmosphere Model. *J. Geophys. Res.*, **115**, D18216.

Ghan, S., R. Easter, J. Hudson, and F.-M. Bréon, 2001: Evaluation of aerosol indirect radiative forcing in MIRAGE. *J. Geophys. Res.*, **106**, 5317–5334.

Ghan, S. J., and S. E. Schwartz, 2007: Aerosol properties and processes - A path from field and laboratory measurements to global climate models. *Bull. Am. Meteor. Soc.*, **88**, 1059–1083.

Ghan, S. J., H. Abdul-Razzak, A. Nenes, Y. Ming, X. Liu, and M. Ovchinnikov, 2011: Droplet nucleation: Physically-based parameterizations and comparative evaluation. *J. Adv. Model. Earth Syst.*, **3**, M10001.

Ghan, S. J., X. Liu, R. C. Easter, R. Zaveri, P. J. Rasch, J.-H. Yoon, and B. Eaton, 2012: Toward a minimal representation of aerosols in climate models: Comparative decomposition of aerosol direct, semi-direct, and indirect radiative forcing. *J. Clim.*, **25**, 6461–6476.

Ginoux, P., J. M. Prospero, T. E. Gill, N. C. Hsu, and M. Zhao, 2012a: Global-scale attribution of anthropogenic and natural dust sources and their emission rates based on MODIS Deep Blue aerosol products. *Rev. Geophys.*, **50**, RG3005.

Ginoux, P., L. Clarisse, C. Clerbaux, P.-F. Coheur, O. Dubovik, N. C. Hsu, and M. Van Damme, 2012b: Mixing of dust and NH_3 observed globally over anthropogenic dust sources *Atmos. Chem. Phys.*, **12**, 7351–7363.

Gioda, A., B. S. Amaral, I. L. G. Monteiro, and T. D. Saint'Pierre, 2011: Chemical composition, sources, solubility, and transport of aerosol trace elements in a tropical region. *J. Environ. Monit.*, **13**, 2134–2142.

Girard, E., J.-P. Blanchet, and Y. Dubois, 2004: Effects of arctic sulphuric acid aerosols on wintertime low-level atmospheric ice crystals, humidity and temperature at Alert, Nunavut. *Atmos. Res.*, **73**, 131–148.

Givati, A., and D. Rosenfeld, 2004: Quantifying precipitation suppression due to air pollution. *J. Appl. Meteorol.*, **43**, 1038–1056.

Golaz, J. C., V. E. Larson, and W. R. Cotton, 2002: A PDF-based model for boundary layer clouds. Part I: Method and model description. *J. Atmos. Sci.*, **59**, 3540–3551.

Golaz, J. C., M. Salzmann, L. J. Donner, L. W. Horowitz, Y. Ming, and M. Zhao, 2011: Sensitivity of the aerosol indirect effect to subgrid variability in the cloud parameterization of the GFDL atmosphere general circulation model AM3. *J. Clim.*, **24**, 3145–3160.

Good, N., et al., 2010: Consistency between parameterisations of aerosol hygroscopicity and CCN activity during the RHaMBLe discovery cruise. *Atmos. Chem. Phys.*, **10**, 3189–3203.

Gordon, N. D., and J. R. Norris, 2010: Cluster analysis of midlatitude oceanic cloud regimes: Mean properties and temperature sensitivity. *Atmos. Chem. Phys.*, **10**, 6435–6459.

Goren, T., and D. Rosenfeld, 2012: Satellite observations of ship emission induced transitions from broken to closed cell marine stratocumulus over large areas. *J. Geophys. Res.*, **117**, D17206.

Grabowski, W. W., and P. K. Smolarkiewicz, 1999: CRCP: A Cloud Resolving Convection Parameterization for modeling the tropical convecting atmosphere. *Physica D*, **133**, 171–178.

Grabowski, W. W., X. Wu, M. W. Moncrieff, and W. D. Hall, 1998: Cloud-resolving modeling of cloud systems during Phase III of GATE. Part II: Effects of resolution and the third spatial dimension. *J. Atmos. Sci.*, **55**, 3264–3282.

Grandey, B. S., and P. Stier, 2010: A critical look at spatial scale choices in satellite-based aerosol indirect effect studies. *Atmos. Chem. Phys.*, **10**, 11459–11470.

Grandpeix, J.-Y., and J.-P. Lafore, 2010: A density current parameterization coupled with Emanuel's convection scheme. Part I: The models. *J. Atmos. Sci.*, **67**, 881–897.

Granier, C., et al., 2011: Evolution of anthropogenic and biomass burning emissions of air pollutants at global and regional scales during the 1980–2010 period. *Clim. Change*, **109**, 163–190.

Gregory, J., and M. Webb, 2008: Tropospheric adjustment induces a cloud component in CO_2 forcing. *J. Clim.*, **21**, 58–71.

Gregory, J. M., et al., 2004: A new method for diagnosing radiative forcing and climate sensitivity. *Geophys. Res. Lett.*, **31**, L03205.

Grote, R., and U. Niinemets, 2008: Modeling volatile isoprenoid emissions - a story with split ends. *Plant Biology*, **10**, 8–28.

Guenther, A., T. Karl, P. Harley, C. Wiedinmyer, P. I. Palmer, and C. Geron, 2006: Estimates of global terrestrial isoprene emissions using MEGAN (Model of Emissions of Gases and Aerosols from Nature). *Atmos. Chem. Phys.*, **6**, 3181–3210.

Guenther, A. B., X. Jiang, C. L. Heald, T. Sakulyanontvittaya, T. Duhl, L. K. Emmons, and X. Wang, 2012: The Model of Emissions of Gases and Aerosols from Nature version 2.1 (MEGAN2.1): An extended and updated framework for modeling biogenic emissions. *Geosci. Model Dev.*, **5**, 1471–1492.

Gullu, H. G., I. Ölmez, and G. Tuncel, 2000: Temporal variability of atmospheric trace element concentrations over the eastern Mediterranean Sea. *Spectrochim. Acta*, **B55**, 1135–1150.

Guo, H., J. C. Golaz, L. J. Donner, V. E. Larson, D. P. Schanen, and B. M. Griffin, 2010: Multi-variate probability density functions with dynamics for cloud droplet activation in large-scale models: Single column tests. *Geosci. Model Dev.*, **3**, 475–486.

Hadley, O. L., and T. W. Kirchstetter, 2012: Black-carbon reduction of snow albedo. *Nature Clim. Change*, **2**, 437–440.

Haerter, J. O., and P. Berg, 2009: Unexpected rise in extreme precipitation caused by a shift in rain type? *Nature Geosci.*, **2**, 372–373.

Haerter, J. O., P. Berg, and S. Hagemann, 2010: Heavy rain intensity distributions on varying time scales and at different temperatures. *J. Geophys. Res.*, **115**, D17102.

Hagler, G. S. W., et al., 2006: Source areas and chemical composition of fine particulate matter in the Pearl River Delta region of China. *Atmos. Environ.*, **40**, 3802–3815..

Halfon, N., Z. Levin, and P. Alpert, 2009: Temporal rainfall fluctuations in Israel and their possible link to urban and air pollution effects. *Environ. Res. Lett.*, **4**, 025001.

Halloran, P. R., T. G. Bell, and I. J. Totterdell, 2010: Can we trust empirical marine DMS parameterisations within projections of future climate? *Biogeosciences*, **7**, 1645–1656.

Hallquist, M., et al., 2009: The formation, properties and impact of secondary organic aerosol: Current and emerging issues. *Atmos. Chem. Phys.*, **9**, 5155–5236.

Hamwey, R. M., 2007: Active amplification of the terrestrial albedo to mitigate climate change: An exploratory study. *Mitigat. Adapt. Strat. Global Change*, **12**, 419–439.

Han, Y.-J., T.-S. Kim, and H. Kim, 2008: Ionic constituents and source analysis of $PM_{2.5}$ in three Korean cities. *Atmos. Environ.*, **42**, 4735–4746.

Hand, V. L., G. Capes, D. J. Vaughan, P. Formenti, J. M. Haywood, and H. Coe, 2010: Evidence of internal mixing of African dust and biomass burning particles by individual particle analysis using electron beam techniques. *J. Geophys. Res.*, **115**, D13301.

Hansell, R. A., et al., 2010: An assessment of the surface longwave direct radiative effect of airborne Saharan dust during the NAMMA field campaign. *J. Atmos. Sci.*, **67**, 1048–1065.

Hansen, J., and L. Nazarenko, 2004: Soot climate forcing via snow and ice albedos. *Proc. Natl. Acad. Sci. U.S.A.*, **101**, 423–428.

Hansen, J., M. Sato, P. Kharecha, G. Russell, D. W. Lea, and M. Siddall, 2007: Climate change and trace gases. *Philos. Trans. R. Soc. London A*, **365**, 1925–1954.

Hansen, J., et al., 1984: Climate sensitivity: Analysis of feedback mechanisms. In: *Climate Processes and Climate Sensitivity*, Geophysical Monograph Series, Vol. 29 [J. E. Hansen and T. Takahashi (eds.)]. American Geophysical Union, Washington, DC, USA, pp. 130–163.

Hansen, J., et al., 2005: Efficacy of climate forcings. *J. Geophys. Res.*, **110**, D18104.

Hara, K., et al., 2003: Mixing states of individual aerosol particles in spring Arctic troposphere during ASTAR 2000 campaign. *J. Geophys. Res.*, **108**, 4209.

Hardwick Jones, R., S. Westra, and A. Sharma, 2010: Observed relationships between extreme sub-daily precipitation, surface temperature, and relative humidity. *Geophys. Res. Lett.*, **37**, L22805.

Harrington, J. Y., D. Lamb, and R. Carver, 2009: Parameterization of surface kinetic effects for bulk microphysical models: Influences on simulated cirrus dynamics and structure. *J. Geophys. Res.*, **114**, D06212.

Harrison, E. F., P. Minnis, B. R. Barkstrom, V. Ramanathan, R. D. Cess, and G. G. Gibson, 1990: Seasonal variation of cloud radiative forcing derrived from the Earth Radiation Budget Experiment. *J. Geophys. Res.*, **95**, 18687–18703.

Harrison, R., and M. Ambaum, 2008: Enhancement of cloud formation by droplet charging. *Proc. R. Soc. London A*, **464**, 2561–2573.

Harrison, R. G., 2008: Discrimination between cosmic ray and solar irradiance effects on clouds, and evidence for geophysical modulation of cloud thickness. *Proc. R. Soc. London A*, **464**, 2575–2590.

Harrison, R. G., and D. B. Stephenson, 2006: Empirical evidence for a nonlinear effect of galactic cosmic rays on clouds. *Proc. R. Soc. London A*, **462**, 1221–1233.

Harrison, R. G., and M. H. P. Ambaum, 2010: Observing Forbush decreases in cloud at Shetland. *J. Atmos. Sol. Terres. Phys.*, **72**, 1408–1414.

Harrop, B. E., and D. L. Hartmann, 2012: Testing the role of radiation in determining tropical cloud-top temperature. *J. Clim.*, **25**, 5731–5747.

Hartmann, D. L., and K. Larson, 2002: An important constraint on tropical cloud-climate feedback. *Geophys. Res. Lett.*, **29**, 1951.

Hasekamp, O. P., 2010: Capability of multi-viewing-angle photo-polarimetric measurements for the simultaneous retrieval of aerosol and cloud properties. *Atmos. Meas. Tech.*, **3**, 839–851.

Haynes, J. M., C. Jakob, W. B. Rossow, G. Tselioudis, and J. Brown, 2011: Major characteristics of Southern Ocean cloud regimes and their effects on the energy budget. *J. Clim.*, **24**, 5061–5080.

Haywood, J., and O. Boucher, 2000: Estimates of the direct and indirect radiative forcing due to tropospheric aerosols: A review. *Rev. Geophys.*, **38**, 513–543.

Haywood, J., and M. Schulz, 2007: Causes of the reduction in uncertainty in the anthropogenic radiative forcing of climate between IPCC (2001) and IPCC (2007). *Geophys. Res. Lett.*, **34**, L20701.

Haywood, J. M., A. Jones, N. Bellouin, and D. Stephenson, 2013: Asymmetric forcing from stratospheric aerosols impacts Sahelian rainfall. *Nature Clim. Change*, **3**, 660–665.

Haywood, J. M., et al., 2009: A case study of the radiative forcing of persistent contrails evolving into contrail-induced cirrus. *J. Geophys. Res.*, **114**, D24201.

Haywood, J. M., et al., 2011: Motivation, rationale and key results from the GERBILS Saharan dust measurement campaign. *Q. J. R. Meteorol. Soc.*, **137**, 1106–1116.

Heald, C. L., and D. V. Spracklen, 2009: Atmospheric budget of primary biological aerosol particles from fungal spores. *Geophys. Res. Lett.*, **36**, L09806.

Heald, C. L., D. A. Ridley, S. M. Kreidenweis, and E. E. Drury, 2010: Satellite observations cap the atmospheric organic aerosol budget. *Geophys. Res. Lett.*, **37**, L24808.

Heald, C. L., et al., 2008: Predicted change in global secondary organic aerosol concentrations in response to future climate, emissions, and land use change. *J. Geophys. Res.*, **113**, D05211.

Heald, C. L., et al., 2011: Exploring the vertical profile of atmospheric organic aerosol: Comparing 17 aircraft field campaigns with a global model. *Atmos. Chem. Phys.*, **11**, 12673–12696.

Heckendorn, P., et al., 2009: The impact of geoengineering aerosols on stratospheric temperature and ozone. *Environ. Res. Lett.*, **4**, 045108.

Hegg, D. A., D. S. Covert, H. H. Jonsson, and R. K. Woods, 2012: A simple relationship between cloud drop number concentration and precursor aerosol concentration for the regions of Earth's large marine stratocumulus decks. *Atmos. Chem. Phys.*, **12**, 1229–1238.

Heintzenberg, J., D. C. Covert, and R. Van Dingenen, 2000: Size distribution and chemical composition of marine aerosols: A compilation and review. *Tellus*, **52**, 1104–1122.

Heintzenberg, J., et al., 2011: Near-global aerosol mapping in the upper troposphere and lowermost stratosphere with data from the CARIBIC project. *Tellus B*, **63**, 875–890.

Held, I. M., and B. J. Soden, 2006: Robust responses of the hydrological cycle to global warming. *J. Clim.*, **19**, 5686–5699.

Held, I. M., and K. M. Shell, 2012: Using relative humidity as a state variable in climate feedback analysis. *J. Clim.*, **25**, 2578–2582.

Hendricks, J., B. Karcher, U. Lohmann, and M. Ponater, 2005: Do aircraft black carbon emissions affect cirrus clouds on the global scale? *Geophys. Res. Lett.*, **32**, L12814.

Heymsfield, A., D. Baumgardner, P. DeMott, P. Forster, K. Gierens, and B. Kärcher, 2010: Contrail microphysics. *Bull. Am. Meteor. Soc.*, **91**, 465–472.

Heymsfield, A. J., and L. M. Miloshevich, 1995: Relative humidity and temperature influences on cirrus formation and evolution: Observations from wave clouds and FIRE II. *J. Atmos. Sci.*, **52**, 4302–4326.

Heymsfield, A. J., et al., 1998: Cloud properties leading to highly reflective tropical cirrus: Interpretations from CEPEX, TOGA COARE, and Kwajalein, Marshall Islands. *J. Geophys. Res.*, **103**, 8805–8812.

Hill, A. A., and S. Dobbie, 2008: The impact of aerosols on non-precipitating marine stratocumulus. II: The semi-direct effect. *Q. J. R. Meteorol. Soc.*, **134**, 1155–1165.

Hill, A. A., G. Feingold, and H. Jiang, 2009: The influence of entrainment and mixing assumption on aerosol-cloud interactions in marine stratocumulus. *J. Atmos. Sci.*, **66**, 1450–1464.

Hill, S., and Y. Ming, 2012: Nonlinear climate response to regional brightening of tropical marine stratocumulus. *Geophys. Res. Lett.*, **39**, L15707.

Hirsikko, A., et al., 2011: Atmospheric ions and nucleation: A review of observations. *Atmos. Chem. Phys.*, **11**, 767–798.

Hodzic, A., J. L. Jimenez, S. Madronich, M. R. Canagaratna, P. F. DeCarlo, L. Kleinman, and J. Fast, 2010: Modeling organic aerosols in a megacity: Potential contribution of semi-volatile and intermediate volatility primary organic compounds to secondary organic aerosol formation. *Atmos. Chem. Phys.*, **10**, 5491–5514.

Hohenegger, C., and C. S. Bretherton, 2011: Simulating deep convection with a shallow convection scheme. *Atmos. Chem. Phys.*, **11**, 10389–10406.

Hohenegger, C., P. Brockhaus, and C. Schar, 2008: Towards climate simulations at cloud-resolving scales. *Meteorol. Z.*, **17**, 383–394.

Hohenegger, C., P. Brockhaus, C. S. Bretherton, and C. Schär, 2009: The soil moisture–precipitation feedback in simulations with explicit and parameterized convection. *J. Clim.*, **22**, 5003–5020.

Holben, B. N., et al., 1998: AERONET - A federated instrument network and data archive for aerosol characterization. *Remote Sens. Environ.*, **66**, 1–16.

Hoose, C., and O. Möhler, 2012: Heterogeneous ice nucleation on atmospheric aerosols: A review of results from laboratory experiments. *Atmos. Chem. Phys.*, **12**, 9817–9854.

Hoose, C., J. E. Kristjánsson, and S. M. Burrows, 2010a: How important is biological ice nucleation in clouds on a global scale? *Environ. Res. Lett.*, **5**, 024009.

Hoose, C., U. Lohmann, R. Erdin, and I. Tegen, 2008: The global influence of dust mineralogical composition on heterogeneous ice nucleation in mixed-phase clouds. *Environ. Res. Lett.*, **3**, 025003.

Hoose, C., J. E. Kristjánsson, J. P. Chen, and A. Hazra, 2010b: A classical-theory-based parameterization of heterogeneous ice nucleation by mineral dust, soot, and biological particles in a global climate model. *J. Atmos. Sci.*, **67**, 2483–2503.

Hoose, C., J. E. Kristjánsson, T. Iversen, A. Kirkevåg, Ø. Seland, and A. Gettelman, 2009: Constraining cloud droplet number concentration in GCMs suppresses the aerosol indirect effect. *Geophys. Res. Lett.*, **36**, L12807.

Hourdin, F., et al., 2013: LMDZ5B: The atmospheric component of the IPSL climate model with revisited parameterizations for clouds and convection. *Clim. Dyn.*, **40**, 2193–2222.

Hoyle, C. R., et al., 2011: A review of the anthropogenic influence on biogenic secondary organic aerosol. *Atmos. Chem. Phys.*, **11**, 321–343.

Hu, M., L. Y. He, Y. H. Zhang, M. Wang, Y. Pyo Kim, and K. C. Moon, 2002: Seasonal variation of ionic species in fine particles at Qingdao. *Atmos. Environ.*, **36**, 5853–5859.

Huang, J., Q. Fu, W. Zhang, X. Wang, R. Zhang, H. Ye, and S. G. Warren, 2011: Dust and black carbon in seasonal snow across Northern China. *Bull. Am. Meteor. Soc.*, **92**, 175–181.

Hudson, J. G., 1993: Cloud condensation nuclei near marine cumulus. *J. Geophys. Res.*, **98**, 2693–2702.

Hudson, J. G., S. Noble, and V. Jha, 2010: Comparisons of CCN with supercooled clouds. *J. Atmos. Sci.*, **67**, 3006–3018.

Hueglin, C., R. Gehrig, U. Baltensperger, M. Gysel, C. Monn, and H. Vonmont, 2005: Chemical characterisation of $PM_{2.5}$, PM_{10} and coarse particles at urban, near-city and rural sites in Switzerland. *Atmos. Environ.*, **39**, 637–651.

Huffman, G. J., et al., 2007: The TRMM multisatellite precipitation analysis (TMPA): Quasi-global, multiyear, combined-sensor precipitation estimates at fine scales. *J. Hydrometeor.*, **8**, 38–55.

Huneeus, N., F. Chevallier, and O. Boucher, 2012: Estimating aerosol emissions by assimilating observed aerosol optical depth in a global aerosol model. *Atmos. Chem. Phys.*, **12**, 4585–4606.

Huneeus, N., et al., 2011: Global dust model intercomparison in AeroCom phase I. *Atmos. Chem. Phys.*, **11**, 7781–7816.

Hurley, J. V., and J. Galewsky, 2010a: A last saturation analysis of ENSO humidity variability in the Subtropical Pacific. *J. Clim.*, **23**, 918–931.

Hurley, J. V., and J. Galewsky, 2010b: A last-saturation diagnosis of subtropical water vapor response to global warming. *Geophys. Res. Lett.*, **37**, L06702.

Iga, S., H. Tomita, Y. Tsushima, and M. Satoh, 2011: Sensitivity of Hadley Circulation to physical parameters and resolution through changing upper-tropospheric ice clouds using a global cloud-system resolving model. *J. Clim.*, **24**, 2666–2679.

Iguchi, T., T. Nakajima, A. P. Khain, K. Saito, T. Takemura, and K. Suzuki, 2008: Modeling the influence of aerosols on cloud microphysical properties in the east Asia region using a mesoscale model coupled with a bin-based cloud microphysics scheme. *J. Geophys. Res.*, **113**, D14215.

Ingram, W., 2010: A very simple model for the water vapour feedback on climate change. *Q. J. R. Meteorol. Soc.*, **136**, 30–40.

Ingram, W., 2013a: A new way of quantifying GCM water vapour feedback. *Clim. Dyn.*, **40**, 913–924.

Ingram, W., 2013b: Some implications of a new approach to the water vapour feedback. *Clim. Dyn.*, **40**, 925–933.

Inoue, T., M. Satoh, Y. Hagihara, H. Miura, and J. Schmetz, 2010: Comparison of high-level clouds represented in a global cloud system-resolving model with CALIPSO/CloudSat and geostationary satellite observations. *J. Geophys. Res.*, **115**, D00H22.

IPCC, 2011: IPCC Expert Meeting Report on Geoengineering, [Edenhofer O, Field C, Pichs-Madruga R, Sokona Y, Stocker T, Barros V, Dahe Q, Minx J, Mach K, Plattner GK, Schlomer S, Hansen G, Mastrandrea M (eds.)]. IPCC Working Group III Technical Support Unit, Potsdam Institute for Climate Impact Research.

Irvine, P. J., A. Ridgwell, and D. J. Lunt, 2011: Climatic effects of surface albedo geoengineering. *J. Geophys. Res.*, **116**, D24112.

Irvine, P. J., R. L. Sriver, and K. Keller, 2012: Tension between reducing sea-level rise and global warming through solar-radiation management. *Nature Clim. Change*, **2**, 97–100.

Irwin, M., N. Good, J. Crosier, T. W. Choularton, and G. McFiggans, 2010: Reconciliation of measurements of hygroscopic growth and critical supersaturation of aerosol particles in central Germany. *Atmos. Chem. Phys.*, **10**, 11737–11752.

Ito, K., N. Xue, and G. Thurston, 2004: Spatial variation of $PM_{2.5}$ chemical species and source-apportioned mass concentrations in New York City. *Atmos. Environ.*, **38**, 5269–5282.

Izrael, Y. A., A. G. Ryaboshapko, and N. N. Petrov, 2009: Comparative analysis of geo-engineering approaches to climate stabilization. *Russ. Meteorol. Hydrol.*, **34**, 335–347.

Jacob, D. J., et al., 2010: The Arctic Research of the Composition of the Troposphere from Aircraft and Satellites (ARCTAS) mission: Design, execution, and first results. *Atmos. Chem. Phys.*, **10**, 5191–5212.

Jacobson, M. Z., 2003: Development of mixed-phase clouds from multiple aerosol size distributions and the effect of the clouds on aerosol removal. *J. Geophys. Res.*, **108**, 4245.

Jacobson, M. Z., 2004: Climate response of fossil fuel and biofuel soot, accounting for soot's feedback to snow and sea ice albedo and emissivity. *J. Geophys. Res.*, **109**, D21201.

Jacobson, M. Z., 2006: Effects of externally-through-internally-mixed soot inclusions within clouds and precipitation on global climate. *J. Phys. Chem. A*, **110**, 6860–6873.

Jacobson, M. Z., 2012: Investigating cloud absorption effects: Global absorption properties of black carbon, tar balls, and soil dust in clouds and aerosols. *J. Geophys. Res.*, **117**, D06205.

Jacobson, M. Z., and D. G. Streets, 2009: Influence of future anthropogenic emissions on climate, natural emissions, and air quality. *J. Geophys. Res.*, **114**, D08118.

Jacobson, M. Z., and J. E. Ten Hoeve, 2012: Effects of urban surfaces and white roofs on global and regional climate. *J. Clim.*, **25**, 1028–1044.

Jaeglé, L., P. K. Quinn, T. S. Bates, B. Alexander, and J. T. Lin, 2011: Global distribution of sea salt aerosols: New constraints from in situ and remote sensing observations. *Atmos. Chem. Phys.*, **11**, 3137–3157.

Jensen, E. J., S. Kinne, and O. B. Toon, 1994: Tropical cirrus cloud radiative forcing: Sensitivity studies. *Geophys. Res. Lett.*, **21**, 2023–2026.

Jensen, E. J., L. Pfister, T. P. Bui, P. Lawson, and D. Baumgardner, 2010: Ice nucleation and cloud microphysical properties in tropical tropopause layer cirrus. *Atmos. Chem. Phys.*, **10**, 1369–1384.

Jeong, M.-J., and Z. Li, 2010: Separating real and apparent effects of cloud, humidity, and dynamics on aerosol optical thickness near cloud edges. *J. Geophys. Res.*, **115**, D00K32.

Jeong, M. J., S. C. Tsay, Q. Ji, N. C. Hsu, R. A. Hansell, and J. Lee, 2008: Ground-based measurements of airborne Saharan dust in marine environment during the NAMMA field experiment. *Geophys. Res. Lett.*, **35**, L20805.

Jethva, H., S. K. Satheesh, J. Srinivasan, and K. K. Moorthy, 2009: How good is the assumption about visible surface reflectance in MODIS aerosol retrieval over land? A comparison with aircraft measurements over an urban site in India. *IEEE Trans. Geosci. Remote Sens.*, **47**, 1990–1998.

Jiang, H. L., H. W. Xue, A. Teller, G. Feingold, and Z. Levin, 2006: Aerosol effects on the lifetime of shallow cumulus. *Geophys. Res. Lett.*, **33**, L14806.

Jiang, J. H., H. Su, M. Schoeberl, S. T. Massie, P. Colarco, S. Platnick, and N. J. Livesey, 2008: Clean and polluted clouds: Relationships among pollution, ice cloud and precipitation in South America. *Geophys. Res. Lett.*, **35**, L14804.

Jimenez, J. L., et al., 2009: Evolution of organic aerosols in the atmosphere. *Science*, **326**, 1525–1529.

Jirak, I. L., and W. R. Cotton, 2006: Effect of air pollution on precipitation along the front range of the Rocky Mountains. *J. Appl. Meteor. Climatol.*, **45**, 236–245.

Johanson, C. M., and Q. Fu, 2009: Hadley cell widening: Model simulations versus observations. *J. Clim.*, **22**, 2713–2725.

Johns, T. C., et al., 2006: The new Hadley Centre Climate Model (HadGEM1): Evaluation of coupled simulations. *J. Clim.*, **19**, 1327–1353.

Johnson, B. T., K. P. Shine, and P. M. Forster, 2004: The semi-direct aerosol effect: Impact of absorbing aerosols on marine stratocumulus. *Q. J. R. Meteorol. Soc.*, **130**, 1407–1422.

Johnson, N. C., and S. P. Xie, 2010: Changes in the sea surface temperature threshold for tropical convection. *Nature Geosci.*, **3**, 842–845.

Jones, A., J. M. Haywood, and O. Boucher, 2007: Aerosol forcing, climate response and climate sensitivity in the Hadley Centre climate model. *J. Geophys. Res.*, **112**, D20211.

Jones, A., J. Haywood, and O. Boucher, 2009: Climate impacts of geoengineering marine stratocumulus clouds. *J. Geophys. Res.*, **114**, D10106.

Jones, A., D. L. Roberts, M. J. Woodage, and C. E. Johnson, 2001: Indirect sulphate aerosol forcing in a climate model with an interactive sulphur cycle. *J. Geophys. Res.*, **106**, 20293–20310.

Jones, A., J. Haywood, O. Boucher, B. Kravitz, and A. Robock, 2010: Geoengineering by stratospheric SO_2 injection: Results from the Met Office HadGEM2 climate model and comparison with the Goddard Institute for Space Studies ModelE. *Atmos. Chem. Phys.*, **10**, 5999–6006.

Joshi, M. M., M. J. Webb, A. C. Maycock, and M. Collins, 2010: Stratospheric water vapour and high climate sensitivity in a version of the HadSM3 climate model. *Atmos. Chem. Phys.*, **10**, 7161–7167.

Joshi, M. M., J. M. Gregory, M. J. Webb, D. M. H. Sexton, and T. C. Johns, 2008: Mechanisms for the land/sea warming contrast exhibited by simulations of climate change. *Clim. Dyn.*, **30**, 455–465.

Kahn, R., 2012: Reducing the uncertainties in direct aerosol radiative forcing. *Surv. Geophys.*, **33**, 701–721.

Kahn, R. A., B. J. Gaitley, J. V. Martonchik, D. J. Diner, K. A. Crean, and B. Holben, 2005: Multiangle Imaging Spectroradiometer (MISR) global aerosol optical depth validation based on 2 years of coincident Aerosol Robotic Network (AERONET) observations. *J. Geophys. Res.*, **110**, D10S04.

Kahn, R. A., B. J. Gaitley, M. J. Garay, D. J. Diner, T. F. Eck, A. Smirnov, and B. N. Holben, 2010: Multiangle Imaging SpectroRadiometer global aerosol product assessment by comparison with the Aerosol Robotic Network. *J. Geophys. Res.*, **115**, D23209.

Kahn, R. A., et al., 2007: Satellite-derived aerosol optical depth over dark water from MISR and MODIS: Comparisons with AERONET and implications for climatological studies. *J. Geophys. Res.*, **112**, D18205.

Kalkstein, A. J., and R. C. Balling Jr, 2004: Impact of unusually clear weather on United States daily temperature range following 9/11/2001 *Clim. Res.*, **26**, 1–4.

Kammermann, L., et al., 2010: Subarctic atmospheric aerosol composition: 3. Measured and modeled properties of cloud condensation nuclei. *J. Geophys. Res.*, **115**, D04202.

Kanakidou, M., et al., 2005: Organic aerosol and global climate modelling: A review. *Atmos. Chem. Phys.*, **5**, 1053–1123.

Kärcher, B., O. Mohler, P. J. DeMott, S. Pechtl, and F. Yu, 2007: Insights into the role of soot aerosols in cirrus cloud formation. *Atmos. Chem. Phys.*, **7**, 4203–4227.

Kaspari, S. D., M. Schwikowski, M. Gysel, M. G. Flanner, S. Kang, S. Hou, and P. A. Mayewski, 2011: Recent increase in black carbon concentrations from a Mt. Everest ice core spanning 1860–2000 AD. *Geophys. Res. Lett.*, **38**, L04703.

Kato, S., et al., 2011: Improvements of top-of-atmosphere and surface irradiance computations with CALIPSO-, CloudSat-, and MODIS-derived cloud and aerosol properties. *J. Geophys. Res.*, **116**, D19209.

Kaufman, Y. J., O. Boucher, D. Tanré, M. Chin, L. A. Remer, and T. Takemura, 2005: Aerosol anthropogenic component estimated from satellite data. *Geophys. Res. Lett.*, **32**, L17804.

Kay, J. E., and A. Gettelman, 2009: Cloud influence on and response to seasonal Arctic sea ice loss. *J. Geophys. Res.*, **114**, D18204.

Kay, J. E., K. Raeder, A. Gettelman, and J. Anderson, 2011: The boundary layer response to recent Arctic sea ice loss and implications for high-latitude climate feedbacks. *J. Clim.*, **24**, 428–447.

Kay, J. E., T. L'Ecuyer, A. Gettelman, G. Stephens, and C. O'Dell, 2008: The contribution of cloud and radiation anomalies to the 2007 Arctic sea ice extent minimum. *Geophys. Res. Lett.*, **35**, L08503.

Kay, J. E., et al., 2012: Exposing global cloud biases in the Community Atmosphere Model (CAM) using satellite observations and their corresponding instrument simulators. *J. Clim.*, **25**, 5190–5207.

Kazil, J., R. G. Harrison, and E. R. Lovejoy, 2008: Tropospheric new particle formation and the role of ions. *Space Sci. Rev.*, **137**, 241–255.

Kazil, J., K. Zhang, P. Stier, J. Feichter, U. Lohmann, and K. O'Brien, 2012: The present-day decadal solar cycle modulation of Earth's radiative forcing via charged H_2SO_4/H_2O aerosol nucleation. *Geophys. Res. Lett.*, **39**, L02805.

Kazil, J., et al., 2010: Aerosol nucleation and its role for clouds and Earth's radiative forcing in the aerosol-climate model ECHAM5–HAM. *Atmos. Chem. Phys.*, **10**, 10733–10752.

Keith, D. W., 2000: Geoengineering the climate: History and prospect. *Annu. Rev. Energ. Environ.*, **25**, 245–284.

Keith, D. W., 2010: Photophoretic levitation of engineered aerosols for geoengineering. *Proc. Natl. Acad. Sci. U.S.A.*, **107**, 16428–16431.

Kerkweg, A., J. Buchholz, L. Ganzeveld, A. Pozzer, H. Tost, and P. Jöckel, 2006: Technical Note: An implementation of the dry removal processes DRY DEPositionand SEDImentation in the Modular Earth Submodel System (MESSy). *Atmos. Chem. Phys.*, **6**, 4617–4632.

Kerminen, V. M., et al., 2010: Atmospheric nucleation: Highlights of the EUCAARI project and future directions. *Atmos. Chem. Phys.*, **10**, 10829–10848.

Kernthaler, S. C., R. Toumi, and J. D. Haigh, 1999: Some doubts concerning a link between cosmic ray fluxes and global cloudiness. *Geophys. Res. Lett.*, **26**, 863–865.

Khain, A., D. Rosenfeld, and A. Pokrovsky, 2005: Aerosol impact on the dynamics and microphysics of deep convective clouds. *Q. J. R. Meteorol. Soc.*, **131**, 2639–2663.

Khain, A., M. Arkhipov, M. Pinsky, Y. Feldman, and Y. Ryabov, 2004: Rain enhancement and fog elimination by seeding with charged droplets. Part 1: Theory and numerical simulations. *J. Appl. Meteorol.*, **43**, 1513–1529.

Khain, A. P., 2009: Notes on state-of-the-art investigations of aerosol effects on precipitation: A critical review. *Environ. Res. Lett.*, **4**, 015004.

Khairoutdinov, M., and Y. Kogan, 2000: A new cloud physics parameterization in a large-eddy simulation model of marine stratocumulus. *Mon. Weather Rev.*, **128**, 229–243.

Khairoutdinov, M., D. Randall, and C. DeMott, 2005: Simulations of the atmospheric general circulation using a cloud-resolving model as a superparameterization of physical processes. *J. Atmos. Sci.*, **62**, 2136–2154.

Khairoutdinov, M. F., and D. A. Randall, 2001: A cloud resolving model as a cloud parameterization in the NCAR Community Climate System Model: Preliminary results. *Geophys. Res. Lett.*, **28**, 3617–3620.

Khairoutdinov, M. F., and C.-E. Yang, 2013: Cloud-resolving modelling of aerosol indirect effects in idealised radiative-convective equilibrium with interactive and fixed sea surface temperature. *Atmos. Chem. Phys.*, **13**, 4133–4144.

Khairoutdinov, M. F., S. K. Krueger, C.-H. Moeng, P. A. Bogenschutz, and D. A. Randall, 2009: Large-eddy simulation of maritime deep tropical convection. *J. Adv. Model. Earth Syst.*, **1**, 15.

Khan, M. F., Y. Shirasuna, K. Hirano, and S. Masunaga, 2010: Characterization of PM2.5, PM2.5–10 and PMN10 in ambient air, Yokohama, Japan. *Atmos. Res.*, **96**, 159–172.

Khare, P., and B. P. Baruah, 2010: Elemental characterization and source identification of $PM_{2.5}$ using multivariate analysis at the suburban site of North-East India. *Atmos. Res.*, **98**, 148–162.

Kharin, V. V., F. W. Zwiers, X. B. Zhang, and G. C. Hegerl, 2007: Changes in temperature and precipitation extremes in the IPCC ensemble of global coupled model simulations. *J. Clim.*, **20**, 1419–1444.

Khvorostyanov, V., and K. Sassen, 1998: Toward the theory of homogeneous nucleation and its parameterization for cloud models. *Geophys. Res. Lett.*, **25**, 3155–3158.

Khvorostyanov, V. I., and J. A. Curry, 2009: Critical humidities of homogeneous and heterogeneous ice nucleation: Inferences from extended classical nucleation theory. *J. Geophys. Res.*, **114**, D04207.

Kim, B. M., S. Teffera, and M. D. Zeldin, 2000: Characterization of $PM_{2.5}$ and PM_{10} in the South Coast air basin of Southern California: Part 1– Spatial variations. *J. Air Waste Manag. Assoc.*, **50**, 2034–2044.

Kim, D., C. Wang, A. M. L. Ekman, M. C. Barth, and P. J. Rasch, 2008: Distribution and direct radiative forcing of carbonaceous and sulfate aerosols in an interactive size-resolving aerosol–climate model. *J. Geophys. Res.*, **113**, D16309.

Kim, D., et al., 2012: The tropical subseasonal variability simulated in the NASA GISS General Circulation Model. *J. Clim.*, **25**, 4641–4659.

Kim, H.-S., J.-B. Huh, P. K. Hopke, T. M. Holsen, and S.-M. Yi, 2007: Characteristics of the major chemical constituents of $PM_{2.5}$ and smog events in Seoul, Korea in 2003 and 2004. *Atmos. Environ.*, **41**, 6762–6770.

Kim, J. M., et al., 2010: Enhanced production of oceanic dimethylsulfide resulting from CO_2-induced grazing activity in a high CO_2 world. *Environ. Sci. Technol.*, **44**, 8140–8143.

King, S. M., et al., 2010: Cloud droplet activation of mixed organic-sulfate particles produced by the photooxidation of isoprene. *Atmos. Chem. Phys.*, **10**, 3953–3964.

Kirchstetter, T. W., T. Novakov, and P. V. Hobbs, 2004: Evidence that the spectral dependence of light absorption by aerosols is affected by organic carbon. *J. Geophys. Res.*, **109**, D21208.

Kirkby, J., 2007: Cosmic rays and climate. *Surv. Geophys.* **28**, 333–375.

Kirkby, J., et al., 2011: Role of sulphuric acid, ammonia and galactic cosmic rays in atmospheric aerosol nucleation. *Nature*, **476**, 429–433.

Kirkevåg, A., T. Iversen, Ø. Seland, J. B. Debernard, T. Storelvmo, and J. E. Kristjánsson, 2008: Aerosol-cloud-climate interactions in the climate model CAM-Oslo. *Tellus A*, **60**, 492–512.

Kirkevåg, A., et al., 2013: Aerosol–climate interactions in the Norwegian Earth System Model – NorESM1–M. *Geoophys. Model Dev.*, **6**, 207–244.

Kleeman, M. J., 2008: A preliminary assessment of the sensitivity of air quality in California to global change. *Clim. Change*, **87**, S273–S292.

Kleidman, R. G., A. Smirnov, R. C. Levy, S. Mattoo, and D. Tanré, 2012: Evaluation and wind speed dependence of MODIS aerosol retrievals over open ocean. *IEEE Trans. Geosci. Remote Sens.*, **50**, 429–435.

Klein, S. A., and D. L. Hartmann, 1993: The seasonal cycle of low stratiform clouds. *J. Clim.*, **6**, 1587–1606.
Klein, S. A., et al., 2009: Intercomparison of model simulations of mixed-phase clouds observed during the ARM Mixed-Phase Arctic Cloud Experiment. I: Single-layer cloud. *Q. J. R. Meteorol. Soc.*, **135**, 979–1002.
Klocke, D., R. Pincus, and J. Quaas, 2011: On constraining estimates of climate sensitivity with present-day observations through model weighting. *J. Clim.*, **24**, 6092–6099.
Kloster, S., et al., 2007: Response of dimethylsulfide (DMS) in the ocean and atmosphere to global warming. *J. Geophys. Res.*, **112**, G03005.
Kloster, S., et al., 2010: Fire dynamics during the 20th century simulated by the Community Land Model. *Biogeosciences*, **7**, 1877–1902.
Knorr, W., V. Lehsten, and A. Arneth, 2012: Determinants and predictability of global wildfire emissions. *Atmos. Chem. Phys.*, **12**, 6845–6861.
Knox, A., et al., 2009: Mass absorption cross-section of ambient black carbon aerosol in relation to chemical age. *Aer. Sci. Technol.*, **43**, 522–532.
Kocak, M., N. Mihalopoulos, and N. Kubilay, 2007: Chemical composition of the fine and coarse fraction of aerosols in the northeastern Mediterranean. *Atmos. Environ.*, **41**, 7351–7368.
Koch, D., and A. D. Del Genio, 2010: Black carbon semi-direct effects on cloud cover: Review and synthesis. *Atmos. Chem. Phys.*, **10**, 7685–7696.
Koch, D., S. Menon, A. Del Genio, R. Ruedy, I. Alienov, and G. A. Schmidt, 2009a: Distinguishing aerosol impacts on climate over the past century. *J. Clim.*, **22**, 2659–2677.
Koch, D., et al., 2009b: Evaluation of black carbon estimations in global aerosol models. *Atmos. Chem. Phys.*, **9**, 9001–9026.
Kodama, C., A. T. Noda, and M. Satoh, 2012: An assessment of the cloud signals simulated by NICAM using ISCCP, CALIPSO, and CloudSat satellite simulators. *J. Geophys. Res.*, **117**, D12210.
Koffi, B., et al., 2012: Application of the CALIOP layer product to evaluate the vertical distribution of aerosols estimated by global models: Part 1. AeroCom phase I results. *J. Geophys. Res.*, **117**, D10201.
Köhler, M., M. Ahlgrimm, and A. Beljaars, 2011: Unified treatment of dry convective and stratocumulus-topped boundary layers in the ECMWF model. *Q. J. R. Meteorol. Soc.*, **137**, 43–57.
Kok, J. F., 2011: A scaling theory for the size distribution of emitted dust aerosols suggests climate models underestimate the size of the global dust cycle. *Proc. Natl. Acad. Sci. U.S.A.*, **108**, 1016–1021.
Kokhanovsky, A. A., et al., 2010: The inter-comparison of major satellite aerosol retrieval algorithms using simulated intensity and polarization characteristics of reflected light. *Atmos. Meas. Tech.*, **3**, 909–932.
Koop, T., B. P. Luo, A. Tsias, and T. Peter, 2000: Water activity as the determinant for homogeneous ice nucleation in aqueous solutions. *Nature*, **406**, 611–614.
Koren, I., G. Feingold, and L. A. Remer, 2010a: The invigoration of deep convective clouds over the Atlantic: Aerosol effect, meteorology or retrieval artifact? *Atmos. Chem. Phys.*, **10**, 8855–8872.
Koren, I., Y. Kaufman, L. Remer, and J. Martins, 2004: Measurement of the effect of Amazon smoke on inhibition of cloud formation. *Science*, **303**, 1342–1345.
Koren, I., J. V. Martins, L. A. Remer, and H. Afargan, 2008: Smoke invigoration versus inhibition of clouds over the Amazon. *Science*, **321**, 946–949.
Koren, I., Y. J. Kaufman, D. Rosenfeld, L. A. Remer, and Y. Rudich, 2005: Aerosol invigoration and restructuring of Atlantic convective clouds. *Geophys. Res. Lett.*, **32**, L14828.
Koren, I., L. A. Remer, Y. J. Kaufman, Y. Rudich, and J. V. Martins, 2007: On the twilight zone between clouds and aerosols. *Geophys. Res. Lett.*, **34**, L08805.
Koren, I., L. A. Remer, O. Altaratz, J. V. Martins, and A. Davidi, 2010b: Aerosol-induced changes of convective cloud anvils produce strong climate warming. *Atmos. Chem. Phys.*, **10**, 5001–5010.
Korhonen, H., K. S. Carslaw, and S. Romakkaniemi, 2010a: Enhancement of marine cloud albedo via controlled sea spray injections: A global model study of the influence of emission rates, microphysics and transport. *Atmos. Chem. Phys.*, **10**, 4133–4143.
Korhonen, H., K. S. Carslaw, P. M. Forster, S. Mikkonen, N. D. Gordon, and H. Kokkola, 2010b: Aerosol climate feedback due to decadal increases in Southern Hemisphere wind speeds. *Geophys. Res. Lett.*, **37**, L02805.
Korolev, A., 2007: Limitations of the Wegener-Bergeron-Findeisen mechanism in the evolution of mixed-phase clouds. *J. Atmos. Sci.*, **64**, 3372–3375.
Korolev, A., and P. R. Field, 2008: The effect of dynamics on mixed-phase clouds: Theoretical considerations. *J. Atmos. Sci.*, **65**, 66–86.
Kostinski, A. B., 2008: Drizzle rates versus cloud depths for marine stratocumuli. *Environ. Res. Lett.*, **3**, 045019.
Kravitz, B., A. Robock, D. Shindell, and M. Miller, 2012: Sensitivity of stratospheric geoengineering with black carbon to aerosol size and altitude of injection. *J. Geophys. Res.*, **117**, D09203.
Kravitz, B., A. Robock, L. Oman, G. Stenchikov, and A. B. Marquardt, 2009: Sulfuric acid deposition from stratospheric geoengineering with sulfate aerosols. *J. Geophys. Res.*, **114**, D14109.
Kravitz, B., A. Robock, O. Boucher, H. Schmidt, K. Taylor, G. Stenchikov, and M. Schulz, 2011: The Geoengineering Model Intercomparison Project (GeoMIP). *Atmos. Sci. Lett.*, **12**, 162–167.
Kristjánsson, J. E., 2002: Studies of the aerosol indirect effect from sulfate and black carbon aerosols. *J. Geophys. Res.*, **107**, 4246.
Kristjánsson, J. E., T. Iversen, A. Kirkevåg, Ø. Seland, and J. Debernard, 2005: Response of the climate system to aerosol direct and indirect forcing: Role of cloud feedbacks. *J. Geophys. Res.*, **110**, D24206.
Kristjánsson, J. E., C. W. Stjern, F. Stordal, A. M. Fjæraa, G. Myhre, and K. Jónasson, 2008: Cosmic rays, cloud condensation nuclei and clouds – a reassessment using MODIS data. *Atmos. Chem. Phys.*, **8**, 7373–7387.
Kroll, J. H., and J. H. Seinfeld, 2008: Chemistry of secondary organic aerosol: Formation and evolution of low-volatility organics in the atmosphere. *Atmos. Environ.*, **42**, 3593–3624.
Krueger, S. K., G. T. McLean, and Q. Fu, 1995: Numerical simulation of the stratus-to-cumulus transition in the subtropical marine boundary layer. 1. Boundary-layer structure. *J. Atmos. Sci.*, **52**, 2839–2850.
Kuang, Z. M., 2008: Modeling the interaction between cumulus convection and linear gravity waves using a limited-domain cloud system-resolving model. *J. Atmos. Sci.*, **65**, 576–591.
Kuang, Z. M., and C. S. Bretherton, 2006: A mass-flux scheme view of a high-resolution simulation of a transition from shallow to deep cumulus convection. *J. Atmos. Sci.*, **63**, 1895–1909.
Kuang, Z. M., and D. L. Hartmann, 2007: Testing the fixed anvil temperature hypothesis in a cloud-resolving model. *J. Clim.*, **20**, 2051–2057.
Kuebbeler, M., U. Lohmann, and J. Feichter, 2012: Effects of stratospheric sulfate aerosol geo-engineering on cirrus clouds. *Geophys. Res. Lett.*, **39**, L23803.
Kueppers, L. M., M. A. Snyder, and L. C. Sloan, 2007: Irrigation cooling effect: Regional climate forcing by land-use change. *Geophys. Res. Lett.*, **34**, L03703.
Kulmala, M., and V. M. Kerminen, 2008: On the formation and growth of atmospheric nanoparticles. *Atmos. Res.*, **90**, 132–150.
Kulmala, M., et al., 2010: Atmospheric data over a solar cycle: No connection between galactic cosmic rays and new particle formation. *Atmos. Chem. Phys.*, **10**, 1885–1898.
Kulmala, M., et al., 2011: General overview: European Integrated project on Aerosol Cloud Climate and Air Quality interactions (EUCAARI) – integrating aerosol research from nano to global scales. *Atmos. Chem. Phys.*, **11**, 13061–13143.
Kumar, P., I. N. Sokolik, and A. Nenes, 2011: Measurements of cloud condensation nuclei activity and droplet activation kinetics of fresh unprocessed regional dust samples and minerals. *Atmos. Chem. Phys.*, **11**, 3527–3541.
Kumar, R., S. S. Srivastava, and K. M. Kumari, 2007: Characteristics of aerosols over suburban and urban site of semiarid region in India: Seasonal and spatial variations. *Aer. Air Qual. Res.*, **7**, 531–549.
Kurten, T., V. Loukonen, H. Vehkamaki, and M. Kulmala, 2008: Amines are likely to enhance neutral and ion-induced sulfuric acid-water nucleation in the atmosphere more effectively than ammonia. *Atmos. Chem. Phys.*, **8**, 4095–4103.
Kuylenstierna, J. C. I., H. Rodhe, S. Cinderby, and K. Hicks, 2001: Acidification in developing countries: Ecosystem sensitivity and the critical load approach on a global scale. *Ambio*, **30**, 20–28.
L'Ecuyer, T. S., and J. H. Jiang, 2010: Touring the atmosphere aboard the A-Train. *Physics Today*, **63**, 36–41.
Laken, B., A. Wolfendale, and D. Kniveton, 2009: Cosmic ray decreases and changes in the liquid water cloud fraction over the oceans. *Geophys. Res. Lett.*, **36**, L23803.
Laken, B., D. Kniveton, and A. Wolfendale, 2011: Forbush decreases, solar irradiance variations, and anomalous cloud changes. *J. Geophys. Res.*, **116**, D09201.
Laken, B., E. Pallé, and H. Miyahara, 2012: A decade of the Moderate Resolution Imaging Spectroradiometer: is a solar–cloud link detectable? *J. Clim.*, **25**, 4430–4440.
Laken, B. A., and J. Čalogović, 2011: Solar irradiance, cosmic rays and cloudiness over daily timescales. *Geophys. Res. Lett.*, **38**, L24811.

Laken, B. A., D. R. Kniveton, and M. R. Frogley, 2010: Cosmic rays linked to rapid mid-latitude cloud changes. *Atmos. Chem. Phys.*, **10**, 10941–10948.
Lambert, F. H., and M. J. Webb, 2008: Dependency of global mean precipitation on surface temperature. *Geophys. Res. Lett.*, **35**, L16706.
Lance, S., et al., 2011: Cloud condensation nuclei as a modulator of ice processes in Arctic mixed-phase clouds. *Atmos. Chem. Phys.*, **11**, 8003–8015.
Lanz, V. A., M. R. Alfarra, U. Baltensperger, B. Buchmann, C. Hueglin, and A. S. H. Prévôt, 2007: Source apportionment of submicron organic aerosols at an urban site by factor analytical modelling of aerosol mass spectra. *Atmos. Chem. Phys.*, **7**, 1503–1522.
Larson, V. E., and J. C. Golaz, 2005: Using probability density functions to derive consistent closure relationships among higher-order moments. *Mon. Weather Rev.*, **133**, 1023–1042.
Larson, V. E., R. Wood, P. R. Field, J.-C. Golaz, T. H. Vonder Haar, and W. R. Cotton, 2001: Systematic biases in the microphysics and thermodynamics of numerical models that ignore subgrid-scale variability. *J. Atmos. Sci.*, **58**, 1117–1128.
Latham, J., 1990: Control of global warming? *Nature*, **347**, 339–340.
Latham, J., et al., 2008: Global temperature stabilization via controlled albedo enhancement of low-level maritime clouds. *Philos. Trans. R. Soc. London A*, **366**, 3969–3987.
Lathière, J., C. N. Hewitt, and D. J. Beerling, 2010: Sensitivity of isoprene emissions from the terrestrial biosphere to 20th century changes in atmospheric CO_2 concentration, climate, and land use. *Global Biogeochem. Cycles*, **24**, GB1004.
Lau, K. M., M. K. Kim, and K. M. Kim, 2006: Asian summer monsoon anomalies induced by aerosol direct forcing: Tthe role of the Tibetan Plateau. *Clim. Dyn.*, **26**, 855–864.
Lavers, D. A., R. P. Allan, E. F. Wood, G. Villarini, D. J. Brayshaw, and A. J. Wade, 2011: Winter floods in Britain are connected to atmospheric rivers. *Geophys. Res. Lett.*, **38**, L23803.
Lebsock, M. D., G. L. Stephens, and C. Kummerow, 2008: Multisensor satellite observations of aerosol effects on warm clouds. *J. Geophys. Res.*, **113**, D15205.
Lebsock, M. D., C. Kummerow, and G. L. Stephens, 2010: An observed tropical oceanic radiative-convective cloud feedback. *J. Clim.*, **23**, 2065–2078.
Leck, C., and E. K. Bigg, 2007: A modified aerosol–cloud–climate feedback hypothesis. *Environ. Chem.*, **4**, 400–403.
Leck, C., and E. K. Bigg, 2008: Comparison of sources and nature of the tropical aerosol with the summer high Arctic aerosol. *Tellus B*, **60**, 118–126.
Lee, D. S., et al., 2009: Aviation and global climate change in the 21st century. *Atmos. Environ.*, **43**, 3520–3537.
Lee, H. S., and B. W. Kang, 2001: Chemical characteristics of principal $PM_{2.5}$ species in Chongju, South Korea. *Atmos. Environ.*, **35**, 739–749.
Lee, K. H., Z. Li, M. S. Wong, J. Xin, Y. Wang, W.-M. Hao, and F. Zhao, 2007: Aerosol single scattering albedo estimated across China from a combination of ground and satellite measurements. *J. Geophys. Res.*, **112**, D22S15.
Lee, L. A., K. S. Carslaw, K. Pringle, G. W. Mann, and D. V. Spracklen, 2011: Emulation of a complex global aerosol model to quantify sensitivity to uncertain parameters. *Atmos. Chem. Phys.*, **11**, 12253–12273.
Lee, S.-S., G. Feingold, and P. Y. Chuang, 2012: Effect of aerosol on cloud-environment interactions in trade cumulus. *J. Atmos. Sci.*, **69**, 3607–3632.
Lee, S. S., 2012: Effect of aerosol on circulations and precipitation in deep convective clouds. *J. Atmos. Sci.*, **69**, 1957–1974.
Lee, Y. H., et al., 2013: Evaluation of preindustrial to present-day black carbon and its albedo forcing from Atmospheric Chemistry and Climate Model Intercomparison Project (ACCMIP). *Atmos. Chem. Phys.*, **13**, 2607–2634.
Lenderink, G., and E. Van Meijgaard, 2008: Increase in hourly precipitation extremes beyond expectations from temperature changes. *Nature Geosci.*, **1**, 511–514.
Lenderink, G., H. Y. Mok, T. C. Lee, and G. J. van Oldenborgh, 2011: Scaling and trends of hourly precipitation extremes in two different climate zones - Hong Kong and the Netherlands. *Hydrol. Earth Syst. Sci.*, **15**, 3033–3041.
Lenschow, P., H. J. Abraham, K. Kutzner, M. Lutz, J. D. Preu, and W. Reichenbacher, 2001: Some ideas about the sources of PM_{10}. *Atmos. Environ.*, **35**, 23–33.
Lenton, T. M., and N. E. Vaughan, 2009: The radiative forcing potential of different climate geoengineering options. *Atmos. Chem. Phys.*, **9**, 5539–5561.
Levin, Z., and W. R. Cotton, 2009: *Aerosol Pollution Impact on Precipitation: A Scientific Review.* Springer Science+Business Media, New York, NY, USA, and Heidelberg, Germany, 386 pp.
Levy, R. C., L. A. Remer, R. G. Kleidman, S. Mattoo, C. Ichoku, R. Kahn, and T. F. Eck, 2010: Global evaluation of the Collection 5 MODIS dark-target aerosol products over land. *Atmos. Chem. Phys.*, **10**, 10399–10420.
Li, J., M. Pósfai, P. V. Hobbs, and P. R. Buseck, 2003: Individual aerosol particles from biomass burning in southern Africa: 2, Compositions and aging of inorganic particles. *J. Geophys. Res.*, **108**, 8484.
Li, Z., K.-H. Lee, Y. Wang, J. Xin, and W.-M. Hao, 2010: First observation-based estimates of cloud-free aerosol radiative forcing across China. *J. Geophys. Res.*, **115**, D00K18.
Li, Z., F. Niu, J. Fan, Y. Liu, D. Rosenfeld, and Y. Ding, 2011: Long-term impacts of aerosols on the vertical development of clouds and precipitation *Nature Geosci.*, **4**, 888–894.
Li, Z., et al., 2009: Uncertainties in satellite remote sensing of aerosols and impact on monitoring its long-term trend: A review and perspective. *Annal. Geophys.*, **27**, 2755–2770.
Liao, H., W. T. Chen, and J. H. Seinfeld, 2006: Role of climate change in global predictions of future tropospheric ozone and aerosols. *J. Geophys. Res.*, **111**, D12304.
Liao, H., Y. Zhang, W. T. Chen, F. Raes, and J. H. Seinfeld, 2009: Effect of chemistry-aerosol-climate coupling on predictions of future climate and future levels of tropospheric ozone and aerosols. *J. Geophys. Res.*, **114**, D10306.
Liepert, B. G., and M. Previdi, 2012: Inter-model variability and biases of the global water cycle in CMIP3 coupled climate models. *Environ. Res. Lett.*, **7**, 014006.
Lim, Y. B., Y. Tan, M. J. Perri, S. P. Seitzinger, and B. J. Turpin, 2010: Aqueous chemistry and its role in secondary organic aerosol (SOA) formation. *Atmos. Chem. Phys.*, **10**, 10521–10539.
Lin, G., J. E. Penner, S. Sillman, D. Taraborrelli, and J. Lelieveld, 2012: Global modeling of SOA formation from dicarbonyls, epoxides, organic nitrates and peroxides. *Atmos. Chem. Phys.*, **12**, 4743–4774.
Lindzen, R. S., and Y.-S. Choi, 2011: On the observational determination of climate sensitivity and its implications. *Asia Pac. J. Atmos. Sci.*, **47**, 377–390.
Liou, K. N., and S. C. Ou, 1989: The role of cloud microphysical processes in climate—An assessment from a one-dimensional perspective. *J. Geophys. Res.*, **94**, 8599–8607.
Liu, W., Y. Wang, A. Russell, and E. S. Edgerton, 2005: Atmospheric aerosol over two urban-rural pairs in the southeastern United States: Chemical composition and possible sources. *Atmos. Environ.*, **39**, 4453–4470.
Liu, X., J. Penner, S. Ghan, and M. Wang, 2007: Inclusion of ice microphysics in the NCAR community atmospheric model version 3 (CAM3). *J. Clim.*, **20**, 4526–4547.
Liu, X., et al., 2012: Toward a minimal representation of aerosols in climate models: Description and evaluation in the Community Atmosphere Model CAM5. *Geosci. Model Dev.*, **5**, 709–739.
Liu, X. H., and J. E. Penner, 2005: Ice nucleation parameterization for global models. *Meteorol. Z.*, **14**, 499–514.
Liu, X. H., J. E. Penner, and M. H. Wang, 2009: Influence of anthropogenic sulfate and black carbon on upper tropospheric clouds in the NCAR CAM3 model coupled to the IMPACT global aerosol model. *J. Geophys. Res.*, **114**, D03204.
Liu, Y., and P. H. Daum, 2002: Anthropogenic aerosols: Indirect warming effect from dispersion forcing. *Nature*, **419**, 580–581.
Liu, Y., J. R. Key, and X. Wang, 2008: The influence of changes in cloud cover on recent surface temperature trends in the Arctic. *J. Clim.*, **21**, 705–715.
Lobell, D., G. Bala, A. Mirin, T. Phillips, R. Maxwell, and D. Rotman, 2009: Regional differences in the influence of irrigation on climate. *J. Clim.*, **22**, 2248–2255.
Lock, A. P., 2009: Factors influencing cloud area at the capping inversion for shallow cumulus clouds. *Q. J. R. Meteorol. Soc.*, **135**, 941–952.
Lodhi, A., B. Ghauri, M. R. Khan, S. Rahmana, and S. Shafiquea, 2009: Particulate matter ($PM_{2.5}$) concentration and source apportionment in Lahore. *J. Brazil. Chem. Soc.*, **20**, 1811–1820.
Loeb, N. G., and N. Manalo-Smith, 2005: Top-of-atmosphere direct radiative effect of aerosols over global oceans from merged CERES and MODIS observations. *J. Clim.*, **18**, 3506–3526.
Loeb, N. G., and G. L. Schuster, 2008: An observational study of the relationship between cloud, aerosol and meteorology in broken low-level cloud conditions. *J. Geophys. Res.*, **113**, D14214.
Loeb, N. G., and W. Y. Su, 2010: Direct aerosol radiative forcing uncertainty based on a radiative perturbation analysis. *J. Clim.*, **23**, 5288–5293.
Loeb, N. G., et al., 2009: Toward optimal closure of the Earth's top-of-atmosphere radiation budget. *J. Clim.*, **22**, 748–766.
Logan, T., B. K. Xi, X. Q. Dong, R. Obrecht, Z. Q. Li, and M. Cribb, 2010: A study of Asian dust plumes using satellite, surface, and aircraft measurements during the INTEX-B field experiment. *J. Geophys. Res.*, **115**, D00K25.

Lohmann, U., 2002a: Possible aerosol effects on ice clouds via contact nucleation. *J. Atmos. Sci.*, **59**, 647–656.
Lohmann, U., 2002b: A glaciation indirect aerosol effect caused by soot aerosols. *Geophys. Res. Lett.*, **29**, 1052.
Lohmann, U., 2004: Can anthropogenic aerosols decrease the snowfall rate? *J. Atmos. Sci.*, **61**, 2457–2468.
Lohmann, U., 2008: Global anthropogenic aerosol effects on convective clouds in ECHAM5–HAM. *Atmos. Chem. Phys.*, **8**, 2115–2131.
Lohmann, U., and J. Feichter, 1997: Impact of sulfate aerosols on albedo and lifetime of clouds: A sensitivity study with the ECHAM4 GCM. *J. Geophys. Res.*, **102**, 13685–13700.
Lohmann, U., and J. Feichter, 2001: Can the direct and semi-direct aerosol effect compete with the indirect effect on a global scale? *Geophys. Res. Lett.*, **28**, 159–161.
Lohmann, U., and B. Kärcher, 2002: First interactive simulations of cirrus clouds formed by homogeneous freezing in the ECHAM general circulation model. *J. Geophys. Res.*, **107**, 4105.
Lohmann, U., and G. Lesins, 2002: Stronger constraints on the anthropogenic indirect aerosol effect. *Science*, **298**, 1012–1015.
Lohmann, U., and J. Feichter, 2005: Global indirect aerosol effects: A review. *Atmos. Chem. Phys.*, **5**, 715–737.
Lohmann, U., and K. Diehl, 2006: Sensitivity studies of the importance of dust ice nuclei for the indirect aerosol effect on stratiform mixed-phase clouds. *J. Atmos. Sci.*, **63**, 968–982.
Lohmann, U., and C. Hoose, 2009: Sensitivity studies of different aerosol indirect effects in mixed-phase clouds. *Atmos. Chem. Phys.*, **9**, 8917–8934.
Lohmann, U., and S. Ferrachat, 2010: Impact of parametric uncertainties on the present-day climate and on the anthropogenic aerosol effect. *Atmos. Chem. Phys.*, **10**, 11373–11383.
Lohmann, U., J. Feichter, J. Penner, and R. Leaitch, 2000: Indirect effect of sulfate and carbonaceous aerosols: A mechanistic treatment. *J. Geophys. Res.*, **105**, 12193–12206.
Lohmann, U., P. Stier, C. Hoose, S. Ferrachat, S. Kloster, E. Roeckner, and J. Zhang, 2007: Cloud microphysics and aerosol indirect effects in the global climate model ECHAM5–HAM. *Atmos. Chem. Phys.*, **7**, 3425–3446.
Lohmann, U., et al., 2010: Total aerosol effect: Radiative forcing or radiative flux perturbation? *Atmos. Chem. Phys.*, **10**, 3235–3246.
Lonati, G., M. Giugliano, P. Butelli, L. Romele, and R. Tardivo, 2005: Major chemical components of $PM_{2.5}$ in Milan (Italy). *Atmos. Environ.*, **39**, 1925–1934.
Lu, M.-L., W. C. Conant, H. H. Jonsson, V. Varutbangkul, R. C. Flagan, and J. H. Seinfeld, 2007: The marine stratus/stratocumulus experiment (MASE): Aerosol-cloud relationships in marine stratocumulus. *J. Geophys. Res.*, **112**, D10209.
Lu, M.-L., G. Feingold, H. H. Jonsson, P. Y. Chuang, H. Gates, R. C. Flagan, and J. H. Seinfeld, 2008: Aerosol-cloud relationships in continental shallow cumulus. *J. Geophys. Res.*, **113**, D15201.
Lu, Z., Q. Zhang, and D. G. Streets, 2011: Sulfur dioxide and primary carbonaceous aerosol emissions in China and India, 1996–2010. *Atmos. Chem. Phys.*, **11**, 9839–9864.
Lu, Z., et al., 2010: Sulfur dioxide emissions in China and sulfur trends in East Asia since 2000. *Atmos. Chem. Phys.*, **10**, 6311–6331.
Lubin, D., and A. M. Vogelmann, 2006: A climatologically significant aerosol longwave indirect effect in the Arctic. *Nature*, **439**, 453–456.
Lunt, D. J., A. Ridgwell, P. J. Valdes, and A. Seale, 2008: "Sunshade World": A fully coupled GCM evaluation of the climatic impacts of geoengineering. *Geophys. Res. Lett.*, **35**, L12710.
Lyapustin, A., et al., 2010: Analysis of snow bidirectional reflectance from ARCTAS Spring-2008 Campaign. *Atmos. Chem. Phys.*, **10**, 4359–4375.
Ma, H. Y., M. Kohler, J. L. F. Li, J. D. Farrara, C. R. Mechoso, R. M. Forbes, and D. E. Waliser, 2012a: Evaluation of an ice cloud parameterization based on a dynamical-microphysical lifetime concept using CloudSat observations and the ERA-Interim reanalysis. *J. Geophys. Res.*, **117**, D05210.
Ma, X., F. Yu, and G. Luo, 2012b: Aerosol direct radiative forcing based on GEOS-Chem-APM and uncertainties. *Atmos. Chem. Phys.*, **12**, 5563–5581.
MacCracken, M. C., 2009: On the possible use of geoengineering to moderate specific climate change impacts. *Environ. Res. Lett.*, **4**, 045107.
Mace, G. G., Q. Q. Zhang, M. Vaughan, R. Marchand, G. Stephens, C. Trepte, and D. Winker, 2009: A description of hydrometeor layer occurrence statistics derived from the first year of merged Cloudsat and CALIPSO data. *J. Geophys. Res.*, **114**, D00A26.
Maenhaut, W., I. Salma, and J. Cafrneyer, 1996: Regional atmospheric aerosol composition and sources in the eastern Transvaal, South Africa, and impact of biomass burning. *J. Geophys. Res.*, **101**, 23613–23650.
Maenhaut, W., M.-T. Fernandez-Jimenez, J. L. Vanderzalm, B. Hooper, M. A. Hooper, and N. J. Tapper, 2000: Aerosol composition at Jabiru, Australia, and impact of biomass burning. *J. Aer. Sci.*, **31**, 745–746.
Magee, N., A. M. Moyle, and D. Lamb, 2006: Experimental determination of the deposition coefficient of small cirrus-like ice crystals near –50°C. *Geophys. Res. Lett.*, **33**, L17813.
Mahowald, N. M., J. F. Lamarque, X. X. Tie, and E. Wolff, 2006a: Sea-salt aerosol response to climate change: Last Glacial Maximum, preindustrial, and doubled carbon dioxide climates. *J. Geophys. Res.*, **111**, D05303.
Mahowald, N. M., D. R. Muhs, S. Levis, P. J. Rasch, M. Yoshioka, C. S. Zender, and C. Luo, 2006b: Change in atmospheric mineral aerosols in response to climate: Last glacial period, preindustrial, modern, and doubled carbon dioxide climates. *J. Geophys. Res.*, **111**, D10202.
Mahowald, N. M., et al., 2009: Atmospheric iron deposition: Global distribution, variability, and human perturbations. *Annu. Rev. Mar. Sci.*, **1**, 245–278.
Mahowald, N. M., et al., 2010: Observed 20th century desert dust variability: impact on climate and biogeochemistry. *Atmos. Chem. Phys.*, **10**, 10875–10893.
Makkonen, R., A. Asmi, V. Kerminen, M. Boy, A. Arneth, P. Hari, and M. Kulmala, 2012a: Air pollution control and decreasing new particle formation lead to strong climate warming. *Atmos. Chem. Phys.*, **12**, 1515–1524.
Makkonen, R., A. Asmi, V. M. Kerminen, M. Boy, A. Arneth, A. Guenther, and M. Kulmala, 2012b: BVOC-aerosol-climate interactions in the global aerosol-climate model ECHAM5.5–HAM2. *Atmos. Chem. Phys.*, **12**, 10077–10096.
Malm, W. C., and B. A. Schichtel, 2004: Spatial and monthly trends in speciated fine particle concentration in the United States. *J. Geophys. Res.*, **109**, D03306.
Malm, W. C., J. F. Sisler, D. Huffman, R. A. Eldred, and T. A. Cahill, 1994: Spatial and seasonal trends in particle concentration and optical extinction in the United States. *J. Geophys. Res.*, **99**, 1347–1370.
Mann, G. W., et al., 2010: Description and evaluation of GLOMAP-mode: A modal global aerosol microphysics model for the UKCA composition-climate model. *Geosci. Model Dev.*, **3**, 519–551.
Manninen, H. E., et al., 2010: EUCAARI ion spectrometer measurements at 12 European sites—analysis of new particle formation events. *Atmos. Chem. Phys.*, **10**, 7907–7927.
Mapes, B., and R. Neale, 2011: Parameterizing convective organization to escape the entrainment dilemma. *J. Adv. Model. Earth Syst.*, **3**, M06004.
Mariani, R. L., and W. Z. d. Mello, 2007: PM2.5–10, PM2.5 and associated water-soluble inorganic species at a coastal urban site in the metropolitan region of Rio de Janeiro. *Atmos. Environ.*, **41**, 2887–2892.
Marlon, J. R., et al., 2008: Climate and human influences on global biomass burning over the past two millennia. *Nature Geosci.*, **1**, 697–702.
Marsh, N. D., and H. Svensmark, 2000: Low cloud properties influenced by cosmic rays. *Phys. Rev. Lett.*, **85**, 5004–5007.
Martin, S. T., et al., 2010a: Sources and properties of Amazonian aerosol particles. *Rev. Geophys.*, **48**, RG2002.
Martin, S. T., et al., 2010b: An overview of the Amazonian Aerosol Characterization Experiment 2008 (AMAZE-08). *Atmos. Chem. Phys.*, **10**, 11415–11438.
Matthews, H. D., 2010: Can carbon cycle geoengineering be a useful complement to ambitious climate mitigation? *Carbon Manag.*, **1**, 135–144.
Matthews, H. D., and K. Caldeira, 2007: Transient climate–carbon simulations of planetary geoengineering. *Proc. Natl. Acad. Sci. U.S.A.*, **104**, 9949–9954.
Mauger, G. S., and J. R. Norris, 2010: Assessing the impact of meteorological history on subtropical cloud fraction. *J. Clim.*, **23**, 2926–2940.
Mauritsen, T., et al., 2011: An Arctic CCN-limited cloud-aerosol regime. *Atmos. Chem. Phys.*, **11**, 165–173.
Mautner, M., 1991: A space-based solar screen against climate warming. *J. Br. Interplanet. Soc.*, **44**, 135–138.
McComiskey, A., and G. Feingold, 2008: Quantifying error in the radiative forcing of the first aerosol indirect effect. *Geophys. Res. Lett.*, **35**, L02810.
McComiskey, A., and G. Feingold, 2012: The scale problem in quantifying aerosol indirect effects. *Atmos. Chem. Phys.*, **12**, 1031–1049.
McComiskey, A., S. Schwartz, B. Schmid, H. Guan, E. Lewis, P. Ricchiazzi, and J. Ogren, 2008: Direct aerosol forcing: Calculation from observables and sensitivities to inputs. *J. Geophys. Res.*, **113**, D09202.
McComiskey, A., et al., 2009: An assessment of aerosol-cloud interactions in marine stratus clouds based on surface remote sensing. *J. Geophys. Res.*, **114**, D09203.

McConnell, J. R., et al., 2007: 20th-century industrial black carbon emissions altered Arctic climate forcing. *Science*, **317**, 1381–1384.
McCormick, M. P., L. W. Thomason, and C. R. Trepte, 1995: Atmospheric effects of the Mt Pinatubo eruption. *Nature*, **373**, 399–404.
McFarquhar, G. M., et al., 2011: Indirect and semi-direct aerosol campaign: The impact of Arctic aerosols on clouds. *Bull. Am. Meteor. Soc.*, **92**, 183–201.
McFiggans, G., et al., 2006: The effect of physical and chemical aerosol properties on warm cloud droplet activation. *Atmos. Chem. Phys.*, **6**, 2593–2649.
McMeeking, G. R., et al., 2010: Black carbon measurements in the boundary layer over western and northern Europe. *Atmos. Chem. Phys.*, **10**, 9393–9414.
Medeiros, B., B. Stevens, I. M. Held, M. Zhao, D. L. Williamson, J. G. Olson, and C. S. Bretherton, 2008: Aquaplanets, climate sensitivity, and low clouds. *J. Clim.*, **21**, 4974–4991.
Meehl, G. A., et al., 2007: Global climate projections. In: *Climate Change 2007: The Physical Science Basis. Contribution of Working Group I to the Fourth Assessment Report of the Intergovernmental Panel on Climate Change* [Solomon, S., D. Qin, M. Manning, Z. Chen, M. Marquis, K. B. Averyt, M. Tignor and H. L. Miller (eds.)] Cambridge University Press, Cambridge, United Kingdom and New York, NY, USA, pp. 747–843.
Menon, S., and L. Rotstayn, 2006: The radiative influence of aerosol effects on liquid-phase cumulus and stratiform clouds based on sensitivity studies with two climate models. *Clim. Dyn.*, **27**, 345–356.
Menon, S., and A. Del Genio, 2007: Evaluating the impacts of carbonaceous aerosols on clouds and climate. In: *Human-Induced Climate Change: An Interdisciplinary Assessment* [M. E. Schlesinger, H. S. Kheshgi, J. Smith, F. C. de la Chesnaye, J. M. Reilly, T. Wilson and C. Kolstad (eds.)]. Cambridge University Press, Cambridge, United Kingdom, and New York, NY, USA, pp. 34–48.
Menon, S., A. D. Del Genio, D. Koch, and G. Tselioudis, 2002: GCM Simulations of the aerosol indirect effect: Sensitivity to cloud parameterization and aerosol burden. *J. Atmos. Sci.*, **59**, 692–713.
Mercado, L. M., N. Bellouin, S. Sitch, O. Boucher, C. Huntingford, M. Wild, and P. M. Cox, 2009: Impact of changes in diffuse radiation on the global land carbon sink. *Nature*, **458**, 1014–1017.
Merikanto, J., D. V. Spracklen, G. W. Mann, S. J. Pickering, and K. S. Carslaw, 2009: Impact of nucleation on global CCN. *Atmos. Chem. Phys.*, **9**, 8601–8616.
Metzger, A., et al., 2010: Evidence for the role of organics in aerosol particle formation under atmospheric conditions. *Proc. Natl. Acad. Sci. U.S.A.*, **107**, 6646–6651.
Miller, R. L., 1997: Tropical thermostats and low cloud cover. *J. Clim.*, **10**, 409–440.
Ming, J., D. Zhang, S. Kang, and W. Tian, 2007a: Aerosol and fresh snow chemistry in the East Rongbuk Glacier on the northern slope of Mt. Qomolangma (Everest). *J. Geophys. Res.*, **112**, D15307.
Ming, J., C. D. Xiao, H. Cachier, D. H. Qin, X. Qin, Z. Q. Li, and J. C. Pu, 2009: Black Carbon (BC) in the snow of glaciers in west China and its potential effects on albedos. *Atmos. Res.*, **92**, 114–123.
Ming, Y., V. Ramaswamy, and G. Persad, 2010: Two opposing effects of absorbing aerosols on global-mean precipitation. *Geophys. Res. Lett.*, **37**, L13701.
Ming, Y., V. Ramaswamy, P. A. Ginoux, L. W. Horowitz, and L. M. Russell, 2005: Geophysical Fluid Dynamics Laboratory general circulation model investigation of the indirect radiative effects of anthropogenic sulfate aerosol. *J. Geophys. Res.*, **110**, D22206.
Ming, Y., V. Ramaswamy, L. J. Donner, V. T. J. Phillips, S. A. Klein, P. A. Ginoux, and L. W. Horowitz, 2007b: Modeling the interactions between aerosols and liquid water clouds with a self-consistent cloud scheme in a general circulation model. *J. Atmos. Sci.*, **64**, 1189–1209.
Minschwaner, K., A. E. Dessler, and P. Sawaengphokhai, 2006: Multimodel analysis of the water vapor feedback in the tropical upper troposphere. *J. Clim.*, **19**, 5455–5464.
Mirme, S., A. Mirme, A. Minikin, A. Petzold, U. Horrak, V. M. Kerminen, and M. Kulmala, 2010: Atmospheric sub-3 nm particles at high altitudes. *Atmos. Chem. Phys.*, **10**, 437–451.
Mishchenko, M. I., et al., 2007: Accurate monitoring of terrestrial aerosols and total solar irradiance—Introducing the Glory mission. *Bull. Am. Meteor. Soc.*, **88**, 677–691.
Mishchenko, M. I., et al., 2012: Aerosol retrievals from channel-1 and -2 AVHRR radiances: Long-term trends updated and revisited. *J. Quant. Spectrosc. Radiat. Transfer*, **113**, 1974–1980.
Mitchell, D. L., and W. Finnegan, 2009: Modification of cirrus clouds to reduce global warming. *Environ. Res. Lett.*, **4**, 045102.
Mitchell, J. F., C. A. Wilson, and W. M. Cunnington, 1987: On CO_2 climate sensitivity and model dependence of results. *Q. J. R. Meteorol. Soc.*, **113**, 293–322.
Miyazaki, Y., S. G. Aggarwal, K. Singh, P. K. Gupta, and K. Kawamura, 2009: Dicarboxylic acids and water-soluble organic carbon in aerosols in New Delhi, India, in winter: Characteristics and formation processes. *J. Geophys. Res.*, **114**, D19206.
Mkoma, S. L., 2008: Physico-chemical characterisation of atmospheric aerosol in Tanzania, with emphasis on the carbonaceous aerosol components and on chemical mass closure. Ph.D. Ghent University, Ghent, Belgium.
Mkoma, S. L., W. Maenhaut, X. G. Chi, W. Wang, and N. Raes, 2009a: Characterisation of PM_{10} atmospheric aerosols for the wet season 2005 at two sites in East Africa. *Atmos. Environ.*, **43**, 631–639.
Mkoma, S. L., W. Maenhaut, X. Chi, W. Wang, and N. Raes, 2009b: Chemical composition and mass closure for PM10 aerosols during the 2005 dry season at a rural site in Morogoro, Tanzania. *X-Ray Spectrom.*, **38**, 293–300.
Mohler, O., et al., 2003: Experimental investigation of homogeneous freezing of sulphuric acid particles in the aerosol chamber AIDA. *Atmos. Chem. Phys.*, **3**, 211–223.
Moorthy, K. K., S. K. Satheesh, S. S. Babu, and C. B. S. Dutt, 2008: Integrated Campaign for Aerosols, gases and Radiation Budget (ICARB): An overview. *J. Earth Syst. Sci.*, **117**, 243–262.
Moosmüller, H., R. Chakrabarty, and W. Arnott, 2009: Aerosol light absorption and its measurement: A review. *J. Quant. Spectrosc. Radiat. Transfer*, **110**, 844–878.
Morales, J. A., D. Pirela, M. G. d. Nava, B. S. d. Borrego, H. Velasquez, and J. Duran, 1998: Inorganic water soluble ions in atmospheric particles over Maracaibo Lake Basin in the western region of Venezuela. *Atmos. Res.*, **46**, 307–320.
Morcrette, J.-J., et al., 2009: Aerosol analysis and forecast in the ECMWF Integrated Forecast System. Part I: Forward modelling. *J. Geophys. Res.*, **114**, D06206.
Moreno-Cruz, J. B., K. W. Ricke, and D. W. Keith, 2011: A simple model to account for regional inequalities in the effectiveness of solar radation management. *Clim. Change*, **110**, 649–668.
Morrison, H., and A. Gettelman, 2008: A new two-moment bulk stratiform cloud microphysics scheme in the community atmosphere model, version 3 (CAM3). Part I: Description and numerical tests. *J. Clim.*, **21**, 3642–3659.
Morrison, H., and W. W. Grabowski, 2011: Cloud-system resolving model simulations of aerosol indirect effects on tropical deep convection and its thermodynamic environment. *Atmos. Chem. Phys.*, **11**, 10503–10523.
Morrison, H., G. de Boer, G. Feingold, J. Harrington, M. D. Shupe, and K. Sulia, 2012: Resilience of persistent Arctic mixed-phase clouds. *Nature Geosci.*, **5**, 11–17.
Moteki, N., and Y. Kondo, 2010: Dependence of laser-induced incandescence on physical properties of black carbon aerosols: Measurements and theoretical interpretation. *Aer. Sci. Technol.*, **44**, 663–675.
Moteki, N., et al., 2007: Evolution of mixing state of black carbon particles: Aircraft measurements over the western Pacific in March 2004. *Geophys. Res. Lett.*, **34**, L11803.
Mouillot, F., A. Narasimha, Y. Balkanski, J. F. Lamarque, and C. B. Field, 2006: Global carbon emissions from biomass burning in the 20th century. *Geophys. Res. Lett.*, **33**, L01801.
Muller, C. J., and P. A. O'Gorman, 2011: An energetic perspective on the regional response of precipitation to climate change. *Nature Clim. Change*, **1**, 266–271.
Muller, C. J., and I. M. Held, 2012: Detailed investigation of the self-aggregation of convection in cloud-resolving simulations. *J. Atmos. Sci.*, **69**, 2551–2565.
Muller, C. J., P. A. O'Gorman, and L. E. Back, 2011: Intensification of precipitation extremes with warming in a cloud-resolving model. *J. Clim.*, **24**, 2784–2800.
Müller, J.-F., et al., 2008: Global isoprene emissions estimated using MEGAN, ECMWF analyses and a detailed canopy environment model. *Atmos. Chem. Phys.*, **8**, 1329–1341.
Murray, B. J., D. O'Sullivan, J. D. Atkinson, and M. E. Webb, 2012: Ice nucleation by particles immersed in supercooled cloud droplets. *Chem. Soc. Rev.*, **41**, 6519–6554.
Myhre, G., 2009: Consistency between satellite-derived and modeled estimates of the direct aerosol effect. *Science*, **325**, 187–190.
Myhre, G., et al., 2007: Comparison of the radiative properties and direct radiative effect of aerosols from a global aerosol model and remote sensing data over ocean. *Tellus B*, **59**, 115–129.
Myhre, G., et al., 2009: Modelled radiative forcing of the direct aerosol effect with multi-observation evaluation. *Atmos. Chem. Phys.*, **9**, 1365–1392.
Myhre, G., et al., 2013: Radiative forcing of the direct aerosol effect from AeroCom Phase II simulations. *Atmos. Chem. Phys.*, **13**, 1853–1877.

Nakajima, T., and M. Schulz, 2009: What do we know about large scale changes of aerosols, clouds, and the radiative budget? In: *Clouds in the Perturbed Climate System: Their Relationship to Energy Balance, Atmospheric Dynamics, and Precipitation* [R. J. Charlson and J. Heintzenberg (eds.)], MIT Press, Cambridge, MA, USA, pp. 401–430.

Nakajima, T., et al., 2007: Overview of the Atmospheric Brown Cloud East Asian Regional Experiment 2005 and a study of the aerosol direct radiative forcing in East Asia. *J. Geophys. Res.*, **112**, D24S91.

Nakayama, T., Y. Matsumi, K. Sato, T. Imamura, A. Yamazaki, and A. Uchiyama, 2010: Laboratory studies on optical properties of secondary organic aerosols generated during the photooxidation of toluene and the ozonolysis of α-pinene. *J. Geophys. Res.*, **115**, D24204.

Nam, C., S. Bony, J.-L. Dufresne, and H. Chepfer, 2012: The 'too few, too bright' tropical low-cloud problem in CMIP5 models. *Geophys. Res. Lett.*, **39**, L21801.

Naud, C. M., A. D. Del Genio, M. Bauer, and W. Kovari, 2010: Cloud vertical distribution across warm and cold fronts in CloudSat-CALIPSO data and a General Circulation Model. *J. Clim.*, **23**, 3397–3415.

Naud, C. M., A. Del Genio, G. G. Mace, S. Benson, E. E. Clothiaux, and P. Kollias, 2008: Impact of dynamics and atmospheric state on cloud vertical overlap. *J. Clim.*, **21**, 1758–1770.

Neale, R. B., J. H. Richter, and M. Jochum, 2008: The impact of convection on ENSO: From a delayed oscillator to a series of events. *J. Clim.*, **21**, 5904–5924.

Neelin, J. D., and I. M. Held, 1987: Modeling tropical convergence based on the moist static energy budget. *Mon. Weather Rev.*, **115**, 3–12.

Neelin, J. D., M. Münnich, H. Su, J. E. Meyerson, and C. E. Holloway, 2006: Tropical drying trends in global warming models and observations. *Proc. Natl. Acad. Sci. U.S.A.*, **103**, 6110–6115.

Neggers, R. A. J., 2009: A dual mass flux framework for boundary layer convection. Part II: Clouds. *J. Atmos. Sci.*, **66**, 1489–1506.

Neggers, R. A. J., M. Kohler, and A. C. M. Beljaars, 2009: A dual mass flux framework for boundary layer convection. Part I: Transport. *J. Atmos. Sci.*, **66**, 1465–1487.

Nicoll, K., and R. G. Harrison, 2010: Experimental determination of layer cloud edge charging from cosmic ray ionization. *Geophys. Res. Lett.*, **37**, L13802.

Niemeier, U., H. Schmidt, and C. Timmreck, 2011: The dependency of geoengineered sulfate aerosol on the emission strategy. *Atmos. Sci. Lett.*, **12**, 189–194.

Nuijens, L., B. Stevens, and A. P. Siebesma, 2009: The environment of precipitating shallow cumulus convection. *J. Atmos. Sci.*, **66**, 1962–1979.

Nyanganyura, D., W. Maenhaut, M. Mathuthu, A. Makarau, and F. X. Meixner, 2007: The chemical composition of tropospheric aerosols and their contributing sources to a continental background site in northern Zimbabwe from 1994 to 2000. *Atmos. Environ.*, **41**, 2644–2659.

O'Dell, C. W., F. J. Wentz, and R. Bennartz, 2008: Cloud liquid water path from satellite-based passive microwave observations: A new climatology over the global oceans. *J. Clim.*, **21**, 1721–1739.

O'Donnell, D., K. Tsigaridis, and J. Feichter, 2011: Estimating the direct and indirect effects of secondary organic aerosols using ECHAM5–HAM. *Atmos. Chem. Phys.*, **11**, 8635–8659.

O'Dowd, C., C. Monahan, and M. Dall'Osto, 2010: On the occurrence of open ocean particle production and growth events. *Geophys. Res. Lett.*, **37**, L19805.

O'Gorman, P. A., 2012: Sensitivity of tropical precipitation extremes to climate change. *Nature Geosci.*, **5**, 697–700.

O'Gorman, P. A., and T. Schneider, 2008: The hydrological cycle over a wide range of climates simulated with an idealized GCM. *J. Clim.*, **21**, 3815–3832.

O'Gorman, P. A., and T. Schneider, 2009: The physical basis for increases in precipitation extremes in simulations of 21st-century climate change. *Proc. Natl. Acad. Sci. U.S.A.*, **106**, 14773–14777.

Oanh, N. T. K., et al., 2006: Particulate air pollution in six Asian cities: Spatial and temporal distributions, and associated sources. *Atmos. Environ.*, **40**, 3367–3380.

Ocko, I. B., V. Ramaswamy, P. Ginoux, Y. Ming, and L. W. Horowitz, 2012: Sensitivity of scattering and absorbing aerosol direct radiative forcing to physical climate factors. *J. Geophys. Res.*, **117**, D20203.

Oleson, K. W., G. B. Bonan, and J. Feddema, 2010: Effects of white roofs on urban temperature in a global climate model. *Geophys. Res. Lett.*, **37**, L03701.

Omar, A. H., et al., 2009: The CALIPSO automated aerosol classification and lidar ratio selection algorithm. *J. Atmos. Ocean. Technol.*, **26**, 1994–2014.

Oouchi, K., A. T. Noda, M. Satoh, B. Wang, S. P. Xie, H. G. Takahashi, and T. Yasunari, 2009: Asian summer monsoon simulated by a global cloud-system-resolving model: Diurnal to intra-seasonal variability. *Geophys. Res. Lett.*, **36**, L11815.

Orellana, M. V., P. A. Matrai, C. Leck, C. D. Rauschenberg, A. M. Lee, and E. Coz, 2011: Marine microgels as a source of cloud condensation nuclei in the high Arctic. *Proc. Natl. Acad. Sci. U.S.A.*, **108**, 13612–13617.

Oreopoulos, L., and S. Platnick, 2008: Radiative susceptibility of cloudy atmospheres to droplet number perturbations: 2. Global analysis from MODIS. *J. Geophys. Res.*, **113**, D14S21.

Osborne, S. R., A. J. Barana, B. T. Johnson, J. M. Haywood, E. Hesse, and S. Newman, 2011: Short-wave and long-wave radiative properties of Saharan dust aerosol. *Q. J. R. Meteorol. Soc.*, **137**, 1149–1167.

Oshima, N., et al., 2012: Wet removal of black carbon in Asian outflow: Aerosol Radiative Forcing in East Asia (A-FORCE) aircraft campaign. *J. Geophys. Res.*, **117**, D03204.

Ovadnevaite, J., et al., 2011: Primary marine organic aerosol: A dichotomy of low hygroscopicity and high CCN activity. *Geophys. Res. Lett.*, **38**, L21806.

Ovchinnikov, M., A. Korolev, and J. Fan, 2011: Effects of ice number concentration on dynamics of a shallow mixed-phase stratiform cloud. *J. Geophys. Res.*, **116**, D00T06.

Paasonen, P., et al., 2010: On the roles of sulphuric acid and low-volatility organic vapours in the initial steps of atmospheric new particle formation. *Atmos. Chem. Phys.*, **10**, 11223–11242.

Paasonen, P., et al., 2013: Warming-induced increase in aerosol number concentration likely to moderate climate change. *Nature Geosci.*, **6**, 438–442.

Pacifico, F., S. P. Harrison, C. D. Jones, and S. Sitch, 2009: Isoprene emissions and climate. *Atmos. Environ.*, **43**, 6121–6135.

Painemal, D., and P. Zuidema, 2010: Microphysical variability in southeast Pacific Stratocumulus clouds: Synoptic conditions and radiative response. *Atmos. Chem. Phys.*, **10**, 6255–6269.

Pallé Bagó, E., and C. J. Butler, 2000: The influence of cosmic rays on terrestrial clouds and global warming. *Astron. Geophys.*, **41**, 4.18–4.22.

Pallé, E., 2005: Possible satellite perspective effects on the reported correlations between solar activity and clouds. *Geophys. Res. Lett.*, **32**, L03802.

Palm, S. P., S. T. Strey, J. Spinhirne, and T. Markus, 2010: Influence of Arctic sea ice extent on polar cloud fraction and vertical structure and implications for regional climate. *J. Geophys. Res.*, **115**, D21209.

Paltridge, G., A. Arking, and M. Pook, 2009: Trends in middle- and upper-level tropospheric humidity from NCEP reanalysis data. *Theor. Appl. Climatol.*, **98**, 351–359.

Paltridge, G. W., 1980: Cloud-radiation feedback to climate. *Q. J. R. Meteorol. Soc.*, **106**, 895–899.

Paredes-Miranda, G., W. P. Arnott, J. L. Jimenez, A. C. Aiken, J. S. Gaffney, and N. A. Marley, 2009: Primary and secondary contributions to aerosol light scattering and absorption in Mexico City during the MILAGRO 2006 campaign. *Atmos. Chem. Phys.*, **9**, 3721–3730.

Park, S., and C. S. Bretherton, 2009: The University of Washington shallow convection and moist turbulence schemes and their impact on climate simulations with the Community Atmosphere Model. *J. Clim.*, **22**, 3449–3469.

Parodi, A., and K. Emanuel, 2009: A theory for buoyancy and velocity scales in deep moist convection. *J. Atmos. Sci.*, **66**, 3449–3463.

Partanen, A.-I., et al., 2012: Direct and indirect effects of sea spray geoengineering and the role of injected particle size. *J. Geophys. Res.*, **117**, D02203.

Pawlowska, H., and J. L. Brenguier, 2003: An observational study of drizzle formation in stratocumulus clouds for general circulation model (GCM) parameterizations. *J. Geophys. Res.*, **108**, 8630.

Pechony, O., and D. T. Shindell, 2010: Driving forces of global wildfires over the past millennium and the forthcoming century. *Proc. Natl. Acad. Sci. U.S.A.*, **107**, 19167–19170.

Pendergrass, A. G., and D. L. Hartmann, 2012: Global-mean precipitation and black carbon in AR4 simulations. *Geophys. Res. Lett.*, **39**, L01703.

Peng, Y. R., and U. Lohmann, 2003: Sensitivity study of the spectral dispersion of the cloud droplet size distribution on the indirect aerosol effect. *Geophys. Res. Lett.*, **30**, 1507.

Penner, J. E., S. Y. Zhang, and C. C. Chuang, 2003: Soot and smoke aerosol may not warm climate. *J. Geophys. Res.*, **108**, 4657.

Penner, J. E., L. Xu, and M. H. Wang, 2011: Satellite methods underestimate indirect climate forcing by aerosols. *Proc. Natl. Acad. Sci. U.S.A.*, **108**, 13404–13408.

Penner, J. E., C. Zhou, and L. Xu, 2012: Consistent estimates from satellites and models for the first aerosol indirect forcing. *Geophys. Res. Lett.*, **39**, L13810.

Penner, J. E., Y. Chen, M. Wang, and X. Liu, 2009: Possible influence of anthropogenic aerosols on cirrus clouds and anthropogenic forcing. *Atmos. Chem. Phys.*, **9**, 879–896.

Penner, J. E., et al., 2006: Model intercomparison of indirect aerosol effects. *Atmos. Chem. Phys.*, **6**, 3391–3405.

Peñuelas, J., and M. Staudt, 2010: BVOCs and global change. *Trends Plant Sci.*, **15**, 133–144.

Perez, N., J. Pey, X. Querol, A. Alastuey, J. M. Lopez, and M. Viana, 2008: Partitioning of major and trace components in PM10–PM2.5–PM1 at an urban site in Southern Europe. *Atmos. Environ.*, **42**, 1677–1691.

Persad, G. G., Y. Ming, and V. Ramaswamy, 2012: Tropical tropospheric-only responses to absorbing aerosols. *J. Clim.*, **25**, 2471–2480.

Peters, K., J. Quaas, and H. Grassl, 2011a: A search for large-scale effects of ship emissions on clouds and radiation in satellite data. *J. Geophys. Res.*, **116**, D24205.

Peters, K., J. Quaas, and N. Bellouin, 2011b: Effects of absorbing aerosols in cloudy skies: A satellite study over the Atlantic Ocean. *Atmos. Chem. Phys.*, **11**, 1393–1404.

Petroff, A., and L. Zhang, 2010: Development and validation of a size-resolved particle dry deposition scheme for application in aerosol transport models. *Geosci. Model Dev.*, **3**, 753–769.

Petters, M. D., and S. M. Kreidenweis, 2007: A single parameter representation of hygroscopic growth and cloud condensation nucleus activity. *Atmos. Chem. Phys.*, **7**, 1961–1971.

Petters, M. D., J. R. Snider, B. Stevens, G. Vali, I. Faloona, and L. M. Russell, 2006: Accumulation mode aerosol, pockets of open cells, and particle nucleation in the remote subtropical Pacific marine boundary layer. *J. Geophys. Res.*, **111**, D02206.

Phillips, V. T. J., P. J. DeMott, and C. Andronache, 2008: An empirical parameterization of heterogeneous ice nucleation for multiple chemical species of aerosol. *J. Atmos. Sci.*, **65**, 2757–2783.

Pierce, J. R., and P. J. Adams, 2007: Efficiency of cloud condensation nuclei formation from ultrafine particles. *Atmos. Chem. Phys.*, **7**, 1367–1379.

Pierce, J. R., and P. J. Adams, 2009a: Uncertainty in global CCN concentrations from uncertain aerosol nucleation and primary emission rates. *Atmos. Chem. Phys.*, **9**, 1339–1356.

Pierce, J. R., and P. J. Adams, 2009b: Can cosmic rays affect cloud condensation nuclei by altering new particle formation rates? *Geophys. Res. Lett.*, **36**, L09820.

Pierce, J. R., D. K. Weisenstein, P. Heckendorn, T. Peter, and D. W. Keith, 2010: Efficient formation of stratospheric aerosol for climate engineering by emission of condensible vapor from aircraft. *Geophys. Res. Lett.*, **37**, L18805.

Pincus, R., and M. B. Baker, 1994: Effect of precipitation on the albedo susceptibility of clouds in the marine boundary-layer. *Nature*, **372**, 250–252.

Pincus, R., and S. A. Klein, 2000: Unresolved spatial variability and microphysical process rates in large-scale models. *J. Geophys. Res.*, **105**, 27059–27065.

Pincus, R., R. Hemler, and S. A. Klein, 2006: Using stochastically generated subcolumns to represent cloud structure in a large-scale model. *Mon. Weather Rev.*, **134**, 3644–3656.

Platnick, S., M. D. King, S. A. Ackerman, W. P. Menzel, B. A. Baum, J. C. Riedi, and R. A. Frey, 2003: The MODIS cloud products: Algorithms and examples from Terra. *IEEE Trans. Geosci. Remote Sens.*, **41**, 459–473.

Ponater, M., S. Marquart, R. Sausen, and U. Schumann, 2005: On contrail climate sensitivity. *Geophys. Res. Lett.*, **32**, L10706.

Pöschl, U., et al., 2010: Rainforest aerosols as biogenic nuclei of clouds and precipitation in the Amazon. *Science*, **329**, 1513–1516.

Pósfai, M., R. Simonics, J. Li, P. V. Hobbs, and P. R. Buseck, 2003: Individual aerosol particles from biomass burning in southern Africa: 1. Compositions and size distributions of carbonaceous particles. *J. Geophys. Res.*, **108**, 8483.

Posselt, R., and U. Lohmann, 2008: Influence of giant CCN on warm rain processes in the ECHAM5 GCM. *Atmos. Chem. Phys.*, **8**, 3769–3788.

Posselt, R., and U. Lohmann, 2009: Sensitivity of the total anthropogenic aerosol effect to the treatment of rain in a global climate model. *Geophys. Res. Lett.*, **36**, L02805.

Pratt, K. A., and K. A. Prather, 2010: Aircraft measurements of vertical profiles of aerosol mixing states. *J. Geophys. Res.*, **115**, D11305.

Prenni, A. J., et al., 2007: Can ice-nucleating aerosols affect arctic seasonal climate? *Bull. Am. Meteor. Soc.*, **88**, 541–550.

Pringle, K. J., H. Tost, A. Pozzer, U. Pöschl, and J. Lelieveld, 2010: Global distribution of the effective aerosol hygroscopicity parameter for CCN activation. *Atmos. Chem. Phys.*, **10**, 5241–5255.

Prisle, N. L., T. Raatikainen, A. Laaksonen, and M. Bilde, 2010: Surfactants in cloud droplet activation: Mixed organic-inorganic particles. *Atmos. Chem. Phys.*, **10**, 5663–5683.

Prisle, N. L., T. Raatikainen, R. Sorjamaa, B. Svenningsson, A. Laaksonen, and M. Bilde, 2008: Surfactant partitioning in cloud droplet activation: A study of C8, C10, C12 and C14 normal fatty acid sodium salts. *Tellus B*, **60**, 416–431.

Pritchard, M. S., and R. C. J. Somerville, 2010: Assessing the diurnal cycle of precipitation in a multi-scale climate model. *J. Adv. Model. Earth Syst.*, **1**, 12.

Prospero, J. M., W. M. Landing, and M. Schulz, 2010: African dust deposition to Florida: Temporal and spatial variability and comparisons to models. *J. Geophys. Res.*, **115**, D13304.

Puma, M. J., and B. I. Cook, 2010: Effects of irrigation on global climate during the 20th century. *J. Geophys. Res.*, **115**, D16120.

Putaud, J.-P., et al., 2004: European aerosol phenomenology-2: Chemical characteristics of particulate matter at kerbside, urban, rural and background sites in Europe. *Atmos. Environ.*, **38**, 2579–2595.

Putman, W. M., and M. Suarez, 2011: Cloud-system resolving simulations with the NASA Goddard Earth Observing System global atmospheric model (GEOS-5). *Geophys. Res. Lett.*, **38**, L16809.

Puxbaum, H., et al., 2004: A dual site study of PM2.5 and PM10 aerosol chemistry in the larger region of Vienna, Austria. *Atmos. Environ.*, **38**, 3949–3958.

Pye, H. O. T., and J. H. Seinfeld, 2010: A global perspective on aerosol from low-volatility organic compounds. *Atmos. Chem. Phys.*, **10**, 4377–4401.

Pye, H. O. T., H. Liao, S. Wu, L. J. Mickley, D. J. Jacob, D. K. Henze, and J. H. Seinfeld, 2009: Effect of changes in climate and emissions on future sulfate-nitrate-ammonium aerosol levels in the United States. *J. Geophys. Res.*, **114**, D01205.

Qu, W. J., X. Y. Zhang, R. Arimoto, D. Wang, Y. Q. Wang, L. W. Yan, and Y. Li, 2008: Chemical composition of the background aerosol at two sites in southwestern and northwestern China: Potential influences of regional transport. *Tellus B*, **60**, 657–673.

Quaas, J., O. Boucher, and F. M. Bréon, 2004: Aerosol indirect effects in POLDER satellite data and the Laboratoire de Météorologie Dynamique-Zoom (LMDZ) general circulation model. *J. Geophys. Res.*, **109**, D08205.

Quaas, J., O. Boucher, and U. Lohmann, 2006: Constraining the total aerosol indirect effect in the LMDZ and ECHAM4 GCMs using MODIS satellite data. *Atmos. Chem. Phys.*, **6**, 947–955.

Quaas, J., N. Bellouin, and O. Boucher, 2011: Which of satellite-based or model-based estimates are closer to reality for aerosol indirect forcing? Reply to Penner et al. *Proc. Natl. Acad. Sci. U.S.A.*, **108**, E1099.

Quaas, J., O. Boucher, N. Bellouin, and S. Kinne, 2008: Satellite-based estimate of the direct and indirect aerosol climate forcing. *J. Geophys. Res.*, **113**, D05204.

Quaas, J., B. Stevens, P. Stier, and U. Lohmann, 2010: Interpreting the cloud cover – aerosol optical depth relationship found in satellite data using a general circulation model. *Atmos. Chem. Phys.*, **10**, 6129–6135.

Quaas, J., et al., 2009: Aerosol indirect effects—general circulation model intercomparison and evaluation with satellite data. *Atmos. Chem. Phys.*, **9**, 8697–8717.

Querol, X., et al., 2001: PM10 and PM2.5 source apportionment in the Barcelona Metropolitan Area, Catalonia, Spain. *Atmos. Environ.*, **35/36**, 6407–6419.

Querol, X., et al., 2009: Variability in regional background aerosols within the Mediterranean. *Atmos. Chem. Phys.*, **9**, 4575–4591.

Querol, X., et al., 2004: Speciation and origin of PM10 and PM2.5 in selected European cities. *Atmos. Environ.*, **38**, 6547–6555.

Querol, X., et al., 2006: Atmospheric particulate matter in Spain: Levels, composition and source origin. CSIC and Ministerio de Medioambiente, Madrid, Spain, 39 pp.

Querol, X., et al., 2008: Spatial and temporal variations in airborne particulate matter (PM10 and PM2.5) across Spain 1999–2005. *Atmos. Environ.*, **42**, 3964–3979.

Quinn, P. K., and T. S. Bates, 2011: The case against climate regulation via oceanic phytoplankton sulphur emissions. *Nature*, **480**, 51–56.

Racherla, P. N., and P. J. Adams, 2006: Sensitivity of global tropospheric ozone and fine particulate matter concentrations to climate change. *J. Geophys. Res.*, **111**, D24103.

Radhi, M., M. A. Box, G. P. Box, R. M. Mitchell, D. D. Cohen, E. Stelcer, and M. D. Keywood, 2010: Optical, physical and chemical characteristics of Australian continental aerosols: Results from a field experiment. *Atmos. Chem. Phys.*, **10**, 5925–5942.

Rae, J. G. L., C. E. Johnson, N. Bellouin, O. Boucher, J. M. Haywood, and A. Jones, 2007: Sensitivity of global sulphate aerosol production to changes in oxidant concentrations and climate. *J. Geophys. Res.*, **112**, D10312.

Raes, F., H. Liao, W.-T. Chen, and J. H. Seinfeld, 2010: Atmospheric chemistry-climate feedbacks. *J. Geophys. Res.*, **115**, D12121.

Ram, K., M. M. Sarin, and P. Hegde, 2010: Long-term record of aerosol optical properties and chemical composition from a high-altitude site (Manora Peak) in Central Himalaya. *Atmos. Chem. Phys.*, **10**, 11791–11803.

Raman, R. S., S. Ramachandran, and N. Rastogi, 2010: Source identification of ambient aerosols over an urban region in western India. *J. Environ. Monit.*, **12**, 1330–1340.

Ramanathan, V., R. D. Cess, E. F. Harrison, P. Minnis, B. R. Barkstrom, E. Ahmad, and D. Hartmann, 1989: Cloud-radiative forcing and climate: Results from the Earth Radiation Budget Experiment. *Science*, **243**, 57–63.

Randall, D., M. Khairoutdinov, A. Arakawa, and W. Grabowski, 2003: Breaking the cloud parameterization deadlock. *Bull. Am. Meteor. Soc.*, **84**, 1547–1564.

Randall, D. A., et al., 2007: Climate models and their evaluation. In: *Climate Change 2007: The Physical Science Basis. Contribution of Working Group I to the Fourth Assessment Report of the Intergovernmental Panel on Climate Change* [Solomon, S., D. Qin, M. Manning, Z. Chen, M. Marquis, K. B. Averyt, M. Tignor and H. L. Miller (eds.)] Cambridge University Press, Cambridge, United Kingdom and New York, NY, USA, pp. 589–662.

Randerson, J. T., Y. Chen, G. R. van der Werf, B. M. Rogers, and D. C. Morton, 2012: Global burned area and biomass burning emissions from small fires. *J. Geophys. Res.*, **117**, G04012.

Randles, C. A., et al., 2013: Intercomparison of shortwave radiative transfer schemes in global aerosol modeling: Results from the AeroCom Radiative Transfer Experiment. *Atmos. Chem. Phys.*, **13**, 2347–2379.

Rap, A., P. M. Forster, J. M. Haywood, A. Jones, and O. Boucher, 2010a: Estimating the climate impact of linear contrails using the UK Met Office climate model. *Geophys. Res. Lett.*, **37**, L20703.

Rap, A., P. Forster, A. Jones, O. Boucher, J. Haywood, N. Bellouin, and R. De Leon, 2010b: Parameterization of contrails in the UK Met Office Climate Model. *J. Geophys. Res.*, **115**, D10205.

Rasch, P. J., P. J. Crutzen, and D. B. Coleman, 2008a: Exploring the geoengineering of climate using stratospheric sulfate aerosols: The role of particle size. *Geophys. Res. Lett.*, **35**, L02809.

Rasch, P. J., C. C. Chen, and J. L. Latham, 2009: Geo-engineering by cloud seeding: influence on sea-ice and the climate system. *Environ. Res. Lett.*, **4**, 045112.

Rasch, P. J., et al., 2008b: An overview of geoengineering of climate using stratospheric sulphate aerosols. *Philos. Trans. R. Soc. London A*, **366**, 4007–4037.

Rastogi, N., and M. M. Sarin, 2005: Long-term characterization of ionic species in aerosols from urban and high-altitude sites in western India: Role of mineral dust and anthropogenic sources. *Atmos. Environ.*, **39**, 5541–5554.

Rauber, R. M., et al., 2007: Rain in shallow cumulus over the ocean - The RICO campaign. *Bull. Am. Meteor. Soc.*, **88**, 1912–1928.

Raymond, D. J., S. L. Sessions, A. H. Sobel, and Z. Fuchs, 2009: The mechanics of gross moist stability. *J. Adv. Model. Earth Syst.*, **1**, 9.

Reddy, M. S., O. Boucher, Y. Balkanski, and M. Schulz, 2005: Aerosol optical depths and direct radiative perturbations by species and source type. *Geophys. Res. Lett.*, **32**, L12803.

Remer, L. A., et al., 2005: The MODIS aerosol algorithm, products, and validation. *J. Atmos. Sci.*, **62**, 947–973.

Rengarajan, R., M. M. Sarin, and A. K. Sudheer, 2007: Carbonaceous and inorganic species in atmospheric aerosols during wintertime over urban and high-altitude sites in North India. *J. Geophys. Res.*, **112**, D21307.

Richter, I., and S. P. Xie, 2008: Muted precipitation increase in global warming simulations: A surface evaporation perspective. *J. Geophys. Res.*, **113**, D24118.

Richter, J. H., and P. J. Rasch, 2008: Effects of convective momentum transport on the atmospheric circulation in the community atmosphere model, version 3. *J. Clim.*, **21**, 1487–1499.

Ricke, K. L., G. Morgan, and M. R. Allen, 2010: Regional climate response to solar-radiation management. *Nature Geosci.*, **3**, 537–541.

Ridgwell, A., J. S. Singarayer, A. M. Hetherington, and P. J. Valdes, 2009: Tackling regional climate change by leaf albedo bio-geoengineering. *Curr. Biol.*, **19**, 146–150.

Rieck, M., L. Nuijens, and B. Stevens, 2012: Marine boundary-layer cloud feedbacks in a constant relative humidity atmosphere. *J. Atmos. Sci.*, **69**, 2538–2550.

Riipinen, I., et al., 2011: Organic condensation: A vital link connecting aerosol formation to cloud condensation nuclei (CCN) concentrations. *Atmos. Chem. Phys.*, **11**, 3865–3878.

Rinaldi, M., et al., 2009: On the representativeness of coastal aerosol studies to open ocean studies: Mace Head – a case study. *Atmos. Chem. Phys.*, **9**, 9635–9646.

Rinaldi, M., et al., 2011: Evidence of a natural marine source of oxalic acid and a possible link to glyoxal. *J. Geophys. Res.*, **116**, D16204.

Ringer, M. A., et al., 2006: Global mean cloud feedbacks in idealized climate change experiments. *Geophys. Res. Lett.*, **33**, L07718.

Rio, C., and F. Hourdin, 2008: A thermal plume model for the convective boundary layer: Representation of cumulus clouds. *J. Atmos. Sci.*, **65**, 407–425.

Rio, C., F. Hourdin, J.-Y. Grandpeix, and J.-P. Lafore, 2009: Shifting the diurnal cycle of parameterized deep convection over land. *Geophys. Res. Lett.*, **36**, L07809.

Rissler, J., B. Svenningsson, E. O. Fors, M. Bilde, and E. Swietlicki, 2010: An evaluation and comparison of cloud condensation nucleus activity models: Predicting particle critical saturation from growth at subsaturation. *J. Geophys. Res.*, **115**, D22208.

Rissler, J., E. Swietlicki, J. Zhou, G. Roberts, M. O. Andreae, L. V. Gatti, and P. Artaxo, 2004: Physical properties of the sub-micrometer aerosol over the Amazon rain forest during the wet-to-dry season transition—comparison of modeled and measured CCN concentrations. *Atmos. Chem. Phys.*, **4**, 2119–2143.

Roberts, G. C., et al., 2010: Characterization of particle cloud droplet activity and composition in the free troposphere and the boundary layer during INTEX-B. *Atmos. Chem. Phys.*, **10**, 6627–6644.

Robinson, A. L., et al., 2007: Rethinking organic aerosols: Semivolatile emissions and photochemical aging. *Science*, **315**, 1259–1262.

Robock, A., L. Oman, and G. Stenchikov, 2008: Regional climate responses to geoengineering with tropical and Arctic SO_2 injections. *J. Geophys. Res.*, **113**, D16101.

Rodriguez, S., X. Querol, A. Alastuey, and F. Plana, 2002: Sources and processes affecting levels and composition of atmospheric aerosol in the western Mediterranean. *J. Geophys. Res.*, **107**, 4777.

Rodrıguez, S., X. Querol, A. Alastuey, M. M. Viana, M. Alarcon, E. Mantilla, and C. R. Ruiz, 2004: Comparative PM10–PM2.5 source contribution study at rural, urban and industrial sites during PM episodes in Eastern Spain. *Sci. Tot. Environ.*, **328**, 95–113.

Rohs, S., R. Spang, F. Rohrer, C. Schiller, and H. Vos, 2010: A correlation study of high-altitude and midaltitude clouds and galactic cosmic rays by MIPAS-Envisat. *J. Geophys. Res.*, **115**, D14212.

Romps, D. M., 2011: Response of tropical precipitation to global warming. *J. Atmos. Sci.*, **68**, 123–138.

Rondanelli, R., and R. S. Lindzen, 2010: Can thin cirrus clouds in the tropics provide a solution to the faint young Sun paradox? *J. Geophys. Res.*, **115**, D02108.

Roosli, M., et al., 2001: Temporal and spatial variation of the chemical composition of PM10 at urban and rural sites in the Basel area, Switzerland. *Atmos. Environ.*, **35**, 3701–3713.

Rose, D., et al., 2011: Cloud condensation nuclei in polluted air and biomass burning smoke near the mega-city Guangzhou, China -Part 2: Size-resolved aerosol chemical composition, diurnal cycles, and externally mixed weakly CCN-active soot particles. *Atmos. Chem. Phys.*, **11**, 2817–2836.

Rosenfeld, D., and G. Gutman, 1994: Retrieving microphysical properties near the tops of potential rain clouds by multi spectral analysis of AVHRR data. *Atmos. Res.*, **34**, 259–283.

Rosenfeld, D., and W. L. Woodley, 2001: Pollution and clouds. *Physics World*, **14**, 33–37.

Rosenfeld, D., and T. L. Bell, 2011: Why do tornados and hailstorms rest on weekends? *J. Geophys. Res.*, **116**, D20211.

Rosenfeld, D., H. Wang, and P. J. Rasch, 2012: The roles of cloud drop effective radius and LWP in determining rain properties in marine stratocumulus. *Geophys. Res. Lett.*, **39**, L13801.

Rosenfeld, D., et al., 2008: Flood or drought: How do aerosols affect precipitation? *Science*, **321**, 1309–1313.

Rotstayn, L. D., 1999: Indirect forcing by anthropogenic aerosols: A global climate model calculation of the effective-radius and cloud-lifetime effects. *J. Geophys. Res.*, **104**, 9369–9380.

Rotstayn, L. D., 2000: On the "tuning" of autoconversion parameterizations in climate models. *J. Geophys. Res.*, **105**, 15495–15508.

Rotstayn, L. D., and J. E. Penner, 2001: Indirect aerosol forcing, quasi forcing, and climate response. *J. Clim.*, **14**, 2960–2975.

Rotstayn, L. D., and Y. G. Liu, 2005: A smaller global estimate of the second indirect aerosol effect. *Geophys. Res. Lett.*, **32**, L05708.

Rotstayn, L. D., and Y. G. Liu, 2009: Cloud droplet spectral dispersion and the indirect aerosol effect: Comparison of two treatments in a GCM. *Geophys. Res. Lett.*, **36**, L10801.

Rotstayn, L. D., et al., 2007: Have Australian rainfall and cloudiness increased due to the remote effects of Asian anthropogenic aerosols? *J. Geophys. Res.*, **112**, D09202.

Royal Society, 2009: Geoengineering the climate, Science, governance and uncertainty. Report 10/09, Royal Society, London, United Kingdom, 82 pp.

Russell, L. M., L. N. Hawkins, A. A. Frossard, P. K. Quinn, and T. S. Bates, 2010: Carbohydrate-like composition of submicron atmospheric particles and their production from ocean bubble bursting. *Proc. Natl. Acad. Sci. U.S.A.*, **107**, 6652–6657.

Rypdal, K., N. Rive, T. K. Berntsen, Z. Klimont, T. K. Mideksa, G. Myhre, and R. B. Skeie, 2009: Costs and global impacts of black carbon abatement strategies. *Tellus B*, **61**, 625–641.

Sacks, W. J., B. I. Cook, N. Buenning, S. Levis, and J. H. Helkowski, 2009: Effects of global irrigation on the near-surface climate. *Clim. Dyn.*, **33**, 159–175.

Safai, P. D., K. B. Budhavant, P. S. P. Rao, K. Ali, and A. Sinha, 2010: Source characterization for aerosol constituents and changing roles of calcium and ammonium aerosols in the neutralization of aerosol acidity at a semi-urban site in SW India. *Atmos. Res.*, **98**, 78–88.

Sahu, L. K., Y. Kondo, Y. Miyazaki, P. Pongkiatkul, and N. T. Kim Oanh, 2011: Seasonal and diurnal variations of black carbon and organic carbon aerosols in Bangkok. *J. Geophys. Res.*, **116**, D15302.

Sakaeda, N., R. Wood, and P. J. Rasch, 2011: Direct and semidirect aerosol effects of southern African biomass burning aerosol. *J. Geophys. Res.*, **116**, D12205.

Salter, S., G. Sortino, and J. Latham, 2008: Sea-going hardware for the cloud albedo method of reversing global warming. *Philos. Trans. R. Soc. London A*, **366**, 3989–4006.

Salvador, P., B. Artınano, X. Querol, A. Alastuey, and M. Costoya, 2007: Characterisation of local and external contributions of atmospheric particulate matter at a background coastal site. *Atmos. Environ.*, **41**, 1–17.

Salzmann, M., et al., 2010: Two-moment bulk stratiform cloud microphysics in the GFDL AM3 GCM: Description, evaluation, and sensitivity tests. *Atmos. Chem. Phys.*, **10**, 8037–8064.

Samset, B. H., et al., 2013: Black carbon vertical profiles strongly affect its radiative forcing uncertainty. *Atmos. Chem. Phys.*, **13**, 2423–2434.

Sanchez-Lorenzo, A., P. Laux, H. J. Hendricks Franssen, J. Calbó, S. Vogl, A. K. Georgoulias, and J. Quaas, 2012: Assessing large-scale weekly cycles in meteorological variables: A review. *Atmos. Chem. Phys.*, **12**, 5755–5771.

Sanderson, M. G., C. D. Jones, W. J. Collins, C. E. Johnson, and R. G. Derwent, 2003: Effect of climate change on isoprene emissions and surface ozone levels. *Geophys. Res. Lett.*, **30**, 1936.

Sandu, I., J.-L. Brenguier, O. Geoffroy, O. Thouron, and V. Masson, 2008: Aerosol impacts on the diurnal cycle of marine stratocumulus. *J. Atmos. Sci.*, **65**, 2705–2718.

Sassen, K., and G. C. Dodd, 1988: Homogeneous nucleation rate for highly supercooled cirrus cloud droplets. *J. Atmos. Sci.*, **45**, 1357–1369.

Satheesh, S. K., and K. K. Moorthy, 2005: Radiative effects of natural aerosols: A review. *Atmos. Environ.*, **39**, 2089–2110.

Satheesh, S. K., K. K. Moorthy, S. S. Babu, V. Vinoj, and C. B. S. Dutt, 2008: Climate implications of large warming by elevated aerosol over India. *Geophys. Res. Lett.*, **35**, L19809.

Sato, T., H. Miura, M. Satoh, Y. N. Takayabu, and Y. Q. Wang, 2009: Diurnal cycle of precipitation in the Tropics simulated in a global cloud-resolving model. *J. Clim.*, **22**, 4809–4826.

Satoh, M., T. Inoue, and H. Miura, 2010: Evaluations of cloud properties of global and local cloud system resolving models using CALIPSO and CloudSat simulators. *J. Geophys. Res.*, **115**, D00H14.

Sausen, R., et al., 2005: Aviation radiative forcing in 2000: An update on IPCC (1999). *Meteorol. Z.*, **14**, 555–561.

Savic-Jovcic, V., and B. Stevens, 2008: The structure and mesoscale organization of precipitating stratocumulus. *J. Atmos. Sci.*, **65**, 1587–1605.

Sawant, A. A., K. Na, X. Zhu, and D. R. Cocker III, 2004: Chemical characterization of outdoor PM2.5 and gas-phase compounds in Mira Loma, California. *Atmos. Environ.*, **38**, 5517–5528.

Schmidt, A., et al., 2012a: Importance of tropospheric volcanic aerosol for indirect radiative forcing of climate. *Atmos. Chem. Phys.*, **12**, 7321–7339.

Schmidt, H., et al., 2012b: Solar irradiance reduction to counteract radiative forcing from a quadrupling of CO_2: Climate responses simulated by four earth system models. *Earth Syst. Dyn.*, **3**, 63–78.

Schmidt, K. S., G. Feingold, P. Pilewskie, H. Jiang, O. Coddington, and M. Wendisch, 2009: Irradiance in polluted cumulus fields: Measured and modeled cloud-aerosol effects. *Geophys. Res. Lett.*, **36**, L07804.

Schreier, M., H. Mannstein, V. Eyring, and H. Bovensmann, 2007: Global ship track distribution and radiative forcing from 1 year of AATSR data. *Geophys. Res. Lett.*, **34**, L17814.

Schulz, M., M. Chin, and S. Kinne, 2009: The Aerosol Model Comparison Project, AeroCom, phase II: Clearing up diversity. *IGAC Newsletter N° 41*, 2–11.

Schulz, M., et al., 2006: Radiative forcing by aerosols as derived from the AeroCom present-day and pre-industrial simulations. *Atmos. Chem. Phys.*, **6**, 5225–5246.

Schumann, U., and K. Graf, 2013: Aviation-induced cirrus and radiation changes at diurnal timescales. *J. Geophys. Res.*, **118**, 2404–2421.

Schwartz, S. E., and J. E. Freiberg, 1981: Mass-transport limitation to the rate of reaction of gases in liquid droplets - Application to oxidation of SO_2 in aqueous solutions. *Atmos. Environ.*, **15**, 1129–1144.

Schwarz, J. P., et al., 2008a: Coatings and their enhancement of black carbon light absorption in the tropical atmosphere. *J. Geophys. Res.*, **113**, D03203.

Schwarz, J. P., et al., 2008b: Measurement of the mixing state, mass, and optical size of individual black carbon particles in urban and biomass burning emissions. *Geophys. Res. Lett.*, **35**, L13810.

Schwarz, J. P., et al., 2010: Global-scale black carbon profiles observed in the remote atmosphere and compared to models. *Geophys. Res. Lett.*, **37**, L18812.

Schwarzenbock, A., S. Mertes, J. Heintzenberg, W. Wobrock, and P. Laj, 2001: Impact of the Bergeron-Findeisen process on the release of aerosol particles during the evolution of cloud ice. *Atmos. Res.*, **58**, 295–313.

Sciare, J., O. Favez, K. Oikonomou, R. Sarda-Estève, H. Cachier, and V. Kazan, 2009: Long-term observation of carbonaceous aerosols in the Austral Ocean: Evidence of a marine biogenic origin. *J. Geophys. Res.*, **114**, D15302.

Seager, R., N. Naik, and G. A. Vecchi, 2010: Thermodynamic and dynamic mechanisms for large-scale changes in the hydrological cycle in response to global warming. *J. Clim.*, **23**, 4651–4668.

Seifert, A., and K. Beheng, 2006: A two-moment cloud microphysics parameterization for mixed-phase clouds, Part II: Maritime versus continental deep convective storms. *Meteorol. Atmos. Phys.*, **92**, 67–88.

Seifert, A., and B. Stevens, 2010: Microphysical scaling relations in a kinematic model of isolated shallow cumulus clouds. *J. Atmos. Sci.*, **67**, 1575–1590.

Seifert, A., and G. Zängl, 2010: Scaling relations in warm-rain orographic precipitation. *Meteorol. Z.*, **19**, 417–426.

Seifert, A., C. Köhler, and K. D. Beheng, 2012: Aerosol-cloud-precipitation effects over Germany as simulated by a convective-scale numerical weather prediction model. *Atmos. Chem. Phys.*, **12**, 709–725.

Seitz, R., 2011: Bright water: Hydrosols, water conservation and climate change. *Clim. Change*, **105**, 365–381.

Sekiguchi, M., et al., 2003: A study of the direct and indirect effects of aerosols using global satellite data sets of aerosol and cloud parameters. *J. Geophys. Res.*, **108**, 4699.

Seland, Ø., T. Iversen, A. Kirkevåg, and T. Storelvmo, 2008: Aerosol-climate interactions in the CAM-Oslo atmospheric GCM and investigation of associated basic shortcomings. *Tellus A*, **60**, 459–491.

Senior, C. A., and J. F. B. Mitchell, 1993: Carbon dioxide and climate: The impact of cloud parameterization. *J. Clim.*, **6**, 393–418.

Senior, C. A., and J. F. B. Mitchell, 2000: The time-dependence of climate sensitivity. *Geophys. Res. Lett.*, **27**, 2685–2688.

Sesartic, A., U. Lohmann, and T. Storelvmo, 2012: Bacteria in the ECHAM5–HAM global climate model. *Atmos. Chem. Phys.*, **12**, 8645–8661.

Shapiro, E. L., J. Szprengiel, N. Sareen, C. N. Jen, M. R. Giordano, and V. F. McNeill, 2009: Light-absorbing secondary organic material formed by glyoxal in aqueous aerosol mimics. *Atmos. Chem. Phys.*, **9**, 2289–2300.

Sharon, T. M., et al., 2006: Aerosol and cloud microphysical characteristics of rifts and gradients in maritime stratocumulus clouds. *J. Atmos. Sci.*, **63**, 983–997.

Sherwood, S. C., 2002: Aerosols and ice particle size in tropical cumulonimbus. *J. Clim.*, **15**, 1051–1063.

Sherwood, S. C., and C. L. Meyer, 2006: The general circulation and robust relative humidity. *J. Clim.*, **19**, 6278–6290.

Sherwood, S. C., R. Roca, T. M. Weckwerth, and N. G. Andronova, 2010a: Tropospheric water vapor, convection, and climate. *Rev. Geophys.*, **48**, RG2001.

Sherwood, S. C., V. Ramanathan, T. P. Barnett, M. K. Tyree, and E. Roeckner, 1994: Response of an atmospheric general circulation model to radiative forcing of tropical clouds. *J. Geophys. Res.*, **99**, 20829–20845.

Sherwood, S. C., W. Ingram, Y. Tsushima, M. Satoh, M. Roberts, P. L. Vidale, and P. A. O'Gorman, 2010b: Relative humidity changes in a warmer climate. *J. Geophys. Res.*, **115**, D09104.

Shindell, D. T., A. Voulgarakis, G. Faluvegi, and G. Milly, 2012: Precipitation response to regional radiative forcing. *Atmos. Chem. Phys.*, **12**, 6969–6982.

Shindell, D. T., et al., 2013: Radiative forcing in the ACCMIP historical and future climate simulations. *Atmos. Chem. Phys.*, **13**, 2939–2974.

Shiraiwa, M., Y. Kondo, T. Iwamoto, and K. Kita, 2010: Amplification of light absorption of black carbon by organic coating. *Aer. Sci. Technol.*, **44**, 46–54.

Shonk, J. K. P., R. J. Hogan, and J. Manners, 2012: Impact of improved representation of horizontal and vertical cloud structure in a climate model. *Clim. Dyn.*, **38**, 2365–2376.

Shresth, A. B., C. P. Wake, J. E. Dibb, P. A. Mayewski, S. I. Whitlow, G. R. Carmichael, and M. Ferm, 2000: Seasonal variations in aerosol concentrations and compositions in the Nepal Himalaya. *Atmos. Environ.*, **34**, 3349–3363.

Shrivastava, M., et al., 2011: Modeling organic aerosols in a megacity: Comparison of simple and complex representations of the volatility basis set approach. *Atmos. Chem. Phys.*, **11**, 6639–6662.

Shupe, M. D., et al., 2008: A focus on mixed-phase clouds. The status of ground-based observational methods. *Bull. Am. Meteor. Soc.*, **89**, 1549–1562.

Siebesma, A. P., P. M. M. Soares, and J. Teixeira, 2007: A combined eddy-diffusivity mass-flux approach for the convective boundary layer. *J. Atmos. Sci.*, **64**, 1230–1248.

Siebesma, A. P., et al., 2003: A large eddy simulation intercomparison study of shallow cumulus convection. *J. Atmos. Sci.*, **60**, 1201–1219.

Siebesma, A. P., et al., 2009: Cloud-controlling factors. In: *Clouds in the Perturbed Climate System: Their Relationship to Energy Balance, Atmospheric Dynamics, and Precipitation* [J. Heintzenberg and R. J. Charlson (eds.)]. MIT Press, Cambridge, MA, USA, pp. 269–290.

Singh, M. S., and P. A. O'Gorman, 2012: Upward shift of the atmospheric general circulation under global warming: Theory and simulations. *J. Clim.*, **25**, 8259–8276.

Sipilä, M., et al., 2010: The role of sulfuric acid in atmospheric nucleation. *Science*, **327**, 1243–1246.

Skeie, R. B., T. Berntsen, G. Myhre, C. A. Pedersen, J. Ström, S. Gerland, and J. A. Ogren, 2011: Black carbon in the atmosphere and snow, from pre-industrial times until present. *Atmos. Chem. Phys.*, **11**, 6809–6836.

Small, J. D., P. Y. Chuang, G. Feingold, and H. Jiang, 2009: Can aerosol decrease cloud lifetime? *Geophys. Res. Lett.*, **36**, L16806.

Smith, J. N., et al., 2010: Observations of aminium salts in atmospheric nanoparticles and possible climatic implications. *Proc. Natl. Acad. Sci. U.S.A.*, **107**, 6634–6639.

Smith, S. J., and P. J. Rasch, 2012: The long-term policy context for solar radiation management. *Clim. Change*, doi: 10.1007/s10584-012-0577-3.

Snow-Kropla, E. J., J. R. Pierce, D. M. Westervelt, and W. Trivitayanurak, 2011: Cosmic rays, aerosol formation and cloud-condensation nuclei: Sensitivities to model uncertainties. *Atmos. Chem. Phys.*, **11**, 4001–4013.

Soden, B. J., and I. M. Held, 2006: An assessment of climate feedbacks in coupled ocean-atmosphere models. *J. Clim.*, **19**, 3354–3360.

Soden, B. J., and G. A. Vecchi, 2011: The vertical distribution of cloud feedback in coupled ocean-atmosphere models. *Geophys. Res. Lett.*, **38**, L12704.

Soden, B. J., I. M. Held, R. Colman, K. M. Shell, J. T. Kiehl, and C. A. Shields, 2008: Quantifying climate feedbacks using radiative kernels. *J. Clim.*, **21**, 3504–3520.

Sofiev, M., et al., 2009: An operational system for the assimilation of the satellite information on wild-land fires for the needs of air quality modelling and forecasting. *Atmos. Chem. Phys.*, **9**, 6833–6847.

Sohn, B. J., T. Nakajima, M. Satoh, and H. S. Jang, 2010: Impact of different definitions of clear-sky flux on the determination of longwave cloud radiative forcing: NICAM simulation results. *Atmos. Chem. Phys.*, **10**, 11641–11646.

Solomon, S., K. H. Rosenlof, R. W. Portmann, J. S. Daniel, S. M. Davis, T. J. Sanford, and G.-K. Plattner, 2010: Contributions of stratospheric water vapor to decadal changes in the rate of global warming. *Science*, **327**, 1219–1223.

Somerville, R. C. J., and L. A. Remer, 1984: Cloud optical-thickness feedbacks in the CO_2 climate problem. *J. Geophys. Res.*, **89**, 9668–9672.

Sommeria, G., and J. W. Deardorff, 1977: Subgrid-scale condensation in models of nonprecipitating clouds. *J. Atmos. Sci.*, **34**, 344–355.

Song, X., and G. J. Zhang, 2011: Microphysics parameterization for convective clouds in a global climate model: Description and single-column model tests. *J. Geophys. Res.*, **116**, D02201.

Song, X. L., and G. J. Zhang, 2009: Convection parameterization, tropical Pacific double ITCZ, and upper-ocean biases in the NCAR CCSM3. Part I: Climatology and atmospheric feedback. *J. Clim.*, **22**, 4299–4315.

Sorooshian, A., N. L. Ng, A. W. H. Chan, G. Feingold, R. C. Flagan, and J. H. Seinfeld, 2007: Particulate organic acids and overall water-soluble aerosol composition measurements from the 2006 Gulf of Mexico Atmospheric Composition and Climate Study (GoMACCS). *J. Geophys. Res.*, **112**, D13201.

Spencer, R. W., and W. D. Braswell, 2008: Potential biases in feedback diagnosis from observational data: A simple model demonstration. *J. Clim.*, **21**, 5624–5628.

Spencer, R. W., and W. D. Braswell, 2010: On the diagnosis of radiative feedback in the presence of unknown radiative forcing. *J. Geophys. Res.*, **115**, D16109.

Spracklen, D. V., L. J. Mickley, J. A. Logan, R. C. Hudman, R. Yevich, M. D. Flannigan, and A. L. Westerling, 2009: Impacts of climate change from 2000 to 2050 on wildfire activity and carbonaceous aerosol concentrations in the western United States. *J. Geophys. Res.*, **114**, D20301.

Spracklen, D. V., et al., 2008: Contribution of particle formation to global cloud condensation nuclei concentrations. *Geophys. Res. Lett.*, **35**, L06808.

Spracklen, D. V., et al., 2011: Aerosol mass spectrometer constraint on the global secondary organic aerosol budget. *Atmos. Chem. Phys.*, **11**, 12109–12136.

Stan, C., et al., 2010: An ocean-atmosphere climate simulation with an embedded cloud resolving model. *Geophys. Res. Lett.*, **37**, L01702.

Stephens, G. L., M. Wild, P. W. Stackhouse, T. L'Ecuyer, S. Kato, and D. S. Henderson, 2012: The global character of the flux of downward longwave radiation. *J. Clim.*, **25**, 2329–2340.

Stephens, G. L., et al., 2002: The Cloudsat mission and the A-train—A new dimension of space-based observations of clouds and precipitation. *Bull. Am. Meteor. Soc.*, **83**, 1771–1790.

Stephens, G. L., et al., 2008: CloudSat mission: Performance and early science after the first year of operation. *J. Geophys. Res.*, **113**, D00A18.

Stephens, G. L., et al., 2010: Dreary state of precipitation in global models. *J. Geophys. Res.*, **115**, D24211.

Stevens, B., and A. Seifert, 2008: Understanding macrophysical outcomes of microphysical choices in simulations of shallow cumulus convection. *J. Meteorol. Soc. Jpn.*, **86**, 143–162.

Stevens, B., and G. Feingold, 2009: Untangling aerosol effects on clouds and precipitation in a buffered system. *Nature*, **461**, 607–613.

Stevens, B., and J.-L. Brenguier, 2009: Cloud-controlling factors: Low clouds. In: *Clouds in the Perturbed Climate System: Their Relationship to Energy Balance, Atmospheric Dynamics, and Precipitation* [J. Heintzenberg and R. J. Charlson (eds.)]. MIT Press, Cambridge, MA, USA, pp. 173–196.

Stevens, B., W. R. Cotton, G. Feingold, and C.-H. Moeng, 1998: Large-eddy simulations of strongly precipitating, shallow, stratocumulus-topped boundary layers. *J. Atmos. Sci.*, **55**, 3616–3638.

Stevens, B., et al., 2005a: Pockets of open cells and drizzle in marine stratocumulus. *Bull. Am. Meteor. Soc.*, **86**, 51–57.

Stevens, B., et al., 2005b: Evaluation of large-eddy simulations via observations of nocturnal marine stratocumulus. *Mon. Weather Rev.*, **133**, 1443–1462.

Stier, P., J. H. Seinfeld, S. Kinne, and O. Boucher, 2007: Aerosol absorption and radiative forcing. *Atmos. Chem. Phys.*, **7**, 5237–5261.

Stier, P., J. H. Seinfeld, S. Kinne, J. Feichter, and O. Boucher, 2006: Impact of nonabsorbing anthropogenic aerosols on clear-sky atmospheric absorption. *J. Geophys. Res.*, **111**, D18201.

Stier, P., et al., 2005: The Aerosol-Climate Model ECHAM5–HAM. *Atmos. Chem. Phys.*, **5**, 1125–1156.

Stier, P., et al., 2013: Host model uncertainties in aerosol forcing estimates: Results from the AeroCom Prescribed intercomparison study. *Atmos. Chem. Phys.*, **13**, 3245–3270.

Stjern, C. W., 2011: Weekly cycles in precipitation and other meteorological variables in a polluted region of Europe. *Atmos. Chem. Phys.*, **11**, 4095–4104.

Stone, E., J. Schauer, T. A. Quraishi, and A. Mahmood, 2010: Chemical characterization and source apportionment of fine and coarse particulate matter in Lahore, Pakistan. *Atmos. Environ.*, **44**, 1062–1070.

Stone, R. S., et al., 2008: Radiative impact of boreal smoke in the Arctic: Observed and modeled. *J. Geophys. Res.*, **113**, D14S16.

Storelvmo, T., J. E. Kristjánsson, and U. Lohmann, 2008a: Aerosol influence on mixed-phase clouds in CAM-Oslo. *J. Atmos. Sci.*, **65**, 3214–3230.

Storelvmo, T., C. Hoose, and P. Eriksson, 2011: Global modeling of mixed-phase clouds: The albedo and lifetime effects of aerosols. *J. Geophys. Res.*, **116**, D05207.

Storelvmo, T., J. E. Kristjánsson, S. J. Ghan, A. Kirkevåg, Ø. Seland, and T. Iversen, 2006: Predicting cloud droplet number concentration in Community Atmosphere Model (CAM)-Oslo. *J. Geophys. Res.*, **111**, D24208.

Storelvmo, T., J. E. Kristjánsson, U. Lohmann, T. Iversen, A. Kirkevåg, and Ø. Seland, 2008b: Modeling of the Wegener–Bergeron–Findeisen process–implications for aerosol indirect effects. *Environ. Res. Lett.*, **3**, 045001.

Storelvmo, T., J. E. Kristjánsson, U. Lohmann, T. Iversen, A. Kirkevåg, and Ø. Seland, 2010: Corrigendum: Modeling of the Wegener–Bergeron–Findeisen process—implications for aerosol indirect effects. *Environ. Res. Lett.*, **5**, 019801

Storelvmo, T., J. E. Kristjánsson, H. Muri, M. Pfeffer, D. Barahona, and A. Nenes, 2013: Cirrus cloud seeding has potential to cool climate *Geophys. Res. Lett.*, **40**, 178–182.

Storer, R. L., and S. C. van den Heever, 2013: Microphysical processes evident in aerosol forcing of tropical deep convective clouds. *J. Atmos. Sci.*, **70**, 430–446.

Stramler, K., A. D. Del Genio, and W. B. Rossow, 2011: Synoptically driven Arctic winter states. *J. Clim.*, **24**, 1747–1762.

Stratmann, F., O. Moehler, R. Shaw, and W. Heike, 2009: Laboratory cloud simulation: Capabilities and future directions. In: *Clouds in the Perturbed Climate System: Their Relationship to Energy Balance, Atmospheric Dynamics, and Precipitation* [J. Heintzenberg and R. J. Charlson (eds.)]. MIT Press, Cambridge, MA, USA, pp. 149–172.

Struthers, H., et al., 2011: The effect of sea ice loss on sea salt aerosol concentrations and the radiative balance in the Arctic. *Atmos. Chem. Phys.*, **11**, 3459–3477.

Stubenrauch, C. J., S. Cros, A. Guignard, and N. Lamquin, 2010: A 6–year global cloud climatology from the Atmospheric InfraRed Sounder AIRS and a statistical analysis in synergy with CALIPSO and CloudSat. *Atmos. Chem. Phys.*, **10**, 7197–7214.

Stubenrauch, C. J., et al., 2013: Assessment of global cloud datasets from satellites: Project and database initiated by the GEWEX Radiation Panel. *Bull. Am. Meteor. Soc.*, **94**, 1031–1049.

Stuber, N., and P. Forster, 2007: The impact of diurnal variations of air traffic on contrail radiative forcing. *Atmos. Chem. Phys.*, **7**, 3153–3162.

Su, W., N. G. Loeb, G. L. Schuster, M. Chin, and F. G. Rose, 2013: Global all-sky shortwave direct radiative forcing of anthropogenic aerosols from combined satellite observations and GOCART simulations. *J. Geophys. Res.*, **118**, 655–669.

Su, W. Y., et al., 2008: Aerosol and cloud interaction observed from high spectral resolution lidar data. *J. Geophys. Res.*, **113**, D24202.

Sugiyama, M., H. Shiogama, and S. Emori, 2010: Precipitation extreme changes exceeding moisture content increases in MIROC and IPCC climate models. *Proc. Natl. Acad. Sci. U.S.A.*, **107**, 571–575.

Suzuki, K., G. L. Stephens, S. C. van den Heever, and T. Y. Nakajima, 2011: Diagnosis of the warm rain process in cloud-resolving models using joint CloudSat and MODIS observations. *J. Atmos. Sci.*, **68**, 2655–2670.

Suzuki, K., T. Nakajima, M. Satoh, H. Tomita, T. Takemura, T. Y. Nakajima, and G. L. Stephens, 2008: Global cloud-system-resolving simulation of aerosol effect on warm clouds. *Geophys. Res. Lett.*, **35**, L19817.

Svensmark, H., T. Bondo, and J. Svensmark, 2009: Cosmic ray decreases affect atmospheric aerosols and clouds. *Geophys. Res. Lett.*, **36**, L15101.

Tackett, J. L., and L. Di Girolamo, 2009: Enhanced aerosol backscatter adjacent to tropical trade wind clouds revealed by satellite-based lidar. *Geophys. Res. Lett.*, **36**, L14804.

Takahashi, K., 2009: The global hydrological cycle and atmospheric shortwave absorption in climate models under CO_2 forcing. *J. Clim.*, **22**, 5667–5675.

Takemura, T., 2012: Distributions and climate effects of atmospheric aerosols from the preindustrial era to 2100 along Representative Concentration Pathways (RCPs) simulated using the global aerosol model SPRINTARS. *Atmos. Chem. Phys.*, **12**, 11555–11572.

Takemura, T., and T. Uchida, 2011: Global climate modeling of regional changes in cloud, precipitation, and radiation budget due to the aerosol semi-direct effect of black carbon. *Sola*, **7**, 181–184.

Takemura, T., T. Nozawa, S. Emori, T. Y. Nakajima, and T. Nakajima, 2005: Simulation of climate response to aerosol direct and indirect effects with aerosol transport-radiation model. *J. Geophys. Res.*, **110**, D02202.

Tanré, D., M. Herman, and Y. J. Kaufman, 1996: Information on aerosol size distribution contained in solar reflected spectral radiances. *J. Geophys. Res.*, **101**, 19043–19060.

Tanré, D., Y. J. Kaufman, M. Herman, and S. Mattoo, 1997: Remote sensing of aerosol properties over oceans using the MODIS/EOS spectral radiances. *J. Geophys. Res.*, **102**, 16971–16988.

Tanré, D., et al., 2011: Remote sensing of aerosols by using polarized, directional and spectral measurements within the A-Train: The PARASOL mission. *Atmos. Meas. Tech.*, **4**, 1383–1395.

Tao, W.-K., J.-P. Chen, Z. Li, C. Wang, and C. Zhang, 2012: Impact of aerosols on convective clouds and precipitation. *Rev. Geophys.*, **50**, RG2001.

Tao, W.-K., et al., 2009: A Multiscale Modeling System: Developments, applications, and critical issues. *Bull. Am. Meteor. Soc.*, **90**, 515–534.

Tegen, I., M. Werner, S. P. Harrison, and K. E. Kohfeld, 2004: Relative importance of climate and land use in determining present and future global soil dust emission. *Geophys. Res. Lett.*, **31**, L05105.

Theodosi, C., U. Im, A. Bougiatioti, P. Zarmpas, O. Yenigun, and N. Mihalopoulos, 2010: Aerosol chemical composition over Istanbul. *Sci. Tot. Environ.*, **408**, 2482–2491.

Thomas, G. E., et al., 2010: Validation of the GRAPE single view aerosol retrieval for ATSR-2 and insights into the long term global AOD trend over the ocean. *Atmos. Chem. Phys.*, **10**, 4849–4866.

Tilmes, S., R. Müller, and R. Salawitch, 2008: The sensitivity of polar ozone depletion to proposed geoengineering schemes. *Science*, **320**, 1201–1204.

Tilmes, S., R. R. Garcia, E. D. Kinnison, A. Gettelman, and P. J. Rasch, 2009: Impact of geo-engineered aerosols on troposphere and stratosphere. *J. Geophys. Res.*, **114**, D12305.

Tilmes, S., et al., 2012: Impact of very short-lived halogens on stratospheric ozone abundance and UV radiation in a geo-engineered atmosphere. *Atmos. Chem. Phys.*, **12**, 10945–10955.

Tinsley, B. A., 2008: The global atmospheric electric circuit and its effects on cloud microphysics. *Rep. Prog. Phys.*, **71**, 066801.

Tobin, I., S. Bony, and R. Roca, 2012: Observational evidence for relationships between the degree of aggregation of deep convection, water vapor, surface fluxes, and radiation. *J. Clim.*, **25**, 6885–6904.

Tomassini, L., et al., 2013: The respective roles of surface temperature driven feedbacks and tropospheric adjustment to CO_2 in CMIP5 transient climate simulations. *Clim. Dyn.*, doi:10.1007/s00382-013-1682-3.

Tomita, H., H. Miura, S. Iga, T. Nasuno, and M. Satoh, 2005: A global cloud-resolving simulation: Preliminary results from an aqua planet experiment. *Geophys. Res. Lett.*, **32**, L08805.

Tompkins, A. M., and G. C. Craig, 1998: Radiative–convective equilibrium in a three-dimensional cloud-ensemble model. *Q. J. R. Meteorol. Soc.*, **124**, 2073–2097.

Tompkins, A. M., K. Gierens, and G. Radel, 2007: Ice supersaturation in the ECMWF integrated forecast system. *Q. J. R. Meteorol. Soc.*, **133**, 53–63.

Torres, O., P. K. Bhartia, J. R. Herman, A. Sinyuk, P. Ginoux, and B. Holben, 2002: A long-term record of aerosol optical depth from TOMS observations and comparison to AERONET measurements. *J. Atmos. Sci.*, **59**, 398–413.

Torres, O., et al., 2007: Aerosols and surface UV products from Ozone Monitoring Instrument observations: An overview. *J. Geophys. Res.*, **112**, D24S47.

Trenberth, K. E., and A. Dai, 2007: Effects of Mount Pinatubo volcanic eruption on the hydrological cycle as an analog of geoengineering. *Geophys. Res. Lett.*, **34**, L15702.

Trenberth, K. E., and J. T. Fasullo, 2009: Global warming due to increasing absorbed solar radiation. *Geophys. Res. Lett.*, **36**, L07706.

Trenberth, K. E., and J. T. Fasullo, 2010: Simulation of present-day and twenty-first-century energy budgets of the Southern Oceans. *J. Clim.*, **23**, 440–454.

Trenberth, K. E., et al., 2007: Observations: Surface and atmospheric climate change. In: *Climate Change 2007: The Physical Science Basis. Contribution of Working Group I to the Fourth Assessment Report of the Intergovernmental Panel on Climate Change* [Solomon, S., D. Qin, M. Manning, Z. Chen, M. Marquis, K. B. Averyt, M. Tignor and H. L. Miller (eds.)] Cambridge University Press, Cambridge, United Kingdom and New York, NY, USA, pp. 235–336.

Tselioudis, G., and W. B. Rossow, 2006: Climate feedback implied by observed radiation and precipitation changes with midlatitude storm strength and frequency. *Geophys. Res. Lett.*, **33**, L02704.

Tsigaridis, K., and M. Kanakidou, 2007: Secondary organic aerosol importance in the future atmosphere. *Atmos. Environ.*, **41**, 4682–4692.

Tsushima, Y., et al., 2006: Importance of the mixed-phase cloud distribution in the control climatefor assessing the response of clouds to carbon dioxide increase:A multi-model study. *Clim. Dyn.*, **27**, 113–126.

Tsimpidi, A. P., et al., 2010: Evaluation of the volatility basis-set approach for the simulation of organic aerosol formation in the Mexico City metropolitan area. *Atmos. Chem. Phys.*, **10**, 525–546.
Tuttle, J. D., and R. E. Carbone, 2011: Inferences of weekly cycles in summertime rainfall. *J. Geophys. Res.*, **116**, D20213.
Twohy, C. H., and J. R. Anderson, 2008: Droplet nuclei in non-precipitating clouds: Composition and size matter. *Environ. Res. Lett.*, **3**, 045002.
Twohy, C. H., J. A. Coakley, Jr., and W. R. Tahnk, 2009: Effect of changes in relative humidity on aerosol scattering near clouds. *J. Geophys. Res.*, **114**, D05205.
Twohy, C. H., et al., 2005: Evaluation of the aerosol indirect effect in marine stratocumulus clouds: Droplet number, size, liquid water path, and radiative impact. *J. Geophys. Res.*, **110**, D08203.
Twomey, S., 1977: Influence of pollution on shortwave albedo of clouds. *J. Atmos. Sci.*, **34**, 1149–1152.
Udelhofen, P. M., and R. D. Cess, 2001: Cloud cover variations over the United States: An influence of cosmic rays or solar variability? *Geophys. Res. Lett.*, **28**, 2617–2620.
Ulbrich, I. M., M. R. Canagaratna, Q. Zhang, D. R. Worsnop, and J. L. Jimenez, 2009: Interpretation of organic components from Positive Matrix Factorization of aerosol mass spectrometric data. *Atmos. Chem. Phys.*, **9**, 2891–2918.
Unger, N., S. Menon, D. M. Koch, and D. T. Shindell, 2009: Impacts of aerosol-cloud interactions on past and future changes in tropospheric composition. *Atmos. Chem. Phys.*, **9**, 4115–4129.
Unger, N., D. T. Shindell, D. M. Koch, M. Amann, J. Cofala, and D. G. Streets, 2006: Influences of man-made emissions and climate changes on tropospheric ozone, methane, and sulfate at 2030 from a broad range of possible futures. *J. Geophys. Res.*, **111**, D12313.
Usoskin, I. G., and G. A. Kovaltsov, 2008: Cosmic rays and climate of the Earth: Possible connection. *C. R. Geosci.*, **340**, 441–450.
Uttal, T., et al., 2002: Surface heat budget of the Arctic Ocean. *Bull. Am. Meteor. Soc.*, **83**, 255–275.
Vali, G., 1985: Atmospheric ice nucleation—A review. *J. Rech. Atmos.*, **19**, 105–115.
van den Heever, S. C., G. L. Stephens, and N. B. Wood, 2011: Aerosol indirect effects on tropical convection characteristics under conditions of radiative-convective equilibrium. *J. Atmos. Sci.*, **68**, 699–718.
vanZanten, M. C., B. Stevens, G. Vali, and D. H. Lenschow, 2005: Observations of drizzle in nocturnal marine stratocumulus. *J. Atmos. Sci.*, **62**, 88–106.
vanZanten, M. C., et al., 2011: Controls on precipitation and cloudiness in simulations of trade-wind cumulus as observed during RICO. *J. Adv. Model. Earth Syst.*, **3**, M06001.
Várnai, T., and A. Marshak, 2009: MODIS observations of enhanced clear sky reflectance near clouds. *Geophys. Res. Lett.*, **36**, L06807.
Vavrus, S., M. M. Holland, and D. A. Bailey, 2011: Changes in Arctic clouds during intervals of rapid sea ice loss. *Clim. Dyn.*, **36**, 1475–1489.
Vavrus, S., D. Waliser, A. Schweiger, and J. Francis, 2009: Simulations of 20th and 21st century Arctic cloud amount in the global climate models assessed in the IPCC AR4. *Clim. Dyn.*, **33**, 1099–1115.
Verheggen, B., et al., 2007: Aerosol partitioning between the interstitial and the condensed phase in mixed-phase clouds. *J. Geophys. Res.*, **112**, D23202.
Verlinde, J., et al., 2007: The mixed-phase Arctic cloud experiment. *Bull. Am. Meteor. Soc.*, **88**, 205–221.
Vial, J., J.-L. Dufresne, and S. Bony, 2013: On the interpretation of inter-model spread in CMIP5 climate sensitivity estimates. *Climate Dynamics*, doi:10.1007/s00382-013-1725-9.
Viana, M., W. Maenhaut, X. Chi, X. Querol, and A. lastuey, 2007: Comparative chemical mass closure of fine and coarse aerosols at two sites in South and West Europe: Implications for EU air pollution policies. *Atmos. Environ.*, **41**, 315–326.
Viana, M., X. Chi, W. Maenhaut, X. Querol, A. Alastuey, P. Mikuska, and Z. Vecera, 2006: Organic and elemental carbon concentrations during summer and winter sampling campaigns in Barcelona, Spain. *Atmos. Environ.*, **40**, 2180–2193.
Viana, M., et al., 2008: Characterising exposure to PM aerosols for an epidemiological study. *Atmos. Environ.*, **42**, 1552–1568.
Vignati, E., M. Karl, M. Krol, J. Wilson, P. Stier, and F. Cavalli, 2010: Sources of uncertainties in modelling black carbon at the global scale. *Atmos. Chem. Phys.*, **10**, 2595–2611.
Vogelmann, A. M., T. P. Ackerman, and R. P. Turco, 1992: Enhancements in biologically effective ultraviolet radiation following volcanic eruptions. *Nature*, **359**, 47–49.
Vogelmann, A. M., et al., 2012: RACORO extended-term aircraft observations of boundary layer clouds. *Bull. Am. Meteor. Soc.*, **93**, 861–878.
Vogt, M., S. Vallina, and R. von Glasow, 2008: Correspondence on "Enhancing the natural cycle to slow global warming". *Atmos. Environ.*, **42**, 4803–4805.
Volkamer, R., et al., 2006: Secondary organic aerosol formation from anthropogenic air pollution: Rapid and higher than expected. *Geophys. Res. Lett.*, **33**, L17811.
Volodin, E. M., 2008: Relation between temperature sensitivity to doubled carbon dioxide and the distribution of clouds in current climate models. *Izvestiya Atmos. Ocean. Phys.*, **44**, 288–299.
Waliser, D. E., J. L. F. Li, T. S. L'Ecuyer, and W. T. Chen, 2011: The impact of precipitating ice and snow on the radiation balance in global climate models. *Geophys. Res. Lett.*, **38**, L06802.
Wang, G., H. Wang, Y. Yu, S. Gao, J. Feng, S. Gao, and L. Wang, 2003: Chemical characterization of water-soluble components of PM10 and PM2.5 atmospheric aerosols in five locations of Nanjing, China. *Atmos. Environ.*, **37**, 2893–2902.
Wang, H., and D. Shooter, 2001: Water soluble ions of atmospheric aerosols in three New Zealand cities: Seasonal changes and sources. *Atmos. Environ.*, **35**, 6031–6040.
Wang, H., K. Kawamuraa, and D. Shooter, 2005a: Carbonaceous and ionic components in wintertime atmospheric aerosols from two New Zealand cities: Implications for solid fuel combustion. *Atmos. Environ.*, **39**, 5865–5875.
Wang, H., P. J. Rasch, and G. Feingold, 2011a: Manipulating marine stratocumulus cloud amount and albedo: A process-modelling study of aerosol-cloud-precipitation interactions in response to injection of cloud condensation nuclei. *Atmos. Chem. Phys.*, **11**, 4237–4249.
Wang, H. L., and G. Feingold, 2009a: Modeling mesoscale cellular structures and drizzle in marine stratocumulus. Part I: Impact of drizzle on the formation and evolution of open cells. *J. Atmos. Sci.*, **66**, 3237–3256.
Wang, H. L., and G. Feingold, 2009b: Modeling mesoscale cellular structures and drizzle in marine stratocumulus. Part II: The microphysics and dynamics of the boundary region between open and closed cells. *J. Atmos. Sci.*, **66**, 3257–3275.
Wang, L., A. F. Khalizov, J. Zheng, W. Xu, Y. Ma, V. Lal, and R. Y. Zhang, 2010a: Atmospheric nanoparticles formed from heterogeneous reactions of organics. *Nature Geosci.*, **3**, 238–242.
Wang, M., and J. Penner, 2009: Aerosol indirect forcing in a global model with particle nucleation. *Atmos. Chem. Phys.*, **9**, 239–260.
Wang, M., et al., 2011b: Aerosol indirect effects in a multi-scale aerosol-climate model PNNL-MMF. *Atmos. Chem. Phys.*, **11**, 5431–5455.
Wang, M., et al., 2012: Constraining cloud lifetime effects of aerosols using A-Train satellite observations. *Geophys. Res. Lett.*, **39**, L15709.
Wang, T., S. Li, Y. Shen, J. Deng, and M. Xie, 2010b: Investigations on direct and indirect effect of nitrate on temperature and precipitation in China using a regional climate chemistry modeling system. *J. Geophys. Res.*, **115**, D00K26.
Wang, Y., G. Zhuang, A. Tang, H. Yuan, Y. Sun, S. Chen, and A. Zheng, 2005b: The ion chemistry and the source of PM 2.5 aerosol in Beijing. *Atmos. Environ.* **39**, 3771–3784.
Wang, Y., et al., 2006: The ion chemistry, seasonal cycle, and sources of PM2.5 and TSP aerosol in Shanghai. *Atmos. Environ.*, **40**, 2935–2952.
Wang, Z. L., H. Zhang, and X. S. Shen, 2011c: Radiative forcing and climate response due to black carbon in snow and ice. *Adv. Atmos. Sci.*, **28**, 1336–1344.
Waquet, F., J. Riedi, L. C. Labonnote, P. Goloub, B. Cairns, J.-L. Deuzé, and D. Tanré, 2009: Aerosol remote sensing over clouds using A-Train observations. *J. Atmos. Sci.*, **66**, 2468–2480.
Warneke, C., et al., 2010: An important contribution to springtime Arctic aerosol from biomass burning in Russia. *Geophys. Res. Lett.*, **37**, L01801.
Warren, S. G., 2013: Can black carbon in snow be detected by remote sensing? *J. Geophys. Res.*, **118**, 779–786.
Watanabe, M., S. Emori, M. Satoh, and H. Miura, 2009: A PDF-based hybrid prognostic cloud scheme for general circulation models. *Clim. Dyn.*, **33**, 795–816.
Webb, M. J., and A. Lock, 2013: Coupling between subtropical cloud feedback and the local hydrological cycle in a climate model. *Clim. Dyn.*, **41**, 1923–1939.
Webb, M. J., F. H. Lambert, and J. M. Gregory, 2013: Origins of differences in climate sensitivity, forcing and feedback in climate models. *Clim. Dyn.*, **40**, 677–707.
Weinstein, J. P., S. R. Hedges, and S. Kimbrough, 2010: Characterization and aerosol mass balance of PM2.5 and PM10 collected in Conakry, Guinea during the 2004 Harmattan period. *Chemosphere*, **78**, 980–988.
Wen, G., A. Marshak, R. F. Cahalan, L. A. Remer, and R. G. Kleidman, 2007: 3–D aerosol-cloud radiative interaction observed in collocated MODIS and ASTER images of cumulus cloud fields. *J. Geophys. Res.*, **112**, D13204.
Wendisch, M., et al., 2008: Radiative and dynamic effects of absorbing aerosol particles over the Pearl River Delta, China. *Atmos. Environ.*, **42**, 6405–6416.

Westra, S., L. V. Alexander, and F. W. Zwiers, 2013: Global increasing trends in annual maximum daily precipitation. *J. Clim.*, **26**, 3904–3918.

Wetherald, R. T., and S. Manabe, 1980: Cloud cover and climate sensitivity. *J. Atmos. Sci.*, **37**, 1485–1510.

Wex, H., G. McFiggans, S. Henning, and F. Stratmann, 2010: Influence of the external mixing state of atmospheric aerosol on derived CCN number concentrations. *Geophys. Res. Lett.*, **37**, L10805.

Wielicki, B. A., and L. Parker, 1992: On the determination of cloud cover from satellite sensors: The effect of sensor spatial resolution. *J. Geophys. Res.*, **97**, 12799–12823.

Wilcox, E. M., 2010: Stratocumulus cloud thickening beneath layers of absorbing smoke aerosol. *Atmos. Chem. Phys.*, **10**, 11769–11777.

Williams, K. D., and G. Tselioudis, 2007: GCM intercomparison of global cloud regimes: Present-day evaluation and climate change response. *Clim. Dyn.*, **29**, 231–250.

Williams, K. D., and M. J. Webb, 2009: A quantitative performance assessment of cloud regimes in climate models. *Clim. Dyn.*, **33**, 141–157.

Williams, K. D., A. Jones, D. L. Roberts, C. A. Senior, and M. J. Woodage, 2001: The response of the climate system to the indirect effects of anthropogenic sulfate aerosol. *Clim. Dyn.*, **17**, 845–856.

Williams, K. D., et al., 2006: Evaluation of a component of the cloud response to climate change in an intercomparison of climate models. *Clim. Dyn.*, **26**, 145–165.

Wingenter, O. W., S. M. Elliot, and D. R. Blake, 2007: Enhancing the natural sulfur cycle to slow global warming *Atmos. Environ.*, **41**, 7373–7375.

Winker, D. M., J. L. Tackett, B. J. Getzewich, Z. Liu, M. A. Vaughan, and R. R. Rogers, 2013: The global 3–D distribution of tropospheric aerosols as characterized by CALIOP. *Atmos. Chem. Phys.*, **13**, 3345–3361.

Winker, D. M., et al., 2009: Overview of the CALIPSO mission and CALIOP data processing algorithms. *J. Atmos. Ocean. Technol.*, **26**, 2310–2323.

Winker, D. M., et al., 2010: The CALIPSO mission: A global 3D view of aerosols and clouds. *Bull. Am. Meteor. Soc.*, **91**, 1211–1229.

Wood, R., 2005: Drizzle in stratiform boundary layer clouds. Part II: Microphysical aspects. *J. Atmos. Sci.*, **62**, 3034–3050.

Wood, R., 2007: Cancellation of aerosol indirect effects in marine stratocumulus through cloud thinning. *J. Atmos. Sci.*, **64**, 2657–2669.

Wood, R., and C. S. Bretherton, 2006: On the relationship between stratiform low cloud cover and lower-tropospheric stability. *J. Clim.*, **19**, 6425–6432.

Wood, R., C. S. Bretherton, D. Leon, A. D. Clarke, P. Zuidema, G. Allen, and H. Coe, 2011a: An aircraft case study of the spatial transition from closed to open mesoscale cellular convection over the Southeast Pacific. *Atmos. Chem. Phys.*, **11**, 2341–2370.

Wood, R., et al., 2011b: The VAMOS Ocean-Cloud-Atmosphere-Land Study Regional Experiment (VOCALS-REx): Goals, platforms, and field operations. *Atmos. Chem. Phys.*, **11**, 627–654.

Woodhouse, M. T., G. W. Mann, K. S. Carslaw, and O. Boucher, 2008: The impact of oceanic iron fertilisation on cloud condensation nuclei. *Atmos. Environ.*, **42**, 5728–5730.

Woodhouse, M. T., K. S. Carslaw, G. W. Mann, S. M. Vallina, M. Vogt, P. R. Halloran, and O. Boucher, 2010: Low sensitivity of cloud condensation nuclei to changes in the sea-air flux of dimethyl-sulphide. *Atmos. Chem. Phys.*, **10**, 7545–7559.

Woodward, S., D. L. Roberts, and R. A. Betts, 2005: A simulation of the effect of climate change-induced desertification on mineral dust aerosol. *Geophys. Res. Lett.*, **32**, L18810.

Wu, S., L. J. Mickley, J. O. Kaplan, and D. J. Jacob, 2012: Impacts of changes in land use and land cover on atmospheric chemistry and air quality over the 21st century. *Atmos. Chem. Phys.*, **12**, 1597–1609.

Wyant, M. C., C. S. Bretherton, and P. N. Blossey, 2009: Subtropical low cloud response to a warmer climate in a superparameterized climate model. Part I: Regime sorting and physical mechanisms. *J. Adv. Model. Earth Syst.*, **1**, 7.

Wyant, M. C., C. S. Bretherton, P. N. Blossey, and M. Khairoutdinov, 2012: Fast cloud adjustment to increasing CO_2 in a superparameterized climate model. *J. Adv. Model. Earth Syst.*, **4**, M05001.

Wyant, M. C., et al., 2006: A comparison of low-latitude cloud properties and their response to climate change in three AGCMs sorted into regimes using mid-tropospheric vertical velocity. *Clim. Dyn.*, **27**, 261–279.

Xiao, H.-Y., and C.-Q. Liu, 2004: Chemical characteristics of water-soluble components in TSP over Guiyang, SW China, 2003. *Atmos. Environ.*, **38**, 6297–6306.

Xie, S.-P., C. Deser, G. A. Vecchi, J. Ma, H. Teng, and A. T. Wittenberg, 2010: Global warming pattern formation: Sea surface temperature and rainfall. *J. Clim.*, **23**, 966–986.

Xu, B., J. Cao, D. R. Joswiak, X. Liu, H. Zhao, and J. He, 2012: Post-depositional enrichment of black soot in snow-pack and accelerated melting of Tibetan glaciers. *Environ. Res. Lett.*, **7**, 014022.

Xu, B. Q., et al., 2009: Black soot and the survival of Tibetan glaciers. *Proc. Natl. Acad. Sci. U.S.A.*, **106**, 22114–22118.

Xu, K. M., A. N. Cheng, and M. H. Zhang, 2010: Cloud-resolving simulation of low-cloud feedback to an increase in sea surface temperature. *J. Atmos. Sci.*, **67**, 730–748.

Xu, K. M., T. Wong, B. A. Wielicki, L. Parker, B. Lin, Z. A. Eitzen, and M. Branson, 2007: Statistical analyses of satellite cloud object data from CERES. Part II: Tropical convective cloud objects during 1998 El Niño and evidence for supporting the fixed anvil temperature hypothesis. *J. Clim.*, **20**, 819–842.

Xu, K. M., et al., 2002: An intercomparison of cloud-resolving models with the atmospheric radiation measurement summer 1997 intensive observation period data. *Q. J. R. Meteorol. Soc.*, **128**, 593–624.

Xue, H., G. Feingold, and B. Stevens, 2008: Aerosol effects on clouds, precipitation, and the organization of shallow cumulus convection. *J. Atmos. Sci.*, **65**, 392–406.

Yang, Q., et al., 2011: Assessing regional scale predictions of aerosols, marine stratocumulus, and their interactions during VOCALS-REx using WRF-Chem. *Atmos. Chem. Phys.*, **11**, 11951–11975.

Yao, X., et al., 2002: The water-soluble ionic composition of PM2.5 in Shanghai and Beijing, China. *Atmos. Environ.*, **36**, 4223–4234.

Ye, B., et al., 2003: Concentration and chemical composition of PM2.5 in Shanghai for a 1–year period. *Atmos. Environ.*, **37**, 499–510.

Yin, J., and R. M. Harrison, 2008: Pragmatic mass closure study for PM1.0, PM2.5 and PM10 at roadside, urban background and rural sites. *Atmos. Environ.*, **42**, 980–988.

Yin, J. H., 2005: A consistent poleward shift of the storm tracks in simulations of 21st century climate. *Geophys. Res. Lett.*, **32**, L18701.

Yokohata, T., S. Emori, T. Nozawa, Y. Tsushima, T. Ogura, and M. Kimoto, 2005: Climate response to volcanic forcing: Validation of climate sensitivity of a coupled atmosphere-ocean general circulation model. *Geophys. Res. Lett.*, **32**, L21710.

Yokohata, T., M. J. Webb, M. Collins, K. D. Williams, M. Yoshimori, J. C. Hargreaves, and J. D. Annan, 2010: Structural similarities and differences in climate responses to CO_2 increase between two perturbed physics ensembles. *J. Clim.*, **23**, 1392–1410.

Yokohata, T., et al., 2008: Comparison of equilibrium and transient responses to CO_2 increase in eight state-of-the-art climate models. *Tellus A*, **60**, 946–961.

Yoshimori, M., and A. J. Broccoli, 2008: Equilibrium response of an atmosphere-mixed layer ocean model to different radiative forcing agents: Global and zonal mean response. *J. Clim.*, **21**, 4399–4423.

Yoshimori, M., T. Yokohata, and A. Abe-Ouchi, 2009: A comparison of climate feedback strength between CO_2 doubling and LGM experiments. *J. Clim.*, **22**, 3374–3395.

Young, I. R., S. Zieger, and A. V. Babanin, 2011: Global trends in wind speed and wave height. *Science*, **332**, 451–455.

Yttri, K. E., 2007: Concentrations of particulate matter (PM10, PM2.5) in Norway. Annual and seasonal trends and spatial variability. In: *EMEP Particulate Matter Assessment Report, Part B, report EMEP/CCC-Report 8/2007*, Norwegian Institute for Air Research, Oslo, Norway, pp. 292–307.

Yu, F., 2011: A secondary organic aerosol formation model considering successive oxidation aging and kinetic condensation of organic compounds: Global scale implications. *Atmos. Chem. Phys.*, **11**, 1083–1099.

Yu, F., and G. Luo, 2009: Simulation of particle size distribution with a global aerosol model: Contribution of nucleation to aerosol and CCN number concentrations. *Atmos. Chem. Phys.*, **9**, 7691–7710.

Yu, H., R. McGraw, and S. Lee, 2012: Effects of amines on formation of sub-3 nm particles and their subsequent growth. *Geophys. Res. Lett.*, **39**, L02807.

Yu, H., et al., 2006: A review of measurement-based assessments of the aerosol direct radiative effect and forcing. *Atmos. Chem. Phys.*, **6**, 613–666.

Yu, H. B., M. Chin, D. M. Winker, A. H. Omar, Z. Y. Liu, C. Kittaka, and T. Diehl, 2010: Global view of aerosol vertical distributions from CALIPSO lidar measurements and GOCART simulations: Regional and seasonal variations. *J. Geophys. Res.*, **115**, D00H30.

Yuan, T., L. A. Remer, and H. Yu, 2011: Microphysical, macrophysical and radiative signatures of volcanic aerosols in trade wind cumulus observed by the A-Train. *Atmos. Chem. Phys.*, **11**, 7119–7132.

Yuekui, Y., and L. Di Girolamo, 2008: Impacts of 3–D radiative effects on satellite cloud detection and their consequences on cloud fraction and aerosol optical depth retrievals. *J. Geophys. Res.*, **113**, D04213.

Yuter, S. E., M. A. Miller, M. D. Parker, P. M. Markowski, Y. Richardson, H. Brooks, and J. M. Straka, 2013: Comment on "Why do tornados and hailstorms rest on weekends?" by D. Rosenfeld and T. Bell. *J. Geophys. Res. Atmos.*, **118**, 7332–7338.

Zarzycki, C. M., and T. C. Bond, 2010: How much can the vertical distribution of black carbon affect its global direct radiative forcing? *Geophys. Res. Lett.*, **37**, L20807.

Zelinka, M. D., and D. L. Hartmann, 2010: Why is longwave cloud feedback positive? *J. Geophys. Res.*, **115**, D16117.

Zelinka, M. D., and D. L. Hartmann, 2011: The observed sensitivity of high clouds to mean surface temperature anomalies in the tropics. *J. Geophys. Res.*, **116**, D23103.

Zelinka, M. D., S. A. Klein, and D. L. Hartmann, 2012a: Computing and partitioning cloud feedbacks using cloud property histograms. Part I: Cloud radiative kernels. *J. Clim.*, **25**, 3715–3735.

Zelinka, M. D., S. A. Klein, and D. L. Hartmann, 2012b: Computing and partitioning cloud feedbacks using cloud property histograms. Part II: Attribution to changes in cloud amount, altitude, and optical depth. *J. Clim.*, **25**, 3736–3754.

Zelinka, M. D., S. A. Klein, K. E. Taylor, T. Andrews, M. J. Webb, J. M. Gregory, and P. M. Forster, 2013: Contributions of different cloud types to feedbacks and rapid adjustments in CMIP5. *J. Clim.*, **26**, 5007–5027.

Zhang, G. J., A. M. Vogelmann, M. P. Jensen, W. D. Collins, and E. P. Luke, 2010: Relating satellite-observed cloud properties from MODIS to meteorological conditions for marine boundary layer clouds. *J. Clim.*, **23**, 1374–1391.

Zhang, M. H., and C. Bretherton, 2008: Mechanisms of low cloud-climate feedback in idealized single-column simulations with the Community Atmospheric Model, version 3 (CAM3). *J. Clim.*, **21**, 4859–4878.

Zhang, Q., D. R. Worsnop, M. R. Canagaratna, and J. L. Jimenez, 2005a: Hydrocarbon-like and oxygenated organic aerosols in Pittsburgh: Insights into sources and processes of organic aerosols. *Atmos. Chem. Phys.*, **5**, 3289–3311.

Zhang, Q., M. R. Alfarra, D. R. Worsnop, J. D. Allan, H. Coe, M. R. Canagaratna, and J. L. Jimenez, 2005b: Deconvolution and quantification of hydrocarbon-like and oxygenated organic aerosols based on aerosol mass spectrometry. *Environ. Sci. Technol.*, **39**, 4938–4952.

Zhang, Q., et al., 2007a: Ubiquity and dominance of oxygenated species in organic aerosols in anthropogenically-influenced Northern Hemisphere midlatitudes. *Geophys. Res. Lett.*, **34**, L13801.

Zhang, R. Y., A. Khalizov, L. Wang, M. Hu, and W. Xu, 2012a: Nucleation and growth of nanoparticles in the atmosphere. *Chem. Rev.*, **112**, 1957–2011.

Zhang, X. B., et al., 2007b: Detection of human influence on twentieth-century precipitation trends. *Nature*, **448**, 461–465.

Zhang, X. Y., R. Arimoto, Z. S. An, J. J. Cao, and D. Wang, 2001: Atmospheric dust aerosol over the Tibetian Plateau. *J. Geophys. Res.*, **106**, 18471–18476.

Zhang, X. Y., Y. Q. Wang, X. C. Zhang, W. Guo, and S. L. Gong, 2008: Carbonaceous aerosol composition over various regions of China during 2006. *J. Geophys. Res.*, **113**, D14111.

Zhang, X. Y., J. J. Cao, L. M. Li, R. Arimoto, Y. Cheng, B. Huebert, and D. Wang, 2002: Characterization of atmospheric aerosol over Xian in the south margin of the loess plateau, China. *Atmos. Environ.*, **36**, 4189–4199.

Zhang, X. Y., Y. Q. Wang, T. Niu, X. C. Zhang, S. L. Gong, Y. M. Zhang, and J. Y. Sun, 2012b: Atmospheric aerosol compositions in China: Spatial/temporal variability, chemical signature, regional haze distribution and comparisons with global aerosols. *Atmos. Chem. Phys.*, **12**, 779–799.

Zhang, Y., 2008: Online-coupled meteorology and chemistry models: History, current status, and outlook. *Atmos. Chem. Phys.*, **8**, 2895–2932.

Zhang, Y. M., X. Y. Zhang, J. Y. Sun, W. L. Lin, S. L. Gong, X. J. Shen, and S. Yang, 2011: Characterization of new particle and secondary aerosol formation during summertime in Beijing, China. *Tellus B*, **63**, 382–394.

Zhao, T. L., S. L. Gong, X. Y. Zhang, A. A. Mawgoud, and Y. P. Shao, 2006: An assessment of dust emission schemes in modeling east Asian dust storms. *J. Geophys. Res.*, **111**, D05S90.

Zhao, T. X.-P., et al., 2008a: Study of long-term trend in aerosol optical thickness observed from operational AVHRR satellite instrument. *J. Geophys. Res.*, **113**, D07201.

Zhao, T. X. P., N. G. Loeb, I. Laszlo, and M. Zhou, 2011: Global component aerosol direct radiative effect at the top of atmosphere. *Int. J. Remote Sens.*, **32**, 633–655.

Zhao, T. X. P., H. B. Yu, I. Laszlo, M. Chin, and W. C. Conant, 2008b: Derivation of component aerosol direct radiative forcing at the top of atmosphere for clear-sky oceans. *J. Quant. Spectrosc. Radiat. Transfer*, **109**, 1162–1186.

Zhu, P., B. A. Albrecht, V. P. Ghate, and Z. D. Zhu, 2010: Multiple-scale simulations of stratocumulus clouds. *J. Geophys. Res.*, **115**, D23201.

Zhu, P., et al., 2012: A limited area model (LAM) intercomparison study of a TWP-ICE active monsoon mesoscale convective event. *J. Geophys. Res.*, **117**, D11208.

Zhuang, B. L., L. Liu, F. H. Shen, T. J. Wang, and Y. Han, 2010: Semidirect radiative forcing of internal mixed black carbon cloud droplet and its regional climatic effect over China. *J. Geophys. Res.*, **115**, D00K19.

Ziemann, P. J., and R. Atkinson, 2012: Kinetics, products, and mechanisms of secondary organic aerosol formation. *Chem. Soc. Rev.*, **41**, 6582–6605.

Zubler, E. M., U. Lohmann, D. Lüthi, C. Schär, and A. Muhlbauer, 2011: Statistical analysis of aerosol effects on simulated mixed-phase clouds and precipitation in the Alps. *J. Atmos. Sci.*, **68**, 1474–1492.

Zuidema, P., et al., 2005: An arctic springtime mixed-phase cloudy boundary layer observed during SHEBA. *J. Atmos. Sci.*, **62**, 160–176.

Zuidema, P., et al., 2012: On trade wind cumulus cold pools. *J. Atmos. Sci.*, **69**, 258–280.